
MICROALGAL BIOREFINERY FOR FOOD APPLICATION: PROCESS DEVELOPMENT FOR THERMO-RESISTANT ANTIOXIDANTS PRODUCTION

Luigi D'Elia

Dottorato in Biotecnologie – XXXIII ciclo

Università di Napoli Federico II



Dottorato in Biotecnologie – XXXIII ciclo

Università di Napoli Federico II



**MICROALGAL BIOREFINERY
FOR FOOD APPLICATION:
PROCESS DEVELOPMENT
FOR THERMO-RESISTANT
ANTIOXIDANTS PRODUCTION**

Luigi D'Elia

Dottorando: Luigi D'Elia

Relatore: Prof.ssa Daria Maria Monti

Coordinatore: Prof. Marco Moracci

Settore Scientifico Disciplinare: BIO/10

RIASSUNTO.....	1
SUMMARY.....	6
1.Introduction.....	7
1.1 Photosynthetic microorganisms.....	9
1.2High-value compounds from Microalgae and Cyanobacteria.....	9
1.3Microalgae as source of natural antioxidants for food application.....	14
1.4Current market of bioactive food compounds from microalgae.....	15
1.5 Green chemistry and microalgae.....	16
1.6 Green innovative techniques for the extraction of molecules.....	16
1.7 Switchable solvents.....	17
1.8 The aim of thesis.....	21
1.9 References.....	22
2. Microorganisms from harsh and extreme environments: a collection of living strains at ACUF (Naples, Italy).....	33
2.1 The ACUF collection.....	33
2.2 History and aims.....	33
2.3 Microalgae from thermoacidic habitats.....	35
2.4 Algal biofilms and cultural heritage.....	35
2.5 Biotechnological applications and toxicity tests.....	35
2.6 Facilities and culture maintenance.....	36
2.7. Strain isolation procedures.....	37
2.8 Characterization and monitoring of cultures.....	38
2.9 Overview of the available strains and representativeness of cultures.....	38
2.10 Perspectives.....	41
2.11 References.....	42
3. Thermo resistant antioxidants from photoautotrophic microorganisms: screening and characterization.....	47
3.1 Introduction.....	48
3.2 Materials and methods.....	51
3.3 Results.....	56
3.4 Discussion.....	68
3.5 References.....	69
4. Hydrophobic molecules from <i>Spirulina platensis</i> grown in <i>Thin Layer Photobioreactor</i> at ATlbiotech company.....	78
4.1 Introduction.....	78
4.2 Materials and methods.....	79

4.3 Results and Discussion.....	82
4.4 Conclusion.....	85
4.5 References.....	86
5. Switchable solvent selective extraction of hydrophobic antioxidants from <i>Synechococcus bigranulatus</i>	91
5.1 Introduction.....	92
5.2 Materials and Methods.....	93
5.3 Results.....	98
5.4 Discussion.....	105
5.6 References.....	106
GENERAL DISCUSSION.....	113
APPENDIX.....	117

Riassunto

Nei prodotti alimentari industriali, per prevenire l'ossidazione del cibo con conseguente irrancidimento, vengono utilizzati principalmente antiossidanti sintetici, come il butilidrossianisolo (BHA) e il butilidrossitolone (BHT), la cui tossicità e gli effetti negativi sulla salute sono ampiamente documentati. Pertanto, l'aumento della consapevolezza da parte dei consumatori dei possibili effetti dannosi del cibo sulla salute ha portato ad una richiesta sempre maggiore di cibi naturali, considerati sicuri e salutari. Di conseguenza, l'industria del settore alimentare sta cercando di adeguarsi alle richieste, cercando di favorire e dare maggiore impulso alla ricerca e allo studio di additivi innovativi di origine naturale.

I principali antiossidanti naturali utilizzati sono molecole estratte da frutta o verdura (es. tocoferoli, carotenoidi e acido ascorbico). Tuttavia, durante varie operazioni di lavorazione degli alimenti, come il trattamento termico o il processo di conservazione, questi antiossidanti possono perdere la loro stabilità ossidativa, con conseguente perdita dell'attività antiossidante.

In questo contesto, microalghe e cianobatteri hanno ricevuto grande attenzione proprio per l'abbondanza di metaboliti secondari con attività antiossidante. Questi microrganismi fotosintetici, ricchi di proteine, lipidi, pigmenti e carboidrati, attualmente sono considerati fabbriche naturali di prodotti ad alto valore aggiunto. Tali microrganismi presentano inoltre diversi vantaggi: (i) hanno cicli di crescita brevi; (ii) possono essere coltivati tutto l'anno; (iii) non necessitano di terreni agricoli o di acqua pulita e (iv) non sottraggono spazi destinati all'agricoltura.

Inizialmente, microalghe e cianobatteri sono stati utilizzati per la produzione di biocarburanti, ma tale scelta si è rivelata un'opzione non economicamente vantaggiosa. Un approccio diverso è stato quindi preso in considerazione: utilizzare tali microrganismi per ottenere molecole ad alto valore aggiunto e sfruttare poi la biomassa esausta. Attualmente, l'estrazione di bioprodotto dalle biomasse naturali si basa su tecnologie che prevedono l'utilizzo di solventi organici, come esano, cloroformio, acetone, metanolo e dietilene, la cui tossicità e il rispettivo danno ambientale indotto sono ormai noti. Inoltre, le grandi quantità di solvente richiesto, il lungo tempo di estrazione e i frequenti pretrattamenti della biomassa determinano un grande dispendio energetico. Ecco perché lo sviluppo di tecniche "verdi" per estrarre composti ad alto valore rappresenta un progresso significativo e una valida alternativa alle tecnologie classiche.

Il concetto di chimica verde è stato introdotto per la prima volta agli inizi degli anni '90 da Anastas. Basato su 12 principi, tra le varie cose, l'utilizzo di solventi sicuri e con minimo impatto ambientale possibile, così da massimizzare la quantità di materia prima che diventa parte del prodotto stesso.

Le attuali tecniche estrattive, definite verdi, riducono o eliminano completamente i solventi tossici, minimizzando l'impatto ambientale; consentono di ridurre i tempi di estrazione e di migliorarne le rese, risultando vantaggiosi anche in termini economici. Va considerato però che la piena fattibilità di questi processi su scala industriale richiede ancora tempo.

Tra le diverse tecniche innovative verdi sono da annoverare quelle che prevedono l'uso dei *solventi commutabili*, studiati per l'estrazione di molecole idrofobiche. Questi solventi sono liquidi non volatili, in grado di passare da una forma idrofobica ad una idrofilica, e viceversa, in risposta ad uno stimolo esterno. Un vantaggio di questi solventi consiste nel fatto che è possibile recuperare le molecole estratte senza processi di distillazione, ma semplicemente cambiando la polarità del solvente.

Nell'ottica della chimica verde, lo scopo del seguente progetto di dottorato è stato la messa a punto di tecniche verdi per l'estrazione di molecole antiossidanti termoresistenti a partire da microalghe o cianobatteri, da applicare come conservanti alimentari.

A tal fine l'attenzione si è concentrata sullo studio dei ceppi disponibili presso la Collezione Algale dell'Università Federico II di Napoli (ACUF). Fondata nel 1973 dal Professor Taddei, l'ACUF nasce come raccolta di *Cyanidium caldarium*. Oggi sono mantenuti oltre 800 microrganismi fotosintetici vivi da quasi tutti i continenti, principalmente appartenenti a Cianobatteri, Chlorophyta, Rhodophyta e Bacillariophyceae. Considerando la grande biodiversità di microalghe disponibile presso tale centro, è stato condotto uno screening su venticinque ceppi tra microalghe e cianobatteri al fine di identificare i più promettenti per la produzione di antiossidanti. I parametri utilizzati ai fini dello screening sono stati la velocità di crescita e il potere antiossidante dell'estratto in etanolo di ciascun ceppo. Dall'integrazione di questi due parametri sono stati selezionati *Enallax sp.*, *Synechococcus bigranulatus* e *Galdieria sulphuraria*. Successivamente, è stata valutata l'attività antiossidante degli estratti selezionati, prima e dopo il trattamento di pastorizzazione. I risultati hanno chiaramente mostrato che l'attività antiossidante degli estratti era completamente preservata anche dopo il trattamento termico,

poiché erano in grado di proteggere le cellule dai danni indotti dai raggi UVA.

Il passo successivo è stato la produzione massiva dei ceppi selezionati in fotobioreattori tubolari a colonna con un volume di lavoro 0,8 L e, presso l'azienda ATlbiotech la produzione massiva di *Spirulina platensis* in un fotobioreattore a strato sottile. Entrambi i fotobioreattori hanno mostrato una buona produttività.

Successivamente, con il solvente commutabile "verde" N-Etilbutilammia (EBA) sono state estratte le molecole antiossidanti dalla biomassa prodotta nei fotobioreattori. Le rese delle molecole idrofobiche ottenute con l'EBA sono state poi paragonate alle rese ottenute con il metodo convenzionale Bligh-Dyer (cloroformio/metanolo) e nessuna differenza significativa è stata osservata.

Nel caso del cianobatterio *S. bigranulatus*, il recupero delle molecole estratte è stato condotto con tre strategie diverse ai fini di valutare la più efficiente: nella strategia (i) la commutazione del solvente da non-polare a polare è stata indotta mediante CO₂, SS(CO₂); nella strategia (ii) la commutazione è avvenuta mediante una riduzione di temperatura SS(LCST) e nella strategia (iii) sono stati condotti due cicli di commutazione, il primo indotto dalla temperatura e il secondo dalla CO₂, SS(LCST-CO₂).

Sorprendentemente, la strategia SS(LCST-CO₂) ha permesso di recuperare due frazioni distinte, una frazione arancione (OF) ricca di β-carotene, e una frazione verde (GF) ricca di zeaxantina, rendendo il processo altamente selettivo e più efficiente delle tecniche convenzionali utilizzate in parallelo. Inoltre, la natura del solvente non ha influenzato la biocompatibilità delle molecole estratte né l'attività antiossidante, che è stata conservata anche dopo il processo di pastorizzazione degli estratti.

Ancora, la capacità del solvente di estrarre antiossidanti dalla biomassa non pretrattata, dimostra la capacità dell'EBA, nella sua forma non polare, di distruggere le pareti e le membrane delle cellule algali. Quindi, l'eliminazione delle fasi di essiccazione e distruzione cellulare provoca una riduzione del consumo energetico del processo di estrazione che lo rende vantaggioso economicamente.

Infine, la possibilità di recupero e riuso del solvente, la capacità di estrarre molecole idrofobiche da biomassa non pretrattata, la selettività di estrazione e la facile separazione soluto-solvente rendono i solventi commutabili una valida alternativa alle tecniche convenzionali.

Pertanto, sulla base dei risultati ottenuti è possibile considerare microalghe e cianobatteri una fonte promettente di antiossidanti naturali termo-resistenti da applicare come conservanti alimentari.

*Gli esperimenti di estrazione con i solventi commutabili sono stati effettuati nel laboratorio del Prof.dr.ir. D.W.F. (Wim) Brilman presso il Dipartimento di Sustainable Process technology (SPT), TNW faculty UNIVERSITY OF TWENTE

*La biomassa di *S. Platensis* è stata prodotta presso l'azienda ATlbiotech s.r.l. di Castel Baronia (AV), Italia, sotto la supervisione dell'Ing. Domenico Liotto

SUMMARY

Due to the toxicity of synthetic antioxidants used as food additives, nowadays the request for natural ones is mandatory. Moreover, many natural antioxidants lose their biological activity after food thermal process treatment. Among natural sources, microalgae and cyanobacteria emerged in the last years as good antioxidants producers.

The aim of the present PhD project was the production of thermo-resistant antioxidants from microalgae and cyanobacteria to be applied in the food industry, obtained with green extraction processes and/or solvents.

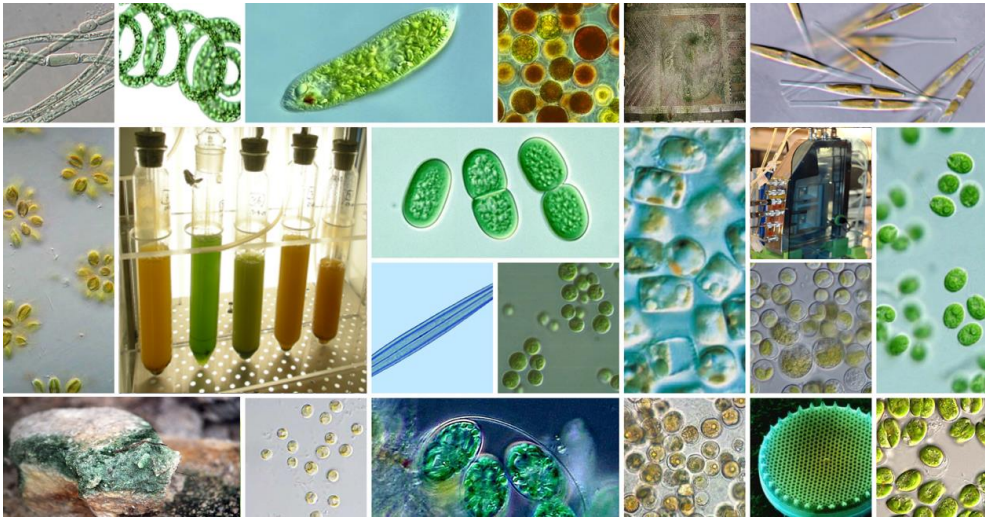
First, a screening on twenty-five strains between microalgae and cyanobacteria, obtained from the Algal collection of University Federico II (ACUF), was carried out. The biomass was extracted in ethanol, considered a GRAS (Generally Recognized As Safe) solvent. Based on growth rate and *in vitro* antioxidant activity of the extracts, *Enallax sp.*, *Synechococcus bigranulatus* and *Galdieria sulphuraria* were selected and their biocompatibility was assessed. Then, extracts were validated also for their ability to protect human keratinocytes from UVA induced oxidative stress, before and after the pasteurization process.

Then, the secondary amine N-Ethylbutylamine (EBA) switchable solvent was used to extract antioxidants from biomass obtained from microalgae grown in bubble column photobioreactors (1L) and in thin layer photobioreactor (15L). Switchable solvents are particular liquids that can be converted from hydrophobic to hydrophilic form and *viceversa*, as a response to an external stimulus. The yields of antioxidants molecules obtained with EBA were similar to the yields obtained with a conventional method, Bligh e Dyer (B&D), on the same amount of biomass. Moreover, EBA extraction allowed to selectively extract a β -carotene enriched fraction and a zeaxanthin enriched fraction.

The biocompatibility and antioxidants activity of both fractions, either before and after thermal treatment, open the way to use microalgae and cyanobacteria in food preservation.

Chapter 1

Introduction



1.1 Photosynthetic microorganisms

Microalgae and cyanobacteria (Figure 1) are unicellular microorganisms which use sun radiant energy, carbon dioxide (CO₂) and ions present in the environment for energy and biomass production. Microalgae and cyanobacteria are directly responsible for almost 50% of photosynthesis on earth¹ and they are able to mitigate large amounts of carbon dioxide, as about 1.8 tons of CO₂ are converted in one ton of microalgae². They are present in different ecosystems, as they can grow in fresh or marine water, they do not compete with arable lands, multiply rapidly and can accumulate large amounts of valuable components (pigments, polyunsaturated fatty acids, proteins, lipids and carbohydrates) within a short period of time, compared to conventional crops. These microorganisms are usually classified on the basis of their pigments and morphology.

Cyanobacteria, known in the past as blue-green algae, have a prokaryotic cell and produce chlorophyll *a* as well as phycobiliproteins^{3,4}. Green algae have chlorophylls *a* and *b* and usually do not have accessory light-harvesting pigments⁵. Red algae contain chlorophyll *a* and phycobilisomes that are located on the surface of unstacked thylakoid membranes^{6,7}.

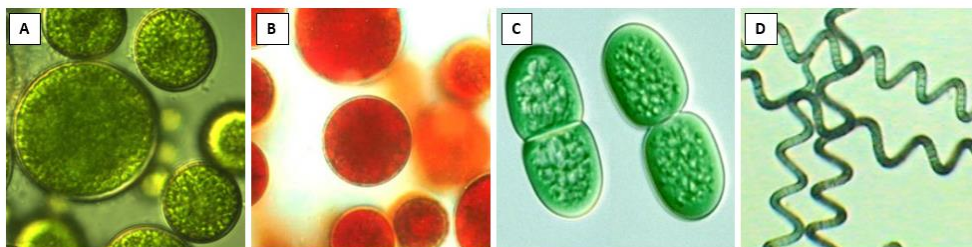


Figure 1. Examples of microalgae and cyanobacteria. A) *Chlorella vulgaris*; B) *Haematococcus pluvialis*; C) *Synechococcus bigranulatus*; D) *Arthrospira platensis*.

1.2 High-value compounds from Microalgae and Cyanobacteria

It has been estimated that about 200,000 species are known among microalgae and cyanobacteria⁸, but only few of them have been studied to exploit their content⁹. Indeed, the metabolic diversity and their ability to grow under different nutritional conditions (autotrophy, heterotrophy and mixotrophy) is the starting point for the synthesis of a huge number of molecules which can be used in different fields. Thus, microalgae can be exploited as a novel and green source of high-value compounds for industrial purposes (Table 1). Some examples of microalgae-derived high-value compounds are:

- Carotenoids:** terpenoids that are derived from a 40-carbon polyene chain and may be complemented by cyclic groups and oxygen-containing functional groups. Based on their organic structure, carotenoids may be classified into two types: carotenes and xanthophylls (Figure 2), which are responsible for the red, brown and yellow color of plants, algae and cyanobacteria¹⁰. Carotenoids play key roles in light harvesting, in the transfer of energy during photosynthesis and in the protection of the photosynthetic apparatus against photooxidative damage¹¹. Noteworthy, carotenoids are able to quench singlet oxygen (1O_2) and free radicals responsible for cell damage. Carotenoids can help in preventing and treating many diseases, such as cancer, cardiovascular disease, diabetes and osteoporosis^{12,13}, as they possess anti-inflammatory and antioxidant activities¹⁴. Due to their striking color characteristics, antioxidant and preservative properties, they are widely used as a natural colorant for the food industry¹⁴. In particular, β -carotene is used as colorant, especially in the preparation of food with elevated fatty acids content (e.g. margarine, butter, soft drinks, cakes and milk-based products)¹⁴. As microalgae usually produce 0.1-0.2% dry weight on average of carotenoids and up to 14% of β -carotene for some species¹⁵⁻¹⁷, it is not surprising that nowadays the β -carotene most used in the food sector is produced by the microalga *Dunaliella salina*¹⁸.

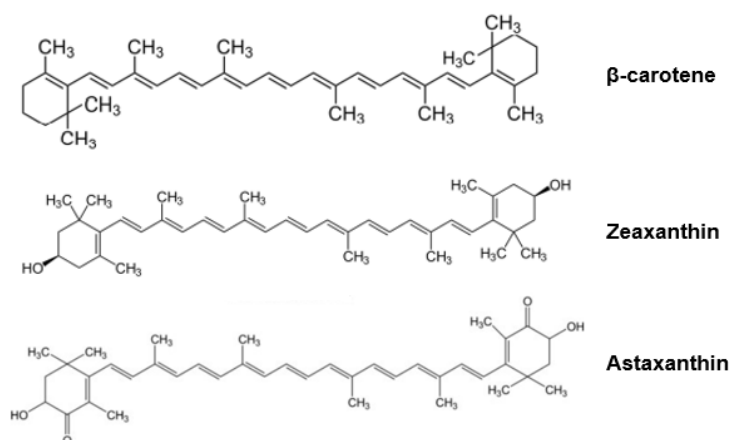


Figure 2. Molecular structure of carotenoids. β -carotene ($C_{40}H_{56}$) belongs to the group of carotenoids consisting of isoprene units. It is the most abundant form of carotenoid and it is the precursor of vitamin A. Zeaxanthin ($C_{40}H_{56}O_2$) is a xanthophyll carotenoid. Zeaxanthin is an isomer of Lutein. Astaxanthin ($C_{40}H_{52}O_4$) is a metabolite of zeaxanthin and/or canthaxanthin, containing both hydroxyl (-OH) and ketone (C=O) functional groups.

- Chlorophylls:** porphyrin-containing compounds with macrocyclic tetrapyrrole nucleus (Figure 3). The pyrrole rings are linked to each other via methine bridges with the double bonds forming a closed, conjugated loop. On the other hand, the closed loop of the conjugated double bonds forms the chromophore imparting light absorption ability to the molecule¹⁴. Chlorophylls are currently used as both food and pharmaceutical colorants and as functional food supplements. Furthermore, Fernandes and colleagues found that chlorophylls can be implicated as chemopreventive agents against the onset of degenerative diseases¹⁹. Due to their vital role in photosynthesis, they are the most abundant and common pigments in plants, algae and cyanobacteria and constitute about 0.5–1.5% of the dry cell matter²⁰. *Chlorella* is the most used species for chlorophyll production^{10,14,21}.

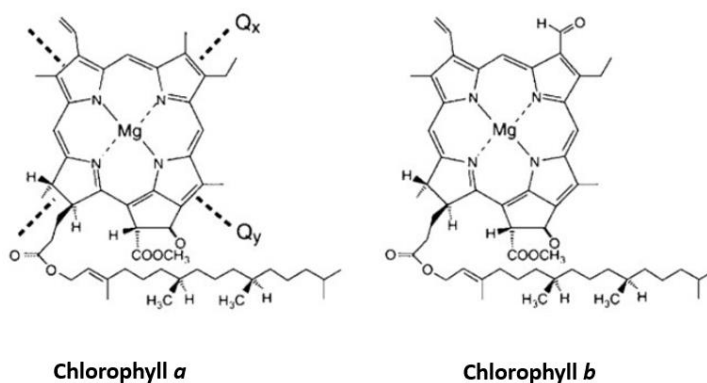


Figure 3. Molecular structure of Chlorophylls. Chlorophyll molecule is a porphyrin ring, coordinated to a central atom of magnesium. Chlorophyll a ($C_{55}H_{72}MgN_4O_5$) is the principal pigment involved in the photosynthesis, whereas chlorophyll b ($C_{55}H_{70}MgN_4O_6$) is the accessory pigment, collecting the energy to be transferred to chlorophyll a.

- Proteins:** Microalgae protein content is higher than that obtained from conventional sources, such as meat, poultry and dairy products. Some species, such as the Chlorophycean show a protein amount between 40-60%, whereas species such as *Spirulina* reach up to 70% with respect to their mass^{22,23}. Algal proteins are mainly used as animal feed, as food or food supplement for human consumption^{24,25}. However, microalgal based functional foods have not flooded the market yet²⁰.

- **Phycobiliproteins:** accessory photosynthetic pigments, they assemble to form phycobilisomes, antenna complex of cyanobacteria, algae and cryptomonads. These pigments are water soluble proteins brilliantly colored. The color is due to the presence of linear tetrapyrrole groups called bilins¹⁰. Two major classes are predominant: phycocyanin (C-phycocyanin, deep blue, and allophycocyanin, light blue) and phycoerythrin (red)¹⁴. Phycobiliproteins exhibit antioxidant, anti-inflammatory, anti-proliferative activity, hepatoprotective, and neuroprotective effects^{26,27}. In addition to these health benefits, these molecules have been used in dietary nutritional supplements and as natural colorant applications in the food, nutraceutical, cosmetic, and biotechnology industry^{20,25}.
- **Lipids:** hydrophobic molecules, which are soluble in most organic solvents^{28,29}. They can be classified into: (i) polar lipids, (ii) neutral lipids and (iii) free fatty acids²⁹. Microalgae and cyanobacteria produce high levels of lipids³⁰, in the range of 20-50% of total biomass dry weight²⁸. Algae fatty acids have been widely studied for biofuel production, but this option is still economically unsustainable³⁰⁻³². On the contrary, the use of omega-3 and omega-6, polyunsaturated fatty acids (Figure 4), as food supplements for their beneficial effects on human health, has received great interest²⁸.

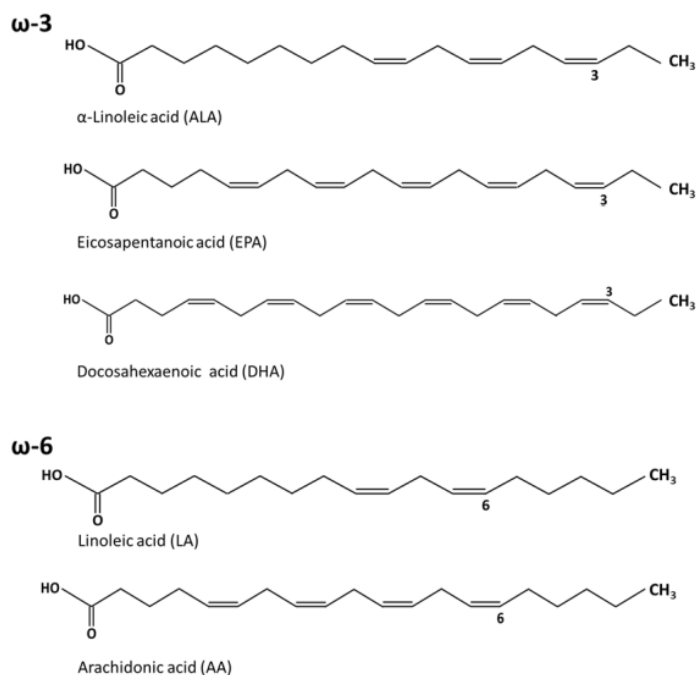


Figure 4. Molecular structure of common ω -3 and ω -6 polyunsaturated fatty acids. Polyunsaturated fatty acids have the first double binding in position 3 (ω -3) or in position 6 (ω -6). All double bindings are in cis formation. The ω -3 fatty acids include alpha-linolenic acid (ALA), eicosapentaenoic acid (EPA), and docosahexaenoic acid (DHA). The ω -6 include linoleic acid (LA) and arachidonic acid (AA).

- **Carbohydrates**, obtained in Calvin cycle during photosynthesis, accounts for 15-60% of the biomass, but the content and the composition may vary among species^{33,34}. They are present in plastids in the form of starch, while in the cell wall as cellulose, glycogen and polysaccharides³⁵. Microalgae carbohydrates are mainly preferred for the production of biofuel, due to the high availability of fermentable sugars, low hemicellulose content and no lignin^{33,34,36}.

Table 1. Lipids, proteins, carbohydrates and carotenoids content of main algae used for food applications. Yields are reported as % with respect to dry weight biomass.

Species	Lipids %	Proteins %	Carbo-hydrates %	Carotenoids %	Ref
<i>Chlorella vulgaris</i>	5-4	40-60	10-50	0.4	23,37,38
<i>Chlorella sp.</i>	10-50	20-45	23-45		38-41
<i>Scenedesmus sp.</i>	25-50	35-52	18-43		39,42-44
<i>Dunaliella</i>	6-25	50-80	5-11	0.5	42,45-47
<i>Spirulina platensis</i>	2-10	45-70	5-13	0.2	41,48,49

1.3 Microalgae as source of natural antioxidants for food application

Antioxidants are molecules able to protect, scavenge, and repair oxidative damage, thereby protecting target structures or molecules from oxidative injuries^{8,50}. From a metabolic point of view, aerobic organisms need oxygen to live, because oxygen is the main source of energy for the cell. However, oxygen can induce oxidative stress, which means a loss of balance between the free radical species and antioxidant levels^{51,52}. Free radicals species are atoms, molecules or ions with unpaired electrons that are highly unstable and active towards chemical reactions with other molecules. They derive from three elements: oxygen, nitrogen and sulphur, thus forming reactive oxygen species (ROS), reactive nitrogen species (RNS) and reactive sulphur species (RSS)^{8,53}. The unbalance between the free radical species and antioxidant levels leads to DNA damage, lipids peroxidation, as well as to the activation of signalling pathways that induce an uncontrolled growth of cells, their inability to differentiate, and the insurgence of a malignant phenotype^{53,54}.

The human body has a natural antioxidant defense mechanism composed of enzymatic (e.g., catalase) or nonenzymatic molecules, such as radical scavengers (e.g., the water-soluble vitamin C and the lipid-soluble vitamin E) and quenchers (e.g., β -carotene)⁵². Although these defense mechanisms are quite effective, they are incomplete

because the human body cannot produce some important antioxidants, which therefore must be taken from the diet^{52,55}.

The main antioxidants acquired from the diet are pigments (carotenes and xanthophylls), polyphenols (flavonoids, phenolic acids) and fatty acids (ω -3 and ω -6 fatty acids) present in many vegetables and fruits^{20,56}.

A completely different use of antioxidants is to use them to prolong the shelf life of foodstuff. Actually, many of them are synthetic, such as butylated hydroxytoluene (BHT) or butylated hydroxyanisole (BHA)⁵⁷. As these components are suspected to be toxic and carcinogens, natural molecules with antioxidant activity have drawn great attention^{58,59}. Moreover, the antioxidant content and their biological activities in foods may be affected by certain processing and thermal treatments⁶⁰. Thus, research is focusing on the discovery of natural molecules with antioxidant activity that can be applied for the preservation of foods without losing their biological activity after industrial treatments of processing and sterilization.

In this context, microalgae and cyanobacteria are emerging as great sources of sustainable antioxidants. Indeed, many algae secondary metabolites are endowed with antioxidant activity. Currently, microalgae derived foods are marketed as healthy foods and are available in the industry as capsules, tablets, powders and liquids. Other secondary metabolites, such as pigments and fatty acids, derived from microalgae, are consolidating their market share as food coloring, food additive, and food supplement⁶¹.

1.4 Current market of bioactive food compounds from microalgae

The use of extracts or the whole algal biomass for human consumption is related to food safety regulations, which vary among countries, and is allowed only for some species^{9,62}. Nowadays, the most commercialized algal species is *Spirulina* (selling price 5-50 USD/Kg). Its phycocyanin, along with^{61,63,64} β -carotene and astaxanthin produced by *Dunaliella* and *Haematococcus*, are widely required as food additives and food colorants⁶¹.

According to a report by Future Market Insights (<https://www.researchandmarkets.com>), the algae pigments market is steadily growing. For example, the actual phycocyanin market is \$ 112.3 million, while the β -carotene is \$ 432.2 million and is expected to increase by 2025 with a CAGR (Compound Annual Growth Rate) of

around 10%. However, when compared to the global market of food and feed products derived from all the other sources, the market portfolio of microalgae-based products is still small⁶⁵.

1.5 Green chemistry and microalgae

In the last decades, increasing concerns about environmental issues has been raised around the world. However, bioactive molecules are still extracted on an industrial scale by conventional methods, such as hexane, chloroform, acetone, methanol and diethyl ether, with a high negative environmental impact. Despite high energy consumption and large amounts of solvents, the yield is often minimal⁶⁶. Thus, the design of green and sustainable extraction methods of natural products is currently a hot research topic in the multidisciplinary area of applied chemistry, biology and technology⁶⁷.

The concept of Green Chemistry was first formulated at the beginning of the '90s⁶⁸. In relation to green extraction of natural products, the definition can be: *“Green Extraction is based on the discovery and design of extraction processes which will reduce energy consumption, allows use of alternative solvents and renewable natural products, and ensure a safe and high quality extract/product”*⁶⁷.

Green chemistry is based on the application of 12 principles⁶⁹. Among those, some are important in the context of circular economy and industrial applications. As an example, the development of processes that maximize the amount of raw material that becomes part of the product itself; the use from industries of chemicals and solvents that are safe for the environment; the efficiency in using energy, and, last but not least, the prevention of wastes.

However, most current industrial production processes still lack efficiency in using feedstocks and produce large amount of wastes, some of which are toxic for the solvents used⁷⁰.

In this context, the development of green extraction technologies to be applied to microalgae well fits into the Green Chemistry philosophy.

1.6 Green innovative techniques for the extraction of molecules

Supercritical fluids extraction (SFE) was widely studied mainly for lipophilic compounds extraction, such as fatty acids, carotenoids, and sterols, rather than polar compounds⁷¹. SFE uses a fluid in supercritical conditions, that is at temperature and pressure above the critical point

of the solvent selected. These conditions allow the solvent to penetrate the matrix and extract molecules that have the same polarity of the solvent^{72,73}. SFE is considered “green” as it uses an economic, non-harmful, non-flammable, and recyclable solvent (CO₂). However, due to the high initial cost of the SFE equipment it is difficult the scaling up on an industrial level^{71–73}.

Another innovative technique that allows a good extraction of hydrophobic molecules from microalgae is the Microwave Assisted Extraction (MAE). This technique uses microwaves to heat the solvent, which can easily penetrate into the matrix, thus facilitating the extraction of target compounds⁷⁴. MAE has the advantage of (i) requiring short extraction time, and (ii) it could be used at an industrial level. However, the high energy for radiation power and high temperature required can affect the bioactivity of the extracted compounds^{71,75}.

Ionic liquids (ILs), composed of a large number of inorganic or organic cations, are a valid alternative to volatile solvent for hydrophobic molecules extraction. However, although many of them have been proved to be not harmful for humans, the application at industrial level is unrealistic, due to their costs and the environmental impact^{76,77}.

In recent years, a second generation of ILs has been developed: switchable solvents (SSs).

1.7 Switchable solvents

Switchable solvents (SSs) (Figure 5) are non-volatile liquids that can be converted from a non-ionic (hydrophobic) form to an ionic (hydrophilic) form and *viceversa* in response to an external stimulus, such as temperature⁷⁸. This innovative method allows to recover hydrophobic and hydrophilic molecules from the extraction solvent, based on phase splitting, which might offer an energy efficient alternative^{79,80}. In addition, they can be easily applied at an industrial scale and may allow a highly selective extraction⁸¹.

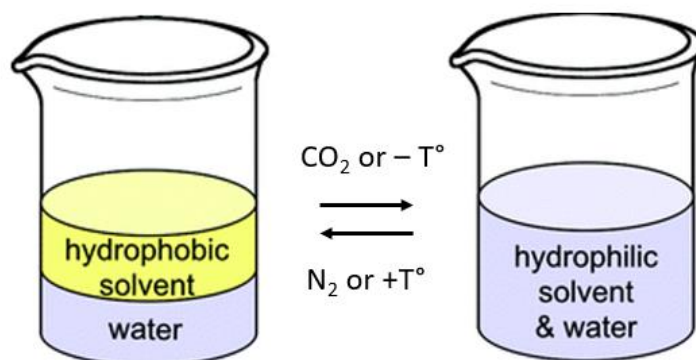


Figure 5. Switching mechanisms of SSs. The different polarity of the liquid under the two different conditions is illustrated by the miscibility of the solvent in water in presence of CO_2 or by decreasing the temperature. Image is taken from *Green chemistry* 13, 3, 3, 2011.

The first SS system consisted of an equimolar mixture of an alcohol and an amidine such as 1,8-diazabicyclo-[5.4.0]-undec-7-ene (DBU) (Figure 6)⁷⁸. Unfortunately, this two-component system was difficult to control, thus a single component system was developed⁷⁸. The solvents of this new system are primary, secondary or tertiary amines^{82–84}. These new SSs have been found to be toxic⁸⁵. However, their recovery after the extraction process and the possibility to re-use them, renders SSs “green” solvents^{86,87}.

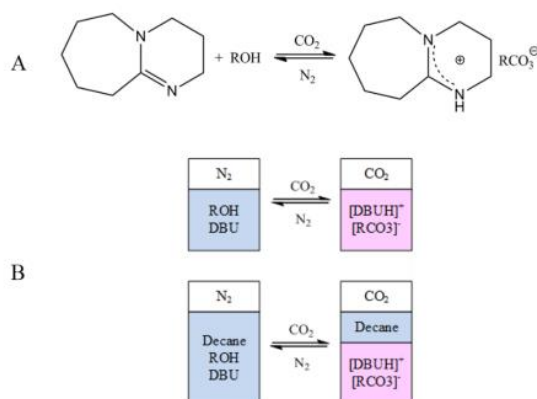


Figure 6. Switchable mechanism of alcohol/amidinium mixture. (A) Protonation equilibrium of DBU in the presence of an alcohol and carbon dioxide. (B) The different polarity of each liquid under the two conditions is illustrated by the miscibility of decane with the hexanol/DBU mixture under nitrogen, a decane phase separates out once the solvent mixture becomes polar in the presence of CO_2 . This process is reversible. Image is taken from *Nature* 436, 7054, 8 2005.

Primary amines

The N,N,N'-tributylpentanamidine was reported as a suitable switchable hydrophilicity solvent (SHS) (Figure 7).

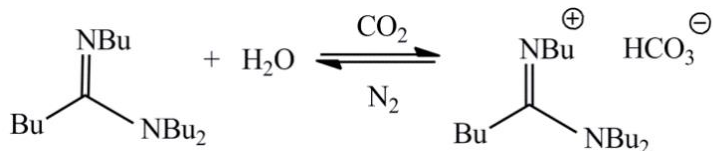


Figure 7. Switching mechanism of primary amines. The amine is hydrophobic at room temperature, and it switches in its hydrophilic form after exposure to CO₂ at atmospheric pressure in presence of water. Then, exposure to N₂ or heat solvent can revert the molecule to its original state. Image is taken from *Green chemistry*, 12, 5, 5 2010.

Secondary amines

Among secondary amines, N-ethyl butyl amine (EBA), N-ethyl propyl amine (EPA), di-propyl amine (DPA), and benzyl methyl amine (BMA) can function as a switchable solvents (Figure 8)^{83,88}.

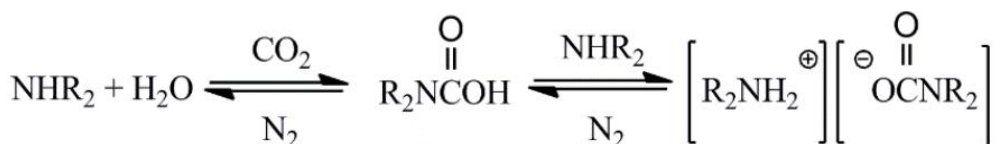


Figure 8. Switching mechanism of secondary amines. The amine, in presence of water and CO₂, forms carbamate salts via carbamic acids. Then, in the presence of N₂ the reaction equilibrium shifts to the right and the system returns to its original state. Image is taken from *Journal of Organic Chemistry* 73, 1, 1 2008.

Noteworthy, the switching of the above reported secondary amines happens at room temperature⁸³.

Tertiary amines

Tertiary amines are hydrophobic solvents which become hydrophilic in the presence of CO₂ and revert in the hydrophobic form in the presence of N₂ (Figure 9).

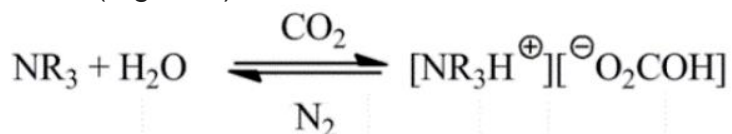


Figure 9. Switching mechanisms of tertiary amines. The reaction between tertiary amine, water and CO₂ gives a bicarbonate salt and a protonated SS. The reaction reverts by insufflating N₂ into the system.

Due to the reaction stoichiometry an equimolar amount of H₂O is required, in contrast to primary and secondary amines. Tertiary amines are normally less reactive towards CO₂ than secondary amines, which may lead to longer reaction times before observing the switch of the solvent, but the reaction requires less energy input to revert the reaction⁸⁴.

SSs are considered “green” solvents as they are simple to recover and the possibility of recycle them determines a lower energy consumption of the system, with a consequent reduction in the costs of the whole process^{73,86,89}.

In the last years, several authors have used secondary or tertiary amines for the extraction of compounds from microalgae (Table 2). Samorì (2013) used the tertiary amine N, N-dimethyl cyclohexyl amine (DMCHA) for extracting and recovering lipids directly from either wet algae paste biomass and algae slurry⁷⁹. Du and colleagues (2013) proposed a process for lipid extraction from wet algae using a secondary amine⁸⁸. Later, Cicci (2018) showed the ability of tertiary amines to extract hydrophobic and hydrophilic molecules from different microalgae, in order to fully exploit the circularity of the extraction process⁸⁰. Only recently, Liu (2020) exploited the selective extraction capacity of these solvents, for the extraction of astaxanthin from *Haematococcus pluvialis* for food applications⁸¹.

Thus, switchable solvents, due to their eco-friendly properties, are a good alternative to conventional solvents in the scaling up of extractions of molecules from microalgae at an industrial level.

Table 2. Yields of hydrophobic and hydrophilic compounds extracted by switchable solvents (SSs) from several microalgal species. Yields are reported as % with respect to dry weight biomass.

Species	Solvent	Hydrophobic compounds %	Hydrophilic compounds %	Ref
<i>Nannochloropsis gaditana</i>	N,N-dimethyl-cyclohexylamine	57.9 ± 1.3	-	18
<i>Tetraselmis suecica</i>	N,N-dimethyl-cyclohexylamine	31.9 ± 1.5	-	18
<i>Desmodesmus communis</i>	N,N-dimethyl-cyclohexylamine	29.2 ± 0.9	-	18
<i>Desmodesmus sp.</i>	N-Ethylbutylamine	16.8 ± 0.5	-	19
<i>Scenedesmus dimorphus</i>	N,N-dimethyl-cyclohexylamine	35.6 ± 1.9	41.1 ± 2	20
<i>Haematococcus pluvialis</i>	N-Ethylbutylamine	51.1*		21
	Dipropylamine	53.1*	-	21

*is referred to astaxanthin molecules

1.8 The aim of thesis

The general aim of the present PhD project is the use of Green Chemistry to extract thermo-resistant antioxidants from microalgae or cyanobacteria, to be applied in the food industry. The research activities are presented in three sections.

WP1 – Strain selection and cultivation

A screening on different microalgal or cyanobacteria strains available at the Algal Collection of Federico II, able to grow at medium high temperature (25-40 °C).

WP2 – Extraction of hydrophobic molecules from *Spirulina platensis* cultivated in thin layer photobioreactor at ATI BIOTECH company.

Extraction trials of antioxidant molecules, starting from *S. platensis* slurry biomass, obtained in thin layer photobioreactors by using switchable solvent.

WP3 – Antioxidant extraction and characterization

Extraction and purification of antioxidant compounds from microalgae grown indoor. Extractions have been conducted by using conventional extraction in ethanol and by switchable solvents. Lab-scale purification of the extracted fractions and validation of the antioxidant properties with biological assays *in vitro* and on eukaryotic cells after oxidative stress. Study of the thermo-resistance of extracted antioxidants.

1.9 References

- (1) Moroney, J. V. Algal Photosynthesis. In *Encyclopedia of Life Sciences*; John Wiley & Sons, Ltd: Chichester, UK, 2001. <https://doi.org/10.1038/ngp.els.0000322>.
- (2) Kliphuis, A. M. J.; de Winter, L.; Vejrazka, C.; Martens, D. E.; Janssen, M.; Wijffels, R. H. Photosynthetic Efficiency of *Chlorella Sorokiniana* in a Turbulently Mixed Short Light-Path Photobioreactor. *Biotechnol. Prog.* 2010, 26 (3), 687–696. <https://doi.org/10.1002/btpr.379>.
- (3) Watson, S. B.; Whitton, B. A.; Higgins, S. N.; Paerl, H. W.; Brooks, B. W. Chapter 20 – Harmful Algal Blooms. In *Freshwater Algae of North America*; 2015; pp 873–920. <https://doi.org/10.1016/B978-0-12-385876-4.00020-7>.
- (4) Stirbet, A.; Lazár, D.; Papageorgiou, G. C.; Govindjee. Chlorophyll a Fluorescence in Cyanobacteria: Relation to Photosynthesis. In *Cyanobacteria: From Basic Science to Applications*; Elsevier, 2018; pp 79–130. <https://doi.org/10.1016/B978-0-12-814667-5.00005-2>.
- (5) Leliaert, F.; Smith, D. R.; Moreau, H.; Herron, M. D.; Verbruggen, H.; Delwiche, C. F.; De Clerck, O. Phylogeny and Molecular Evolution of the Green Algae. *CRC. Crit. Rev. Plant Sci.* 2012, 31 (1), 1–46. <https://doi.org/10.1080/07352689.2011.615705>.
- (6) Yoon, H. S.; Hackett, J. D.; Pinto, G.; Bhattacharya, D. The Single, Ancient Origin of Chromist Plastids. *Proc. Natl. Acad. Sci. U. S. A.* 2002, 99 (24), 15507–15512. <https://doi.org/10.1073/pnas.242379899>.
- (7) Yoon, H. S.; Müller, K. M.; Sheath, R. G.; Ott, F. D.; Bhattacharya, D. Defining the Major Lineages of Red Algae (Rhodophyta). *J. Phycol.* 2006, 42 (2), 482–492. <https://doi.org/10.1111/j.1529-8817.2006.00210.x>.
- (8) Sansone, C.; Brunet, C. Promises and Challenges of Microalgal Antioxidant Production. *Antioxidants* 2019, 8 (7), 199. <https://doi.org/10.3390/antiox8070199>.
- (9) Pulz, O.; Gross, W. Valuable Products from Biotechnology of Microalgae. *Applied Microbiology and Biotechnology*. Springer November 6, 2004, pp 635–648. <https://doi.org/10.1007/s00253-004-1647-x>.

- (10) Pangestuti, R.; Suryaningtyas, I. T.; Siahaan, E. A.; Kim, S.-K. Cosmetics and Cosmeceutical Applications of Microalgae Pigments. In *Pigments from Microalgae Handbook*; Springer International Publishing, 2020; pp 611–633. https://doi.org/10.1007/978-3-030-50971-2_25.
- (11) Ye, Z. W.; Jiang, J. G.; Wu, G. H. Biosynthesis and Regulation of Carotenoids in *Dunaliella*: Progresses and Prospects. *Biotechnology Advances*. July 2008, pp 352–360. <https://doi.org/10.1016/j.biotechadv.2008.03.004>.
- (12) Sharma, S.; Katoch, V.; Kumar, S.; Chatterjee, S. Functional Relationship of Vegetable Colors and Bioactive Compounds: Implications in Human Health. *Journal of Nutritional Biochemistry*. Elsevier Inc. June 1, 2021, p 108615. <https://doi.org/10.1016/j.jnutbio.2021.108615>.
- (13) do Nascimento, T. C.; Cazarin, C. B. B.; Maróstica, M. R.; Mercadante, A. Z.; Jacob-Lopes, E.; Zepka, L. Q. Microalgae Carotenoids Intake: Influence on Cholesterol Levels, Lipid Peroxidation and Antioxidant Enzymes. *Food Res. Int.* 2020, 128, 108770. <https://doi.org/10.1016/j.foodres.2019.108770>.
- (14) Nwoba, E. G.; Ogbonna, C. N.; Ishika, T.; Vadiveloo, A. Microalgal Pigments: A Source of Natural Food Colors. In *Microalgae Biotechnology for Food, Health and High Value Products*; Springer Singapore, 2020; pp 81–123. https://doi.org/10.1007/978-981-15-0169-2_3.
- (15) Martins, N.; Roriz, C. L.; Morales, P.; Barros, L.; Ferreira, I. C. F. R. Food Colorants: Challenges, Opportunities and Current Desires of Agro-Industries to Ensure Consumer Expectations and Regulatory Practices. *Trends in Food Science and Technology*. Elsevier Ltd June 2016, pp 1–15. <https://doi.org/10.1016/j.tifs.2016.03.009>.
- (16) Barra, L.; Chandrasekaran, R.; Corato, F.; Brunet, C. The Challenge of Ecophysiological Biodiversity for Biotechnological Applications of Marine Microalgae. *Marine Drugs*. MDPI AG 2014, pp 1641–1675. <https://doi.org/10.3390/md12031641>.
- (17) Yusoff, F. M.; Banerjee, S.; Nagao, N.; Imaizumi, Y.; Shariff, M.; Toda, T. Use of Microalgae Pigments in Aquaculture. In *Pigments from Microalgae Handbook*; Springer International Publishing, 2020; pp 471–513. https://doi.org/10.1007/978-3-030-50971-2_19.
- (18) Novoveská, L.; Ross, M. E.; Stanley, M. S.; Pradelles, R.; Wasiolek, V.; Sassi, J.-F. Microalgal Carotenoids: A Review of Production, Current Markets, Regulations, and Future Direction. *Mar. Drugs* 2019, 17 (11), 640. <https://doi.org/10.3390/md17110640>.
- (19) Fernandes, T. M.; Gomes, B. B.; Lanfer-Marquez, U. M. Apparent Absorption of Chlorophyll from Spinach in an Assay with Dogs. *Innov. Food Sci. Emerg. Technol.* 2007, 8 (3), 426–432. <https://doi.org/10.1016/j.ifset.2007.03.019>.
- (20) Koyande, A. K.; Chew, K. W.; Rambabu, K.; Tao, Y.; Chu, D. T.; Show, P. L. Microalgae: A Potential Alternative to Health Supplementation for Humans. *Food Science and Human Wellness*. Elsevier BV March 2019, pp 16–24. <https://doi.org/10.1016/j.fshw.2019.03.001>.
- (21) Morocho-Jácome, A. L.; Ruscinc, N.; Martinez, R. M.; de Carvalho, J. C. M.; Santos de Almeida, T.; Rosado, C.; Costa, J. G.; Velasco, M. V. R.; Baby, A. R. (Bio)Technological Aspects of Microalgae Pigments for Cosmetics. *Applied Microbiology and Biotechnology*. Springer Science and Business Media Deutschland GmbH November 2020, pp 9513–9522. <https://doi.org/10.1007/s00253-020-10936-x>.
- (22) Bleakley, S.; Hayes, M. Algal Proteins: Extraction, Application, and Challenges Concerning Production. *Foods* 2017, 6 (5), 1–34.

- <https://doi.org/10.3390/foods6050033>.
- (23) Safi, C.; Zebib, B.; Merah, O.; Pontalier, P. Y.; Vaca-Garcia, C. Morphology, Composition, Production, Processing and Applications of *Chlorella Vulgaris*: A Review. *Renewable and Sustainable Energy Reviews*. Elsevier Ltd July 1, 2014, pp 265–278. <https://doi.org/10.1016/j.rser.2014.04.007>.
- (24) Guedes, A. C.; Amaro, H. M.; Sousa-Pinto, I.; Malcata, F. X. Algal Spent Biomass—A Pool of Applications. In *Biofuels from Algae*; Elsevier, 2019; pp 397–433. <https://doi.org/10.1016/b978-0-444-64192-2.00016-0>.
- (25) Alam, M. A.; Xu, J. L.; Wang, Z. *Microalgae Biotechnology for Food, Health and High Value Products*; Springer Singapore, 2020. <https://doi.org/10.1007/978-981-15-0169-2>.
- (26) Imbimbo, P.; Romanucci, V.; Pollio, A.; Fontanarosa, C.; Amoresano, A.; Zarrelli, A.; Olivieri, G.; Monti, D. M. A Cascade Extraction of Active Phycocyanin and Fatty Acids from *Galdieria Phlegrea*. *Appl. Microbiol. Biotechnol.* 2019, *103* (23–24), 9455–9464. <https://doi.org/10.1007/s00253-019-10154-0>.
- (27) Sonani, R. R.; Patel, S.; Bhastana, B.; Jakharia, K.; Chaubey, M. G.; Singh, N. K.; Madamwar, D. Purification and Antioxidant Activity of Phycocyanin from *Synechococcus* Sp. R42DM Isolated from Industrially Polluted Site. *Bioresour. Technol.* 2017, *245*, 325–331. <https://doi.org/10.1016/j.biortech.2017.08.129>.
- (28) Katiyar, R.; Arora, A. Health Promoting Functional Lipids from Microalgae Pool: A Review. *Algal Research*. Elsevier B.V. March 1, 2020. <https://doi.org/10.1016/j.algal.2020.101800>.
- (29) D’Alessandro, E. B.; Antoniosi Filho, N. R. Concepts and Studies on Lipid and Pigments of Microalgae: A Review. *Renewable and Sustainable Energy Reviews*. Elsevier Ltd May 1, 2016, pp 832–841. <https://doi.org/10.1016/j.rser.2015.12.162>.
- (30) Mata, T. M.; Martins, A. A.; Caetano, N. S. Microalgae for Biodiesel Production and Other Applications: A Review. *Renew. Sustain. Energy Rev.* 2010, *14* (1), 217–232. <https://doi.org/10.1016/J.RSER.2009.07.020>.
- (31) Ruiz, J.; Olivieri, G.; de Vree, J.; Bosma, R.; Willems, P.; Reith, J. H.; Eppink, M. H. M.; Kleinegris, D. M. M.; Wijffels, R. H.; Barbosa, M. J. Towards Industrial Products from Microalgae. *Energy Environ. Sci.* 2016, *9* (10), 3036–3043. <https://doi.org/10.1039/C6EE01493C>.
- (32) Eppink, M. H. M.; Olivieri, G.; Reith, H.; van den Berg, C.; Barbosa, M. J.; Wijffels, R. H. From Current Algae Products to Future Biorefinery Practices: A Review. In *Advances in Biochemical Engineering/Biotechnology*; Springer Science and Business Media Deutschland GmbH, 2019; Vol. 166, pp 99–123. https://doi.org/10.1007/10_2016_64.
- (33) Chen, C. Y.; Zhao, X. Q.; Yen, H. W.; Ho, S. H.; Cheng, C. L.; Lee, D. J.; Bai, F. W.; Chang, J. S. Microalgae-Based Carbohydrates for Biofuel Production. *Biochem. Eng. J.* 2013, *78*, 1–10. <https://doi.org/10.1016/j.bej.2013.03.006>.
- (34) Shahid, A.; Khan, F.; Ahmad, N.; Farooq, M.; Mehmood, M. A. Microalgal Carbohydrates and Proteins: Synthesis, Extraction, Applications, and Challenges. In *Microalgae Biotechnology for Food, Health and High Value Products*; Springer Singapore, 2020; pp 433–468. https://doi.org/10.1007/978-981-15-0169-2_14.
- (35) Khan, M. I.; Shin, J. H.; Kim, J. D. The Promising Future of Microalgae: Current Status, Challenges, and Optimization of a Sustainable and Renewable Industry for Biofuels,

- Feed, and Other Products. *Microbial Cell Factories*. BioMed Central Ltd. March 5, 2018. <https://doi.org/10.1186/s12934-018-0879-x>.
- (36) Markou, G.; Angelidaki, I.; Georgakakis, D. Microalgal Carbohydrates: An Overview of the Factors Influencing Carbohydrates Production, and of Main Bioconversion Technologies for Production of Biofuels. *Applied Microbiology and Biotechnology*. Springer November 21, 2012, pp 631–645. <https://doi.org/10.1007/s00253-012-4398-0>.
- (37) Ru, I. T. K.; Sung, Y. Y.; Jusoh, M.; Wahid, M. E. A.; Nagappan, T. *Chlorella Vulgaris* : A Perspective on Its Potential for Combining High Biomass with High Value Bioproducts. *Appl. Phycol.* 2020, 1 (1), 2–11. <https://doi.org/10.1080/26388081.2020.1715256>.
- (38) Ferreira, G. F.; Ríos Pinto, L. F.; Carvalho, P. O.; Coelho, M. B.; Eberlin, M. N.; Maciel Filho, R.; Fregolente, L. V. Biomass and Lipid Characterization of Microalgae Genera *Botryococcus*, *Chlorella*, and *Desmodesmus* Aiming High-Value Fatty Acid Production. *Biomass Convers. Biorefinery* 2019, 1–15. <https://doi.org/10.1007/s13399-019-00566-3>.
- (39) Mathimani, T.; Sekar, M.; Shanmugam, S.; Sabir, J. S. M.; Chi, N. T. L.; Pugazhendhi, A. Relative Abundance of Lipid Types among *Chlorella* Sp. and *Scenedesmus* Sp. and Ameliorating Homogeneous Acid Catalytic Conditions Using Central Composite Design (CCD) for Maximizing Fatty Acid Methyl Ester Yield. *Sci. Total Environ.* 2021, 771, 144700. <https://doi.org/10.1016/j.scitotenv.2020.144700>.
- (40) Chi, N. T. L.; Duc, P. A.; Mathimani, T.; Pugazhendhi, A. Evaluating the Potential of Green Alga *Chlorella* Sp. for High Biomass and Lipid Production in Biodiesel Viewpoint. *Biocatal. Agric. Biotechnol.* 2019, 17, 184–188. <https://doi.org/10.1016/j.bcab.2018.11.011>.
- (41) Alagawany, M.; Taha, A. E.; Noreldin, A.; El-Tarabily, K. A.; Abd El-Hack, M. E. Nutritional Applications of Species of *Spirulina* and *Chlorella* in Farmed Fish: A Review. *Aquaculture* 2021, 542, 736841. <https://doi.org/10.1016/j.aquaculture.2021.736841>.
- (42) Breuer, G.; Lamers, P. P.; Martens, D. E.; Draaisma, R. B.; Wijffels, R. H. The Impact of Nitrogen Starvation on the Dynamics of Triacylglycerol Accumulation in Nine Microalgae Strains. *Bioresour. Technol.* 2012, 124, 217–226. <https://doi.org/10.1016/j.biortech.2012.08.003>.
- (43) Xin, L.; Hong-ying, H.; Ke, G.; Ying-xue, S. Effects of Different Nitrogen and Phosphorus Concentrations on the Growth, Nutrient Uptake, and Lipid Accumulation of a Freshwater Microalga *Scenedesmus* Sp. *Bioresour. Technol.* 2010, 101 (14), 5494–5500. <https://doi.org/10.1016/j.biortech.2010.02.016>.
- (44) Toledo-Cervantes, A.; Garduño Solórzano, G.; Campos, J. E.; Martínez-García, M.; Morales, M. Characterization of *Scenedesmus Obtusiusculus* AT-UAM for High-Energy Molecules Accumulation: Deeper Insight into Biotechnological Potential of Strains of the Same Species. *Biotechnol. Reports* 2018, 17, 16–23. <https://doi.org/10.1016/j.btre.2017.11.009>.
- (45) Mata, T. M.; Martins, A. A.; Caetano, N. S. Microalgae for Biodiesel Production and Other Applications: A Review. *Renewable and Sustainable Energy Reviews*. Pergamon January 1, 2010, pp 217–232. <https://doi.org/10.1016/j.rser.2009.07.020>.
- (46) Sui, Y.; Vlaeminck, S. E. Effects of Salinity, PH and Growth Phase on the Protein Productivity by *Dunaliella Salina*. *J. Chem. Technol. Biotechnol.* 2019, 94 (4), 1032–1040. <https://doi.org/10.1002/jctb.5850>.

- (47) Colusse, G. A.; Mendes, C. R. B.; Duarte, M. E. R.; Carvalho, J. C. de; Noseda, M. D. Effects of Different Culture Media on Physiological Features and Laboratory Scale Production Cost of *Dunaliella Salina*. *Biotechnol. Reports* 2020, 27, e00508. <https://doi.org/10.1016/j.btre.2020.e00508>.
- (48) Lim, H. R.; Khoo, K. S.; Chew, K. W.; Chang, C.-K.; Munawaroh, H. S. H.; Kumar, P. S.; Huy, N. D.; Show, P. L. Perspective of *Spirulina* Culture with Wastewater into a Sustainable Circular Bioeconomy. *Environ. Pollut.* 2021, 284, 117492. <https://doi.org/10.1016/j.envpol.2021.117492>.
- (49) Seghiri, R.; Kharbach, M.; Essamri, A. Functional Composition, Nutritional Properties, and Biological Activities of Moroccan *Spirulina* Microalga. *J. Food Qual.* 2019, 2019. <https://doi.org/10.1155/2019/3707219>.
- (50) Halliwell, B. Biochemistry of Oxidative Stress. *Biochem. Soc. Trans.* 2007, 35 (5), 1147–1150. <https://doi.org/10.1042/BST0351147>.
- (51) Yoshikawa, T.; Naito, Y. *What Is Oxidative Stress?*; 2002; Vol. 45.
- (52) Assunção, M. F. G.; Amaral, R.; Martins, C. B.; Ferreira, J. D.; Ressurreição, S.; Santos, S. D.; Varejão, J. M. T. B.; Santos, L. M. A. Screening Microalgae as Potential Sources of Antioxidants. *J. Appl. Phycol.* 2017, 29 (2), 865–877. <https://doi.org/10.1007/s10811-016-0980-7>.
- (53) Hultqvist, M.; Olsson, L. M.; Gelderman, K. A.; Holmdahl, R. The Protective Role of ROS in Autoimmune Disease. *Trends in Immunology*. Trends Immunol May 2009, pp 201–208. <https://doi.org/10.1016/j.it.2009.03.004>.
- (54) Valko, M.; Leibfritz, D.; Moncol, J.; Cronin, M. T. D.; Mazur, M.; Telser, J. Free Radicals and Antioxidants in Normal Physiological Functions and Human Disease. *International Journal of Biochemistry and Cell Biology*. Int J Biochem Cell Biol 2007, pp 44–84. <https://doi.org/10.1016/j.biocel.2006.07.001>.
- (55) Benzie, I. F. F. Evolution of Antioxidant Defence Mechanisms. *Eur. J. Nutr.* 2000, 39 (2), 53–61. <https://doi.org/10.1007/s003940070030>.
- (56) García, J. L.; de Vicente, M.; Galán, B. Microalgae, Old Sustainable Food and Fashion Nutraceuticals. *Microb. Biotechnol.* 2017, 10 (5), 1017–1024. <https://doi.org/10.1111/1751-7915.12800>.
- (57) Goiris, K.; Muylaert, K.; Fraeye, I.; Foubert, I.; De Brabanter, J.; De Cooman, L. Antioxidant Potential of Microalgae in Relation to Their Phenolic and Carotenoid Content. *J. Appl. Phycol.* 2012, 24 (6), 1477–1486. <https://doi.org/10.1007/s10811-012-9804-6>.
- (58) Matos, J.; Cardoso, C.; Bandarra, N. M.; Afonso, C. Microalgae as Healthy Ingredients for Functional Food: A Review. *Food and Function*. Royal Society of Chemistry August 2017, pp 2672–2685. <https://doi.org/10.1039/c7fo00409e>.
- (59) Villalobos-Delgado, L. H.; Mateo, J.; Caro, I.; Leal Ramos, M.-Y.; Mendez, N. G.; Cansino, R. G.; González Mondragón, E. G. Natural Antioxidants in Fresh and Processed Meat. In *Sustainable Meat Production and Processing*; Elsevier, 2019; pp 207–236. <https://doi.org/10.1016/b978-0-12-814874-7.00011-0>.
- (60) Poljsak, B.; Kovač, V.; Milisav, I. Antioxidants, Food Processing and Health. *Antioxidants* 2021, 10 (3), 1–11. <https://doi.org/10.3390/antiox10030433>.
- (61) Jacob-Lopes, E.; Maroneze, M. M.; Deprá, M. C.; Sartori, R. B.; Dias, R. R.; Zepka, L. Q. Bioactive Food Compounds from Microalgae: An Innovative Framework on

- Industrial Biorefineries. *Current Opinion in Food Science*. Elsevier Ltd February 1, 2019, pp 1–7. <https://doi.org/10.1016/j.cofs.2018.12.003>.
- (62) Sidari, R.; Tofalo, R. A Comprehensive Overview on Microalgal-Fortified/Based Food and Beverages. *Food Reviews International*. Taylor and Francis Inc. 2019, pp 778–805. <https://doi.org/10.1080/87559129.2019.1608557>.
- (63) Chew, K. W.; Yap, J. Y.; Show, P. L.; Suan, N. H.; Juan, J. C.; Ling, T. C.; Lee, D. J.; Chang, J. S. Microalgae Biorefinery: High Value Products Perspectives. *Bioresour. Technol.* 2017, 229, 53–62. <https://doi.org/10.1016/j.biortech.2017.01.006>.
- (64) M. U., N.; Mehar, J. G.; Mudliar, S. N.; Shekh, A. Y. Recent Advances in Microalgal Bioactives for Food, Feed, and Healthcare Products: Commercial Potential, Market Space, and Sustainability. *Compr. Rev. Food Sci. Food Saf.* 2019, 18 (6), 1882–1897. <https://doi.org/10.1111/1541-4337.12500>.
- (65) Nethravathy, M. U.; Mehar, J. G.; Mudliar, S. N.; Shekh, A. Y. Recent Advances in Microalgal Bioactives for Food, Feed, and Healthcare Products: Commercial Potential, Market Space, and Sustainability. *Compr. Rev. Food Sci. Food Saf.* 2019, 18 (6), 1882–1897. <https://doi.org/10.1111/1541-4337.12500>.
- (66) Armenta, S.; Garrigues, S.; Esteve-Turrillas, F. A.; de la Guardia, M. Green Extraction Techniques in Green Analytical Chemistry. *TrAC - Trends in Analytical Chemistry*. Elsevier B.V. July 1, 2019, pp 248–253. <https://doi.org/10.1016/j.trac.2019.03.016>.
- (67) Chemat, F.; Vian, M. A.; Cravotto, G. Green Extraction of Natural Products: Concept and Principles. *Int. J. Mol. Sci.* 2012, 13 (7), 8615–8627. <https://doi.org/10.3390/ijms13078615>.
- (68) Anastas, P.; Eghbali, N. Green Chemistry: Principles and Practice. *Chem. Soc. Rev.* 2010, 39 (1), 301–312. <https://doi.org/10.1039/b918763b>.
- (69) Anastas, P. T.; Warner, J. C. Principles of Green Chemistry. *Green Chem. Theory Pract.* 1998, 29–56.
- (70) Song, J.; Han, B. Green Chemistry: A Tool for the Sustainable Development of the Chemical Industry. *Natl. Sci. Rev.* 2015, 2 (3), 255–256. <https://doi.org/10.1093/nsr/nwu076>.
- (71) Esquivel-Hernández, D. A.; Ibarra-Garza, I. P.; Rodríguez-Rodríguez, J.; Cuéllar-Bermúdez, S. P.; Rostro-Alanis, M. de J.; Alemán-Nava, G. S.; García-Pérez, J. S.; Parra-Saldivar, R. Green Extraction Technologies for High-Value Metabolites from Algae: A Review. *Biofuels, Bioproducts and Biorefining*. John Wiley and Sons Ltd January 1, 2017, pp 215–231. <https://doi.org/10.1002/bbb.1735>.
- (72) Herrero, M.; Castro-Puyana, M.; Mendiola, J. A.; Ibañez, E. Compressed Fluids for the Extraction of Bioactive Compounds. *TrAC - Trends in Analytical Chemistry*. Elsevier B.V. February 1, 2013, pp 67–83. <https://doi.org/10.1016/j.trac.2012.12.008>.
- (73) Imbimbo, P.; D'Elia, L.; Liberti, D.; Olivieri, G.; Monti, D. M. Towards Green Extraction Methods from Microalgae Learning from the Classics. *Applied Microbiology and Biotechnology*. Springer Science and Business Media Deutschland GmbH November 1, 2020, pp 9067–9077. <https://doi.org/10.1007/s00253-020-10839-x>.
- (74) Juin, C.; Chérouvrier, J. R.; Thiéry, V.; Gagez, A. L.; Bérard, J. B.; Joguet, N.; Kaas, R.; Cadoret, J. P.; Picot, L. Microwave-Assisted Extraction of Phycobiliproteins from *Porphyridium Purpureum*. *Appl. Biochem. Biotechnol.* 2015, 175 (1), 1–15. <https://doi.org/10.1007/s12010-014-1250-2>.

- (75) Michalak, I.; Chojnacka, K. Algal Extracts: Technology and Advances. *Engineering in Life Sciences*. Wiley-VCH Verlag November 1, 2014, pp 581–591. <https://doi.org/10.1002/elsc.201400139>.
- (76) Motlagh, S. R.; Harun, R.; Biak, D. R. A.; Hussain, S. A.; Ghani, W. A. W. A. K.; Khezri, R.; Wilfred, C. D.; Elgharbawy, A. A. M. Screening of Suitable Ionic Liquids as Green Solvents for Extraction of Eicosapentaenoic Acid (EPA) from Microalgae Biomass Using COSMO-RS Model. *Molecules* 2019, 24 (4). <https://doi.org/10.3390/molecules24040713>.
- (77) Zhang, Y.; Bakshi, B. R.; Demessie, E. S. Life Cycle Assessment of an Ionic Liquid versus Molecular Solvents and Their Applications. *Environ. Sci. Technol.* 2008, 42 (5), 1724–1730. <https://doi.org/10.1021/es0713983>.
- (78) Jessop, P. G.; Heldebrant, D. J.; Li, X.; Eckert, C. A.; Liotta, C. L. Green Chemistry: Reversible Nonpolar-to-Polar Solvent. *Nature* 2005, 436 (7054), 1102. <https://doi.org/10.1038/nature4361102a>.
- (79) Samorì, C.; Barreiro, D. L.; Vet, R.; Pezzolesi, L.; Brilman, D. W. F.; Galletti, P.; Tagliavini, E. Effective Lipid Extraction from Algae Cultures Using Switchable Solvents. *Green Chem.* 2013, 15 (2), 353–356. <https://doi.org/10.1039/C2GC36730K>.
- (80) Cicci, A.; Sed, G.; Jessop, P. G.; Bravi, M. Circular Extraction: An Innovative Use of Switchable Solvents for the Biomass Biorefinery. *Green Chem.* 2018, 20 (17), 3908–3911. <https://doi.org/10.1039/c8gc01731j>.
- (81) Liu, H.; Huang, W. C.; Guo, N.; Mao, X. Application of Secondary Amine Switchable Hydrophilicity Solvents for Astaxanthin Extraction from Wet *Haematococcus Pluvialis*. *Algal Res.* 2020, 48, 101892. <https://doi.org/10.1016/j.algal.2020.101892>.
- (82) Jessop, P. G.; Phan, L.; Carrier, A.; Robinson, S.; Dürr, C. J.; Harjani, J. R. A Solvent Having Switchable Hydrophilicity. *Green Chem.* 2010, 12 (5), 809–881. <https://doi.org/10.1039/b926885e>.
- (83) Phan, L.; Andreatta, J. R.; Horvey, L. K.; Edie, C. F.; Luco, A. L.; Mirchandani, A.; Darensbourg, D. J.; Jessop, P. G. Switchable-Polarity Solvents Prepared with a Single Liquid Component. *J. Org. Chem.* 2008, 73 (1), 127–132. <https://doi.org/10.1021/jo7017697>.
- (84) Jessop, P. G.; Kozyc, L.; Rahami, Z. G.; Schoenmakers, D.; Boyd, A. R.; Wechsler, D.; Holland, A. M. Tertiary Amine Solvents Having Switchable Hydrophilicity. *Green Chem.* 2011, 13 (3), 619–623. <https://doi.org/10.1039/c0gc00806k>.
- (85) Schuur, B.; Brouwer, T.; Smink, D.; Sprakel, L. M. J. Green Solvents for Sustainable Separation Processes. *Current Opinion in Green and Sustainable Chemistry*. Elsevier B.V. August 1, 2019, pp 57–65. <https://doi.org/10.1016/j.cogsc.2018.12.009>.
- (86) Jeevan Kumar, S. P.; Vijay Kumar, G.; Dash, A.; Scholz, P.; Banerjee, R. Sustainable Green Solvents and Techniques for Lipid Extraction from Microalgae: A Review. *Algal Research*. Elsevier B.V. January 1, 2017, pp 138–147. <https://doi.org/10.1016/j.algal.2016.11.014>.
- (87) Vanderveen, J. R.; Durelle, J.; Jessop, P. G. Design and Evaluation of Switchable-Hydrophilicity Solvents. *Green Chem.* 2014, 16 (3), 1187–1197. <https://doi.org/10.1039/c3gc42164c>.
- (88) Du, Y.; Schuur, B.; Samorì, C.; Tagliavini, E.; Brilman, D. W. F. Secondary Amines as Switchable Solvents for Lipid Extraction from Non-Broken Microalgae. *Bioresour. Technol.* 2013, 149, 253–260. <https://doi.org/10.1016/j.biortech.2013.09.039>.

- (89) Clarke, C. J.; Tu, W. C.; Levers, O.; Bröhl, A.; Hallett, J. P. Green and Sustainable Solvents in Chemical Processes. *Chem. Rev.* 2018, *118* (2), 747–800. <https://doi.org/10.1021/acs.chemrev.7b00571>.

Chapter 2

***Microorganisms from harsh and
extreme environments:
a collection of living strains at ACUF
(Naples, Italy)***



Microorganisms from harsh and extreme environments: a collection of living strains at ACUF (Naples, Italy)

Luigi D'Elia^{1,2}, Angelo Del Mondo^{1*}, Mariano Santoro^{1,3}, Antonino De Natale¹, Gabriele Pinto¹, Antonino Pollio¹

¹Department of Biology, University of Naples "Federico II", Via Cinthia 26, 80126 Naples, Italy

²Department of Chemistry, University of Naples "Federico II", Via Cinthia 26, 80126 Naples, Italy

³InBioS-Centre for Protein Engineering, University of Liège, Sart Tilman, 4000 Liège, Belgium

*Corresponding Author: angelo.delmondo@unina.it

Received: 28 April 2018 / Accepted: 22 July 2018

Abstract: The Algal Collection at the University Federico II (ACUF) is a bioresource center where over 800 live microalgal strains are maintained, mainly belonging to Cyanobacteria, Chlorophyta, Rhodophyta, and Bacillariophyceae. The extremophilic algae maintained at ACUF include thermo-acidophilic and acidotolerant strains, mostly belonging to the Cyanidiophyceae isolated from European and extra-European sites, and also terrestrial isolates from bare rocks and monuments. The main target of the ACUF Center is the study and preservation of the diversity of extremophytic microalgae. This collection is used as a resource for studies about biochemical and evolutionary strategies as well as mechanisms involved in cell functioning under harsh environmental conditions. These organisms can be also useful sources for the production of chemical compounds or other biological products with potential biotechnological applications.

Keywords: Culture collection, extreme environments, microalgae, biodiversity, biotechnology

The ACUF collection

Extreme environments are typically characterized by harsh conditions determined by spatial gradients of chemical and physical factors, consisting of strong variations in temperatures, humidity, salinity, and pH. They are usually represented by hot and cold deserts, hot springs, salt lakes, volcanic and thermal areas, sulfide mines near deep-sea vents as well as terrestrial environments exposed to desiccation and sharp variations of temperature, as bare rocks, but also building facades and monuments. Extremophilic microorganisms are exposed to hostile conditions and are categorized on the basis of their ability to thrive in a specific type of niche (Rampelotto, 2013). During the past 45 years ACUF collection based at the Federico II University of Naples (Italy) has supported the study of photoautotrophic microorganisms dwelling those habitats. The aim of this

article is to present the most significant features of ACUF collection, examples of applied research carried out by the ACUF staff, strains of interest and future directions in the preservation and study of biodiversity. Table 1 provides a complete list of the strains maintained in the ACUF collection classified according to Division, Class, and Order.

History and aims

The culture collection of algae at the Federico II University of Naples was started in 1973 by professor Roberto Taddei, and was initially planned as a collection of *Cyanidium caldarium* Geitler (*sensu lato*) strains from different acidic-thermal sites of Italy (De Luca et al., 1973) and other countries (De Luca et al., 1977). Further investigations on acidic and thermal sites of Italy (Fig. 1a and b) led to the

lect Cyanidiophyceae in the type locality of *C. caldarium* (De Luca et al., 1981). Afterwards, in 2006 and at a later stage in 2011, Pinto and Ciniglia increased considerably the number of Cyanidiophyceae strains in the ACUF collection with the explorations of thermal and acidic sites in Iceland (Fig. 1c) (Ciniglia et al., 2014) and Turkey.

Microalgae from thermoacidic habitats

During the years, ecophysiological and ultrastructural studies were conducted on chlorophycean microalgae isolated from low pH environments, as *Chlamydomonas pitschmannii* Ettl (Pollio et al., 2005), *Stichococcus bacillaris* Nägeli (Pollio et al., 1997), *Pseudococcomyxa simplex* (Mainx) Fott (Albertano et al., 1990) and *Auxenochlorella protothecoides* (Krüger) Kalina et Puncovářová (Albertano and Taddei, 1984) together with the newly described species *Viridella fridericiana* Albertano, Pollio, Taddei (Albertano et al., 1991). Also the chrysophycean *Ochromonas vulcania* Gromov (Albertano et al., 1994) and the bacillariophycean *Pinnularia obscura* Krasske (Ciniglia et al., 2007) thriving in acidic ponds of Southern Italy were collected and studied.

A major focus was dedicated to Cyanidiophyceae. Unicellular terrestrial Rhodophyta have been considered as a single species for a long time, and described for the first time as *Coccochloris orsini* by Meneghini (1839). Almost a century later, this species had been placed in a number of already described genera, falling either to the Cyanophyta or Chlorophyta, until Geitler assigned to this species the generally accepted binomial *Cyanidium caldarium*. The taxon was officially recognized as part of the Rhodophyta by Hirose (1958), who demonstrated the presence of several characteristic rhodophycean features. Later, De Luca et al. (1978) described the new species *Cyanidioschyzon merolae* De Luca, Taddei, Varano, featured by its characteristic size and shape, whereas Merola et al. (1981) differentiated *Galdieria sulphuraria* (Galdieri) Merola from *C. caldarium* based on its ability to grow in the dark. Currently, macroevolutionary studies integrate aspects of biogeography and geography in a phylogenetic context to answer questions related to the world diffusion of *Cyanidium*, *Galdieria*, and *Cyanidioschyzon*. Molecular phylogenetic studies suggest that the Cyanidiales represent one of the most ancient groups of algae, having diverged about 1.3 billion years ago at the base of the Rhodophyta (Müller et al., 2001; Yoon et al., 2002b).

Algal biofilms and cultural heritage

Although most green algae typically thrive in aquatic environments, many species also live partly or permanently under aero-terrestrial conditions; microorganisms living at rock-atmosphere interface experience dehydration regularly,

a phenomenon described as desiccation tolerance (Holzinger and Karsten, 2013). Microbial biofilm development can be observed on virtually all kinds of stone monuments such as castles, caves, churches/cathedrals, fountains, temples, tombs/catacombs, etc. (Fig. 1d, e and f), and can be associated with problems of conservation. Several types of autotrophic and heterotrophic microorganisms such as bacteria, fungi, algae and lichens, are usually observed on stone monuments. The rock substratum provides harsh environmental conditions. Temperature may vary by several tens of degrees during a day, and can be accompanied by rapid desiccation (or freezing); all that implies a limited availability of water (e.g., Walker and Pace, 2007). The ACUF team characterized and studied biofilm communities on stone monuments in the archaeological sites of Campania (Italy), namely Pompeii, Herculaneum, Oplontis, Cumae and Nola among others. Microorganisms retrieved on monuments were analysed in their native biofilm structure by CLS-microscopy, isolated, characterized, and subsequently used as models to perform *in vitro* experiments for understanding the patterns of microbial colonization of stone materials (Marasco et al., 2016; Del Mondo et al., 2017).

Biotechnological applications and toxicity tests

Microalgae can be employed in a wide number of biochemical and biotechnological applications. In recent years, wastewater treatment, biodiesel production, biopolymers and nutraceutical science have become hot topics. In response to the uprising energy crisis, climate change and depletion of natural sources, advantages in the use of microalgae for biotechnological applications are represented by their capability to grow on non-arable lands nearly all year long, thus non competing with conventional agriculture. As a matter of fact, they only require freshwater, non-organic nutrients, and atmospheric CO₂. Moreover, their cultivation may be coupled to industrial processing, i.e. reducing overall carbon dioxide emission or for wastewater treatment. Given this premise, collections of extremophilic microorganisms allow the selection of strains that produce high value compounds with specific features as thermo-resistance or cryo-resistance; this may also prevent environmental microbial contaminants that would not survive the selected growth conditions (Ruiz et al., 2016).

Biofuels production by microalgae appeared promising since the end of the last century: bio-oil extracted from microalgae may be adopted as crude fuels or may be transesterified to biodiesel. In a study conducted by Olivieri et al. (2010) the strain ACUF 158 *S. bacillaris* has been selected as a promising candidate for biofuel production; in fact, this strain is characterized by satisfactory lipid content (33%) and fatty acids distribution; moreover, the high tolerance of this strain to large variations of temperature, salinity and pH allows massive cultures to be operated un-

der severe conditions, thus preventing bacterial and fungal contamination.

Risk characterization is an estimation of the incidence of the adverse effect occurring in an environmental compartment as a result of actual or predicted exposure to a substance. In a study by Ferrari et al. (2003), the occurrence in sewage treatment plant (STP) effluents and ecotoxicity of the pharmaceuticals carbamazepine, clofibrac acid, and diclofenac has been investigated testing growth inhibition of the microalga *Raphidocelis subcapitata* (Korshikov) Nygaard, Komárek, Kristiansen et Skulberg (*Pseudokirchneriella subcapitata* (Korshikov) Hindák). This species is a standard test microalga recommended by U.S. EPA (Environmental Protection Agency, 1989) and OECD guidelines (Organization for Economic Co-operation and Development, 1993). In another study, Ciniglia and co-workers (Ciniglia et al., 2005) examined the toxic effects of Triclosan (2,4,4'-trichloro-2'-hydroxydiethyl ether) on the morphology and sexual and asexual reproduction of *Closterium ehrenbergii* Meneghini ex Ralfs, proposing the species as an ideal target for assessing the

toxicity of pharmaceutical products and personal care products (PPCP).

Finally, it is internationally agreed that water and sanitation are essential to the achievement of many sustainable development goals (WWDR, 2015); the application of microalgae for wastewater treatment represents a suitable technological solution. One of the contributions of ACUF in this area was represented by the treatment of olive oil mill wastewaters with the phenol resistant algae *Ankistrodesmus braunii* (Grunov) Cleve and *Scenedesmus quadricauda* (Turpin) Bréb. which are able to degrade over 50% of low molecular weight phenols contained in oil mill wastewaters and bio-transform them into other non-identified aromatic compounds (Pinto et al., 2003).

Facilities and culture maintenance

The phycological lab at ACUF has established growth rooms and growth cabinets for cultures of cyanobacteria and microalgae at different biomass scales and under dif-

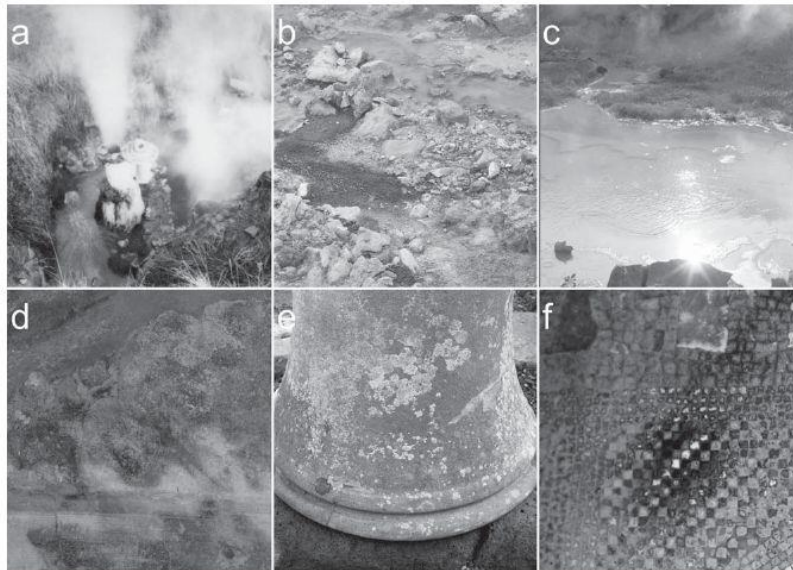


Fig. 1. Algal sampling sites: a) Ali Terme, Spa Granata Cassibile, Messina; b) Piciarelli, Napoli; c) Hveragerði, Iceland. Example of Pompeian biofilms on: d) fresco; e) stone column; f) polychrome mosaic

ferent environmental conditions. Most of ACUF strains are maintained in glass tubes at a range temperatures between 22°C and 26°C with various solid culture media as BG-11, BBM and Allen (using Agar as solidifying agent). Few strains (mostly belonging to Bacillariophyceae) are maintained in liquid cultures at a temperature of 18°C. Cultures grow at an irradiance of 150 $\mu\text{mol photon m}^{-2} \text{s}^{-1}$ with a 16:8 h light-dark cycle. Under these conditions, transfers are made routinely every 1-2 months, although for many species four or six months intervals would be sufficient. An overview of some facilities employed for biomass recovery is displayed in Fig. 2. Different types of photobioreactors and fermenter are used to produce significant amounts of algal biomass for biotechnological applications. The cylindrical photobioreactors are 1 L bubble columns made of glass (0.04 m ID, 0.8 m high, see Fig. 2b); air is sprayed at the photobioreactor bottom by means of a porous ceramic diffuser. Flat photobioreactor systems are made of plexiglass panels (Fig. 2d) spaced by two, 3 mm-thick, silicone sheets conveniently cut out to outline the reactor and separate the plexiglass sheets. Panels absorb only 1% of the incident irradiance (measured by light sensor Li-cor). The

final volume of the culture is 0.3 L. Gas stream is spread into the culture from the bottom of the photobioreactors through four 1mm orifices (Gifuni et al. 2017, 2018).

All photobioreactors are housed in a temperature controlled chamber equipped with lamps at a light irradiance (IL) set at 140 $\mu\text{mol photon m}^{-2} \text{s}^{-1}$. Measurements of photosynthesis and respiration rates (OUR) are carried out on culture sub-samples at the irradiance adopted in climate chambers by means of an Oxygraph (Hansatech) connected to a PC.

Strain isolation procedures

Isolates constitute the main resource for ACUF: the primary focus is to maintain an assessment of algal diversity in unusual terrestrial habitats for mainly three reasons: i) to better understand phylogenetic relationships of the still poorly investigated terrestrial algae and to recover new species; ii) to test and develop new methods for assessing algal diversity in a given habitat; iii) to isolate algal communities from biofilms and in soils to better understand the

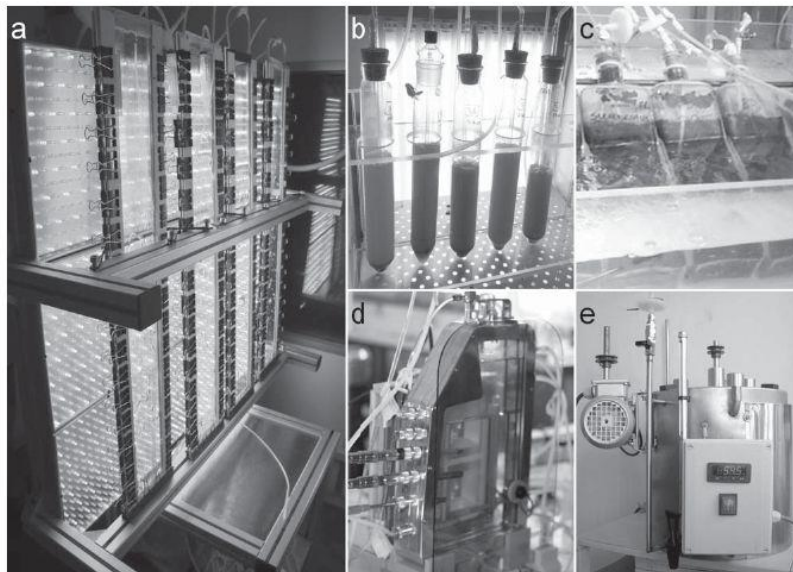


Fig. 2. Different kind of bioreactors a-d, a) ultra-flat; b) bubble column; c) inclined square bubble column; d) flat; e) a fermenter

ecological preferences of terrestrial algae and their interactions with substrates and/or other microorganisms.

Strains in ACUF Collection come from samples collected by members of the host lab and by external depositors. It is a constantly growing Collection of new unique isolates, mainly regarding aero-terrestrial and aquatic habitats. New isolates are subjected to a preliminary screening for morphological traits, growth characteristics, and their phylogenetic relatedness to already known species.

Different culture media have been tested: BBM (Bold, 1949; Bischoff, 1963), BG11 (Rippka et al., 1979) and Allen medium (Allen, 1959) support a consistent growth of the large majority of the strains. For species belonging to the Cyanidophyceae that usually live in habitat with a pH of 1.0 – 3.5, we use Allen medium acidified by H₂SO₄ 7%. Isolation of filamentous microalgae is done at a binocular microscope and the standard techniques of sterile handling in horizontal laminar flow cabinets (HF 72, Gelaire Flow Laboratories) are applied (Rippka et al., 1981).

Characterization and monitoring of cultures

Aim of a polyphasic approach

Until recent times, identification of prokaryotic and eukaryotic microorganisms has been based on morphological features and in a few cases ecological features; the intro-

duction of molecular techniques used for diversity studies has given a significant contribution to integrate the species identification knowledge in the taxonomical context. The integrated approach used at ACUF relies on the morphological and molecular characterization in order to investigate the diversity of microorganisms from extreme ecological habitats. Furthermore, phylogenetic analyses are carried out in order to study biogeography and distribution of different ecotypes of species, with a particular attention to Cyanidophyceae. This kind of approach is also defined “polyphasic” and it is currently used for strain isolation and identification at ACUF as detailed in the workflow in Fig. 3.

Optical, epifluorescence and CLS Microscopy

Strain identification at species level foresees that microphotographs are taken by the light microscope Nikon Eclipse E800 for all strains. At ACUF, also epifluorescence microscopy is used to observe photosynthetic pigment composition and specific cell staining are carried out by using specific dyes as DAPI or concanavalin-A to stain nuclei and extracellular EPS, respectively. Moreover, CLS-Microscopy enables us to study environmental samples on lithic substrates as well as biological structures of interest also in 3D, like plastidial organization (Izabela et al., 2008). Image analysis of Z-stacks allows to analyse specific patterns in meta-community, biological associations

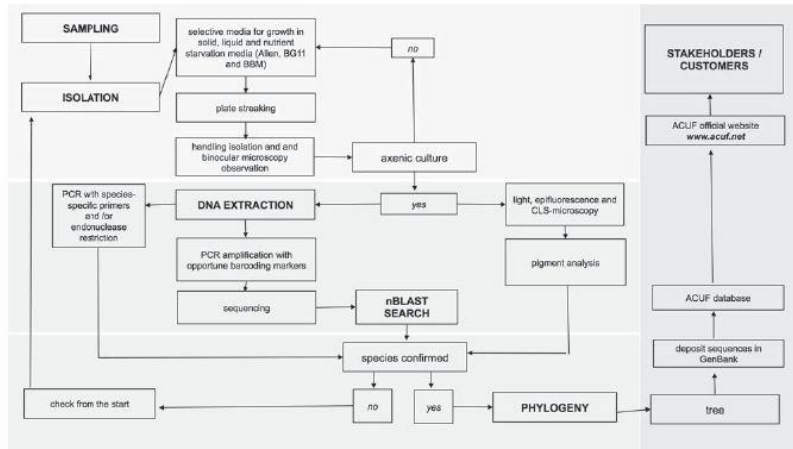


Fig. 3. Workflow of ACUF polyphasic approach for strain isolation and identification

and to monitor interaction of microorganisms with their living substrate.

Pigment analysis

Photosynthetic pigments are revealed at ACUF through spectrophotometric analysis to build a library reference: the procedure consists on determination of chlorophyll a, chlorophyll b, carotenoids and many others, following accurate methods well known in literature (Wellburn, 1994). This allows a first screening of isolated cultures, and the annotation of peculiar pigment composition in microalgae (Aminot and Rey, 2000).

Also hand-fluorometry is used when the available volume of water is not enough for reliable absorbance measurement; however, fluorometers need to be calibrated with chlorophyll standards for a preliminary calibration curve. In some cases, Reversed-Phase High Performance Liquid Chromatography (HPLC) is also used to characterize the quantity of Chlorophyll a and accessories pigments of strains preserved at ACUF Collection.

Molecular analysis and genetic barcoding markers

Cellular lysis for DNA extraction is performed selectively with the aid of bead beater, chemical lysis and freeze-and-thaw, or a combination of these methods. DNA extraction is carried out following the protocol by Doyle and Doyle (1990). Purified DNA is then quantified with NanodropD-1000 (Thermo Fisher Scientific - Wilmington, Delaware USA) and subsequently run on agarose gel electrophoresis for quality evaluation. Amplification by Polymerase Chain Reaction is carried out with primer sets specific for the different algal groups. Purified PCR products are then sequenced by Sanger method and the obtained sequences are compared by BLAST search and used for inferring phylogeny and species-attribution.

A number of molecular markers are used at ACUF for the identification and phylogenetic analyses: (i) ITS1 and ITS2 (internal transcribed spacers) (Wang et al., 2015) are used for barcoding green microalgae; ITS1 has been preferred to investigate phylogenetic relationships in several lineages of green algae (Hall et al., 2010; Cozzolino et al., 1999) whilst the secondary structure of ITS2 has been proposed particularly for the characterization of closely related species among Chlorophyta (Caisová et al., 2013; Fuciková et al., 2013); (ii) the 16S rRNA gene is a broadly used molecular marker for Cyanobacteria and, more generally, for prokaryotes; (iii) the *rbcL* (plastid Rubisco large subunit) gene is a marker that can resolve the attribution of several microalgal species, especially when used in combination with nuclear barcoding markers (Zou et al., 2016). At ACUF, species-specific primers have been designed for the discrimination of Cyanidophyceae.

Specific cases of phylogenetic attribution can be resolved with the help of a number of other markers. Among these, plastidial gene *tufA* (elongation factor (EF)-Tu) (Fama et al., 2002; Vieira et al., 2016) for green algae, and *nifH* (nitrogenase reductase) (Zehr et al., 1997) and *cpcA* (phycocyanin alfa subunit) (Manen and Falquet, 2002) for Cyanobacteria have been proposed. Extending the information deposited in public sequence database – in terms of number of different molecular markers and number of sequences – is fundamental in order to accurately determine the conclusive phylogenetic attribution for known species as well as for novel species described.

Overview of the available strains and representativeness of cultures

Presently, over 800 strains of eukaryotic microalgae and cyanobacteria are cultivated in the ACUF collection. The vast majority of microorganisms held at ACUF collection is composed by Archaeplastida that groups all eukaryotes with plastids derived from primary endosymbiosis: in fact, 89% of the ACUF strains belongs to the Divisions Chlorophyta, Rhodophyta, and Charophyta. About 7% of the entire collection is represented by photosynthetic prokaryotes belonging to different Orders.

The most representative taxonomic groups are Rhodophyta (418), Chlorophyta (277), and Cyanobacteria (58). In particular, among Rhodophyta the vast majority is represented by Cyanidophyceae, while among Chlorophyta, the classes of Trebouxiophyceae and Chlorophyceae account for the widest species diversity. Collection also includes strains sampled in saline or thermo-acidic environments belonging to the divisions of Charophyta (14), Ochrophyta (5), Cryptophyta (3), Haptophyta (3), and Euglenozoa (1) (for further details see Table 1).

The cultured strains were mainly isolated from terrestrial habitats, especially in proximity of hot springs, geysers and sulphuric fumaroles, but also on bare lithic substrates, or monuments (Fig. 4). Most of the species held in collection are known to inhabit terrestrial environments or freshwaters and their surroundings; only a small part thrives preferentially in brackish or marine waters. Some genera, i.e. *Stichococcus* or *Porphyridium*, thrive in moist terrestrial areas, intermittently submerged banks of rivers as well as saltmarshes and soils of sea-cliffs, including brackish and marine situations, thus showing a cosmopolitan growth attitude. Information about general environments of ACUF strains are showed in the Venn's diagram (Fig. 5a).

The geographic localization of our terrestrial and freshwater strains is quite diverse; 132 strains over the total were collected in Italy, whereas the remaining 534 were sampled or acquired from all over the world (Fig. 5b). This is especially true for Cyanidophyceae which have been

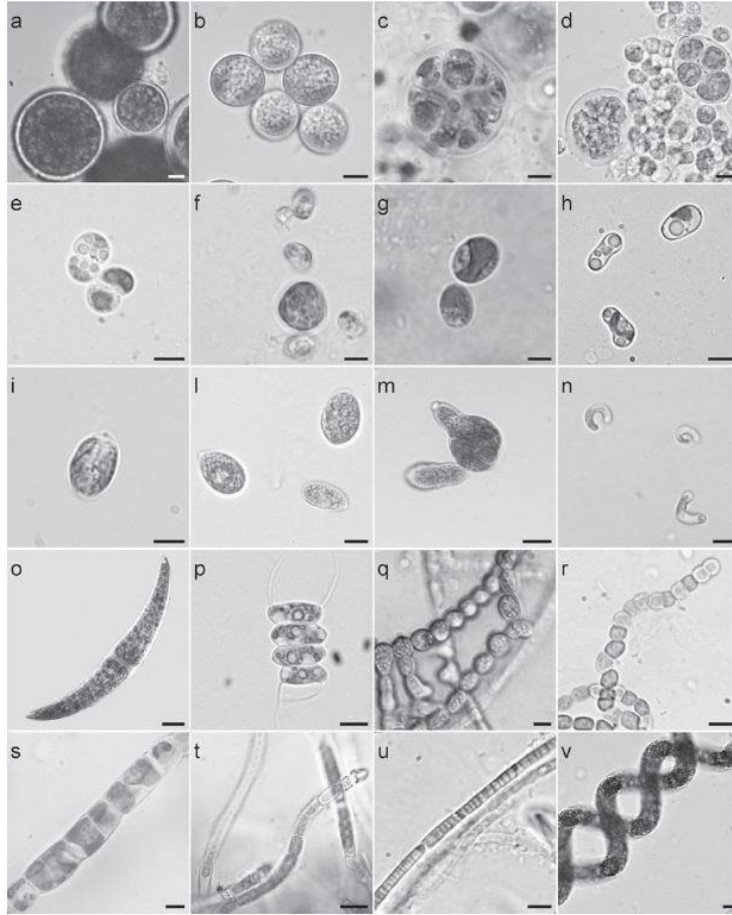


Fig. 4. Examples of microorganisms maintained in the ACUF collection. a) *Haematococcus lacustris* (Girod-Chantrons) Rostaf.; b) *Graesiella emersonii* (Shuhara et Krauss) Nozaki, Katagiri, Nakagawa, Aizawa et Watanabe. c) *Chlorosarcinopsis* sp.; d) *Scenedesmus* sp.; e) *Pseudococcomyxa simplex* (Maux) Fott; f) *Isochrysis galbana* Parke; g) *Viridiella fridericana* Albertano, Pollio et Taddei; h) *Stichococcus bacillaris* Nägeli; i) *Tetraselmis suecica* (Kytlin) Butcher; l) *Oocystis marssonii* Lemm.; m) *Chlorolobion braunii* (Nägeli) Komárek; n) *Raphidocelis subcapitata* (Korslikov) Nygaard, Komárek, Kristiansen et Skulberg; o) *Closterium ehrenbergii* Meneghini ex Ralfs; p) *Scenedesmus quadricauda* (Turpin) Bréb; q) *Westiellopsis* sp.; r) *Anabaena* sp.; s) *Klebsormidium flaccidum* (Kützang) Silva, Mattox et Blackwell; t) *Calothrix membranacea* Schmidle; u) *Leptolyngbya boryana* (Gomont) Anagnostidis et Komárek; v) *Arthrospira platensis* Gomont. Scale bar 5µm

sampled in hot volcanic and/or acidic sites mainly from Iceland, Turkey, and Italy but also strains from USA, former URSS, Mexico, and Japan (Ciniglia et al., 2004; Yoon et al., 2006).

The research projects in which the ACUF staff is involved since 1973 and the sampling campaigns in archaeological sites and volcanic environments in recent years allowed the ACUF collection to own 556 original cultures, 249 of which are strains acquired from other collections and institutes (Fig. 5c).

Perspectives

ACUF collection is continuously enriching its heritage with sampling campaigns in extreme environments and archaeological sites to preserve biodiversity and understand ecological and physiological features of photosynthetic inhabitants of extreme environments. For this aim, also the improvement of strain conservation and countemeasures to contamination are required to keep the collection alive and functioning. Recently, a flow cytometry protocol has been developed at ACUF to discriminate and sort the *C. caldarium* and *G. sulphuraria*, which have very poor and overlapping morphology, without the aid of fluorescent probes.

Microalgae from extreme environments adapt to survive in harsh conditions, facing severe oscillations in nutrient availability and other relevant microclimatic parameters. Hot springs, acidic ponds, stone surfaces, high peaks and salty lakes may host microorganism that enact a marvellous strategy for their living, hiding a precious genetic diversity and, in some cases, even more precious skills.

Since last decade, microalgae have been considered a new frontier in the energy biorefinery field because the "fuel only" (Zhu, 2015) option is difficult to achieve. To reduce the considerable cost of production and harvesting, that represents a true bottleneck in the pipeline, the "biorefinery" concept is extending to all compounds in these microorganisms that may be valuable. Microalgae are rich in

proteins, polyunsaturated fat acids (PUFA), carbohydrates, and pigments with anti-oxydizing activity. ACUF host laboratory is currently involved to expand algal screenings among extremophilic microalgae to find thermostable anti-oxydants (Carfagna et al., 2018), based on previous studies showing the potential use of *Galdiera sulphuraria* in food industry (Graziani et al., 2013).

However, because of the multiple potential in biotechnological applications, the demand for *G. sulphuraria* from the ACUF collection has increased in recent years.

The ACUF holds one of the largest and most diverse collection of Cyanidiales isolated from thermo-acidic environments of different continents. Moreover, it houses many cyanobacterial and algal isolates from monuments and artworks, that could serve as a platform for in vitro studies on biodeterioration.

Among the stakeholders and collaborators, there are: Roy J. Carver Center for Comparative Genomics, University of Iowa - USA, that studied the biodiversity of this genus in partnership with ACUF; Department of Biology, University of York - United Kingdom; University College London - United Kingdom; Botanisches Institut, University of Köln - Germany; Laboratory of Cell Cycles of Algae Institute of Microbiology Algatech - Czech Republic; Fermentalg - France. Besides, an on-going collaboration is presently held between ACUF and ATI-biotech - Italy for research and production of compounds in the field of food sustainability.

Future perspectives are oriented to the investigation and the screening of microalgae from extreme environments for the production of thermostable and valuable compounds that may find wider application in the field of food sustainability, chemicals for industrial employment, and useful coupled bioprocesses for the optimization of phytoremediation strategies and industrial biomass production and harvesting. For this aim, a continuous work in the preservation and study of biodiversity is still required to understand the ecological conditions in which such special strains are found to dwell.

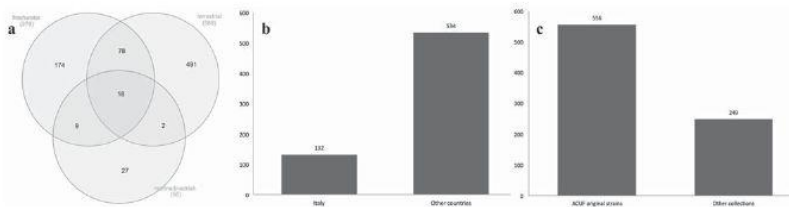


Fig. 5. a) habitats of ACUF algal strains, b, c) supplementary information on ACUF strains

Acknowledgements

The authors gratefully thank Olga Mascolo, Giuseppe Palma, Mariagioia Petraretti and Luca Russo for their valuable technical support.

References

Albertano P, Pinto G, Pollio A., 1994, Ecophysiology and ultrastructure of an acidophilic species of *Ochromonas* (Chrysophyceae, Ochromonadales), *Archiv Für Protistenkunde* 144: 75-82.

Albertano P., Pinto G., Pollio A., Taddei R., 1991, Physiological, biochemical, and ultrastructural characters of some strains of *Viridella fridericiana* (Chlorophyta, Chlorococcales), *Archiv Für Protistenkunde* 139: 117-23.

Albertano P., Pinto G., Pollio A., Taddei R., 1990, Morphology, ultrastructure and ecology of an acidophilic alga, *Pseudococcomyxa simplex* (Maimx) Fott (Chlorococcales), *Algological Studies/Archiv Für Hydrobiologie* 559: 81-95.

Albertano P., Taddei R., 1984, *Chlorella protothecoides* Krüger var. *acidicola*, a new variety from very low pH environments, *Algological Studies/Archiv Für Hydrobiologie* 37: 401-408.

Allen M. B., 1959, Studies with *Cyanidium caldarium*, an anomalously pigmented chlorophyte, *Archiv für Mikrobiologie* 32: 270-277.

Aminot A., Rey F., 2000, Standard procedure for the determination of chlorophyll a by spectroscopic methods international council for the exploration of the sea, Conseil International Pour l'Exploration de La Mer, Copenhagen, Denmark.

Bischoff H. W., Bold H. C., 1963, Some soil algae from enchanted rock and related algal species, *Phycological Studies IV*, Austin Texas Publication 6318: 1-95.

Bold H. C., 1949, The morphology of *Chlamydomonas chlamydogama*, sp. nov. *Bulletin of the Torrey Botanical Club* 76(2): 101-108.

Bordenie F., Denis M., Barami A., Alaoui-Sossé B., Aleya L., 2016, Microbial composition and ecological features of phototrophic biofilms proliferating in the Moidons Caves (France): investigation at the single-cell level, *Environmental Science and Pollution Research* 23(12): 12039-12049.

Caisová L., Marin B., Melkonian M., 2013, A consensus secondary structure of ITS2 in the chlorophyta identified by phylogenetic reconstruction, *Protist* 164 (4): 482-96.

Carfagna S., Landi V., Coraggio F., Salbitani G., Vona V., Pinto G., Pollio A., Ciniglia C., 2018, Different characteristics of C-phycocyanin (C-PC) in two strains of the extremophilic *Galdieria phlegrea*, *Algal Research* 31: 406-12.

Ciniglia C., Yang E. C., Pollio A., Pinto G., Iovinella M., Vitale L., Yoon H. S., 2014, Cyanidophyceae in Iceland: plastid *rbcL* gene elucidates origin and dispersal of extremophilic *Galdieria sulphuraria* and *G. maxima* (Galdieriaceae, Rhodophyta), *Phycologia* 53(6): 542-51.

Ciniglia C., Cennamo P., De Stefano M., Pinto G., Caputo P., Pollio A., 2007, *Pinnularia obscura* Krasske (Bacillariophyceae, Bacillariophyta) from acidic environments: characterization and comparison with other acid-tolerant *Pinnularia* species, *Fundamental and Applied Limnology / Archiv Für Hydrobiologie* 170(1): 29-47.

Ciniglia C., Cascone C., Lo Giudice R., Pinto G., Pollio A., 2005, Application of methods for assessing the genotoxicity of Triclosan to *C. ehrenbergi*, *Journal of Hazardous Materials* 122(3): 227-32.

Ciniglia C., Yoon H. S., Pollio A., Pinto G., Bhattacharya D., 2004, Hidden biodiversity of the extremophilic Cyanidiales red algae, *Molecular Ecology* 13(7): 1827-38.

Cozzolino S., Pinto G., Pollio A., De Luca P., 1999, Lack of trnL intron in the thermoacidophilic red alga *Galdieria sulphuraria* (Galdieri) Merola, *Plant Biosystems* 133(3): 303-5.

De Luca P., Musacchio A., Taddei R., 1981, Acidophilic algae from the fumaroles of Mount Lawu (Java), locus classicus of *Cyanidium caldarium* Geitler, *Giornale Botanico Italiano* 115: 1-9.

De Luca P., Moretti A., Taddei R., 1976-77, Presenza di *Cyanidioschyzon merolae* De Luca, Taddei, Varano in ambienti acidi extraeuropei (U.S.A. e Indonesia), *Delpinoia* n.s. 18-19: 69-76.

De Luca P., Taddei R., Varano L., 1978, *Cyanidioschyzon merolae*: a new alga of thermal acidic environments, *Webbia* 33(1): 37-44.

De Luca P., Moretti A., Taddei R., 1972-73, Nuove stazioni di *Cyanidium caldarium* nell'Italia meridionale ed in Sicilia, *Delpinoia* n.s. 14-15: 49-60.

Del Mondo A., Pinto G., De Natale A., Pollio A., 2017, In vitro colonization experiments for the assessments mycelial growth on a tuff substratum by a *Fusarium solani* strain isolated from the Oplontis (Naples, Italy) archeological site, *International Journal of Conservation Science* 8(4): 651-62.

Doyle J. J., Doyle J. L., 1990, Isolation of plant DNA from fresh tissue, *Focus* 12: 13-15.

Dubelaar G. B. J., Jonker R. R., Jonker R. R., 2000, Flow cytometry as a tool for the study of phytoplankton, *Scientia Marina* 64(2): 135-56.

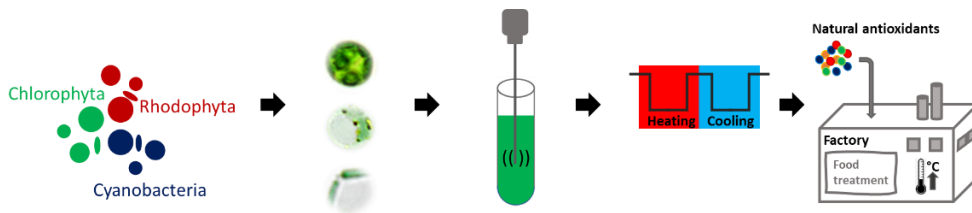
Fama P., Wysor B., Kooistra W. H. C. F., Zuccarello G. C., 2002, Molecular phylogeny of the genus *Caulerpa*

- (Caulerpales, Chlorophyta) inferred from chloroplast *tufA* gene, *Journal of Phycology* 38(5): 1040-50.
- Ferrari B., Paxéus N., Lo Giudice R., Pollio A., Garric J., 2003. Ecotoxicological impact of pharmaceuticals found in treated wastewaters: study of carbamazepine, clofibrac acid, and diclofenac. *Ecotoxicology and Environmental Safety* 55(3): 359-70.
- Fuiková K., Flechtner V. R., Lewis L. A., 2013. Revision of the genus *Bracteacoccus* Tereg (Chlorophyceae, Chlorophyta) based on a phylogenetic approach, *Nova Hedwigia* 96(1-2): 15-59.
- Gambardella R., Moretti A., Musacchio A., 1979-80. Autotocologia ed ultrastruttura di alghe termoacidofile del nord e centro America, *Delpino* n.s. 21-22: 35-45.
- Gifuni I., Olivieri G., Pollio A., Franco T. T., Marzocchella A., 2017. Autotrophic starch production by *Chlamydomonas* species. *Journal of Applied Phycology* 29(1): 105-14.
- Gifuni I., Olivieri G., Pollio A., Marzocchella A., 2018. Identification of an industrial microalgal strain for starch production in biorefinery context: the effect of nitrogen and carbon concentration on starch accumulation. *New Biotechnology* 41: 46-54.
- Graziani G., Schiavo S., Nicolai M. A., Buono S., Fogliano V., Pinto G., Pollio A., 2013. Microalgae as human food: chemical and nutritional characteristics of the thermo-acidophilic microalga *Galdieria sulphuraria*, *Food Function* 4(1): 144-52.
- Hall J. D., Fuoková K., Lo C., Lewis A.L., Karol K. G., 2010. An assessment of proposed DNA barcodes in freshwater green algae. *Cryptogamie, Algologie* 31(4): 529-55.
- Hirose H., 1958. Rearrangement of the systematic position of a thermal alga, *Cyanidium caldarium*, *Botanical Magazine, Tokyo* 71: 347-352.
- Holzinger A., Karsten U. 2013. Desiccation stress and tolerance in green algae: consequences for ultrastructure, physiological and molecular mechanisms, *Frontiers in Plant Science* 4: 327.
- Hyka P., Lickova S., Přibyl P., Melzoch K., Kovar K., 2013. Flow Cytometry for the Development of Biotechnological Processes with Microalgae, *Biotechnology Advances* 31: 2-16.
- Izabela R., Katarzyna G., Borys K., Agnieszka M., Ignacy G.W., Maciej G., 2008. 3D chloroplast structure. In: Allen J.F., Gantt E., Golbeck J.H., Osmond B. (eds) *Photosynthesis. Energy from the Sun*. Springer, Dordrecht.
- Janda J. M., Abbott S. L., 2007. 16S rRNA Gene Sequencing for bacterial identification in the diagnostic laboratory: pluses, perils, and pitfalls, *Journal of Clinical Microbiology* 45: 2761-64.
- Manen J. F., Jacques F., 2002. The *cpcB-cpcA* Locus as a tool for the genetic characterization of the genus *Arthrospira* (Cyanobacteria): evidence for horizontal transfer, *International Journal of Systematic and Evolutionary Microbiology* 52: 861-67.
- Marasco A., Nocerino S., Pinto G., Pollio A., Trojsi G., De Natale A., 2016. Weathering of a Roman mosaic—A biological and quantitative study on in vitro colonization of calcareous tesserae by phototrophic microorganisms, *Plos One* 11.
- Meneghini G., 1839. Nuova specie di alga descritta dal sig. Dott. Giuseppe Meneghini di Padova, *Nuovo Giornale De' Letterati* 39: 67-68.
- Merola A., Castaldo R., De Luca P., Gambardella R., Musacchio A., Taddei R., 1981. Revision of *Cyanidium caldarium*. Three species of acidophilic algae, *Giomale Botanico Italiano* 115: 189-95.
- Müller K. M., Oliveira M. C., Sheath R. G., Bhattacharya D., 2001. Ribosomal DNA phylogeny of the Bangiophycidae (Rhodophyta) and the origin of secondary plastids, *American Journal of Botany* 88: 1390-400.
- Olivieri G., Marzocchella A., Salatino P., Andreozzi R., Pinto G., Pollio A., 2010. Bio-oil production by *Stichococcus* strains in laboratory scale photobioreactors, *Journal of Biotechnology* 150: 18.
- Organization for Economic Co-operation and development, 1993. OECD guidelines for testing of chemicals 201-alga, growth inhibition test. OECD guidelines for the testing of chemicals, vol. 1, Paris.
- Pinto G., Pollio A., Previtera L., Stanzione M., Temussi F., 2003. Removal of low molecular weight phenols from olive oil mill wastewater using microalgae, *Biotechnology Letters* 25: 1657-59.
- Pinto G., Taddei R., 1976-77. Le alghe delle acque e dei suoli acidi italiani, *Delpino* n.s. 18-19: 77-106.
- Pollio A., Aliotta G., Pinto G., Paterno M., Bevilacqua A., 1997. Ecophysiological characters and biochemical composition of *Stichococcus bacillaris* Naegeli strains from low pH environments, *Algalogical Studies/Archiv Für Hydrobiologie* S84: 129-43.
- Pollio A., Cennamo P., Ciniglia C., De Stefano M., Pinto G., Huss V. A., 2005. *Chlamydomonas pilschmannii* Ettl, a little known species from thermoacidic environments, *Protist* 156: 287-302.
- Rampelotto P., 2013. Extremophiles and extreme environments, *Life* 3: 482-85.
- Rippka R., Deruelles J., Waterbury J., Herdman M., Stanier R., 1979. Generic assignments, strain histories and properties of pure cultures of cyanobacteria, *Journal of General Microbiology*, 111: 1-61.
- Rippka R., Waterbury J. B., Stanier R. Y., 1981. Isolation and purification of cyanobacteria: some general principles. In: Starr M. P., Trüper H. G., Balows A., Schlegel H. G. (eds) *The Prokaryotes*. Springer, Berlin, Heidelberg, 212-20.
- Ruiz G.J., Olivieri G., de Vree J., Bosma R., Willems P., Reith H., Eppink M., Kleinegris D., Wijffels R., Barbo-

- sa M. J., 2016, Towards industrial products from microalgae, *Energy and Environmental Science*, 9(10):3036-3043.
- Trask B. J., van den Engh G. J., Elgershuizen J. H., 1982, analysis of phytoplankton by flow cytometry, *Cytometry* 2(4): 258-64.
- U.S. EPA, 1989, Algal (*Selenastrum capricornutum*) growth test. Short - term methods for estimating the chronic toxicity of effluents and receiving waters to freshwater organisms, Environmental Monitoring Systems Laboratory, Environmental Protection Agency, Cincinnati, Ohio.
- Vieira H.H., Bagatini I. L., Guinart C. M., Vieira H. A. A., 2016, tufA Gene as molecular marker for freshwater Chlorophyceae, *Algae* 31: 155-65.
- Walker J. J., Pace N. R., 2007, Endolithic microbial ecosystems, *Annual Review of Microbiology* 61: 331-47.
- Wang X. C., Chang L., Liang H., Bengtsson-Palme J., Chen H., Zhang J. H., Cai D., Li J. Q., 2015, ITS1 a DNA barcode better than ITS2 in eukaryotes? *Molecular Ecology Resources* 15(3): 573 -86.
- Wellbum A. R., 1994, The spectral determination of chlorophylls a and b, as well as total carotenoids, using various solvents with spectrophotometers of different resolution, *Journal of Plant Physiology* 144: 307-13.
- WWAP (United Nations World Water Assessment Programme), 2015, The United Nations World Water Development Report 2015: Water for a sustainable world, Paris, UNESCO.
- Yoon H. S., Hackett J. D., Pinto G., Bhattacharya D., 2002 Nonlinear partial differential equations and applications: from the cover: the single, ancient origin of chromist plastids, *Proceedings of the National Academy of Sciences* 99: 15507-12.
- Yoon H. S., Cmgilia C., Wu M., Comeron J. M., Pinto G., Pollio A., Bhattacharya D., 2006, Establishment of endolithic populations of extremophilic Cyanidiales (Rhodophyta), *BMC Evolutionary Biology* 6: 78.
- Zehr J. P., Mellon M. T., Hioms W. D., 1997, Phylogeny of cyanobacterial nifH genes: evolutionary implications and potential applications to natural assemblages, *Microbiology* 143: 1443-50.
- Zhu L., 2015, Biorefinery as a promising approach to promote microalgae industry: an innovative framework, *Renewable and Sustainable Energy Reviews* 41: 1376-84.
- Zou S., Fei C., Wang C., Gao Z., Bao Y., He M., Wang C., 2016, How DNA barcoding can be more effective in microalgae identification: a case of cryptic diversity revelation in *Scenedesmus* (Chlorophyceae), *Scientific Reports* 6: 36822.

Chapter 3

Thermo resistant antioxidants from photoautotrophic microorganisms: screening and characterization



Submitted to Journal of Applied Microbiology

Thermo resistant antioxidants from photoautotrophic
microorganisms: screening and characterization

Luigi D'Elia¹, Paola Imbimbo¹, Davide Liberti¹, Francesco Bolinesi², Olga Mangoni², Antonino Pollio², Giuseppe Olivieri^{3,4*}, Daria Maria Monti^{1*}

¹Department of Chemical Sciences, University of Naples Federico II, via Cinthia 4, 80126, Naples, Italy

²Department of Biology, University of Naples Federico II, via Cinthia 4, 80126, Naples, Italy

³Bioprocess Engineering Group, Wageningen University and Research, Droevendaalsesteeg 1, 6700AA, Wageningen, the Netherlands

⁴Department of Chemical, Materials and Industrial Engineering, University of Naples Federico II, Piazzale Tecchio 80, 80125, Naples, Italy

*Corresponding Authors: G.O. giuseppe.olivieri@wur.nl; D.M.M. mdmonti@unina.it

Abstract

Aims. The demand for natural antioxidants to be used in food industry is increasing, as synthetic antioxidants are toxic and have high production costs. Specifically, food processing and preservation require antioxidants resistant to thermal sterilization processes. In this study, twenty-five strains among microalgae and cyanobacteria were screened as antioxidants producers.

Methods and Results. The pigment content of all extracts was determined spectrophotometrically. The species *Enallax* sp., *Synechococcus bigranulatus* and *Galdieria sulphuraria* showed the highest content of chlorophyll *a* and total carotenoids. *In vitro* stability and antioxidant activity of the ethanolic extracts were performed. The results revealed that extracts obtained from the previously mentioned species were stable at room temperature and exhibited *in vitro* free radical scavenging potential with IC₅₀ values of 0.099 ± 0.001, 0.048 ± 0.001 and 0.129 ± 0.02 mg mL⁻¹, respectively. Biocompatibility assay showed that the extracts were not toxic on immortalized cell lines. The

antioxidant activity was also tested on a cell-based model by measuring intracellular ROS levels after sodium arsenite treatment. Noteworthy, extracts were able to exert the same protective effect, before and after the pasteurization process.

Conclusions. Our results clearly indicate that the feasibility of obtaining biologically active antioxidants from microalgae.

Significance and Impact of Study. Green solvents can be used to obtain thermo-resistant antioxidants from cyanobacteria and microalgae which can be used in the food industry. Thus, the substitution of synthetic pigments with natural ones is now practicable.

Key points

- Microalgae and cyanobacteria contain natural antioxidants
- Ethanolic extracts show antioxidant activity in vitro and on a cell-based system
- Ethanolic extracts are resistant to pasteurization and active as antioxidants

Keywords

Microalgae; pigments; natural antioxidants; ABTS; H₂-DCFDA; pasteurization.

3.1 Introduction

Due to the toxicity of synthetic antioxidants, natural molecules with antioxidant activity have drawn great attention for their potential use as food preservatives or nutraceuticals^{1,2}. Nowadays, microalgae and cyanobacteria are emerging as an important source of sustainable antioxidants.

These microorganisms can survive in several environments, such as hot terrestrial and marine habitats, considered inhospitable for most life forms^{3,4}.

In recent years, several photosynthetic microorganisms have found application in industrial processes and in food industry for two reasons: (i) they can grow in harsh environmental conditions, so they are not susceptible to microbial contamination⁵; (ii) they produce molecules resistant to high temperatures, ionic strength and extreme pH values⁶⁻⁹. Moreover, high value compounds from algae and cyanobacteria are more effective than synthetic ones in food application¹⁰.

Microalgae and cyanobacteria are photosynthetic single-cell organisms, which are usually classified on the basis of their pigments, photosynthetic storage products and morphology^{11–13}. Cyanobacteria, known in the past as blue-green algae, have a prokaryotic cell and produce chlorophyll *a* as well as phycobiliproteins^{14,15}. Green algae have chlorophylls *a* and *b*, and usually do not have accessory light-harvesting pigments¹⁶. Red algae contain chlorophyll *a* and phycobilisomes that are located on the surface of unstacked thylakoid membranes^{17,18}.

In general, microalgae and cyanobacteria, present in different ecosystems, account for a large part of the total ecosystem biomass and productivity, and can be exploited to generate several value-added products of nutraceutical and industrial relevance⁶. Noteworthy, these microorganisms have the great advantage to be able to grow in wastewater and on non-arable lands, and to produce a huge number of secondary metabolites endowed with biological activity.

Currently, only few microalgae strains are commercialized. The dry biomass of *Chlorella* and *Arthrospira* is used as a food supplement due to the high content of proteins rich in essential amino acids¹⁰. The biomass of *Nannochloropsis species*, *Isochrysis species*, *Nitzschia species*, *Phaeodactylum species*, and *Porphyridium cruentum*, is rich in ω -3 fatty acids such as eicosapentaenoic (EPA) and docosahexaenoic (DHA), which exert beneficial effects on human health^{10,19,20}.

Moreover, microalgae produce a huge array of antioxidants, whose physiological function is to harvest the light at different wavelengths, and to protect cells from the continuous exposure to high levels of oxygen and radical stress^{21–24}. These are and mainly pigments, such as carotenoids and phycobiliproteins²⁵. These pigments can be widely used in the food industry as food colorants to replace synthetic dyes, or as additives to prolong the shelf-life of food products. Nevertheless, to date, *Spirulina Blue* is the only natural blue food coloring used in the food industry²⁶.

Unfortunately, to date, several factors need to be considered when developing food products from seaweeds and microalgae: (i) consumer awareness and demand; (ii) bioavailability; (iii) over time stability of bioactive compounds, and (iv) cost-effectiveness of the process. Therefore, the use of the whole algal biomass and extracts for human consumption must be related to food safety regulations, which vary among countries¹³.

To this regard, microalgae have received approval by different regulations. *Chlorella pyrenoidosa*, *Chlorella vulgaris* and

Heterochlorella luteoviridis are species not subjected to the Novel Foods Regulation, as they have been on the food market before 15 May 1997²⁷. Astaxanthin from *Haematococcus pluvialis*, oil from *Schizochytrium* sp., *Nannochloropsis gaditana* and *Phaeodactylum tricorutum* were approved as novel food ingredients between 2004-2017 under regulation (EC) No. 258/97^{10,28}. In order to simplify the current authorization procedures, a new regulation on novel food has been established with effective validity at the end of 2017¹⁰. According to this regulation, a novel food category has been proposed, i.e. “food consisting of, isolated from or produced from, microorganisms, fungi or algae”¹⁰. Also, the Food and Drug Administration (FDA, United States),

Food Standards Australia New Zealand (FSANZ) and Ministry of health, Labour and Welfare in Japan, approved safe biomasses and extracts of several microalgae as novel food ingredients¹⁰. Today, algae-based food products market is in expansion, as the world population is increasingly aware in the purchase of healthy food with a low environmental impact²⁹. As an example, the global carotenoid market is projected to increase to 2.0 billion USD by 2026³⁰. The production of carotenoids, such as β -carotene from *Dunaliella salina*, is 3000 t year⁻¹, with a total cost of 104 USD kg⁻¹. This value highlights that microalgal biomass is an expensive material compared to other types of biomasses. As reported by Ruiz et al., in the south of Spain the microalgal biomass cost production is estimated between 3.4 and 5.2 € kg⁻¹ (100 ha, with a productivity of about 27 ton ha⁻¹ Yr⁻¹ for open ponds and between 34 and 61 ton ha⁻¹ Yr⁻¹ for photobioreactors).

Authors highlighted that the cost of biomass is influenced by light exposure, as the same model in the Netherlands shows a cost of biomass between 6.0 and 11.0 € kg⁻¹³¹. In addition, the procedures employed for the extraction of high value compounds from microalgae represent a bottleneck in the exploitation of an algae-based biorefinery³². For example, the overall costs for the production of β -carotene from *D. salina* reflect a cost of 27-53 € day⁻¹³³. To make microalgae competitive to other natural sources, it is necessary to develop innovative and sustainable techniques able to reduce the costs of the whole process.

Another important factor to be considered is the potential toxicity and carcinogenic effect of synthetic antioxidants, as they are often obtained by using toxic solvents^{1,34,35}.

Thus, the idea of using antioxidants from natural sources is mandatory. Here, twenty-five photosynthetic thermotolerant microorganisms were used: 11 Chlorophyta, 4 Rhodophyta and 10 Cyanobacteria strains. Thermotolerant species were used to obtain antioxidants resistant to

the high temperatures reached during the sterilization processes. Extracts were obtained with a green solvent (ethanol), according to the Food Safety Regulation (EC 178/2002) and the mentioned-above Novel Food Regulation (EC 258/97), which limit the type of solvent to be used in the extraction processes. Extracts were screened for their growth rate and their *in vitro* antioxidant activity, and those endowed with the most promising activity were then evaluated for their biocompatibility and for their antioxidant activity on a cell-based model, before and after pasteurization process.

3.2 Materials and methods

Strains and Medium

Twenty-five strains, Chlorophyta, Rhodophyta and Cyanobacteria, were selected from the Algal Collection of the University Federico II (ACUF, www.acuf.net)³⁶. Chlorophyta strains were: *Chlorella vulgaris* Beij (062); *Chlorella zofingiensis* Dönz (252); *Coelastrella terrestris* (Reisigl) Hegewald et N. Hanagata (271); *Chlorella* sp. (684); *Chlorella sorokiniana* Shihira et Krauss (824); *Scenedesmus* sp. (826); *Chlorella sorokiniana* Shihira et Krauss (830); *Enallax* sp. (833); *Scenedesmus* sp. (839); *Scenedesmus* sp. (840); *Westiellopsis prolifera* (845). Cyanobacteria strains were: *Nodularia sphaerocarpa* Bornet et Flahault (033); *Calothrix membranacea* Shmidle (114); *Gloeotrichia* sp. (115); *Anabaena flos-aquae* Healey (249); *Nostoc commune* Vaucher ex Bornet et Flahault (299); *Fischerella ambigua* (Kützing ex Bornet et Flahault) Gomont (304); *Lyngbya major* Meneghini (633); *Synechococcus bigranulatus* Scuria (680); *Synechocystis fuscopigmentos* Kovacic (683); *Chroococcidiopsis* sp. (831). Rhodophyta strains were: *Galdieria sulphuraria* (Galdieri) Merola (064); *Galdieria phlegrea* Pinto G. (291); *Galdieria partita* Sentsova (627) and *Galdieria maxima* Sentsova (671). Chlorophyta inorganic medium was Bold Basal Medium (BBM)³⁷. Cyanobacteria were grown in Blue-Green medium (BG-11)³⁸. The culture medium for Rhodophyta was the Allen medium (Allen, 1968). Media were sterilized in autoclave.

Algal growth

Cultures of 50 mL were grown in flasks on a shaking shaker in a climate room at 39 ± 1 °C equipped with fluorescent lamps with a constant light intensity of 300 PAR $\mu\text{mol}_{\text{photons}} \text{m}^{-2} \text{s}^{-1}$. The irradiance

value was chosen as it corresponded to the average yearly conditions, during outdoor production, in Europe³⁹.

The growth and microalgal concentration of each strain was followed for 14 days by measuring the optical density (O.D.) at 730 nm wavelength. The conversion between the O.D. and the biomass dry weight was determined for each strain at the end of the exponential growth phase. The conversion factor was: 1 O.D. corresponded to 0.2 mg dry weight. The conversion between fresh and dry weight was measured for each strain and the ratio was found to be 5:1, which means that 1 g of fresh biomass corresponded to 200 mg ± 18 of dry weight.

Division per day (k) is directly related to the ratio between the O.D. of each day (t_2) and the initial time (t_1) and inversely related to Δt ⁴⁰:

$$k = \frac{\log_2 (O.D._{t_2} / O.D._{t_1})}{\Delta t}$$

The light yield ($Y_{X/E}$, g mol_{photons}⁻¹) was defined as the ratio of the produced biomass and the light energy irradiated over the cultivation time. Thus:

$$\frac{(x_t - x_{t=0}) \cdot V}{A \cdot I \cdot t}$$

where the produced biomass is the product of the culture volume (V , L) and the biomass concentration produced ($x_t - x_{t=0}$, g L⁻¹) during the culture time (t , s). The irradiated energy is the product of the irradiated surface (A , m²), the irradiance (I , μmol m⁻² s⁻¹) and of the culture time.

Pigments extraction

Antioxidants extractions were performed using ethanol as solvent, as reported by Aremu, with some modifications⁴¹. Briefly, for each extraction, 1 g of harvested biomass, which corresponds to 200 mg of dry weight (D.W.), was suspended in 2 mL of ethanol and disrupted by ultrasonication (in continuous, 40% instrument amplitude) for 4 min on ice. The final volume was adjusted to 20 mL and the mixture was shaken for 24 h at 250 rpm in a dark room at 4 °C. The mixture was then centrifuged at 12000 g for 10 min and the supernatant stored at -20 °C. The supernatant, dried under N₂ stream, was solubilized in ethanol (12 mg mL⁻¹) and stored at -20 °C. the extract represents the ethanol extract (EE).

Spectrophotometric characterization

UV-vis absorption spectra of EE were collected at different time (0, 24 and 48 h) using a quartz cuvette of 1 cm path length. Spectra were collected at 25 °C over 400-700 nm wavelength range using a Varian Cary 5000 UV-vis-NIR spectrophotometer.

Determination of pigments concentration

Pigments concentration was determined spectrophotometrically by acquiring the spectra in the range 400-700 nm. The amount of pigments was calculated using formulae (1)-(3), derived for ethanol extracts⁴²:

$$Chl\ a = 13.36 \cdot A_{664\ nm} - 5.19 \cdot A_{649\ nm} \quad (1)$$

$$Chl\ b = 27.43 \cdot A_{649\ nm} - 8.12 \cdot A_{664\ nm} \quad (2)$$

$$Carotenoids = (1000 \cdot A_{470nm} - 2.13 \cdot Chl\ a - 97.63 \cdot Chl\ b)/209 \quad (3)$$

The results were expressed as mg of pigments g⁻¹ of biomass D.W.

The supernatant, dried under N₂ stream, was solubilized in ethanol (12 mg mL⁻¹) and stored at -20 °C. The extract represents the ethanol extract (EE).

Antioxidants concentration was calculated as the product between biomass antioxidants content (A_{ox}) and biomass concentration (X , g L⁻¹), calculated when the antioxidants content reached the maximum level (t_{smax} , day):

$$P_{antioxidants} = \frac{A_{OX(t_{smax})} \cdot X_{(t_{smax})}}{t_{smax}}$$

Antioxidants productivity ($P_{antioxidants}$, mg L⁻¹ day⁻¹) was assessed as the ratio between the concentration of antioxidant and the culture time at which the antioxidants reach the maximum.

Total carotenoid quantification

The total carotenoid content was determined by spectrophotometrical analysis as described by Gilbert-López et al.⁴³. The ethanolic extracts from *S. bigranulatus*, *Enallax* sp. and *G. sulphuraria* were dissolved in pure methanol in a concentration range from 0.5 to 0.05 mg mL⁻¹. A standard calibration curve of commercial

β -carotene (from 5 to 200 $\mu\text{g mL}^{-1}$) was used to calculate the concentration of total carotenoids. The absorbance of samples was recorded at 470 nm using a plate reader. The total carotenoid content was expressed as the ratio of mg of carotenoids and g of the extract.

Pigments characterization by HPLC

For pigment determination, extracts were resuspended in 100% methanol and analyzed using an HPLC Hewlett Packard (1100 Series). 200 μL of sample was injected and pigments were separated by using a C8 column (3 μm Hyperloop MOS, 10 cm, 4.6 mm internal diameter, Shandon), as described in Vidussi et al.⁴⁴. Solvent A was: 0.5 N aqueous ammonium acetate, 70:30% v/v, and solvent B was MeOH, with the following gradient: min 0, 25% B; min 1, 50% B; min 15, 100% B, min 19, 25% B. For the determination of chlorophylls and carotenoids, a spectrophotometer with a diodes array detector (DAD) was set at 440 nm, making it possible to determine the absorption spectrum of the 350–750 nm interval for each peak, in order to check the purity of each pigment.

ABTS assay

The *in vitro* antioxidant activity of each extract was evaluated by the 2,2'-azinobis-(3-ethylbenzothiazoline-6-sulfonic acid) ABTS assay, according to Rigano et al. with some modifications⁴⁵. Briefly, 7.4 mM ABTS^{•+} was mixed with 140 mM $\text{K}_2\text{S}_2\text{O}_8$ and the solution stabilized for 12 h at room temperature in the dark. The mixture was then diluted with deionized water to obtain an absorbance of 0.70 ± 0.02 unit at 734 nm using a spectrophotometer. Ethanolic extracts (50 μL) were allowed to react with 250 μL of diluted ABTS^{•+} solution for 7 min, and then the absorbance was read at 734 nm. The standard curve was linear between 0 and 20 μM Trolox. Results are expressed as IC_{50} (mg mL^{-1}), i.e. the concentration required to scavenge 50% of free radical ABTS.

Biocompatibility assay

Human keratinocytes (HaCaT, Innoprot, Derio, Spain) and murine fibroblasts (BALB/c-3T3, ATCC, VA, USA) were cultured in Dulbecco's modified Eagle's medium (DMEM) (Sigma-Aldrich, St Louis, MO, USA) supplemented with 10% foetal bovine serum (HyClone, Logan, UT, USA), 2 mM L-glutamine and antibiotics. Cells were grown in a 5% CO_2

humidified atmosphere at 37 °C and seeded in 96-well plates at a density of 2×10^3 cells per well. Ethanol microalgal extracts were added to the cells 24 h after seeding for dose-dependent cytotoxicity assays. After 48 h incubation, cell viability was assessed by the MTT assay as described in Galano et al.⁴⁶. Briefly, 3-(4,5-dimethylthiazol-2-yl)-2,5-diphenyltetrazolium bromide (MTT) reagent dissolved in DMEM in the absence of phenol red (Sigma-Aldrich) was added to the cells (0.5 mg mL^{-1} final concentration). Following 4 h incubation at 37 °C, the culture medium was removed and the resulting formazan salts were dissolved by adding isopropanol containing 0.01 N HCl ($100 \text{ }\mu\text{L}$ per well). Absorbance values were determined at 570 nm using an automatic plate reader (Microbeta Wallac 1420, PerkinElmer, Waltham, MA, USA). Cell survival was expressed as percentage of viable cells in the presence of the ethanol microalgal extract under test compared with control cells grown in the absence of the extract. Three separate analyses were carried out with each sample. Control experiments were performed either by growing cells in the absence of the EE or by adding to the cell cultures identical volumes of ethanol.

Thermal pasteurization

Thermal pasteurization was performed accordingly to the protocol reported by Ferraro et al.⁷. Briefly, EE were heated at 75 °C in a water bath. After 10 min incubation, samples were transferred to a second water bath at 20 °C and then stored at 4 °C until analysis.

Cellular reactive oxygen species (ROS) assay

The antioxidant activity of EEs before and after pasteurization was determined by measuring intracellular ROS levels, according to the protocol previously reported⁴⁷ with modifications. HaCaT cells were pre-incubated for 2 h with $80 \text{ }\mu\text{g mL}^{-1}$ of raw or pasteurized extract. At the end of incubation, cells were treated with $25 \text{ }\mu\text{M}$ 2',7'-dichlorodihydrofluorescein diacetate ($\text{H}_2\text{-DCFDA}$) for 45 min at 37 °C in complete medium without phenol red. Then, cells were incubated with $300 \text{ }\mu\text{M}$ NaAsO_2 (SA) for 1 h at 37 °C. Finally, cells were washed with warm PBS plus (phosphate buffer saline supplemented with 1 mM CaCl_2 , 0.5 mM MgCl_2 , and 30 mM glucose). The fluorescence of DCF was detected at an emission wavelength of 525 nm and an excitation wavelength of 488 nm using a Perkin-Elmer LS50 spectrofluorometer (Shelton, CT, USA). Emission spectra were acquired at a scanning speed of 300 nm min^{-1} , with 5 nm slit width both for excitation and

emission. ROS levels were expressed as percentage of fluorescence intensity of the sample under test, compared to untreated cells. Three independent experiments were carried out, each one with three determinations.

Statistical analysis

All the experiments were performed in triplicate. Results are presented as mean of results obtained after three independent experiments (mean \pm SD or mean \pm SEM) and compared by one-way ANOVA according to the Bonferroni's method (post-hoc) using Graphpad Prism for Windows, version 6.01.

3.3 Results

Biomass production

Commercial-scale cultivation of photosynthetic microorganisms is fundamental for the biomass generation process, and photobioreactors (PBRs) are often used as they allow a good control of all the experimental set up. 11 Chlorophyta, 4 Rhodophyta and 10 Cyanobacteria strains were grown at 40 °C for 14 days. Most of the strains showed an adaptation period of 3-5 days followed by an exponential growth phase and ultimately a stationary phase (Figures S1-S3). Strains *Westiellopsis prolifera* (845), *Nodularia sphaerocarpa* (033), *Calothrix membranacea* (114), *Nostoc commune* (299), *Fischerella ambigua* (304) and *Lyngbya major* (633), did not adapt to the chosen experimental conditions and were discarded. For all the other microalgal cells, division per day (k) and light yield were calculated and reported in Figure 1. Among the three phyla, *Scenedesmus sp.* (826), *Chroococciopsis sp.* (831) and *Galdieria phlegrea* (291) showed the lowest division per day (grey bars). On the other hand, the species endowed with the highest division per day and light yield were: *Enallax sp.* (833) ($0.593 \pm 0.12 \text{ day}^{-1}$; $0.488 \pm 0.09 \text{ g mol}_{\text{photons}}^{-1}$) for Chlorophyta; *Synechococcus bigranulatus* (680) ($0.566 \pm 0.04 \text{ day}^{-1}$; $0.373 \pm 0.03 \text{ g mol}_{\text{photons}}^{-1}$) for Cyanobacteria, and *Galdieria sulphuraria* (064) ($0.565 \pm 0.02 \text{ day}^{-1}$; $0.065 \pm 0.02 \text{ g mol}_{\text{photons}}^{-1}$) for Rhodophyta.

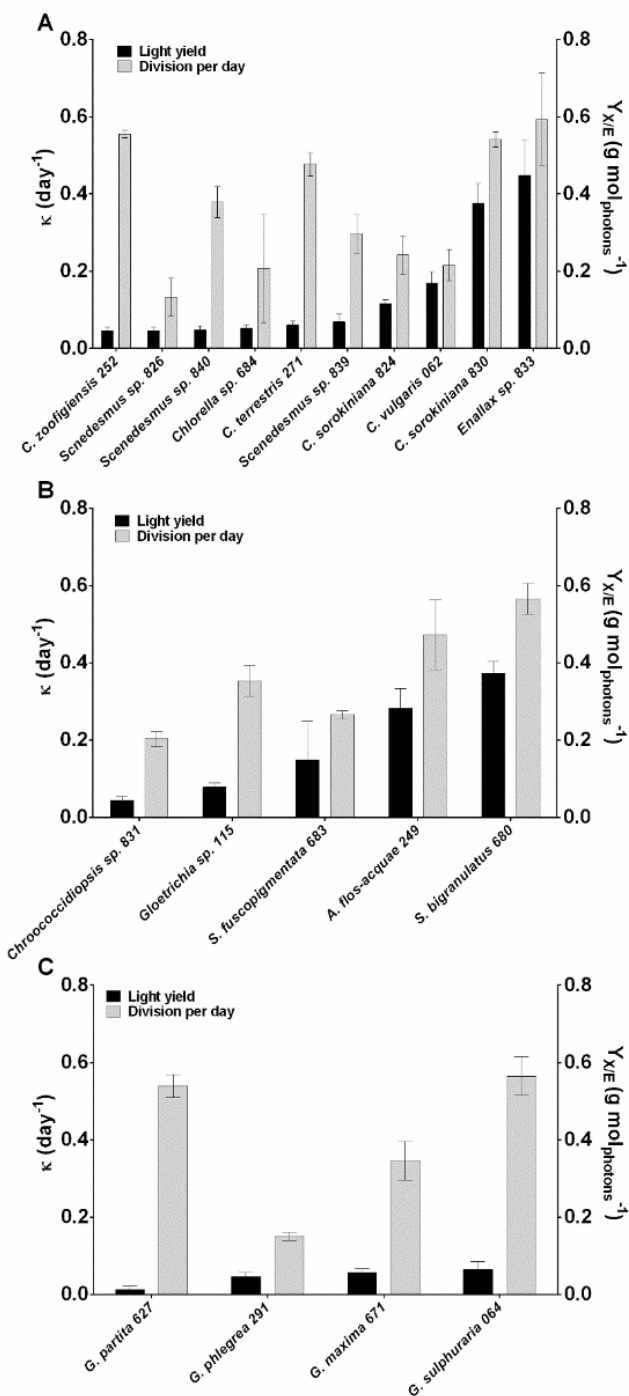


Figure 1. Analysis of microalgal growth. Divisions per day (k) and light yield (Y) of Chlorophyta (A), Cyanobacteria (B) and Rhodophyta (C) strains. Divisions per day (grey bars) and light yield (black bars) were calculated at exponentially phase. Data expressed as mean \pm SD (n=3).

Pigment extraction and quantification

Ethanol was used to extract antioxidants from microalgae, as it is considered a safe solvent for humans. Pigments concentration was obtained by using the formulas from Chen and Vaidyanathan⁴² (Table S1). In this study, chlorophyll *a* (Figure 2, white bars) was higher in *Scenedesmus sp.* (839) and *Enallax sp.* (833) for Chlorophyta species (Figure 2A), whereas, among Cyanobacteria, *S. bigranulatus* seemed to be the best antioxidants producer (Figure 2B). In the case of Cyanidiales, instead, the chlorophyll *a* content was very similar (Figure 2B).

As for chlorophyll *b* content (Figure 2, grey bars), a slight variation in Chlorophyta species was observed, although no chlorophyll *b* in Cyanobacteria and Rhodophyta was observed (Figure 2B-C). When total carotenoids were determined, the Chlorophyta with the highest value was *Enallax sp.* (20.7 ± 3.4 mg g⁻¹ biomass D.W.), whereas in case of Cyanobacteria *S. bigranulatus* showed the highest carotenoid level (5.4 ± 1.0 mg g⁻¹ biomass D.W.) and *G. sulphuraria* (2.5 ± 0.5 mg g⁻¹ biomass D.W.) among Rhodophyta.

Thus, based on the overall results, *Enallax sp.*, *S. bigranulatus* and *G. sulphuraria* were chosen for further experiments.

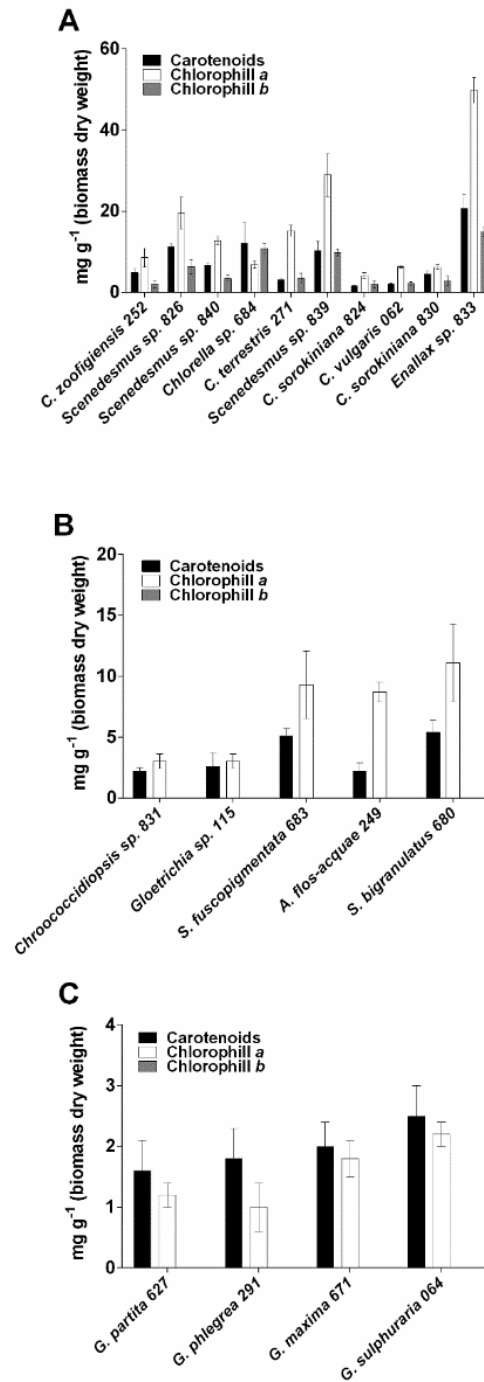


Figure 2. Analysis of pigments content in different microalgal strains. Chlorophyll a (white bars), chlorophyll b (grey bars) and total carotenoids (black bars) present in the ethanol extracts from Chlorophyta (A), Cyanobacteria (B) and Rhodophyta (C). Each content is expressed as mg of extract pigment per g of biomass dry weight.

Determination of carotenoid content in selected strains

Starting from the ethanolic extract of *Enallax sp.*, *S. bigranulatus* and *G. sulphuraria* the total carotenoids content was determined spectrophotometrically. The results are reported in Table 1. The carotenoid content is expressed as mg of carotenoids extracted per g of ethanol dry extract. It is interesting to notice that the conventional extraction allowed obtaining 924 mg of carotenoids per g of dry extract from *Enallax sp.*, whereas 565 mg and 394.5 mg of carotenoids were recovered from *S. bigranulatus* and *G. sulphuraria*, respectively.

Table 2. Comparison between extract yields and carotenoids content of selected strains.

Strain	$\text{mg}_{\text{extract}} \text{g}_{\text{dried biomass}}^{-1}$	$\text{mg}_{\text{carotenoids}} \text{g}_{\text{extract}}^{-1}$
<i>Enallax sp.</i>	256.4 ± 16.7	924.0 ± 39.6
<i>S. bigranulatus</i>	216.6 ± 6.6	565.0 ± 19.8
<i>G. sulphuraria</i>	42.9 ± 0.9	394.5 ± 31.2

Pigments characterization by HPLC of selected strains extract

Table 2 reports the list of pigments obtained in *Enallax sp.*, *S. bigranulatus* and *G. sulphuraria*, using the method reported in Vidussi et al. ⁴⁴, which does not allow the identification of phycobilins.

As shown in Table 2 and in Figure 3, HPLC analyses allowed to identify, among the eleven pigments eluted, violaxanthin (peak 2), lutein (peak 4), chlorophylls a and b (peaks 6-11), and β -carotene (peak 11) in *Enallax sp.* Peaks 1, 3, 5 were xanthophylls not identified. In *S. bigranulatus*, zeaxanthin (peak 3), chlorophyll a - and its isomer - (peaks 7, 8), and β -carotene (peak 10), were identified. Peaks 1, 2, 4, 5, 6, 9 were xanthophylls not identified. In *G. sulphuraria*, among the nine eluted pigment, only two were xanthophylls not identified (peaks 2, 9), whereas zeaxanthin (peak 1), chlorophyll a - and its isomers - (peak 3-5), phaeophytins (peaks 6, 7) and β -carotene (peak 9) were identified.

Table 3. List of pigments obtained for *Enallax sp.*, *S. bigranulatus*, *G. sulphuraria*, with related retention time and absorption peak at different wavelength (nm).

number peak	pigment	Retention time (min)	λ (nm)	λ (nm)	λ (nm)
<i>Enallax sp.</i>					
1	xanthophyll	6.563	417	440	469
2	violaxanthin	7.278	416	439	468
3	xanthophyll	9.737	-	449	472
4	lutein	9.908	421	445	473
5	xanthophyll	11.135	416	440	466
6	chlorophyll b	12.313	467	601	653
7	chlorophyll b*	12.845	463	601	653
8	chlorophyll a*	14.105	426	617	664
9	chlorophyll a	14.445	432	618	665
10	chlorophyll a*	14.727	432	618	666
11	β -carotene	16.872	426	450	476
<i>S. bigranulatus</i>					
1	xanthophyll	7.498	426	449	477
2	xanthophyll	8.648	427	450	477
3	zeaxanthin	9.758	426	450	477
4	xantophyll	10.445	422	444	471
5	xanthophyll	11.302	422	444	470
6	xanthophyll	12.147	421	445	471
7	chlorophyll a*	14.129	428	618	647
8	chlorophyll a	14.472	432	618	665

CHAPTER 3

9	xanthophyll	16.719	422	445	471
10	β -carotene	17.055	426	450	476
<i>G. sulphuraria</i>					
1	zeaxanthin	12.184	426	450	477
2	xanthophyll	14.174	421	444	471
3	chlorophyll a	14.476	430	616	664
4	chlorophyll a*	14.696	421	615	655
5	chlorophyll a*	15.936	404	616	666
6	phaeophytin	16.268	407	502, 533, 609	665
7	phaeophytin	16.740	408	502, 533, 609	665
8	xanthophyll	16.929	420	444	471
9	β -carotene	12.184	427	450	477

Values in bold represent the maximum adsorption wavelength for each pigment. The symbol * meanings isomer. The number of each pigment reflects the sequence of elution on chromatograms (Figure 3).

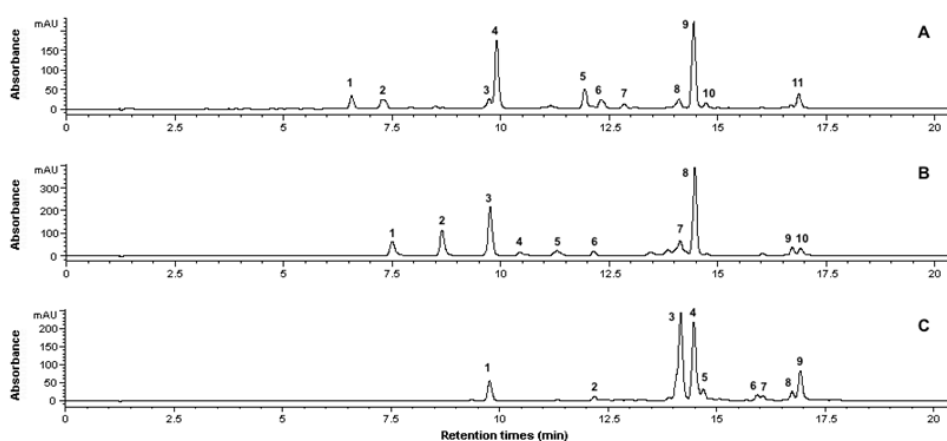


Figure 3. Representative HPLC chromatograms of carotenoids extracted in (A) *Enallax* sp.; (B) *S. bigranulatus*; (C) *G. sulphuraria*. Peak numbers and their identification are reported in Table 3.

In vitro determination of the antioxidant activity of ethanol extracts

The selected strains showed an antioxidant productivity of $6.3 \pm 0.9 \text{ mg L}^{-1} \text{ day}^{-1}$ (*Enallax sp.*); $8 \pm 1.5 \text{ mg L}^{-1} \text{ day}^{-1}$ (*S. bigranulatus*) and $6.0 \pm 0.4 \text{ mg L}^{-1} \text{ day}^{-1}$ (*G. sulphuraria*). Then, the ABTS scavenging assay was performed. Even if the reliability of this analysis is controversial, it is widely used to test the antioxidant activity of different molecules^{48–50}. The results of the screening are shown in Table 3. *C. sorokiniana* (684) followed by *Enallax sp.* (833) for the Chlorophyta species. In the case of Cyanobacteria, ethanol extracts from *S. bigranulatus* (680) and *Anabaena flos-aquae* (249) showed the highest antioxidant power, whereas *G. sulphuraria* (064) showed the best antioxidant power among Rhodophyta. Thus, on the basis of the division per day, on the total pigments content and on the *in vitro* antioxidant activity, one strain for each phylum was selected for further experiments: *Enallax sp.* (833), *S. bigranulatus* (680) and *G. sulphuraria* (064).

Table 4. Antioxidant activity of ethanol extracts expressed as IC₅₀, i.e. the concentration required to scavenge 50% of free radical ABTS.

Phylum	Species	ACUF N°	IC ₅₀ (mg mL ⁻¹)
Chlorophyta	<i>Chlorella vulgaris</i>	62	0.104 ± 0.04
	<i>Chlorella zoofigiensis</i>	252	0.218 ± 0.04
	<i>Coelastrella terrestris</i>	271	0.125 ± 0.01
	<i>Chlorella sp.</i>	684	0.132 ± 0.01
	<i>Chlorella sorokiniana</i>	824	0.075 ± 0.02
	<i>Scenedesmus sp.</i>	826	0.117 ± 0.01
	<i>Chlorella sorokiniana</i>	830	0.250 ± 0.01
	<i>Enallax sp.</i>	833	0.099 ± 0.001
	<i>Scenedesmus sp.</i>	839	0.150 ± 0.05
	<i>Scenedesmus sp.</i>	840	0.178 ± 0.03
Cyanobacteria	<i>Gloetrichia sp.</i>	115	0.156 ± 0.01
	<i>Anabaena flos-acquae</i>	249	0.047 ± 0.01
	<i>Synechococcus bigranulatus</i>	680	0.048 ± 0.001

	<i>Synechocystis fuscopigmentata</i>	683	0.092 ± 0.04
	<i>Chroococcidiopsis</i> sp.	831	0.035 ± 0.004
Rodophyta	<i>Galdieria sulphuraria</i>	64	0.129 ± 0.02
	<i>Galdieria phlegrea</i>	291	0.185 ± 0.06
	<i>Galdieria partita</i>	627	>>2
	<i>Galdieria maxima</i>	671	0.147 ± 0.03

Ethanol extract stability

To assess the stability of ethanol extracts, spectra of each selected strain were acquired at different time of storage. The UV-vis absorption spectra of extracts from *Enallax* sp., *S. bigranulatus* and *G. sulphuraria* are reported in Figure 4. After 48 h storage, a loss of absorbance was found: 33% for *Enallax* sp., 7% for *S. bigranulatus* and 34% for *G. sulphuraria*, thus suggesting an overall stability of all the extracts overtime.

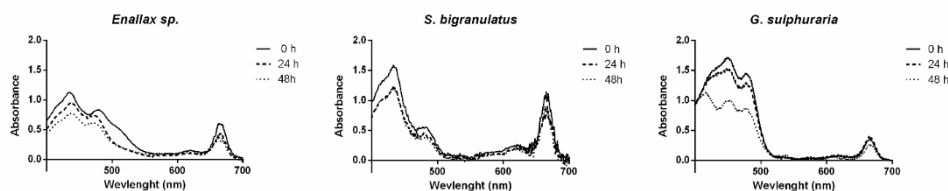


Figure 4. UV-vis absorption spectra of *Enallax* sp., *S. bigranulatus* and *G. sulphuraria* extracts. Samples were concentrated 0.12 mg mL⁻¹. Spectra were acquired at 25 °C, in the range 400-700 nm. Spectra are reported at time 0 (-), after 24 h (---) and 48 h (···) storage.

Ethanol extract biocompatibility on immortalized eukaryotic cells

In order to verify if the ethanol extracts could be used in the food industry, the biocompatibility of the selected strains extracts was verified by MTT assay on eukaryotic immortalized cells: HaCaT (human keratinocytes) and BALB/c-3T3 (murine fibroblasts) cells. Cells were plated, and 24 h after seeding, increasing amount (from 5 µg mL⁻¹ to 100 µg L⁻¹) of *S. bigranulatus*, *Enallax* sp. and *G. sulphuraria* extracts were added to the cells, taking into account that the average of the IC₅₀ of the tested samples was lower than 50 µg mL⁻¹. After 48 h incubation, cell viability was assessed by the MTT (3-(4,5-dimethylthiazol-2-yl)-2,5-diphenyltetrazolium bromide) assay and cell survival was expressed as the percentage of viable cells in the

presence of extract compared to that of control samples. Two groups of cells were used as control, i.e. cells untreated with the extract and cells supplemented with identical volumes of buffer. Each sample was tested in two independent analyses, each carried out in triplicates (Figure 5). MTT assays showed that the molecules extracted in ethanol resulted to be biocompatible with both the cell lines analyzed.

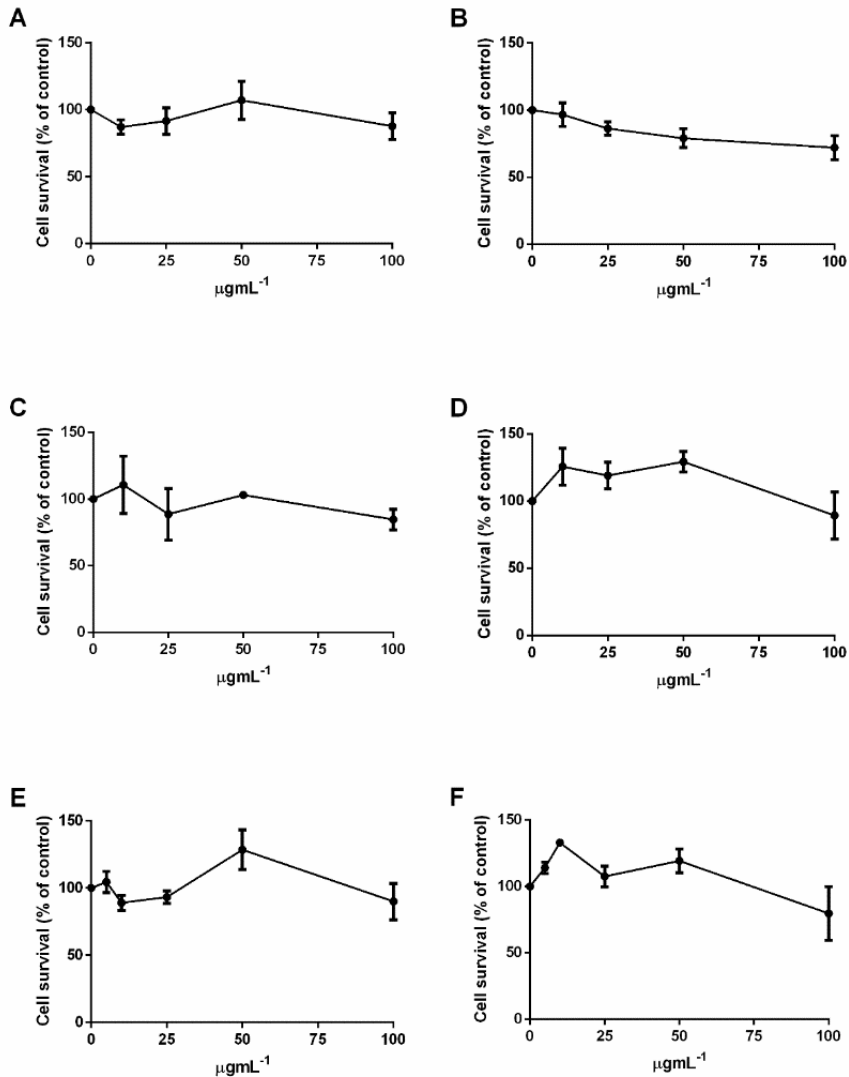


Figure 5. Effect of ethanol extracts from *S. bigranulatus*, *Enallax sp.* and *G. sulphuraria* on the viability of immortalized cells. Dose-response curve of cells incubated for 48 h in the presence of increasing concentration (5-100 $\mu\text{g mL}^{-1}$) of each extract. **A, C, E**, HaCaT cells; **B, D, F**, BALB/c-3T3 cells. Cells were incubated with *S. bigranulatus* extracts (**A, B**); *Enallax sp.* (**C, D**); *G. sulphuraria* (**E, F**). Cell viability was assessed by the MTT assay and expressed as described in Materials and Methods section. Values are given as means \pm SD (n \geq 3).

Antioxidants thermo-resistance

To verify if high temperature treatments affect the bioactivity of ethanol extracts, a comparison between the antioxidant activity of raw and of pasteurized extracts (i.e. heated at 75°C for 10 min) was performed. Cells were incubated for 2 h with 80 µg mL⁻¹ of either raw or pasteurized extracts prior to SA exposure. At the end of the experiment, ROS levels were measured by using 2,7-dichlorodihydrofluorescein diacetate (H₂-DCFDA). As shown in Figure 6, no alteration in ROS levels was observed when cells were incubated with the two molecules (white and grey bars), whereas a significant increase in ROS levels was observed when cells were exposed to SA (black bars).

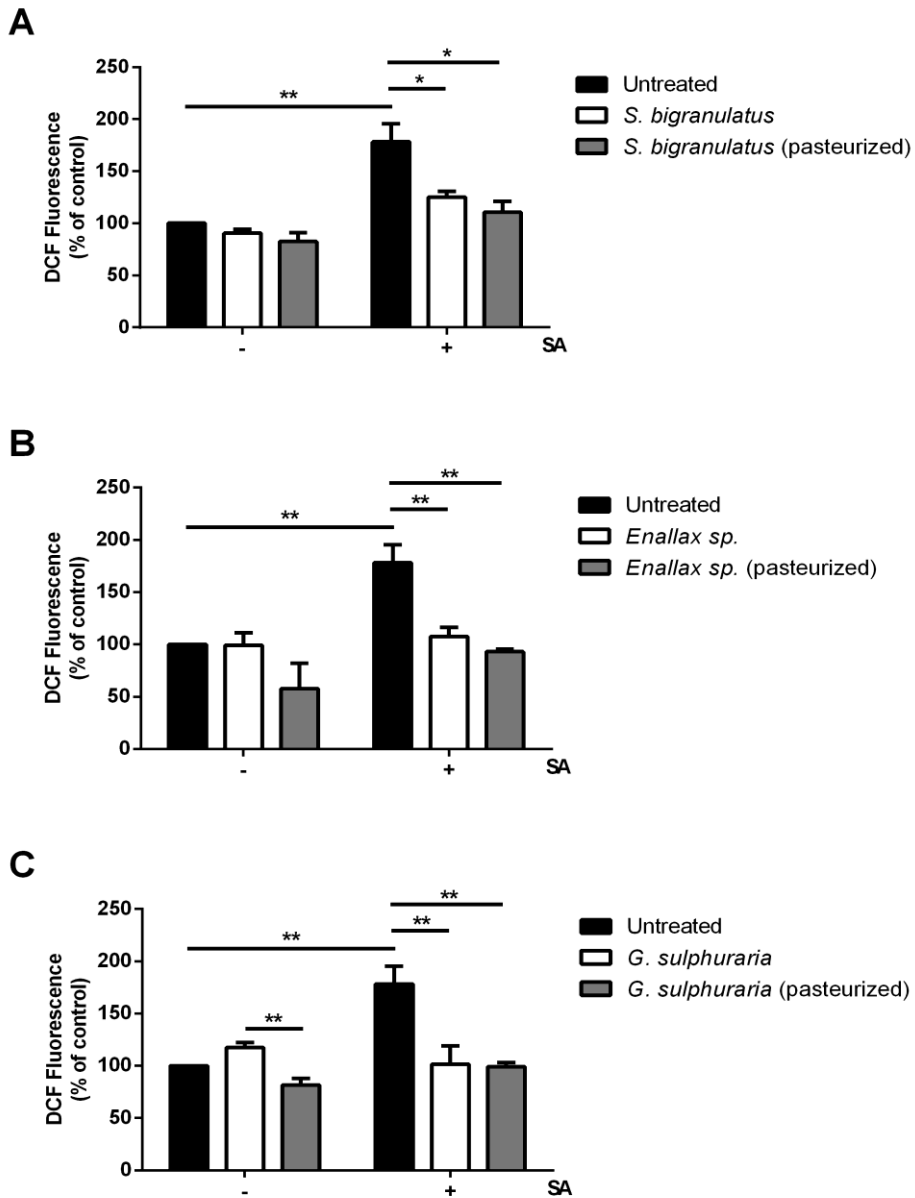


Figure 6. Comparison of antioxidant activity between raw and pasteurized extracts from *S. bigranulatus*, *Enallax sp.* and *G. sulphuraria* on SA-stressed HaCaT cells. Intracellular ROS levels were determined by DCFDA assay on: **A**, *S. bigranulatus*; **B**, *Enallax sp.*; **C**, *G. sulphuraria*. Cells were pre-incubated in the presence of 80 $\mu\text{g mL}^{-1}$ of unpasteurized (white bars) and 80 $\mu\text{g mL}^{-1}$ of pasteurized extract (grey bars) for 2 h, prior of SA treatment (300 μM , 60 min). Black bars refer to untreated cells in the absence (-) or in the presence (+) of SA. Values are expressed as percentage with respect to control (i.e. untreated) cells. Data are shown as means \pm standard deviation (S.D.). Three independent measurements were carried out. * indicates $p < 0.05$; ** indicates $p < 0.01$.

3.4 Discussion

The threshold of legally permitted synthetic food additives that can be used in the food industry is decreasing due to their suspected role as promoters of carcinoma, and their toxic effects on liver and kidney⁵¹. It has been demonstrated that natural β -carotene is superior to the synthetic one. In particular, the so called “natural β -carotene” is a mixture of carotenoids and nutrients, which are absent in synthetic β -carotene⁵². Hence, the substitution of synthetic pigments with natural ones is becoming mandatory. Moreover, during the thermal processes applied for food preservation, antioxidant molecules could lose their activity.

The aim of this work was to identify microalgae able to produce antioxidants resistant to thermal stress, to be used in the food industry. For this reason, ethanol was used as solvent^{48,53}. The growth of several strains from different phyla, able to grow between 40-70 °C, was followed overtime⁵⁴ and *Enallax sp.*, *S. bigranulatus* and *G. sulphuraria* were found to have the highest division per day and light yields. These results well correlate with antioxidant productivity, and can be compared with those obtained by Silva⁵⁵ for *S. bigranulatus*, and by Graziani⁵⁶ for *G. sulphuraria*. The highest content of pigments is observed in *Enallax sp.* and *S. bigranulatus* with a chlorophyll a content of 49.8 ± 3.2 mg g_{d.w.}⁻¹ and 11.1 ± 3.2 mg g_{d.w.}⁻¹, and a carotenoid content of 20.7 ± 3.4 mg g_{d.w.}⁻¹ and 5.4 ± 1.0 mg g_{d.w.}⁻¹. Nevertheless, the carotenoid content found in the used biomass samples falls within the range given by Spolaore⁵⁷, who found an average carotenoid content of 0.1-0.2 % of dry weight biomass. On the other hand, a high pigments content has been reported for *Galdieria* species, when the biomass was broken by French press or bead-beater⁵⁸. Cyanidiales are known to usually possess a strong cell wall (Merola et al. 1981) which protects cells from most of the extraction techniques used. Thus, in this experimental system, ultrasound treatment may not be sufficient to disrupt the biomass and to release pigments. However, Rubashvili analysed the carotenoid content of various agro-industrial wastes, and found that β -carotene content of tomato skin, tangerine peel and orange peel was 0.083-0.127, 0.256-0.321 and 0.416-0.591 mg g_{dried peel}⁻¹ respectively⁵⁹. These data clearly indicate that algal and cyanobacterial biomass are more advantageous for the extraction of these antioxidant molecules. Indeed, it has to be considered that these phytochemicals vary in structure and function from vegetable to vegetable and from cultivar to cultivar, and their level is strictly related

to the level of maturity, postharvest handling, processing, and geographical position⁶⁰.

The ethanol extracts of selected strains were analysed by HPLC, in order to collect more information about the specific pigments (carotenoids and chlorophylls). The main peaks of each species were identified^{56,61–63}. The overall picture showed a high variability of xanthophylls, both identified and not identified, among samples. The presence of pigments, such as xanthophylls, strongly depends on growth conditions, in particular light intensity and temperature⁶¹. In *G. sulphuraria* we found relatively high amount of chlorophylls and phaeophytin compared to other species, and *Enallax* sp. was the only species lacking zeaxanthin and presenting lutein and violaxanthin.

The biocompatibility results fully agree with those reported in literature. As an example, some authors found that antioxidants were toxic at high concentration, whereas low doses have a protective effect^{45,64,65}. Based on biocompatibility results, 80 µg mL⁻¹ of each extract was selected as the optimal concentration to be used to analyse the free radical scavenger activity against oxidative stress induced by SA before and after pasteurizing of extracts. Noteworthy, SA-induced ROS production was strongly inhibited when cells were pre-treated with both raw (30-40% decrease) and pasteurized (40-50% decrease) extracts of selected strains.

Thus, the antioxidants present in *Enallax* sp., *S. bigranulatus* and *G. sulphuraria* can be easily extracted in ethanol, are biologically active and resistant to pasteurization. This opens the way to the use of microalgal and cyanobacteria extracts in food preservation.

3.5 References

- (1) Villalobos-Delgado, L. H.; Mateo, J.; Caro, I.; Leal Ramos, M.-Y.; Mendez, N. G.; Cansino, R. G.; González Mondragón, E. G. Natural Antioxidants in Fresh and Processed Meat. In *Sustainable Meat Production and Processing*; Elsevier, 2019; pp 207–236. <https://doi.org/10.1016/b978-0-12-814874-7.00011-0>.
- (2) Liu, X.; Luo, G.; Wang, L.; Yuan, W. Optimization of Antioxidant Extraction from Edible Brown Algae *Ascophyllum Nodosum* Using Response Surface Methodology. *Food Bioprod. Process.* 2019, 114, 205–215. <https://doi.org/10.1016/J.FBP.2019.01.003>.
- (3) Elleuche, S.; Schäfers, C.; Blank, S.; Schröder, C.; Antranikian, G. Exploration of Extremophiles for High Temperature Biotechnological Processes. *Current Opinion in Microbiology.* June 2015, pp 113–119. <https://doi.org/10.1016/j.mib.2015.05.011>.
- (4) Urbietta, M. S.; Donati, E. R.; Chan, K. G.; Shahar, S.; Sin, L. L.; Goh, K. M. Thermophiles in the Genomic Era: Biodiversity, Science, and Applications. *Biotechnology Advances.* November 2015, pp 633–647. <https://doi.org/10.1016/j.biotechadv.2015.04.007>.

CHAPTER 3

- (5) Bhandiwad, A.; Guseva, A.; Lynd, L. Metabolic Engineering of *Thermoanaerobacterium Thermosaccharolyticum* for Increased n-Butanol Production. *Adv. Microbiol.* 2013, 03 (01), 46–51. <https://doi.org/10.4236/aim.2013.31007>.
- (6) Patel, A.; Matsakas, L.; Rova, U.; Christakopoulos, P. A Perspective on Biotechnological Applications of Thermophilic Microalgae and Cyanobacteria. *Bioresource Technology.* April 2019, pp 424–434. <https://doi.org/10.1016/j.biortech.2019.01.063>.
- (7) Ferraro, G.; Imbimbo, P.; Marseglia, A.; Illiano, A.; Fontanarosa, C.; Amoresano, A.; Olivieri, G.; Pollio, A.; Monti, D. M.; Merlino, A. A Thermophilic C-Phycocyanin with Unprecedented Biophysical and Biochemical Properties. *Int. J. Biol. Macromol.* 2020, 150, 38–51. <https://doi.org/10.1016/j.ijbiomac.2020.02.045>.
- (8) Malavasi, V.; Soru, S.; Cao, G. Extremophile Microalgae: The Potential for Biotechnological Application. *Journal of Phycology.* Blackwell Publishing Inc. February 2020, pp 559–573. <https://doi.org/10.1111/jpy.12965>.
- (9) Zuccaro, G.; Yousuf, A.; Pollio, A.; Steyer, J.-P. Microalgae Cultivation Systems. In *Microalgae Cultivation for Biofuels Production*; Elsevier, 2020; pp 11–29. <https://doi.org/10.1016/b978-0-12-817536-1.00002-3>.
- (10) Sidari, R.; Tofalo, R. A Comprehensive Overview on Microalgal-Fortified/Based Food and Beverages. *Food Reviews International.* Taylor and Francis Inc. 2019, pp 778–805. <https://doi.org/10.1080/87559129.2019.1608557>.
- (11) Metting, F. B. Biodiversity and Application of Microalgae. *J. Ind. Microbiol. Biotechnol.* 1996, 17 (5–6), 477–489. <https://doi.org/10.1007/bf01574779>.
- (12) Gualtieri, P. Morphology of Photoreceptor Systems in Microalgae. *Micron.* Pergamon June 2001, pp 411–426. [https://doi.org/10.1016/S0968-4328\(00\)00016-0](https://doi.org/10.1016/S0968-4328(00)00016-0).
- (13) Pulz, O.; Gross, W. Valuable Products from Biotechnology of Microalgae. *Applied Microbiology and Biotechnology.* Springer November 6, 2004, pp 635–648. <https://doi.org/10.1007/s00253-004-1647-x>.
- (14) Watson, S. B.; Whitton, B. A.; Higgins, S. N.; Paerl, H. W.; Brooks, B. W. Chapter 20 – Harmful Algal Blooms. In *Freshwater Algae of North America*; 2015; pp 873–920. <https://doi.org/10.1016/B978-0-12-385876-4.00020-7>.
- (15) Stirbet, A.; Lazár, D.; Papageorgiou, G. C.; Govindjee. Chlorophyll a Fluorescence in Cyanobacteria: Relation to Photosynthesis. In *Cyanobacteria: From Basic Science to Applications*; Elsevier, 2018; pp 79–130. <https://doi.org/10.1016/B978-0-12-814667-5.00005-2>.
- (16) Leliaert, F.; Smith, D. R.; Moreau, H.; Herron, M. D.; Verbruggen, H.; Delwiche, C. F.; De Clerck, O. Phylogeny and Molecular Evolution of the Green Algae. *CRC. Crit. Rev. Plant Sci.* 2012, 31 (1), 1–46. <https://doi.org/10.1080/07352689.2011.615705>.
- (17) Yoon, H. S.; Hackett, J. D.; Pinto, G.; Bhattacharya, D. The Single, Ancient Origin of Chromist Plastids. *Proc. Natl. Acad. Sci. U. S. A.* 2002, 99 (24), 15507–15512. <https://doi.org/10.1073/pnas.242379899>.
- (18) Yoon, H. S.; Müller, K. M.; Sheath, R. G.; Ott, F. D.; Bhattacharya, D. Defining the

- Major Lineages of Red Algae (Rhodophyta). *J. Phycol.* 2006, 42 (2), 482–492. <https://doi.org/10.1111/j.1529-8817.2006.00210.x>.
- (19) Jiménez Callejón, M. J.; Robles Medina, A.; González Moreno, P. A.; Esteban Cerdán, L.; Orta Guillén, S.; Molina Grima, E. Simultaneous Extraction and Fractionation of Lipids from the Microalga *Nannochloropsis* Sp. for the Production of EPA-Rich Polar Lipid Concentrates. *J. Appl. Phycol.* 2020, 32 (2), 1117–1128. <https://doi.org/10.1007/s10811-020-02037-z>.
- (20) Derwenskus, F.; Schäfer, B.; Müller, J.; Frick, K.; Gille, A.; Briviba, K.; Schmid-Staiger, U.; Hirth, T. Coproduction of EPA and Fucoxanthin with *P. Tricornutum* – A Promising Approach for Up- and Downstream Processing. *Chemie-Ingenieur-Technik* 2020, 92 (11), 1780–1789. <https://doi.org/10.1002/cite.202000046>.
- (21) Sampath-Wiley, P.; Neefus, C. D.; Jahnke, L. S. Seasonal Effects of Sun Exposure and Emersion on Intertidal Seaweed Physiology: Fluctuations in Antioxidant Contents, Photosynthetic Pigments and Photosynthetic Efficiency in the Red Alga *Porphyra Umbilicalis* Kützting (Rhodophyta, Bangiales). *J. Exp. Mar. Bio. Ecol.* 2008, 361 (2), 83–91. <https://doi.org/10.1016/j.jembe.2008.05.001>.
- (22) Gouveia, L.; Marques, A. E.; Sousa, J. M.; Moura, P.; Bandarra, N. M. Microalgae – Source of Natural Bioactive Molecules as Functional Ingredients. *Food Sci. Technol. Bull. Funct. Foods* 2010, 7 (2), 21–37. <https://doi.org/10.1616/1476-2137.15884>.
- (23) Matos, J.; Cardoso, C.; Bandarra, N. M.; Afonso, C. Microalgae as Healthy Ingredients for Functional Food: A Review. *Food and Function*. Royal Society of Chemistry August 1, 2017, pp 2672–2685. <https://doi.org/10.1039/c7fo00409e>.
- (24) Koyande, A. K.; Chew, K. W.; Rambabu, K.; Tao, Y.; Chu, D. T.; Show, P. L. Microalgae: A Potential Alternative to Health Supplementation for Humans. *Food Science and Human Wellness*. Elsevier BV March 2019, pp 16–24. <https://doi.org/10.1016/j.fshw.2019.03.001>.
- (25) Keddar, M. N.; Ballesteros-Gómez, A.; Amiali, M.; Siles, J. A.; Zerrouki, D.; Martín, M. A.; Rubio, S. Efficient Extraction of Hydrophilic and Lipophilic Antioxidants from Microalgae with Supramolecular Solvents. *Sep. Purif. Technol.* 2020, 251, 117327. <https://doi.org/10.1016/j.seppur.2020.117327>.
- (26) Böcker, L.; Ortman, S.; Surber, J.; Leeb, E.; Reineke, K.; Mathys, A. Biphasic Short Time Heat Degradation of the Blue Microalgae Protein Phycocyanin from *Arthrospira Platensis*. *Innov. Food Sci. Emerg. Technol.* 2019, 52 (November 2018), 116–121. <https://doi.org/10.1016/j.ifset.2018.11.007>.
- (27) Champenois, J.; Marfaing, H.; Pierre, R. Review of the Taxonomic Revision of *Chlorella* and Consequences for Its Food Uses in Europe. *J. Appl. Phycol.* 2015, 27 (5), 1845–1851. <https://doi.org/10.1007/s10811-014-0431-2>.
- (28) Regulation (EC) No 258/97. Implementation of Regulation (EC) No 258/97 of the European Parliament and of the Council of 27 January 1997 Concerning Novel Foods and Novel Food Ingredients. Directorate General Health and Consumer Protection. *extwprlegs1.fao.org* 2002, No. 258.
- (29) Barsanti, L.; Gualtieri, P. Is Exploitation of Microalgae Economically and Energetically Sustainable? *Algal Research*. Elsevier B.V. April 2018, pp 107–115.

- <https://doi.org/10.1016/j.algal.2018.02.001>.
- (30) Harvey, P. J.; Ben-Amotz, A. Towards a Sustainable Dunaliella Salina Microalgal Biorefinery for 9-Cis β -Carotene Production. *Algal Res.* 2020, 50, 102002. <https://doi.org/10.1016/j.algal.2020.102002>.
- (31) Ruiz, J.; Olivieri, G.; De Vree, J.; Bosma, R.; Willems, P.; Reith, J. H.; Eppink, M. H. M.; Kleinegris, D. M. M.; Wijffels, R. H.; Barbosa, M. J. Towards Industrial Products from Microalgae. *Energy and Environmental Science*. The Royal Society of Chemistry October 2016, pp 3036–3043. <https://doi.org/10.1039/c6ee01493c>.
- (32) Slegers, P. M.; Olivieri, G.; Breitmayer, E.; Sijtsma, L.; Eppink, M. H. M.; Wijffels, R. H.; Reith, J. H. Design of Value Chains for Microalgal Biorefinery at Industrial Scale: Process Integration and Techno-Economic Analysis. *Front. Bioeng. Biotechnol.* 2020, 8, 1048. <https://doi.org/10.3389/fbioe.2020.550758>.
- (33) Sangiorgio, P.; Verardi, A.; Editors, G.; Bardone, E.; Marzocchella, A.; Bravi, M.; Marino, T.; Casella, P.; Ferraro, A.; Hristoforou, E.; Molino, A.; Musmarra, D.; Fermi, E.; Enea, I. Natural Beta-Carotene: A Microalgae Derivate for Nutraceutical Applications Natural Beta-Carotene: A Microalgae Derivate for Nutraceutical Applications Energy and Sustainable Economic Development, Territorial and Production System Sustainability Departmen. In *CHEMICAL ENGINEERING TRANSACTIONS*; 2020; Vol. 79, p 2020. <https://doi.org/10.3303/CET2079018>.
- (34) Cheng, S.-H.; Khoo, H. E.; Kong, K. W.; Prasad, K. N.; Galanakis, C. M. Extraction of Carotenoids and Applications. In *Carotenoids: Properties, Processing and Applications*; Elsevier, 2020; pp 259–288. <https://doi.org/10.1016/b978-0-12-817067-0.00008-7>.
- (35) Marzorati, S.; Schievano, A.; Idà, A.; Verotta, L. Carotenoids, Chlorophylls and Phycocyanin from Spirulina: Supercritical CO₂ and Water Extraction Methods for Added Value Products Cascade. *Green Chem.* 2020, 22 (1), 187–196. <https://doi.org/10.1039/c9gc03292d>.
- (36) D’Elia, L.; Del Mondo, A.; Santoro, M.; De Natale, A.; Pinto, G.; Pollio, A. Microorganisms from Harsh and Extreme Environments: A Collection of Living Strains at ACUF (Naples, Italy). *Ecol. Quest.* 2018, 29 (3), 63–74. <https://doi.org/10.12775/EQ.2018.023>.
- (37) Bold, H. C. The Morphology of Chlamydomonas Chlamydogama , Sp . Nov . *Bull. Torrey Bot. Club* 1949, 76 (2), 101–108.
- (38) Rippka, R.; Deruelles, J.; Waterbury, J. B. Generic Assignments, Strain Histories and Properties of Pure Cultures of Cyanobacteria. *J. Gen. Microbiol.* 1979, 111 (1), 1–61. <https://doi.org/10.1099/00221287-111-1-1>.
- (39) Pruvost, J.; Cornet, J. F.; Goetz, V.; Legrand, J. Theoretical Investigation of Biomass Productivities Achievable in Solar Rectangular Photobioreactors for the Cyanobacterium Arthrospira Platensis. *Biotechnol. Prog.* 2012, 28 (3), 699–714. <https://doi.org/10.1002/btpr.1540>.
- (40) Andersen, R. ALGAL CULTURING TECHNIQUES. *J. Phycol.* 2005, 41 (4), 906–908. <https://doi.org/10.1111/j.1529-8817.2005.00114.x>.

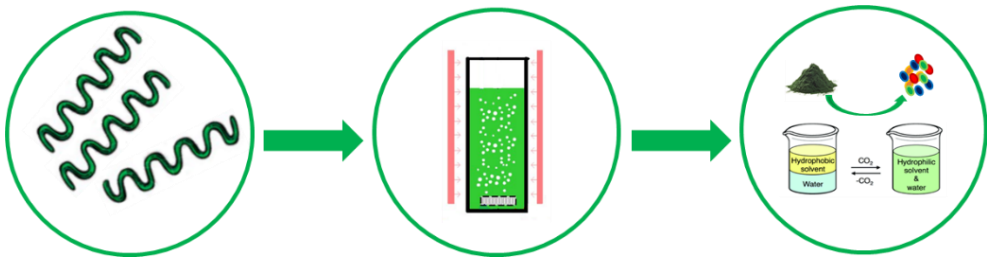
- (41) Aremu, A. O.; Masondo, N. A.; Molnár, Z.; Stirk, W. A.; Ördög, V.; Van Staden, J. Changes in Phytochemical Content and Pharmacological Activities of Three *Chlorella* Strains Grown in Different Nitrogen Conditions. *J. Appl. Phycol.* 2016, 28 (1), 149–159. <https://doi.org/10.1007/s10811-015-0568-7>.
- (42) Chen, Y.; Vaidyanathan, S. Simultaneous Assay of Pigments, Carbohydrates, Proteins and Lipids in Microalgae. *Anal. Chim. Acta* 2013, 776, 31–40. <https://doi.org/10.1016/j.aca.2013.03.005>.
- (43) Gilbert-López, B.; Mendiola, J. A.; Fontecha, J.; Van Den Broek, L. A. M.; Sijtsma, L.; Cifuentes, A.; Herrero, M.; Ibáñez, E. Downstream Processing of *Isochrysis Galbana*: A Step towards Microalgal Biorefinery. *Green Chem.* 2015, 17 (9), 4599–4609. <https://doi.org/10.1039/c5gc01256b>.
- (44) Vidussi, F.; Claustre, H.; Bustillos-Guzmán, J.; Cailliau, C.; Marty, J.-C. Determination of Chlorophylls and Carotenoids of Marine Phytoplankton: Separation of Chlorophyll a from Divinylchlorophyll a and Zeaxanthin from Lutein. *J. Plankton Res.* 1996, 18 (12), 2377–2382. <https://doi.org/10.1093/plankt/18.12.2377>.
- (45) Rigano, M. M.; Raiola, A.; Tenore, G. C.; Monti, D. M.; Del Giudice, R.; Frusciante, L.; Barone, A. Quantitative Trait Loci Pyramiding Can Improve the Nutritional Potential of Tomato (*Solanum Lycopersicum*) Fruits. *J. Agric. Food Chem.* 2014, 62 (47). <https://doi.org/10.1021/jf502573n>.
- (46) Galano, E.; Arciello, A.; Piccoli, R.; Monti, D. M.; Amoresano, A. A Proteomic Approach to Investigate the Effects of Cadmium and Lead on Human Primary Renal Cells. *Metallomics* 2014, 6 (3), 587–597. <https://doi.org/10.1039/c3mt00344b>.
- (47) Sobeh, M.; Youssef, F. S.; Esmat, A.; Petruk, G.; El-Khatib, A. H.; Monti, D. M.; Ashour, M. L.; Wink, M. High Resolution UPLC-MS/MS Profiling of Polyphenolics in the Methanol Extract of *Syzygium Samarangense* Leaves and Its Hepatoprotective Activity in Rats with CCl₄-Induced Hepatic Damage. *Food Chem. Toxicol.* 2018, 113 (December 2017), 145–153. <https://doi.org/10.1016/j.fct.2018.01.031>.
- (48) Assunção, M. F. G.; Amaral, R.; Martins, C. B.; Ferreira, J. D.; Ressurreição, S.; Santos, S. D.; Varejão, J. M. T. B.; Santos, L. M. A. Screening Microalgae as Potential Sources of Antioxidants. *J. Appl. Phycol.* 2017, 29 (2), 865–877. <https://doi.org/10.1007/s10811-016-0980-7>.
- (49) Goiris, K.; Muylaert, K.; Fraeye, I.; Foubert, I.; De Brabanter, J.; De Cooman, L. Antioxidant Potential of Microalgae in Relation to Their Phenolic and Carotenoid Content. *J. Appl. Phycol.* 2012, 24 (6), 1477–1486. <https://doi.org/10.1007/s10811-012-9804-6>.
- (50) Lauritano, C.; Andersen, J. H.; Hansen, E.; Albrigtsen, M.; Escalera, L.; Esposito, F.; Helland, K.; Hanssen, K.; Romano, G.; Ianora, A. Bioactivity Screening of Microalgae for Antioxidant, Anti-Inflammatory, Anticancer, Anti-Diabetes, and Antibacterial Activities. *Front. Mar. Sci.* 2016, 3 (MAY), 1–2. <https://doi.org/10.3389/fmars.2016.00068>.
- (51) El-Baky, A.; . F. K. E. B.; . G. S. E.-B. *Spirulina* Species as a Source of Carotenoids and A-Tocopherol and Its Anticarcinoma Factors. *Biotechnology(Faisalabad)* 2003, 2 (3), 222–240. <https://doi.org/10.3923/biotech.2003.222.240>.

- (52) Varfolomeev, S. D.; Wasserman, L. A. Microalgae as Source of Biofuel, Food, Fodder, and Medicines. *Applied Biochemistry and Microbiology*. Springer December 2011, pp 789–807. <https://doi.org/10.1134/S0003683811090079>.
- (53) Bulut, O.; Akın, D.; Sönmez, Ç.; Öktem, A.; Yücel, M.; Öktem, H. A. Phenolic Compounds, Carotenoids, and Antioxidant Capacities of a Thermo-Tolerant *Scenedesmus* Sp. (Chlorophyta) Extracted with Different Solvents. *J. Appl. Phycol.* 2019, 31 (3), 1675–1683. <https://doi.org/10.1007/s10811-018-1726-5>.
- (54) Varshney, P.; Mikulic, P.; Vonshak, A.; Beardall, J.; Wangikar, P. P. Extremophilic Micro-Algae and Their Potential Contribution in Biotechnology. *Bioresource Technology*. Elsevier Ltd May 2015, pp 363–372. <https://doi.org/10.1016/j.biortech.2014.11.040>.
- (55) Silva, C. S. P.; Silva-Stenico, M. E.; Fiore, M. F.; de Castro, H. F.; Da Rós, P. C. M. Optimization of the Cultivation Conditions for *Synechococcus* Sp. PCC7942 (Cyanobacterium) to Be Used as Feedstock for Biodiesel Production. *Algal Res.* 2014, 3 (1), 1–7. <https://doi.org/10.1016/j.algal.2013.11.012>.
- (56) Graziani, G.; Schiavo, S.; Nicolai, M. A.; Buono, S.; Fogliano, V.; Pinto, G.; Pollio, A. Microalgae as Human Food: Chemical and Nutritional Characteristics of the Thermo-Acidophilic Microalga *Galdieria Sulphuraria*. *Food Funct.* 2013, 4 (1), 144–152. <https://doi.org/10.1039/c2fo30198a>.
- (57) Spolaore, P.; Joannis-Cassan, C.; Duran, E.; Isambert, A. Commercial Applications of Microalgae. *J. Biosci. Bioeng.* 2006, 101 (2), 87–96. <https://doi.org/10.1263/jbb.101.87>.
- (58) Imbimbo, P.; Bueno, M.; D'Elia, L.; Pollio, A.; Ibañez, E.; Olivieri, G.; Monti, D. M. Green Compressed Fluid Technologies To Extract Antioxidants and Lipids from *Galdieria Phlegrea* in a Biorefinery Approach. *ACS Sustain. Chem. Eng.* 2020, 8 (7), 2939–2947. <https://doi.org/10.1021/acssuschemeng.9b07505>.
- (59) Rubashvili, I.; Tsitsagi, M.; Ebralidze, K.; Tsitsishvili, V.; Eprikashvili, L.; Chkhaidze, M.; Zautashvili, M. Extraction and Analysis of the Major Carotenoids of Agro-Industrial Waste Materials Using Sequential Extraction Techniques and High Performance Liquid Chromatography. *Eurasian J. Anal. Chem.* 2018, 13 (2). <https://doi.org/10.29333/ejac/82931>.
- (60) Jideani, A. I. O.; Silungwe, H.; Takalani, T.; Omolola, A. O.; Udeh, H. O.; Anyasi, T. A. Antioxidant-Rich Natural Fruit and Vegetable Products and Human Health. *Int. J. Food Prop.* 2021, 24 (1), 41–67. <https://doi.org/10.1080/10942912.2020.1866597>.
- (61) Moore, L. R.; Goericke, R.; Chisholm, S. W. Comparative Physiology of *Synechococcus* and *Prochlorococcus*: Influence of Light and Temperature on Growth, Pigments, Fluorescence and Absorptive Properties. *Mar. Ecol. Prog. Ser.* 1995, 116 (1–3), 259–276. <https://doi.org/10.3354/meps116259>.
- (62) Zimmermann, J. D. ar. F.; Sydney, E. B.; Cerri, M. L.; de Carvalho, I. K.; Schafranski, K.; Sydney, A. C. N.; Vitali, L.; Gonçalves, S.; Micke, G. A.; Soccol, C. R.; Demiate, I. M. Growth Kinetics, Phenolic Compounds Profile and Pigments Analysis of *Galdieria Sulphuraria* Cultivated in Whey Permeate in Shake-Flasks and Stirred-Tank Bioreactor. *J. Water Process Eng.* 2020, 38, 101598. <https://doi.org/10.1016/j.jwpe.2020.101598>.

- (63) Goecke, F.; Noda, J.; Paliocha, M.; Gislerød, H. R. Revision of *Coelastrella* (Scenedesmaceae, Chlorophyta) and First Register of This Green Coccoid Microalga for Continental Norway. *World J. Microbiol. Biotechnol.* 2020, 36 (10), 149. <https://doi.org/10.1007/s11274-020-02897-0>.
- (64) Imbimbo, P.; Romanucci, V.; Pollio, A.; Fontanarosa, C.; Amoresano, A.; Zarrelli, A.; Olivieri, G.; Monti, D. M. A Cascade Extraction of Active Phycocyanin and Fatty Acids from *Galdieria Phlegrea*. *Appl. Microbiol. Biotechnol.* 2019, 103 (23–24), 9455–9464. <https://doi.org/10.1007/s00253-019-10154-0>.
- (65) Petruk, G.; Gifuni, I.; Illiano, A.; Roxo, M.; Pinto, G.; Amoresano, A.; Marzocchella, A.; Piccoli, R.; Wink, M.; Olivieri, G.; Monti, D. M. Simultaneous Production of Antioxidants and Starch from the Microalga *Chlorella Sorokiniana*. *Algal Res.* 2018, 34, 164–174. <https://doi.org/10.1016/j.algal.2018.07.012>.

Chapter 4

*Hydrophobic molecules from *Spirulina platensis* grown in Thin Layer Photobioreactor at ATbiotech company*



Hydrophobic molecules from *Spirulina platensis* grown in *Thin Layer Photobioreactor* at ATlbiotech company

Abstract

The control of the growth parameters of microalgae and prevention of contamination in open ponds at an industrial scale is still difficult today. To overcome these problems, algae can be grown in photobioreactors, which are difficult and expensive to be implemented on an industrial scale. Other costs responsible for a slow market entry of microalgae are due to the use of conventional solvents, very harmful to the environment, to extract high values compounds. So, the aim of this chapter was to assess the growth of *Spirulina platensis* in a prototype thin-layer photobioreactor at the ATI-biotech company and, from a point of view of green chemistry, to extract antioxidants by using N-Ethylbutylamine switchable solvent.

4.1 Introduction

In recent years, microalgae and cyanobacteria have been considered sunlight-driven cell factories, as they can convert CO₂ in high values products¹. Rich in lipids, proteins and carbohydrates, they may become a valuable source to obtain energy, fuels, pharmaceutical molecules, cosmetics, food and feed².

However, even if from a theoretical point of view microalgae and cyanobacteria represent a huge and very convenient alternative to conventional feedstocks, three main drawbacks limit their use at large scale: (i) cultivation, (ii) harvesting, and (iii) downstream costs³⁻⁷.

The main problems related to algal processes are the costs associated to the control of growth parameters and risks related to contaminations^{8,9}.

To control them, microalgae and cyanobacteria are generally grown in photobioreactors (PBRs), which also allow obtaining high productivity yields and keeping the cultures axenic^{10,11}.

Moreover, the extraction processes account for up to 60% of the total expenditure of manufacturing microalgae-based^{12,13}. Noteworthy, the major conventional extraction techniques of hydrophobic compounds use organic solvents with many side effects on the environment and on human health. Therefore, the use of green innovative and safe extraction techniques is required¹⁴⁻¹⁶.

In this study, the green switchable solvent N-Ethylbutylamine (EBA), considered one of the most efficient secondary amines in extracting

CHAPTER 4

hydrophobic molecules from algal biomass¹⁷, was used to extract hydrophobic molecules from *Spirulina platensis* slurry, grown in thin layer photobioreactor. This work was carried out at ATI-biotech company.

Switchable solvents are particular non-volatile liquids that change their chemical and physical properties, in particular the polarity in response to an external supply of CO₂. Then, by removing CO₂ from the system using an inert gas, the solvent comes in its original state and can be reused for a second extraction process. Therefore, the recovery and reuse of the solvent in the extraction process, as well as the low energy consumption make switchable solvents green, economically and competitive.

4.2 Materials and methods

Thin layer Photobioreactor

A Thin Layer photobioreactor (Figure1) was made at ATI-biotech company. The reactor consisted of two glass sides (that enabled artificial illumination) supported by an aluminium structure. Two LED lamps (amberlight) were used for illumination and were located horizontally on each side of the reactor. The total volume of the photobioreactor was 15 L with a height of 90 cm, a breadth of 65 cm and a depth of 2.5 cm. The working volume was 11 L.

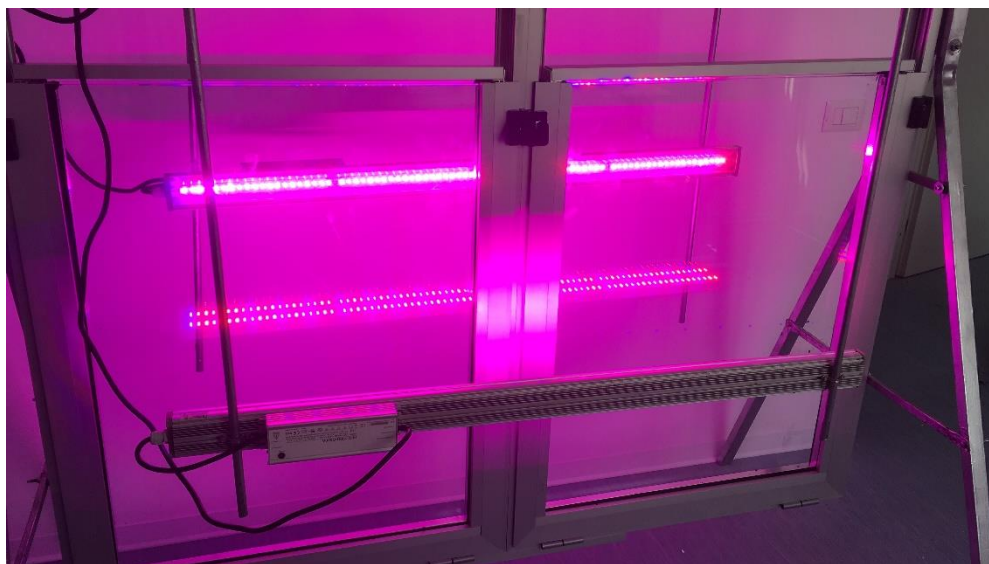


Figure 1. Thin layer photobioreactor prototype, 15 L, irradiated by two LED lamps. Light emitted was Blue 450nm and Red 620nm - 660nm - 735nm.

CHAPTER 4

Microorganisms and media composition

Spirulina platensis was cultivated in 1L bubble column photobioreactor (0.8L working volume) and in 15L thin layer photobioreactor (11L working volume), the initial concentration was 0.1 g L⁻¹, in Zarrouk liquid standard medium¹⁸ containing 2.50 g L⁻¹ sodium nitrates.

The aeration/mixing of cultures was provided by feeding air at the bottom of photobioreactors and 0.2 µm filters were used to sterilize air flow inlet and outlet. The cultures were maintained in a room under a 12 h light/12 h dark photoperiod at 30 °C, illuminated with two lamps which provided an irradiance of 40 µmol_{photons} m⁻² s⁻¹.

Analytical procedures

The concentration of cells (X) was determined daily using optical density measurements at 730 nm for 12 days. The conversion between the O.D. and the biomass dry weight was determined at the end of the exponential growth phase. The conversion factor was: 1 O.D. corresponded to 1.4 mg dry weight. The pH of the medium was acquired every day. The biomass concentration, biomass productivity, specific growth rate and doubling time were determined spectrophotometrically from fresh biomass. Cell productivity, specific growth rate and doubling time were calculated based on the following relations.

Cell productivity

Cell productivity (P_x) was calculated as the ratio of the variation in the concentration of cells ($X_f - X_i$) to cultivation time (T_c):

$$P_x = (X_f - X_i) / T_c$$

where X_f is the final concentration of cells at the time of cultivation T and X_i is the concentration of inoculum cells.

Specific growth rate and doubling time

The specific growth rate is given by the following equation:

$$\mu = \frac{\ln x_2 - \ln x_1}{t_2 - t_1}$$

Where the concentration of biomass at the time interval t_1 and t_2 is x_1 and x_2 .

CHAPTER 4

The doubling time (T_2) of the crop is defined by:

$$T_2 = \frac{\ln}{\mu} = \frac{0.6931}{\mu}$$

Conventional hydrophobic molecules extraction

Hydrophobic molecules were extracted starting from wet biomass (1g), according to the original B&D method¹⁹, and the content was determined gravimetrically.

Switchable solvents extraction

Slurry biomass (2 g L⁻¹) was mixed with N-Ethylbutylamine (EBA) in a ratio of 1:2 (wt/wt). The mixture was magnetically stirred at room temperature for 18h to ensure extraction of hydrophobic molecules. Then, the mixture was centrifuged at 9000g at r.t. and the supernatant (which contains EBA and hydrophobic molecules) was mixed with water in a ratio of 1:2 (wt/wt), forming a biphasic system. CO₂ was bubbled through the system for 30 min at 2vvm (volume volume per minute) to allow EBA to switch in its polar form (switching forward). The sample was centrifuged at 9000g at r.t., and, at the end of centrifugation, EBA and water formed a homogeneous phase with a small lipid layer on the top. The hydrophobic molecules were recovered by chloroform. The total amount of the extracted product was measured gravimetrically (after evaporating the solvent) and reported as a percentage on algae dry weight.

Pigments quantification

To determine pigments concentration, both extracts (B&D and EBA) were resuspended in methanol (10 mg mL⁻¹). Pigments concentration was determined spectrophotometrically; spectra were acquired in the range 400-700 nm. The amount of pigments was calculated using formulae (1)-(3), derived for methanol solvent²⁰:

$$\text{Chl } a = 15.65 \cdot A_{666 \text{ nm}} - 7.34 \cdot A_{653 \text{ nm}} \quad (1)$$

$$\text{Chl } b = 27.05 \cdot A_{653 \text{ nm}} - 11.21 \cdot A_{666 \text{ nm}} \quad (2)$$

$$\text{Carotenoids} = \frac{1000 \cdot A_{470 \text{ nm}} - 2.86 \cdot \text{Chl } a - 192.2 \cdot \text{Chl } b}{221} \quad (3)$$

The results were expressed as mg of pigments g⁻¹ of biomass dry weight.

CHAPTER 4

4.3 Results and Discussion

Growth and Biomass Productivity

Spirulina platensis growth rate and biomass yield depend on nutrients availability, pH, light and temperature. Growth rate was analyzed in two closed systems: a thin layer PBR and a bubble column PBR. The experiment was done in order to verify if any difference was present in the two closed systems which have differences in the final volume, and in the irradiation surface. Cell growth was followed daily by measuring the optical density at 730 nm. Figure 2 shows the growth curve in the bubble column PBR (A) and in the thin layer PBR (B), both housed in a climate room at 30°C, the best growth temperature for this cyanobacterium²¹.

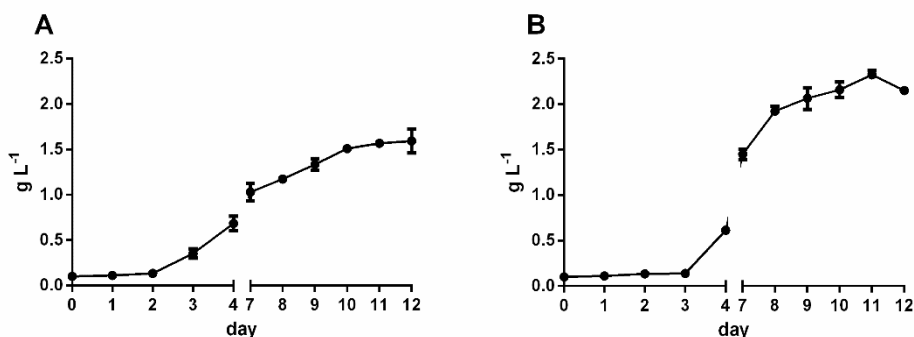


Figure 2. Growth curves of *S. platensis* in A) bubble column photobioreactor and in B) thin layer PBR, at 30°C with a light intensity of 40 $\mu\text{mol}_{\text{photons}} \text{m}^{-2} \text{s}^{-1}$. Growth is expressed as biomass dry weight concentration as a function of time.

In both cell cultures it is possible to observe the initial lag phase (about 3 days) followed by an exponential phase which reaches a plateau after 12 days. Values for maximum specific growth rate (μ), doubling time (T_2), biomass concentration (X) and biomass productivity (P_x) are shown in Table 1.

Table 1. Specific growth rate (μ), doubling time (T_2), biomass concentration (X) and biomass productivity (P_x) of *S. platensis*

PBR	μ (h ⁻¹)	T_2 (h ⁻¹)	X (g L ⁻¹ d.w.)	P_x (g L ⁻¹ h ⁻¹ d.w.)
Bubble column	0.024 ± 0.001	28.4 ± 0.6	1.6 ± 0.2	0.0072 ± 0.0003
Thin layer	0.031 ± 0.001	22.0 ± 0.1	2.3 ± 0.1	0.01 ± 0.0004

Biomass productivity was higher in the thin layer PBR ($10.5 \pm 0.4 \text{ mg L}^{-1} \text{ h}^{-1} \text{ d.w.}$) with respect to that achieved in the bubble column PBR ($7.2 \pm 0.3 \text{ mg L}^{-1} \text{ h}^{-1} \text{ d.w.}$). This may be due to a difference in the light penetration between the two PBRs, as in the thin layer PBR the light incidence surface is major, thus availability of light for each cell increases, with a consequent increase in growth rate. During the experiment, pH was measured, as this parameter is one of those affecting the microalgal cell metabolism. Figure 3 shows the pH trend of both cultures. The observed values were similar between the two cultures, and in agreement with data reported in literature (pH 9.5-10.5). Indeed, as reported by Ai et al., the pH level of the medium increased during photosynthesis as a consequence of nutrient uptake, such as bicarbonate and nitrate²².

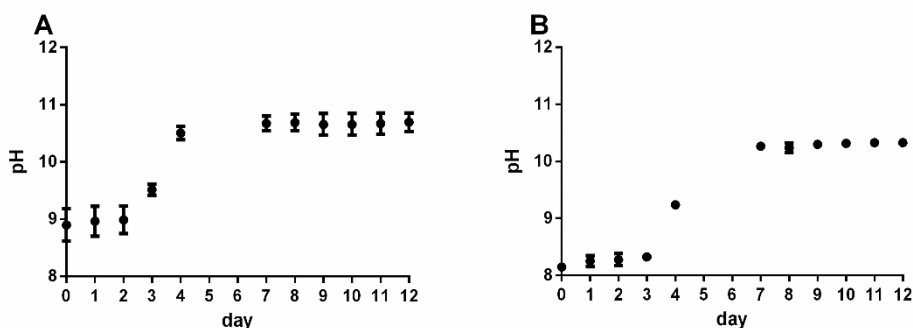


Figure 3. pH monitoring during cultivation of *S. platensis*. A) pH trend in bubble column PBR and B) pH trend in thin layer PBR. The pH value is reported as a function of time.

Hydrophobic molecules extraction

The ability of N-Ethylbutylamine switchable solvent (EBA) to extract and recover antioxidants directly from *S. platensis* slurry was verified by comparing the results with the conventional Bligh & Dyer extraction.

Initially, EBA was mixed with slurry biomass ($2 \text{ g L}^{-1} \text{ d.w.}$) to ensure the extraction of molecules. Then, after removing the residual algal biomass by centrifugation, the organic layer (EBA plus extracted hydrophobic molecules) was mixed with water. By bubbling CO_2 into the system, the solvent switched in its polar form, soluble in water. Then, the mixture was centrifuged, and the extracted hydrophobic molecules floated on the surface of the system. At this point, extracted compounds were collected with chloroform. The yield of extracted molecules was $6.9 \pm 1 \%$ (Figure 4, grey bar), whereas the B&D

CHAPTER 4

method allowed to recover 4.9 ± 0.5 % of hydrophobic molecules (Figure 4, black bar).

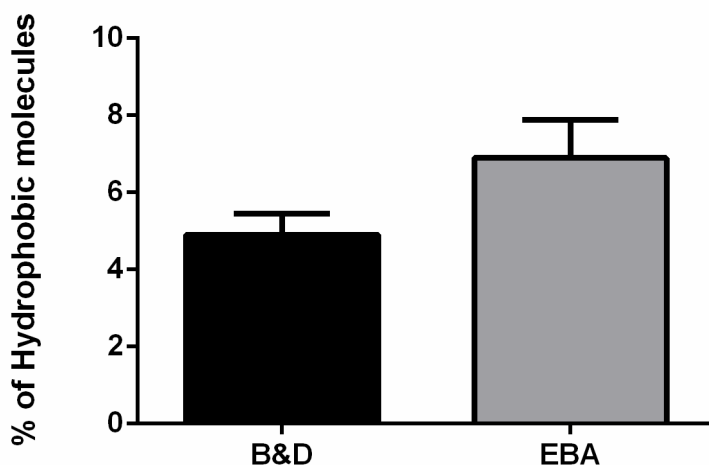


Figure 4. Hydrophobic molecules extracted from *S. platensis* biomass. Yields are reported as % with respect to dry weight biomass. B&D is referred to Bligh & Dyer, EBA to extraction by switchable solvent. Results are reported as means \pm S.D. of at least two independent experiments.

Algae and cyanobacteria cell wall microstructure differs among species. The cyanobacterium *Spirulina platensis* has a relatively fragile cell wall, composed mainly of murein and no cellulose, therefore it can be easily destroyed even with mild treatments, such as maceration in organic solvents. Other algal species, such as Chlorophycean, have a cell wall rich in cellulose and hemicellulose and *H. pluvialis* exhibits a thick tri-laminar cell wall composed of cellulose and sporopollenin. Thus, these algal cell wall are less permeable and extremely resistant to mechanical treatments. Generally speaking, the efficiency of extracting components from microalgae is inversely related to the rigidity of cell wall. In the case of switchable solvents extraction, several studies showed that the solvents are able to completely destroy the algae cell wall in species with a fragile cell wall, whereas, when algae have a strong cell wall, secondary and tertiary amine can destroy only the cell membrane leaving intact cell wall²³.

By comparing the hydrophobic fraction yields obtained with both extraction methods, no significant differences were observed. This means that EBA is able to destroy the cell wall of *Spirulina* cells and allows the extraction of hydrophobic molecules similarly to conventional methods, such as B&D. Noteworthy, EBA was able to

extract molecules directly from algal culture, which represent a great advantage from an energy expenditure point of view. These results are in agreement with those reported in literature, in which the ability of EBA to extract hydrophobic molecules either non-broken wet biomass or algal culture has been demonstrated^{17,24}.

Pigments quantification

The carotenoids content in both extracts was similar, as reported in Table 1. This value is comparable to that obtained by Marzorati et al., who used supercritical CO₂ as an extraction method²⁵. In the B&D extract, chlorophyll a ($45.8 \pm 5.1 \text{ mg}_{\text{pigments}} \text{ g}_{\text{extract}}^{-1}$) was much higher than in the EBA extract ($20.1 \pm 0.8 \text{ mg}_{\text{pigments}} \text{ g}_{\text{extract}}^{-1}$). No chlorophyll b was found in both extracts. In both cases, the extraction of chlorophylls was performed by maceration. However, the difference in the yield of chlorophylls between B&D and EBA may be due to the fact that B&D extraction was done on dry biomass. Indeed, it is known that drying cells will enhance cell disruption, thus improving chlorophyll extraction^{23,26}.

Table 1. Comparison of pigments content of *S. platensis* obtained with B&D and EBA switchable solvent. Pigments content is expressed as mg of extract on g of dry weight biomass

extraction method	total carotenoids (mg _{pigments} g _{extract} ⁻¹)	chlorophyll a (mg _{pigments} g _{extract} ⁻¹)	chlorophyll b (mg _{pigments} g _{extract} ⁻¹)
B&D	4.5 ± 1.0	44.4 ± 3.2	-
EBA	5.0 ± 0.6	20.1 ± 0.8	-

4.4 Conclusion

The results of this work show that thin-layer PBRs are very promising for the controlled production of algal biomass and allow higher productivity than tubular PBRs. In addition, switchable solvents are a great alternative in the development of energy-efficient extraction technology for hydrophobic molecules from the aqueous suspension of unbroken algae.

4.5 References

- (1) Ruiz, J.; Olivieri, G.; de Vree, J.; Bosma, R.; Willems, P.; Reith, J. H.; Eppink, M. H. M.; Kleinegris, D. M. M.; Wijffels, R. H.; Barbosa, M. J. Towards Industrial Products from Microalgae. *Energy Environ. Sci.* **2016**, 9 (10), 3036–3043. <https://doi.org/10.1039/C6EE01493C>.
- (2) Matos, J.; Cardoso, C.; Bandarra, N. M.; Afonso, C. Microalgae as Healthy Ingredients for Functional Food: A Review. *Food and Function*. Royal Society of Chemistry August 2017, pp 2672–2685. <https://doi.org/10.1039/c7fo00409e>.
- (3) Günerken, E.; D'Hondt, E.; Eppink, M. H. M.; Garcia-Gonzalez, L.; Elst, K.; Wijffels, R. H. Cell Disruption for Microalgae Biorefineries. *Biotechnology Advances*. Elsevier Inc. March 1, 2015, pp 243–260. <https://doi.org/10.1016/j.biotechadv.2015.01.008>.
- (4) Zhang, T. Y.; Hu, H. Y.; Wu, Y. H.; Zhuang, L. L.; Xu, X. Q.; Wang, X. X.; Dao, G. H. Promising Solutions to Solve the Bottlenecks in the Large-Scale Cultivation of Microalgae for Biomass/Bioenergy Production. *Renewable and Sustainable Energy Reviews*. Elsevier Ltd July 1, 2016, pp 1602–1614. <https://doi.org/10.1016/j.rser.2016.02.008>.
- (5) Lee, S. Y.; Cho, J. M.; Chang, Y. K.; Oh, Y. K. Cell Disruption and Lipid Extraction for Microalgal Biorefineries: A Review. *Bioresource Technology*. Elsevier Ltd November 1, 2017, pp 1317–1328. <https://doi.org/10.1016/j.biortech.2017.06.038>.
- (6) Gifuni, I.; Pollio, A.; Safi, C.; Marzocchella, A.; Olivieri, G. Current Bottlenecks and Challenges of the Microalgal Biorefinery. *Trends in Biotechnology*. Elsevier Ltd March 1, 2019, pp 242–252. <https://doi.org/10.1016/j.tibtech.2018.09.006>.
- (7) Imbimbo, P.; D'Elia, L.; Liberti, D.; Olivieri, G.; Monti, D. M. Towards Green Extraction Methods from Microalgae Learning from the Classics. *Applied Microbiology and Biotechnology*. Springer Science and Business Media Deutschland GmbH November 1, 2020, pp 9067–9077. <https://doi.org/10.1007/s00253-020-10839-x>.
- (8) Wang, H.; Zhang, W.; Chen, L.; Wang, J.; Liu, T. The Contamination and Control of Biological Pollutants in Mass Cultivation of Microalgae. *Bioresource Technology*. Elsevier Ltd January 1, 2013, pp 745–750. <https://doi.org/10.1016/j.biortech.2012.10.158>.
- (9) Molina, D.; de Carvalho, J. C.; Júnior, A. I. M.; Faulds, C.; Bertrand, E.; Socol, C. R. Biological Contamination and Its Chemical Control in Microalgal Mass Cultures. *Applied Microbiology and Biotechnology*. Springer December 1, 2019, pp 9345–9358. <https://doi.org/10.1007/s00253-019-10193-7>.
- (10) Benedetti, S.; Benvenuti, F.; Pagliarani, S.; Francogli, S.; Scoglio, S.; Canestrari, F. Antioxidant Properties of a Novel Phycocyanin Extract from the Blue-Green Alga *Aphanizomenon Flos-Aquae*. *Life Sci.* **2004**, 75 (19), 2353–2362. <https://doi.org/10.1016/j.lfs.2004.06.004>.
- (11) Liu, X.; Luo, G.; Wang, L.; Yuan, W. Optimization of Antioxidant Extraction from Edible Brown Algae *Ascophyllum Nodosum* Using Response Surface Methodology. *Food Bioprod. Process.* **2019**, 114, 205–215. <https://doi.org/10.1016/J.FBP.2019.01.003>.
- (12) Jacob-Lopes, E.; Maroneze, M. M.; Deprá, M. C.; Sartori, R. B.; Dias, R. R.; Zepka, L. Q. Bioactive Food Compounds from Microalgae: An Innovative Framework on Industrial Biorefineries. *Current Opinion in Food Science*. Elsevier Ltd February 1,

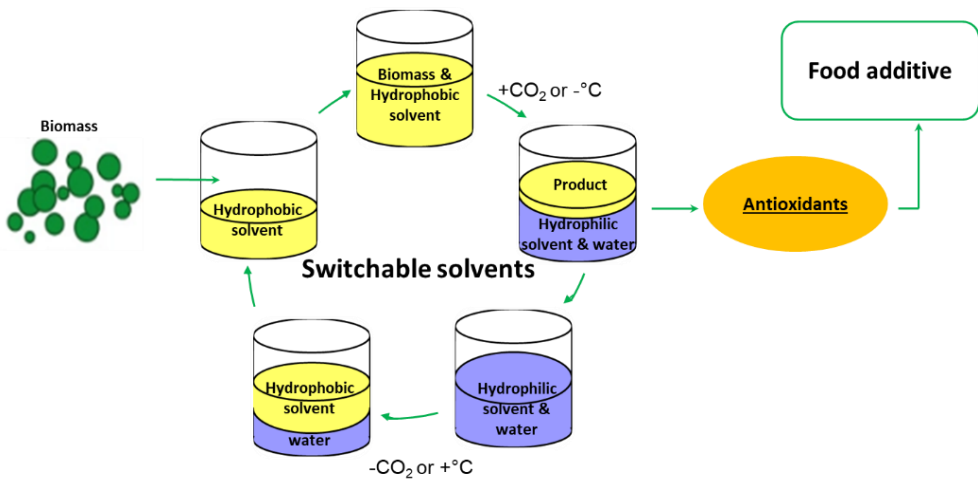
- 2019, pp 1–7. <https://doi.org/10.1016/j.cofs.2018.12.003>.
- (13) Chew, K. W.; Yap, J. Y.; Show, P. L.; Suan, N. H.; Juan, J. C.; Ling, T. C.; Lee, D. J.; Chang, J. S. Microalgae Biorefinery: High Value Products Perspectives. *Bioresour. Technol.* **2017**, *229*, 53–62. <https://doi.org/10.1016/j.biortech.2017.01.006>.
- (14) Khan, M. I.; Shin, J. H.; Kim, J. D. The Promising Future of Microalgae: Current Status, Challenges, and Optimization of a Sustainable and Renewable Industry for Biofuels, Feed, and Other Products. *Microbial Cell Factories*. BioMed Central Ltd. March 5, 2018. <https://doi.org/10.1186/s12934-018-0879-x>.
- (15) Eppink, M. H. M.; Olivieri, G.; Reith, H.; van den Berg, C.; Barbosa, M. J.; Wijffels, R. H. From Current Algae Products to Future Biorefinery Practices: A Review. In *Advances in Biochemical Engineering/Biotechnology*; Springer Science and Business Media Deutschland GmbH, 2019; Vol. 166, pp 99–123. https://doi.org/10.1007/10_2016_64.
- (16) Gilbert-López, B.; Mendiola, J. A.; Fontecha, J.; Van Den Broek, L. A. M.; Sijtsma, L.; Cifuentes, A.; Herrero, M.; Ibáñez, E. Downstream Processing of Isochrysis Galbana: A Step towards Microalgal Biorefinery. *Green Chem.* **2015**, *17* (9), 4599–4609. <https://doi.org/10.1039/c5gc01256b>.
- (17) Du, Y.; Schuur, B.; Samorì, C.; Tagliavini, E.; Brilman, D. W. F. Secondary Amines as Switchable Solvents for Lipid Extraction from Non-Broken Microalgae. *Bioresour. Technol.* **2013**, *149*, 253–260. <https://doi.org/10.1016/j.biortech.2013.09.039>.
- (18) ZARROUK; C. Contribution a l'etude d'une Cyanophyce. Influence de Divers Facteurs Physiques et Chimiques Sur La Croissance et La Photosynthese de *Spirulina Mixima*. *Thesis. Univ. Paris, Fr.* **1966**.
- (19) BLIGH, E. G.; DYER, W. J. A Rapid Method of Total Lipid Extraction and Purification. *Can. J. Biochem. Physiol.* **1959**, *37* (8), 911–917. <https://doi.org/10.1139/o59-099>.
- (20) Chen, Y.; Vaidyanathan, S. Simultaneous Assay of Pigments, Carbohydrates, Proteins and Lipids in Microalgae. *Anal. Chim. Acta* **2013**, *776*, 31–40. <https://doi.org/10.1016/j.aca.2013.03.005>.
- (21) Colla, L. M.; Oliveira Reinehr, C.; Reichert, C.; Costa, J. A. V. Production of Biomass and Nutraceutical Compounds by *Spirulina Platensis* under Different Temperature and Nitrogen Regimes. *Bioresour. Technol.* **2007**, *98* (7), 1489–1493. <https://doi.org/10.1016/j.biortech.2005.09.030>.
- (22) Ai, W.; Guo, S.; Qin, L.; Tang, Y. Development of a Ground-Based Space Micro-Algae Photo-Bioreactor. *Adv. Sp. Res.* **2008**, *41* (5), 742–747. <https://doi.org/10.1016/j.asr.2007.06.060>.
- (23) Halim, R.; Hosikian, A.; Lim, S.; Danquah, M. K. Chlorophyll Extraction from Microalgae: A Review on the Process Engineering Aspects. *International Journal of Chemical Engineering*. 2010. <https://doi.org/10.1155/2010/391632>.
- (24) Samorì, C.; Barreiro, D. L.; Vet, R.; Pezzolesi, L.; Brilman, D. W. F.; Galletti, P.; Tagliavini, E. Effective Lipid Extraction from Algae Cultures Using Switchable Solvents. *Green Chem.* **2013**, *15* (2), 353–356. <https://doi.org/10.1039/C2GC36730K>.
- (25) Marzorati, S.; Schievano, A.; Idà, A.; Verotta, L. Carotenoids, Chlorophylls and Phycocyanin from *Spirulina*: Supercritical CO₂ and Water Extraction Methods for Added Value Products Cascade. *Green Chem.* **2020**, *22* (1), 187–196. <https://doi.org/10.1039/c9gc03292d>.

CHAPTER 4

- (26) Safi, C.; Zebib, B.; Merah, O.; Pontalier, P. Y.; Vaca-Garcia, C. Morphology, Composition, Production, Processing and Applications of Chlorella Vulgaris: A Review. *Renewable and Sustainable Energy Reviews*. Elsevier Ltd July 1, 2014, pp 265–278. <https://doi.org/10.1016/j.rser.2014.04.007>.

Chapter 5

*Switchable solvent selective extraction of hydrophobic antioxidants from *Synechococcus bigranulatus**



Submitted to **ACS Sustainable Chemistry & Engineering**

**Switchable solvent selective extraction of hydrophobic
antioxidants from *Synechococcus bigranulatus***

Luigi D'Elia^a, Paola Imbimbo^a, Davide Liberti^a, Francesco Bolinesi^b,
Antonino Pollio^b, Olga Mangoni^b, Derk Willem Frederik Brillman^e
Giuseppe Olivieri^{c,d}, Daria Maria Monti^{a,f*}

^a Department of Chemical Science, University of Naples Federico II, via
Cinthia 4, 80126, Naples, Italy

^b Department of Biology, University of Naples Federico II, via Cinthia 4,
80126, Naples, Italy

^c Bioprocess Engineering Group, Wageningen University and
Research, Droevendaalsesteeg 1, 6700AA, Wageningen, the
Netherlands

^d Department of Chemical, Materials and Industrial Engineering,
University of Naples Federico II, Piazzale Tecchio 80, 80125, Napoli,
Italy

^e University of Twente, Sustainable Process Technology Group (SPT),
Green Energy Initiative, Faculty of Science and Technology, PO Box
217, 7500 AE Enschede, The Netherlands

^f Istituto Nazionale di Biostrutture e Biosistemi (INBB), Rome, Italy

Abstract

In this study, hydrophobic molecules, in particular carotenoids, were extracted from *Synechococcus bigranulatus* ACUF680 fresh and frozen biomass, using secondary amine switchable solvent N-Ethylbutylamine (EBA). EBA was able to extract hydrophobic molecules from both fresh and frozen biomass at the same extent of the conventional procedure. In particular, two fractions, enriched specifically in zeaxanthin or β -carotene, were obtained. The yields of both fractions were higher than those obtained by conventional methods. These fractions showed *in vitro* antioxidant activity and biocompatibility on immortalized human cells. Moreover both fractions are able to protect cells from oxidative stress, both before and after thermal treatment. Results clearly indicate that EBA is a perfect candidate to specifically extract β -carotene and zeaxanthin from the wet biomass of *Synechococcus bigranulatus*, without affecting their biological activity. The possibility to avoid cell disruption or energy-

CHAPTER 5

intensive equipment to broke the cells, to use either fresh or frozen biomass are important factors that will allow the use of SS on an industrial scale.

5.1 Introduction

In the last decades, the search for energy from renewable sources and the increasing demand of consumers for healthy foods, have driven the attention also toward microalgae and cyanobacteria¹⁻⁴. These phototrophic microorganisms can be rich in high value biological compounds, such as proteins, polysaccharides, polyunsaturated fatty acids, vitamins and pigments with special biological activities, thus they can potentially be exploited in several industrial sectors and meet many new consumer wishes⁴⁻⁶.

Today, algae and cyanobacteria are used only in the food industry as an additive for functional food and as food supplements. Nevertheless, the increasing demand for natural antioxidants, as a healthy alternative to synthetic additives in industrial food, has strengthened microalgae and cyanobacteria as a valid source of natural antioxidants⁷⁻¹³. In addition, natural carotenoids exhibit greater stability than synthetic ones¹⁴.

The main antioxidants produced by microalgae and cyanobacteria are polyphenols and pigments¹⁵. Among pigments, carotenoids show the highest antioxidant activity. These tetraterpenes are accessory pigments of the light-harvesting photosystems, which exhibit yellow, orange, red and purple colour. They are divided into two groups: carotenes and xanthophylls. Carotenoids mostly used in the global market are astaxanthin, β -carotene, lutein, canthaxanthin, lycopene, and zeaxanthin¹⁶.

To date, antioxidants extraction is usually performed by using organic solvents^{10,17,18}. However, these benchmark technologies suffer from several drawbacks, making the whole process unsustainable: (i) the use of high amounts of solvent; (ii) the need of a large amount of energy to recover solvent by evaporation; (iii) the need of more than one extraction step; (iv) the recovery of a single class of molecules^{19,20 21}.

These drawbacks are even more consistent in the case of antioxidants from microalgae, as they already suffer from upstream processes. Thus, the optimization of a green extraction technique, able to replace conventional ones seems to be a good starting point for lowering the costs. So far, it has been reported that the new green extraction techniques performed at high pressure, such as supercritical fluid extraction (SFE) and pressurised liquid extraction (PLE) are more

CHAPTER 5

sustainable and can be competitive in the effectiveness of the extraction of hydrophobic molecules^{22,23}. However, these innovative technologies show some drawbacks: (i) biomass pretreatment; (ii) impossibility to extract hydrophilic molecules; (iii) high investments costs and (iv) difficulty to scale up the process at an industrial scale^{21,24}. In this context, a new class of solvents is emerging: switchable solvents.

Switchable solvents (SSs), first reported by Jessop and Liotta^{25,26} are liquids that can be converted from non-polar form to polar form and *vice versa*. The switching of the solvent in the hydrophilic form (switch forward) is done by bubbling CO₂ through the solvent. The reverse reaction is induced by removing CO₂ from the system with an inert gas such as N₂ and is enhanced by heating²⁷. Noteworthy, the circularity of the extraction process on wet biomass involves a significant reduction in energy requirements because the separation of the solvent from the extract is not performed by evaporation^{28,29}.

Recently, a study carried out by Du et al. reported that the secondary amine N-Ethylbutylamine (EBA) shows a lower critical solution temperature (LCST) behaviour, which means a change in EBA polarity with temperature³⁰. This system is expected to be a cost and energy efficient alternative process configuration to the CO₂ switching system³⁰.

Here, EBA was chosen to set up an innovative procedure to selectively extract hydrophobic antioxidants from the cyanobacterium *Synechococcus bigranulatus*.

First, the carotenoids were extracted from the biomass using the switchable solvent in its lower polar (lipophilic) form. Then, by decreasing the temperature of the system, from 22°C to 0°C, the solvent switched into its polar form, thus allowing the separation of the nonpolar hydrophobic molecules from the SS. After having collected the hydrophobic molecules, the solvent can be returned to its original state by increasing the temperature at 22°C. When the SS returned into its original state the system showed two phases. The upper phase is the solvent in the “lipophilic” form, whereas the lower phase is the aqueous one with hydrophilic molecules. Hydrophobic molecules were finally characterized from a chemical and biological point of view.

5.2 Materials and Methods

Reagents

All solvents and chemicals, unless differently specified, were from Sigma–Aldrich.

CHAPTER 5

Microalgal Strain and Culture Conditions

Synechococcus bigranulatus was provided from the Algal Collection of the University Federico II (ACUF number 680)³¹. Cells were grown in autotrophic conditions in bubble column photobioreactors characterized by 800 mL working volume in BG11 medium. The photobioreactors were housed in a climate chamber at 37 ± 1 °C equipped with fluorescent lamps with a constant light intensity of 300 PAR $\mu\text{mol}_{\text{photons}} \text{m}^{-2} \text{s}^{-1}$. The aeration of cultures was provided by feeding air at the bottom of the photobioreactors. Cell density was inferred from the absorbance measured at a wavelength of 730 nm. The culture was harvested at the end of exponential phase and biomass concentration was about 0.8 g L^{-1} dry weight.

Water content of *S. bigranulatus*

The dry weight content of the harvested wet microalgae paste was determined from the difference in the weight of the sample before and after drying at 60 °C for 24 h. The water content did not change significantly among samples and was 73.1 ± 3.3 %.

Protein extraction and quantification

The biomass was harvested by centrifugation at 1200g for 30 min at room temperature. Then, 1.5 g of wet biomass, which corresponds to about 400 mg d.w., was resuspended in 50 mM sodium acetate pH 5.5³². Cells were disrupted by ultrasonication (30 seconds, 30 seconds of 40% instrument amplitude) for 45 minutes. After centrifugation at 5000g at 4 °C for 30 min, proteins were recovered in the supernatant and their concentration was measured by BCA Assay Kit.

Conventional extraction of total hydrophobic molecules

Conventional extraction of hydrophobic molecules from wet algal biomass (1g) was done according to the original B&D method³³.

Hydrophobic molecules extraction by N-Ethylbutylamine

To extract hydrophobic molecules from *S. bigranulatus* by EBA, wet biomass (~1.5 g) was mixed with EBA in a ratio of 1:2 (wt/wt). The mixture was magnetically stirred at room temperature for 18h to ensure extraction of hydrophobic molecules. Then, the mixture was centrifuged at 9000g at r.t. and the supernatant (which contains EBA and hydrophobic molecules) was mixed with water in a ratio of 1:2 (wt/wt), forming a biphasic system. Then, three experimental approaches were followed.

CHAPTER 5

Strategy 1: CO₂ - N₂ switching method

CO₂ was insufflated into the system for 30 min at 2vvm (volume volume per minute) to allow EBA to switch in its polar form (switching forward). The sample was centrifuged at 9000g at r.t. and at the end of centrifugation, EBA and water formed a homogeneous phase with a small lipid layer on the top. The hydrophobic molecules were recovered by chloroform with a syringe. The total amount of the extracted product was measured gravimetrically (after evaporating the solvent) and reported as a percentage on algae dry weight.

To recover extracted hydrophilic molecules, N₂ was bubbled through the system to remove CO₂ (switch back) and to allow EBA to return in the hydrophobic form. The sample was centrifuged at 9000g at r.t.. However, the two phases separation was not observed.

Strategy 2: Temperature switching method (Lower Critical Solution Temperature, LCST)

The supernatant was cooled to 0 °C for 2h, to allow the switch of EBA in its polar form. The sample was centrifuged at 9000g at 0 °C. The result was a water phase with a lipid layer on the top and an orange layer on the wall of the tube. To recover both the lipid phase and the orange layer, chloroform was added on the lipid layer, mixed and centrifuged at 9000g at 0 °C for 10 min. A two phase system was observed, with the hydrophobic molecules on the bottom. The total amount of the extracted products was recovered with a syringe and measured gravimetrically (after evaporating the solvent) and reported as a percentage on algae dry weight basis. To extract hydrophilic molecules, the water phase was incubated in the presence of the residual biomass for 2h at 0°C. The sample was centrifuged at 9000g at 0 °C for 10 min. Then, to collect hydrophilic molecules, the supernatant was heated to 22°C to allow EBA to switch back to the non-polar form. The sample was centrifuged at 9000g at 0 °C for 10 min to allow the formation of two phases. The aqueous fraction, containing hydrophilic molecules, was collected and total proteins were determined by BCA assay and SDS-PAGE.

Strategy 3: switch forward-switch back-switch forward

To recover the lipid layer and the orange layer separately, a different approach was used, starting from the 2nd strategy. The supernatant was cooled to 0 °C for 2h, centrifuged at 9000g at 0 °C.

CHAPTER 5

The result was a water phase with a lipid layer on the top and an orange layer on the wall of the tube. In this case, the orange layer (named orange fraction) was recovered first by methanol or heptane, after having transferred the water phase and the lipid layer to another tube. The system was heated to 22°C to allow EBA switch back to the non-polar form. The sample was centrifuged at 9000g at 0 °C to allow the formation of two phases. The upper phase contained EBA and the hydrophobic molecules. The upper phase was transferred to a new tube and mixed with water in a ratio of 1:2 (wt/wt), forming a biphasic system. Then, CO₂ was insufflated into the system for 30 min at 2vvm, the sample was centrifuged at 9000g at r.t. to recover the lipid layer (named green fraction) on the top by chloroform.

The total amount of the extracted products was measured gravimetrically (after evaporating the solvent) and reported as a percentage on algae dry weight.

ABTS assay

The *in vitro* antioxidant activity of orange and green fractions were evaluated by the 2,2'-azinobis-(3-ethylbenzothiazoline-6-sulfonic acid) ABTS assay, according to Rigano et al. with some modifications³⁴. Briefly, 7.4 mM ABTS^{•+} was mixed with 140 mM K₂S₂O₈ and the solution stabilized for 12h at room temperature in the dark. The mixture was then diluted with water to obtain an absorbance of 0.70 ± 0.02 unit at 734 nm using a spectrophotometer. Each extract (50 µL) was allowed to react with 250 µL of diluted ABTS^{•+} solution for 7 min, and then the absorbance was read at 734 nm. The standard curve was linear between 0 and 20 µM Trolox. Results are expressed as IC₅₀ (mg mL⁻¹), i.e. the concentration required to scavenge 50% of free radical ABTS.

Cell culture and Biocompatibility assay

Human immortalized keratinocytes (HaCaT, Innoprot, Spain) and immortalized murine fibroblasts (BALB/c 3T3, ATCC, Manassas, Vi, USA) were cultured in 10% fetal bovine serum in Dulbecco's modified Eagle's medium, in the presence of 1% antibiotics and 2 mM L-glutamine, in a 5% CO₂ humidified atmosphere at 37 °C. HaCaT cells were seeded in 96-well plates at a density of 2 × 10³ cells well⁻¹ and BALB/c 3T3 at a density of 3 × 10³ cells well⁻¹. 24h after seeding, increasing concentrations of the orange and green fractions (from 10 to 200 µg mL⁻¹) were added to the cells for 48h. At the end of the incubation, cell viability was measured by the tetrazolium salt colorimetric assay (MTT assay), as previously described³⁵. Cell

CHAPTER 5

survival was expressed as the percentage of viable cells in the presence of the extracts compared to control cells (represented by the average obtained between untreated cells and cells supplemented with the highest concentration of buffer). Each sample was tested in three independent analyses, each carried out in triplicates.

Thermal pasteurization

Thermal pasteurization was performed accordingly to the protocol reported by Ferraro et al.³⁶. Briefly, orange and green fractions were heated at 75 °C in a water bath. After 10 min incubation, samples were transferred to a second water bath at 20 °C and then stored at 4 °C until analysis.

Cellular reactive oxygen species (ROS) assay

To evaluate the protective effect of orange and green fractions against oxidative stress, DCFDA assay was carried out, according to the protocol reported by Petruk et al.³⁷ with some modifications. Briefly, 24h after seeding, cells were incubated in the presence of 25 µg mL⁻¹ of either raw or pasteurized orange and green extract for 2h and irradiated by UVA light for 10 min (100 J cm⁻²). Fluorescence intensity of the probe (2', 7'-dichlorofluorescein, DCF) was measured at an emission wavelength of 525 nm and an excitation wavelength of 488 nm using a Perkin-Elmer LS50 spectrofluorometer. Emission spectra were acquired at a scanning speed of 300 nm min⁻¹, with 5 slit width for both excitation and emission. ROS production was expressed as percentage of DCF fluorescence intensity of the samples under test, compared to untreated samples. Three independent experiments were carried out, each one with three determinations.

Pigments identification by HPLC

For the determination of the pigments content, extracts were resuspended in 100% methanol and analyzed by isocratic HPLC (Hewlett Packard, 1100 Series) in a reverse-phase (C8 column 3 µm Hyperloop MOS, 10 cm, 4.6 mm internal diameter, Shandon) as described in Vidussi et al.³⁸. Mobile phase consisted of MeOH: 0.5 N aqueous ammonium acetate, 70:30% v/v (solvent A), and MeOH (solvent B), with a gradient (minute; percent of solvent A- percent of solvent B): 0;75-25, 1;50-50, 15;0-100, and 19;75-25. For the determination of chlorophylls and carotenoids, a spectrophotometer with a diodes array detector (DAD) was set at 440 nm, making it possible to determine the absorption spectrum of the 350–750 nm

CHAPTER 5

interval for each peak, in order to check the purity of single pigments. The calibration of the instrument was carried out using external standard pigments provided by the International Agency for 14C determination-VKI Water Quality Institute. The identification of pigments was based considering retention time, spectral characteristics, and chromatography with certified commercial standards (International Agency for 14C determinations, Denmark). Quantification was based on the absorbance at 440 nm and the factor response (peak area/pigment concentration) value for each pigment, as described by Mantoura and Repeta³⁹.-

5.3 Results

Extraction and recovery of hydrophobic molecules from Synechococcus bigranulatus through switchable solvents

To verify the ability of N-Ethylbutylamine (EBA) switchable solvent to extract hydrophobic molecules from the selected microalgal strain, a direct comparison with a reference extraction method (Bligh & Dyer, B&D) was performed. *S. bigranulatus* wet biomass was mixed with EBA. Then, to separate hydrophobic molecules from EBA, the solvent was switched to the hydrophilic form (switch forward) by two procedures: (i) by bubbling CO₂ through the system (SS-CO₂ switch-forward) and (ii) by decreasing temperature (SS-LCST switch-forward, Lower Critical Solution Temperature). In addition, in a third experimental approach, the recovery of the hydrophobic fraction was carried out by changing the temperature first and then by insufflating CO₂ (SS-LCST- CO₂), as described in details in Materials and Methods section. The extracted hydrophobic molecules were measured gravimetrically and reported as a percentage with respect to dry weight biomass (Figure 1 and Table 1). Results clearly show that EBA was able to extract hydrophobic molecules from the algae at the same extent of the B&D procedure. This result indicates that it is possible to obtain hydrophobic molecules starting from a wet biomass, thus reducing the costs of the whole process, which are affected by drying, milling and temperature.

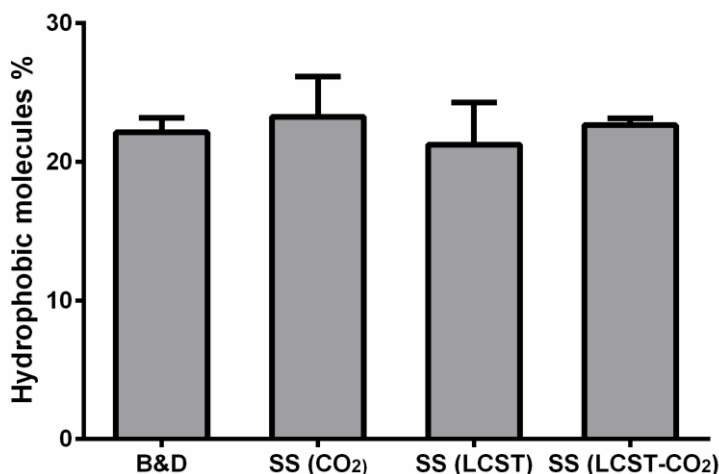


Figure 1. Hydrophobic molecules from *S. bigranulatus* biomass. Yields are reported as % with respect to dry weight biomass. B&D is referred to Bligh & Dyer; SS (CO₂) to extraction by switchable solvent and CO₂; SS (LCST) to extraction by switchable solvent and LCST; SS (LCST-CO₂) to extraction by switchable solvent and the combination of LCST and CO₂. Results are reported as means ± S.D. of at least three independent experiments.

N-Ethylbutylamine for carotenoids extraction

The procedure SS(LCST-CO₂) was chosen as the extraction procedure for further experiments. Noteworthy, during the extraction performed by SS(LCST-CO₂), an orange layer, on the wall of the tube, was observed. This fraction was recovered by using heptane, whereas the green fraction was recovered after a second cycle of switch-forward by using chloroform, as described in the Materials and Method section. Fresh and frozen (stored at -20 °C) biomass were analyzed in parallel experiments. The yields of orange (OF) and green (GF) fractions are reported in Figure 2. No significant differences were observed between the two starting materials, as shown in Figure 2 and reported in Table 2. This result suggests that the extraction can be done according to the experimental purpose, i.e. on either just harvested biomass or on a stored one.

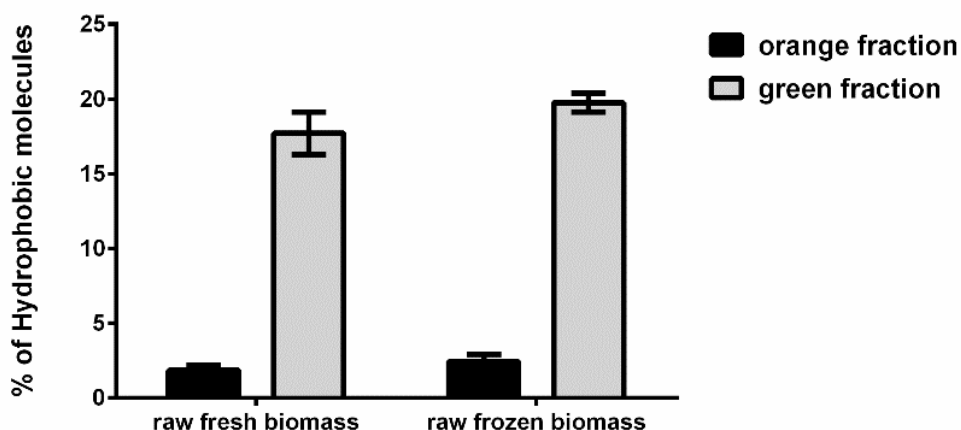


Figure 2. Yields of hydrophobic molecules in orange fraction and green fractions. Black bars are referred to the orange fraction; grey bars are referred to the green fraction. Yields are referred to extracts from fresh or frozen biomass. Results are reported as means \pm S.D. of at least three independent experiments.

Proteins extraction

After the extraction of hydrophobic molecules, EBA solvent, in its polar form, was used to extract proteins on the residual biomass, as described in Materials and Method section. In this case, ultrasounds were used as reference procedure. According to the BCA procedure, the SS (LCST-CO₂) method allowed to recover about 10% proteins, a value 3-fold lower than in the case of ultrasonication. However, when samples were analysed by SDS-PAGE, no proteins were observed in the sample SS (LCST-CO₂) (Figure 3), thus indicating that the yield indicated by the BCA procedure is affected by the presence of EBA itself. The polar form of EBA was also used on the whole biomass, to verify its ability to extract hydrophilic molecules. However, no hydrophilic molecules were obtained, probably because EBA was not able to destroy the biomass (data not shown).

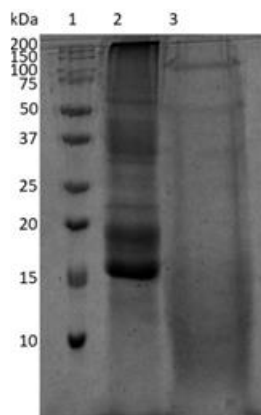


Figure 3. Proteins extracted from *S. bigranulatus*. SDS-PAGE analysis of protein extracted by ultrasounds and SS(LCST-CO₂) extraction. Lane 1: molecular weight markers; lane 2: soluble proteins extracted by ultrasounds (30 µg); lane 3: soluble proteins extracted by EBA (30 µg). The SDS-PAGE was stained by Blue Coomassie.

HPLC analysis

First, HPLC analysis was performed to identify the molecules present in OF and GF. Results clearly show that OF is enriched in β -carotene, whereas GF is enriched in zeaxanthin. Indeed, when the ratio Zeaxanthin/ β -carotene was measured in both fractions, a ratio of 0.07 ± 0.06 was found in the OF and 4.4 ± 1.5 in the GF, whereas the ratio in extract obtained by conventional method was about 1. In particular, zeaxanthin values ranged between 0.3 - $10.6 \mu\text{g mL}^{-1}$ in the GF, whereas β -carotene ranged between 1.7 - $7.5 \mu\text{g mL}^{-1}$ in the OF. A mean value of $0.06 \mu\text{g mL}^{-1}$ was observed instead for both molecules in the extract obtained by a conventional method.

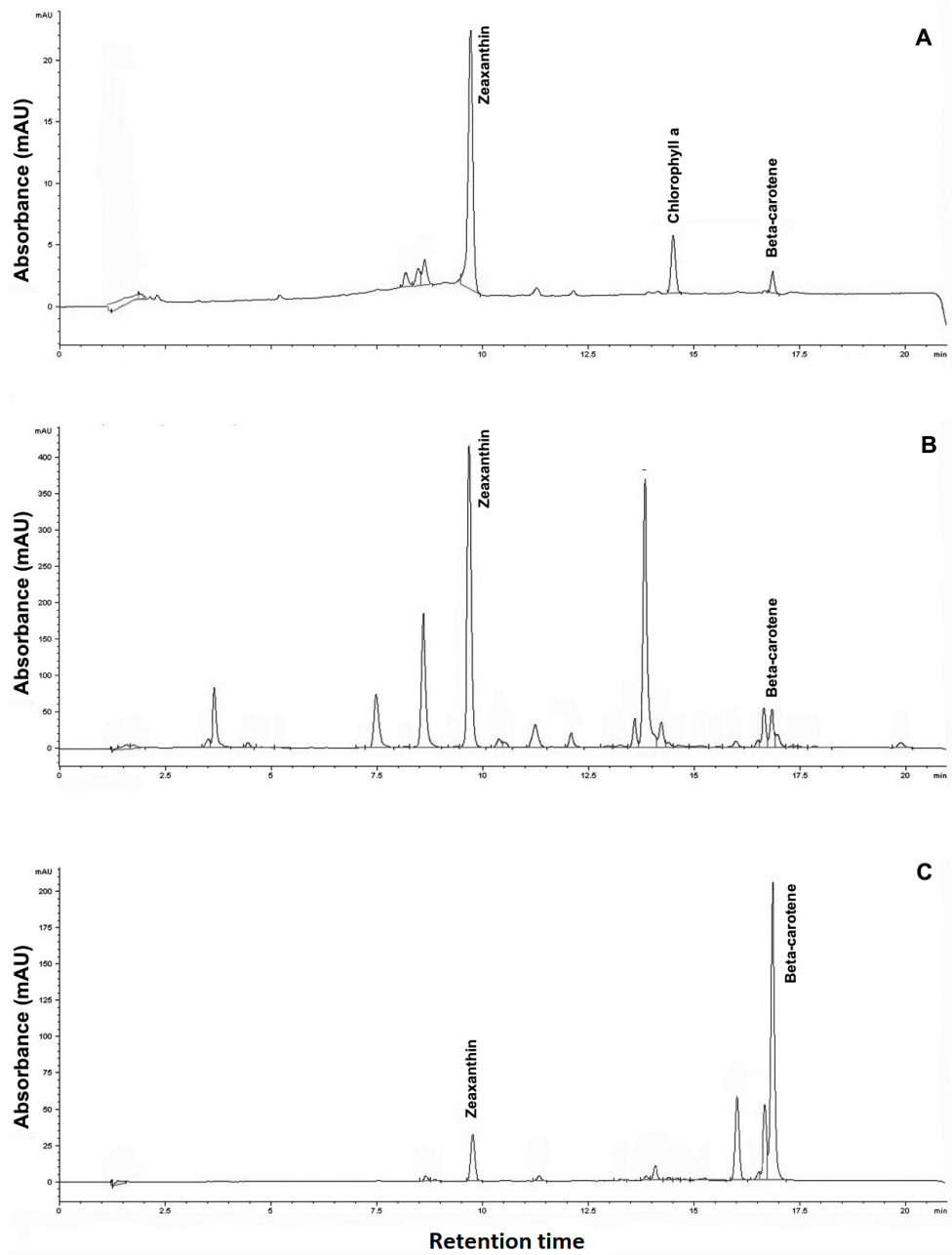


Figure 4. Representative HPLC chromatograms of antioxidants extracted from *S. bigranulatus*. (A) Raw extract obtained by conventional extraction; (B) GF and (C) OF.

CHAPTER 5

ABTS assay

To verify if OF and GF contained molecules endowed with antioxidant activity, the *in vitro* antioxidant activity was tested by the ABTS assay. Results are shown in Figure 5 and clearly indicate that both fractions had antioxidant activity. The IC₅₀ values, which correspond to the concentration of the extract that can inhibit 50% of the radical, were 0.024 ± 0.008 and 0.056 ± 0.013 mg mL⁻¹ for the OF and GF, respectively.

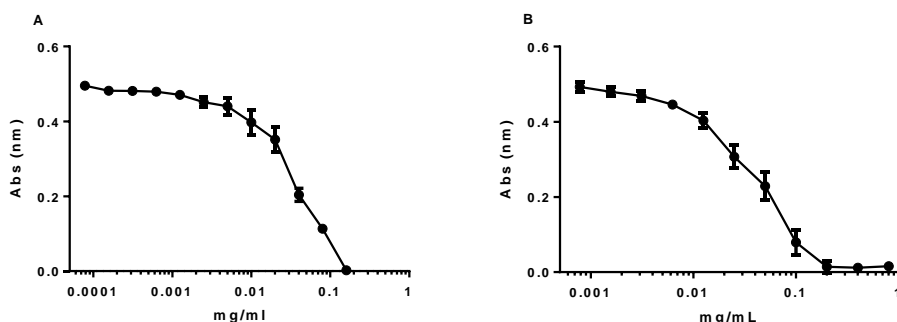


Figure 5. ABTS assay on OF and GF. The ABTS scavenging activity of orange (A) and green (B) fractions (mg mL⁻¹) from *S. bigranulatus*. Data shown are means \pm S.D. of three independent experiments.

Evaluation of the biocompatibility of orange and green fractions on eukaryotic cells.

The biocompatibility of OF and GF was evaluated by the MTT assay on two immortalized eukaryotic cell lines: HaCaT (human keratinocytes) and BALB/c-3T3 (murine fibroblasts). Cells were incubated in the presence of each extract for 48h, and cell survival was determined as described in Materials and Methods section. As shown in Figure 6, the GF did not show cell mortality on both cell lines tested, up to $200 \mu\text{g mL}^{-1}$ (A-B), whereas the OF (C-D) showed a low level of toxicity only on HaCaT cells (IC₅₀ value of $152 \pm 7 \mu\text{g mL}^{-1}$). Noteworthy, the solvent used to recover the OF is important, as, when methanol was used, cell mortality was achieved at a very low concentration of the extract, with an IC₅₀ value of $31 \pm 8 \mu\text{g mL}^{-1}$ and $43 \pm 4 \mu\text{g mL}^{-1}$ on HaCaT cells and BALB/c 3T3 cells, respectively (E-F).

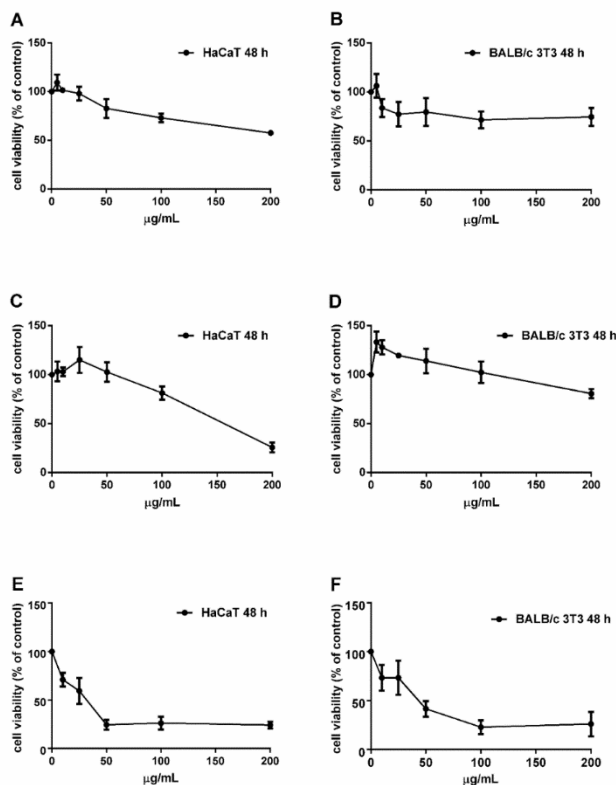


Figure 6. Cell viability of OF and GF on eukaryotic cells. HaCaT and BALB/c 3T3 were incubated for 48 h with increasing concentrations (10– 200 $\mu\text{g mL}^{-1}$) of GF (A-B), OF collected with heptane (C-D) and OF collected with methanol (E-F). Cell viability was assessed by the MTT assay, and cell survival expressed as a percentage of viable cells in the presence of the extracts under test, with respect to control cells grown in the absence of the extracts. Data shown are means \pm S.D. of three independent experiments.

Evaluation of antioxidant activity of OF and GF on eukaryotic cells.

In order to verify if the two extracts showed antioxidant activity also on a cell-based system, HaCaT cells were used. UVA was chosen as a source of oxidative stress and extracts were tested at 25 $\mu\text{g mL}^{-1}$. In particular, cells were incubated for 2 h with each extract prior to UVA exposure. Then, the DCFDA probe was used to measure ROS levels. Moreover, to verify if the extracts could be used in food industry, thus if they were resistant to high temperature treatments, a comparison between the antioxidant activity of raw and pasteurized extracts (i.e. heated at 75°C for 10 min) was performed. As shown in Figure 7, no effect on ROS levels was observed when cells were incubated with the raw orange and green fraction extracts, whereas when the cells were incubated with pasteurized orange and green extracts, an increase in intracellular ROS levels is observed in the absence of any treatment.

UVA induced a significant increase in intracellular ROS levels (180%) with respect to untreated cells (black bars). When cells were pre-incubated with any of the extract, no alteration in ROS levels was observed, thus suggesting that the extracts were able to protect cells from stress injury. These results indicate that thermal procedures do not affect the antioxidant activity of both fractions.

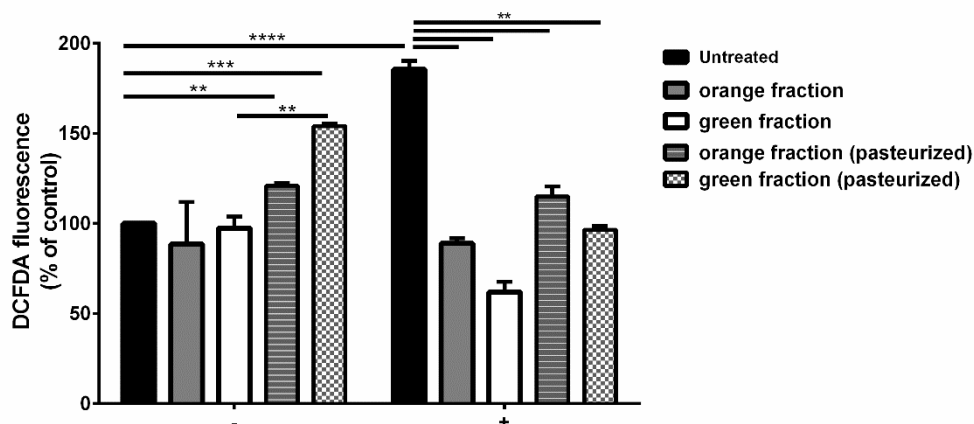


Figure 7. Antioxidant effect of the orange and green extracts from *S. bigranulatus* on UVA-stressed HaCaT cells. Cells were preincubated in the presence of $25 \mu\text{g mL}^{-1}$ of raw and pasteurized extracts for 2 h, prior to be irradiated by UVA (100 J cm^{-2}). For each experimental condition, ROS production was measured and results were reported as percentage with respect to untreated cells. Black bars: untreated cells; grey bars: cells incubated with OF; white bars: cells incubated with GF; gray striped bars: cells incubated with pasteurized OF; white squared bars: cells incubated with pasteurized GF. Data shown are means \pm S.D. of three independent experiment. ** indicates $p < 0.005$, *** indicates $p < 0.0005$ and **** indicates $p < 0.0001$.

5.4 Discussion

In the last decades, microalgae and cyanobacteria have been suggested as a very promising source for energy, food and cosmeceutical application. However, direct extraction of the desired biomolecules from the algal culture media, or at least from the wet biomass after a pre-concentration step, would be useful to decrease the downstream costs of microalgae-derived products. In addition, with current organic solvent systems, the results are still unsatisfactory.

Recently, new extraction techniques have been developed, such as ultrasonic waves, ionic liquids, acid-base, supercritical CO_2 and switchable solvents, which show an improvement in extraction efficiency.

Switchable solvents are widely used to extract hydrophobic molecules from algae raw biomass^{20,27,40}. In this work, the secondary

amine EBA was used on the cyanobacterium *S. bigranulatus*. Yields of hydrophobic molecules clearly show that EBA has the same extraction power than conventional methods.

However, EBA was not able to extract proteins on either unbroken or broken biomass. This results seems to be in contrast with data reported in literature, as they found about 40% of proteins from different microalgae by using the tertiary amine *N,N*-dimethyl-cyclohexylamine (DMCHA)²⁹. Noteworthy, in the present paper, by using the same colorimetric assay, about 10% of proteins seemed to be present, but the data was not confirmed by SDS-PAGE analysis, thus suggesting an interference of the SS with the colorimetric assay.

Surprisingly, EBA allowed the selective extraction of β -carotene and zeaxanthin. the selectivity found was in agreement with data recently reported on astaxanthin extraction from *H. pluvialis*²². This selectivity allowed to obtain a β -carotene enriched fraction a zeaxanthin enriched fraction, as clearly demonstrated by HPLC analysis. Furthermore, the yields of both hydrophobic molecules were found to be 5-170 fold higher those that obtained by conventional methods^{20,41}. In addition, EBA had the same extraction power on both frozen and fresh biomass. This result is very important from an industrial point of view, as it is possible to process the biomass anytime with the same yields and, in case of fresh biomass, to lower the downstream costs.

From a biological point of view, the isolated molecules were fully biocompatible, active as antioxidants and thermo-stable. In particular, the *in vitro* results showed lower IC₅₀ values than those reported in literature with different microalgae^{42,43}. Both fractions were able to protect immortalized human keratinocytes from oxidative stress induced by UVA. This ability was fully maintained also after thermal treatment, i.e. pasteurization.

In conclusion, EBA seems to be an excellent candidate for β -carotene and zeaxanthin extraction, as it is able to selectively extract both molecules with higher yields with respect to conventional methods, it does not affect their biological activity, it does not require any cell disruption or energy-intensive equipment to broke the cells, it can be used on either fresh or frozen biomass. All these parameters would decrease the total costs of the downstream process, thus allowing the use of SS on an industrial scale. ,

5.6 References

- (1) Spolaore, P.; Joannis-Cassan, C.; Duran, E.; Isambert, A. Commercial Applications of Microalgae. *J. Biosci. Bioeng.* 2006, 101 (2), 87–96.

- <https://doi.org/10.1263/jbb.101.87>.
- (2) Zhu, L. Biorefinery as a Promising Approach to Promote Microalgae Industry: An Innovative Framework. *Renew. Sustain. Energy Rev.* 2015, *41*, 1376–1384. <https://doi.org/10.1016/J.RSER.2014.09.040>.
 - (3) Ruiz, J.; Olivieri, G.; de Vree, J.; Bosma, R.; Willems, P.; Reith, J. H.; Eppink, M. H. M.; Kleinegris, D. M. M.; Wijffels, R. H.; Barbosa, M. J. Towards Industrial Products from Microalgae. *Energy Environ. Sci.* 2016, *9* (10), 3036–3043. <https://doi.org/10.1039/C6EE01493C>.
 - (4) Draaisma, R. B.; Wijffels, R. H.; Slegers, P. M.; Brentner, L. B.; Roy, A.; Barbosa, M. J. Food Commodities from Microalgae. *Current Opinion in Biotechnology.* Elsevier Current Trends April 1, 2013, pp 169–177. <https://doi.org/10.1016/j.copbio.2012.09.012>.
 - (5) Dolganyuk, V.; Belova, D.; Babich, O.; Prosekov, A.; Ivanova, S.; Katsarov, D.; Patyukov, N.; Sukhikh, S. Microalgae: A Promising Source of Valuable Bioproducts. *Biomolecules.* MDPI AG August 1, 2020, pp 1–24. <https://doi.org/10.3390/biom10081153>.
 - (6) Pulz, O.; Gross, W. Valuable Products from Biotechnology of Microalgae. *Applied Microbiology and Biotechnology.* Springer November 6, 2004, pp 635–648. <https://doi.org/10.1007/s00253-004-1647-x>.
 - (7) Shebis, Y.; Iluz, D.; Kinel-Tahan, Y.; Dubinsky, Z.; Yehoshua, Y. Natural Antioxidants: Function and Sources. *Food Nutr. Sci.* 2013, *04* (06), 643–649. <https://doi.org/10.4236/fns.2013.46083>.
 - (8) Ribeiro, J. S.; Santos, M. J. M. C.; Silva, L. K. R.; Pereira, L. C. L.; Santos, I. A.; da Silva Lannes, S. C.; da Silva, M. V. Natural Antioxidants Used in Meat Products: A Brief Review. *Meat Science.* Elsevier Ltd February 1, 2019, pp 181–188. <https://doi.org/10.1016/j.meatsci.2018.10.016>.
 - (9) Goiris, K.; Muylaert, K.; Fraeye, I.; Foubert, I.; De Brabanter, J.; De Cooman, L. Antioxidant Potential of Microalgae in Relation to Their Phenolic and Carotenoid Content. *J. Appl. Phycol.* 2012, *24* (6), 1477–1486. <https://doi.org/10.1007/s10811-012-9804-6>.
 - (10) Lourenço, S. C.; Moldão-Martins, M.; Alves, V. D. Antioxidants of Natural Plant Origins: From Sources to Food Industry Applications. *Molecules.* MDPI AG 2019. <https://doi.org/10.3390/molecules24224132>.
 - (11) Zhao, Z.; Rasool, M. A.; Chen, C.; Ma, S.; Wang, L.; Huang, G. Identification and Screening of Multiple Tropical Microalgal Strains for Antioxidant Activity in Vitro. *Food Biosci.* 2020, *36*, 100649. <https://doi.org/10.1016/j.fbio.2020.100649>.
 - (12) Villalobos-Delgado, L. H.; Mateo, J.; Caro, I.; Leal Ramos, M.-Y.; Mendez, N. G.; Cansino, R. G.; González Mondragón, E. G. Natural Antioxidants in Fresh and Processed Meat. In *Sustainable Meat Production and Processing*; Elsevier, 2019; pp 207–236. <https://doi.org/10.1016/b978-0-12-814874-7.00011-0>.
 - (13) Liu, X.; Luo, G.; Wang, L.; Yuan, W. Optimization of Antioxidant Extraction from Edible Brown Algae *Ascophyllum Nodosum* Using Response Surface Methodology. *Food Bioprod. Process.* 2019, *114*, 205–215. <https://doi.org/10.1016/j.fbp.2019.01.003>.
 - (14) Ambati, R. R.; Gogisetty, D.; Aswathanarayana, R. G.; Ravi, S.; Bikkina, P. N.; Bo, L.; Yuepeng, S. Industrial Potential of Carotenoid Pigments from Microalgae: Current Trends and Future Prospects. *Critical Reviews in Food Science and Nutrition.* Taylor

- and Francis Inc. July 4, 2019, pp 1880–1902. <https://doi.org/10.1080/10408398.2018.1432561>.
- (15) Sansone, C.; Brunet, C. Promises and Challenges of Microalgal Antioxidant Production. *Antioxidants* 2019, 8 (7), 199. <https://doi.org/10.3390/antiox8070199>.
- (16) Jacob-Lopes, E.; Maroneze, M. M.; Deprá, M. C.; Sartori, R. B.; Dias, R. R.; Zepka, L. Q. Bioactive Food Compounds from Microalgae: An Innovative Framework on Industrial Biorefineries. *Current Opinion in Food Science*. Elsevier Ltd February 1, 2019, pp 1–7. <https://doi.org/10.1016/j.cofs.2018.12.003>.
- (17) Hidalgo, G. I.; Almajano, M. P. Red Fruits: Extraction of Antioxidants, Phenolic Content, and Radical Scavenging Determination: A Review. *Antioxidants*. MDPI AG March 1, 2017, p 7. <https://doi.org/10.3390/antiox6010007>.
- (18) Selvamuthukumar, M.; Shi, J. Recent Advances in Extraction of Antioxidants from Plant By-Products Processing Industries. *Food Quality and Safety*. Oxford University Press March 1, 2017, pp 61–81. <https://doi.org/10.1093/fqsafe/fyx004>.
- (19) Mäki-Arvela, P.; Hachemi, I.; Murzin, D. Y. Comparative Study of the Extraction Methods for Recovery of Carotenoids from Algae: Extraction Kinetics and Effect of Different Extraction Parameters. *J. Chem. Technol. Biotechnol.* 2014, 89 (11), 1607–1626. <https://doi.org/10.1002/jctb.4461>.
- (20) Imbimbo, P.; D'Elia, L.; Liberti, D.; Olivieri, G.; Monti, D. M. Towards Green Extraction Methods from Microalgae Learning from the Classics. *Applied Microbiology and Biotechnology*. Springer Science and Business Media Deutschland GmbH November 1, 2020, pp 9067–9077. <https://doi.org/10.1007/s00253-020-10839-x>.
- (21) Du, Y.; Schuur, B.; Kersten, S. R. A.; Brillman, D. W. F. Opportunities for Switchable Solvents for Lipid Extraction from Wet Algal Biomass: An Energy Evaluation. *Algal Research*. Elsevier September 1, 2015, pp 271–283. <https://doi.org/10.1016/j.algal.2015.07.004>.
- (22) Liu, H.; Huang, W. C.; Guo, N.; Mao, X. Application of Secondary Amine Switchable Hydrophilicity Solvents for Astaxanthin Extraction from Wet Haematococcus Pluvialis. *Algal Res.* 2020, 48, 101892. <https://doi.org/10.1016/j.algal.2020.101892>.
- (23) Sanzo, G.; Mehariya, S.; Martino, M.; Larocca, V.; Casella, P.; Chianese, S.; Musmarra, D.; Balducci, R.; Molino, A. Supercritical Carbon Dioxide Extraction of Astaxanthin, Lutein, and Fatty Acids from Haematococcus Pluvialis Microalgae. *Mar. Drugs* 2018, 16 (9), 334. <https://doi.org/10.3390/md16090334>.
- (24) Pawliszyn, J. Kinetic Model of Supercritical Fluid Extraction. *J. Chromatogr. Sci.* 1993, 31 (1), 31–37. <https://doi.org/10.1093/chromsci/31.1.31>.
- (25) Jessop, P. G.; Heldebrant, D. J.; Li, X.; Eckert, C. A.; Liotta, C. L. Green Chemistry: Reversible Nonpolar-to-Polar Solvent. *Nature* 2005, 436 (7054), 1102. <https://doi.org/10.1038/nature4361102a>.
- (26) Phan, L.; Andreatta, J. R.; Horvey, L. K.; Edie, C. F.; Luco, A.-L.; Mirchandani, A.; Darensbourg, D. J.; Jessop, P. G. Switchable-Polarity Solvents Prepared with a Single Liquid Component. 2007. <https://doi.org/10.1021/ie070552r>.
- (27) Du, Y.; Schuur, B.; Samori, C.; Tagliavini, E.; Brillman, D. W. F. Secondary Amines as Switchable Solvents for Lipid Extraction from Non-Broken Microalgae. *Bioresour. Technol.* 2013, 149, 253–260. <https://doi.org/10.1016/j.biortech.2013.09.039>.
- (28) Du, Y.; Schuur, B.; Brillman, D. W. F. Maximizing Lipid Yield in Neochloris

- Oleoabundans Algae Extraction by Stressing and Using Multiple Extraction Stages with N-Ethylbutylamine as Switchable Solvent. *Ind. Eng. Chem. Res.* 2017, 56 (28), 8073–8080. <https://doi.org/10.1021/acs.iecr.7b01032>.
- (29) Cicci, A.; Sed, G.; Jessop, P. G.; Bravi, M. Circular Extraction: An Innovative Use of Switchable Solvents for the Biomass Biorefinery. *Green Chem.* 2018, 20 (17), 3908–3911. <https://doi.org/10.1039/c8gc01731j>.
- (30) Du, Y.; Cyprichová, V.; Hoppe, K.; Schuur, B.; Brilman, W. Process Evaluation of Swing Strategies to Recover N-Ethylbutylamine after Wet Lipid Extraction from Microalgae. *Sep. Purif. Technol.* 2020, 233, 115819. <https://doi.org/10.1016/j.seppur.2019.115819>.
- (31) D’Elia, L.; Del Mondo, A.; Santoro, M.; De Natale, A.; Pinto, G.; Pollio, A. Microorganisms from Harsh and Extreme Environments: A Collection of Living Strains at ACUF (Naples, Italy). *Ecol. Quest.* 2018, 29 (3), 63–74. <https://doi.org/10.12775/EQ.2018.023>.
- (32) Wu, H.-L.; Wang, G.-H.; Xiang, W.-Z.; Li, T.; He, H. Stability and Antioxidant Activity of Food-Grade Phycocyanin Isolated from *Spirulina Platensis*. *Int. J. Food Prop.* 2016, 19 (10), 2349–2362. <https://doi.org/10.1080/10942912.2015.1038564>.
- (33) BLIGH, E. G.; DYER, W. J. A Rapid Method of Total Lipid Extraction and Purification. *Can. J. Biochem. Physiol.* 1959, 37 (8), 911–917. <https://doi.org/10.1139/o59-099>.
- (34) Rigano, M. M.; Raiola, A.; Tenore, G. C.; Monti, D. M.; Del Giudice, R.; Frusciante, L.; Barone, A. Quantitative Trait Loci Pyramiding Can Improve the Nutritional Potential of Tomato (*Solanum Lycopersicum*) Fruits. *J. Agric. Food Chem.* 2014, 62 (47), 11519–11527. <https://doi.org/10.1021/jf502573n>.
- (35) Petruk, G.; Gifuni, I.; Illiano, A.; Roxo, M.; Pinto, G.; Amoresano, A.; Marzocchella, A.; Piccoli, R.; Wink, M.; Olivieri, G.; Monti, D. M. Simultaneous Production of Antioxidants and Starch from the Microalga *Chlorella Sorokiniana*. *Algal Res.* 2018, 34, 164–174. <https://doi.org/10.1016/j.algal.2018.07.012>.
- (36) Ferraro, G.; Imbimbo, P.; Marseglia, A.; Illiano, A.; Fontanarosa, C.; Amoresano, A.; Olivieri, G.; Pollio, A.; Monti, D. M.; Merlino, A. A Thermophilic C-Phycocyanin with Unprecedented Biophysical and Biochemical Properties. *Int. J. Biol. Macromol.* 2020, 150, 38–51. <https://doi.org/10.1016/j.ijbiomac.2020.02.045>.
- (37) Petruk, G.; Raiola, A.; Del Giudice, R.; Barone, A.; Frusciante, L.; Rigano, M. M.; Monti, D. M. An Ascorbic Acid-Enriched Tomato Genotype to Fight UVA-Induced Oxidative Stress in Normal Human Keratinocytes. *J. Photochem. Photobiol. B Biol.* 2016, 163, 284–289. <https://doi.org/10.1016/j.jphotobiol.2016.08.047>.
- (38) Vidussi, F.; Claustre, H.; Bustillos-Guzmán, J.; Cailliau, C.; Marty, J.-C. Determination of Chlorophylls and Carotenoids of Marine Phytoplankton: Separation of Chlorophyll a from Divinylchlorophyll a and Zeaxanthin from Lutein. *J. Plankton Res.* 1996, 18 (12), 2377–2382. <https://doi.org/10.1093/plankt/18.12.2377>.
- (39) Mantoura, R. F. C.; Repeta, D. J. *Calibration Methods for HPLC*; na, 1997.
- (40) Samori, C.; Barreiro, D. L.; Vet, R.; Pezzolesi, L.; Brilman, D. W. F.; Galletti, P.; Tagliavini, E. Effective Lipid Extraction from Algae Cultures Using Switchable Solvents. *Green Chem.* 2013, 15 (2), 353–356. <https://doi.org/10.1039/C2GC36730K>.
- (41) Fabrowska, J.; Messyasz, B.; Szyling, J.; Walkowiak, J.; Łęska, B. Isolation of Chlorophylls and Carotenoids from Freshwater Algae Using Different Extraction Methods. *Phycol. Res.* 2018, 66 (1), 52–57. <https://doi.org/10.1111/pre.12191>.

CHAPTER 5

- (42) Assunção, M. F. G.; Amaral, R.; Martins, C. B.; Ferreira, J. D.; Ressurreição, S.; Santos, S. D.; Varejão, J. M. T. B.; Santos, L. M. A. Screening Microalgae as Potential Sources of Antioxidants. *J. Appl. Phycol.* 2017, 29 (2), 865–877. <https://doi.org/10.1007/s10811-016-0980-7>.
- (43) Guedes, A.; Gião, M.; Seabra, R.; Ferreira, A.; Tamagnini, P.; Moradas-Ferreira, P.; Malcata, F. Evaluation of the Antioxidant Activity of Cell Extracts from Microalgae. *Mar. Drugs* 2013, 11 (12), 1256–1270. <https://doi.org/10.3390/md11041256>.

Chapter 6

General Discussion

6.1 General discussion

Nowadays, antioxidants are used to prevent food oxidation, which may result also in food rancidity. However, evidence is emerging on their adverse health effects, thus research is now focusing to replace these synthetic antioxidants with natural ones^{1,2}. The main natural antioxidants used are those extracted from fruits or vegetables (e.g. tocopherols, carotenoids and ascorbic acid). Nevertheless, during food processing treatments, such as heat/thermal treatment or during the storage process, antioxidants may lose their stability, resulting in loss of the antioxidant activity^{3,4}. Moreover, there is an increasing interest and awareness of consumers in the consumption of healthy foods, which contributes to the identification of natural antioxidant molecules resistant to processing techniques and preservation methods. In this context, microalgae and cyanobacteria, due to the abundance of secondary metabolites, have received great attention in recent years as a natural source of antioxidants.

The aim of this PhD project was to demonstrate the feasibility of the production of thermoresistant antioxidants to be applied as food preservatives from one or more strains of photosynthetic microorganisms.

To this purpose, the attention was first focused on the study of the strains available at the Algal Collection of University Federico II of Naples (ACUF) (Chapters 2 and 3). Founded in 1973 by *professor* Roberto Taddei, the ACUF was born as a collection of *Cyanidium caldarium*; however, today over 800 live photosynthetic microorganisms (mainly belonging to Cyanobacteria, Chlorophyta, Rhodophyta, and Bacillariophyceae) from almost all continents are maintained. Considering the great biodiversity of microalgae available at the ACUF collection, 25 strains were selected between microalgae and cyanobacteria in order to identify the most promising. Among these, *Enallax* sp., *S. bigranulatus* and *G. sulphuraria* were selected. Then, the antioxidant activity of the selected extracts was evaluated, before and after pasteurization treatment. The results showed that the antioxidant activity of extracts was fully preserved even after the thermal treatment, as the extracts were able to protect cells from UVA-induced damage. Based on these results, the selected strains were considered promising as a producer of heat resistant antioxidants to be applied as food preservatives.

Then, a massive production of selected strains was performed at a relevant scale by using bubble column photobioreactor and thin layer photobioreactor (15L operating volume) at ATlbiotech company

(Chapter 4). Both PBRs allowed to obtain high biomass yields. However, increased productivity was observed in the thin layer PBR, most likely for the major irradiation surface that results in more photons available for each individual algal cell^{5,6}. Hence, if the main advantage of thin layer photobioreactors is the high surface/volume ratio, it should be considered that size and rigidity may represent a limit. For this reason, closed tube systems are often easier to realize at an industrial scale. A solution for the feasible application of thin layer photobioreactors would be their integration in the building surfaces, as already proposed by Pruvost et al^{6,7}

As microalgae downstream, and in particular the component extraction, processing has high costs, one possibility to decrease them is using green solvents. In this context, a switchable solvent (SS), and specifically the secondary amine N-Ethylbutylamine (EBA), was used to extract antioxidants from microalgal biomass produced in photobioreactors. In particular, *S. platensis* and *S. bigranulatus* were selected and hydrophobic antioxidants were extracted.

Compared to conventional organic solvent extractions performed on the same biomass, the SS extractions allowed achieving similar yields of hydrophobic molecules in a short time and with less solvent consumption. Surprisingly, when the extraction of molecules was induced by the SS(LCST-CO₂) strategy (Chapter 5), it was possible to recover two fractions, the orange fraction (OF) rich in β -carotene and the green fraction (GF) rich in zeaxanthin, thus rendering the process highly selectively. Furthermore, the nature of the solvent did not affect the biocompatibility of the extracted molecules or the antioxidant activity, preserved even after the pasteurization process of the extracts.

In addition, the ability of the solvent to extract antioxidants from both slurry biomass and wet paste biomass, proved the ability of N-Ethylbutylamine, in its non-polar form, to destroy algal cell walls and membranes. Hence, considering that the drying process and cell disruption steps are responsible for up to 25%⁸ of the energy consumption of the extraction process, this approach would allow a significant decrease in the overall costs^{9,10}.

Moreover, different procedures can be applied to switch SS chemical-physical properties, such as changes in CO₂ or temperature. Recent studies have demonstrated that lowering the temperature induces a lower solvent loss and higher efficiency with respect to CO₂¹¹. Last but not least, using temperature to induce the switching of the solvent is less energy-intensive than CO₂¹¹.

However, several bottlenecks still limit the use of SS and their scalability at an industrial level, such as the contamination of the

residual biomass by the solvent after the extraction process, the release of the solvent in water and the toxicity of the solvent^{12,13}.

To overcome these problems, Du and colleagues investigated the purification of residual biomass and water from the solvent after the extraction process¹¹. They found that it is possible recover the solvent from the biomass by multiple washes with water, and then the solvent was separated from the water by liquid extraction with a polar solvent followed by distillation¹¹. Alternatively, SS properties can be improved during chemical synthesis by adding functional groups into the structure¹⁴.

However, the above described approaches negatively affect the extraction process costs.

Another important bottleneck of extractions performed by SS, is that it has still to be proven their further ability of extracting also proteins from algal biomass. A recent paper¹⁵ stated that the procedure was successful, but only colorimetric analyses were performed. These data are in contrast to what observed in Chapter 5. Indeed, even if the colorimetric assay showed the presence of proteins, no proteins were visible after the SDS-PAGE analysis, thus suggesting an interference of the amine with the colorimetric assay.

In conclusion, the green properties of the SSs, their ability to extract hydrophobic molecules from unbroken biomass, the extraction selectivity and the easy solute-solvent separation are a good starting point for their use at an industrial scale, but many questions and technical factors have to be clarified and set up before rendering these solvents applicable at industrial scale^{13,15–17}.

5.2 References

- (1) Koyande, A. K.; Chew, K. W.; Rambabu, K.; Tao, Y.; Chu, D. T.; Show, P. L. Microalgae: A Potential Alternative to Health Supplementation for Humans. *Food Science and Human Wellness*. Elsevier BV March 2019, pp 16–24. <https://doi.org/10.1016/j.fshw.2019.03.001>.
- (2) Goiris, K.; Muylaert, K.; Fraeye, I.; Foubert, I.; De Brabanter, J.; De Cooman, L. Antioxidant Potential of Microalgae in Relation to Their Phenolic and Carotenoid Content. <https://doi.org/10.1007/s10811-012-9804-6>.
- (3) Pokorný, J. P. *Natural Antioxidant Functionality during Food Processing*.
- (4) Poljsak, B.; Kovač, V.; Milisav, I. Antioxidants, Food Processing and Health. *Antioxidants* 2021, 10 (3), 1–11. <https://doi.org/10.3390/antiox10030433>.
- (5) Soni, R. A.; Sudhakar, K.; Rana, R. S. Comparative Study on the Growth Performance of Spirulina Platensis on Modifying Culture Media. *Energy Reports* 2019, 5, 327–336. <https://doi.org/10.1016/j.egy.2019.02.009>.

- (6) Gifuni, I.; Pollio, A.; Marzocchella, A.; Olivieri, G. New Ultra-Flat Photobioreactor for Intensive Microalgal Production: The Effect of Light Irradiance. *Algal Res.* 2018, *34*, 134–142. <https://doi.org/10.1016/j.algal.2018.07.014>.
- (7) Pruvost, J.; Le Gouic, B.; Lepine, O.; Legrand, J.; Le Borgne, F. Microalgae Culture in Building-Integrated Photobioreactors: Biomass Production Modelling and Energetic Analysis. *Chem. Eng. J.* 2016, *284*, 850–861. <https://doi.org/10.1016/j.cej.2015.08.118>.
- (8) Razon, L. F.; Tan, R. R. Net Energy Analysis of the Production of Biodiesel and Biogas from the Microalgae: *Haematococcus Pluvialis* and *Nannochloropsis*. *Appl. Energy* 2011, *88* (10), 3507–3514. <https://doi.org/10.1016/j.apenergy.2010.12.052>.
- (9) Ismail, M.; Al-Zuhair, S. Thermo-Responsive Switchable Solvents for Simultaneous Microalgae Cell Disruption, Oil Extraction-Reaction, and Product Separation for Biodiesel Production. *Biocatal. Agric. Biotechnol.* 2020, *26*, 101667. <https://doi.org/10.1016/j.bcab.2020.101667>.
- (10) Gifuni, I.; Pollio, A.; Safi, C.; Marzocchella, A.; Olivieri, G. Current Bottlenecks and Challenges of the Microalgal Biorefinery. *Trends in Biotechnology*. Elsevier Ltd March 1, 2019, pp 242–252. <https://doi.org/10.1016/j.tibtech.2018.09.006>.
- (11) Du, Y.; Cyprichová, V.; Hoppe, K.; Schuur, B.; Brilman, W. Process Evaluation of Swing Strategies to Recover N-Ethylbutylamine after Wet Lipid Extraction from Microalgae. *Sep. Purif. Technol.* 2020, *233*, 115819. <https://doi.org/10.1016/j.seppur.2019.115819>.
- (12) Du, Y.; Schuur, B.; Kersten, S. R. A.; Brilman, D. W. F. Opportunities for Switchable Solvents for Lipid Extraction from Wet Algal Biomass: An Energy Evaluation. *Algal Research*. Elsevier September 1, 2015, pp 271–283. <https://doi.org/10.1016/j.algal.2015.07.004>.
- (13) Liu, H.; Huang, W. C.; Guo, N.; Mao, X. Application of Secondary Amine Switchable Hydrophilicity Solvents for Astaxanthin Extraction from Wet *Haematococcus Pluvialis*. *Algal Res.* 2020, *48*, 101892. <https://doi.org/10.1016/j.algal.2020.101892>.
- (14) Clarke, C. J.; Tu, W. C.; Levers, O.; Bröhl, A.; Hallett, J. P. Green and Sustainable Solvents in Chemical Processes. *Chem. Rev.* 2018, *118* (2), 747–800. <https://doi.org/10.1021/acs.chemrev.7b00571>.
- (15) Cicci, A.; Sed, G.; Jessop, P. G.; Bravi, M. Circular Extraction: An Innovative Use of Switchable Solvents for the Biomass Biorefinery. *Green Chem.* 2018, *20* (17), 3908–3911. <https://doi.org/10.1039/c8gc01731j>.
- (16) Samorì, C.; Barreiro, D. L.; Vet, R.; Pezolesi, L.; Brilman, D. W. F.; Galletti, P.; Tagliavini, E. Effective Lipid Extraction from Algae Cultures Using Switchable Solvents. *Green Chem.* 2013, *15* (2), 353–356. <https://doi.org/10.1039/C2GC36730K>.
- (17) Du, Y.; Schuur, B.; Kersten, S. R. A.; Brilman, D. W. F. (Wim). Multistage Wet Lipid Extraction from Fresh Water Stressed *Neochloris Oleoabundans* Slurry – Experiments and Modelling. *Algal Res.* 2018, *31*, 21–30. <https://doi.org/10.1016/j.algal.2018.01.001>.

APPENDIX**List of scientific publications:**

I-D'Elia, L., Santoro, M., Del Mondo, A., De Natale A., Pollio A. (2018). **Microorganisms from harsh and extreme environments: a collection of living strains at ACUF (Napoli, Italy).** ECOLOGICAL QUESTIONS, 29(3). (ISSN:1644-7298)
<http://dx.doi.org/10.12775/EQ.2018.023>

II-Cucciolito, M. E., De Luca Bossa, F., Esposito, R., Ferraro, G., Iadonisi, A., Petruk, G., D'Elia, L., Romanetti, C., Traboni, S., Tuzi, A., Monti, D. M., Merlino, A., Ruffo, F. (2018). C-Glycosylation in platinum-based agents: a viable strategy to improve cytotoxicity and selectivity. Inorganic Chemistry Frontiers, 5(11), 2921–2933.
doi.org/10.1039/C8QI00664D

III-Petruk, G., Monti, D. M., Ferraro, G., Pica, A., D'Elia, L., Pane, F., Merlino, A. (2019). Encapsulation of the Dinuclear Trithiolato-Bridged Arene Ruthenium Complex Diruthenium-1 in an Apoferritin Nanocage: Structure and Cytotoxicity. ChemMedChem, 14(5), 594–602.
<https://doi.org/10.1002/cmdc.201800805>

IV-Imbimbo P., Bueno M., D'Elia L., Pollio A., Elena Ibañez, Olivieri G., Monti D. M. (2019). Green pressurised fluid technology for the extraction of antioxidants from *Galdieria phlegrea* in a biorefinery approach. ACS Sustain ACS CHEM Eng 8:2939-2947.
<https://doi.org/10.1021/acssuschemeng.9b07505>

V-Barone R., de Napoli L., Mayol L., Paolucci M., Volpe MG., D'Elia L., Pollio A., Guida M., Gambino E., Carraturo F., Marra R., Vinale F., Woo SL., Lorito M. (2020). Autotrophic and Heterotrophic Growth Conditions Modify Biomolecule Production in the Microalga *Galdieria sulphuraria* (Cyanidiophyceae, Rhodophyta). Mar Drugs 18:169. <https://doi.org/10.3390/md18030169>

VI-Tresin F., Stoppa V., Baron M., Biffis A., Annunziata A., D'Elia L., Monti DM., Ruffo F., Roverso M., Sgarbossa P., Bogialli S., Tubaro C. (2020) Synthesis and biological studies on dinuclear gold(II) complexes with Di-(N-Heterocyclic Carbene) ligands

functionalized with carbohydrates. Molecules 25:3850.
<https://doi.org/10.3390/molecules25173850>

VII-Imbimbo P., D'Elia L., Liberti D., Olivieri G., Monti DM. (2020) Towards green extraction methods from microalgae learning from the classics. Appl. Microbiol. Biotechnol. 104:9067–9077.
<https://doi.org/10.1007/s00253-020-10839-x>

VIII- Rezq S., Alsemeh AE., D'Elia L., El-Shazly AM., Monti DM., Sobeh M, Mahmoud MF (2020) Thymus algeriensis and Thymus fontanesii exert neuroprotective effect against chronic constriction injury-induced neuropathic pain in rats. Sci Rep 10:1–15. <https://doi.org/10.1038/s41598-020-77424-0>

List of scientific communications:

- **Organizing committee** of the II Industrial Biotechnology Congress “BioID&A: Biotechnology Identity and Application”. (Naples, October 28, 2019)

- **D'Elia L.**, Del Mondo A., Santoro M., De Natale A., Pinto G. Pollio A. THE CYANIDIALES OF ALGAL COLLECTION OF UNIVERSITY FEDERICO II (ACUF). Società Italiana di Ecologia XXVII. 12 15 September 2017 Napoli (Italy)

- Imbimbo, P., Bueno, M., **D'Elia, L.**, Olivieri, G., Pollio, A., Monti, M.D., Ibañez, E. “Green compressed fluids technologies for downstream processing of Galdiera phlegrea in a biorefinery approach” . IX reunion de expertos en tecnologías de fluidos supercriticos, 2018 (Madrid, June 13-15, 2018)

- Panzella L., **D'Elia L.**, Petruck, G., Monti D.M., DIschia, M. Melanin with potent photoprotective and antioxidant activities for dermo-cosmetic applications. 10th International Conference on Skin Ageing and Challenges (Porto, Portugal, February 25- 27, 2019)

- **D'Elia. L.**, Imbimbo P., Olivieri G., Pollio, A., Monti, D.M. Identification, isolation and characterization of thermoresistant antioxidants from extremophile microalgae. 2° Workshop Bio/10 Campania (Naples, Italy May 17, 2019)

- Srećkovic, N., Mihalovic, V., Stankovic, J.S.K., **D'Elia L.**, Monti, D.M. Antioxidant and cytotoxic activities of rosmarinic acid- rich *Salvia platensis* L. extracts. Serbian Biochemical Society, ninth conference, University of Belgrade – Kolarac Endowment (Belgrade, Serbia, November 14-16, 2019)

- **D'Elia, L.**, Imbimbo, P., Liberti L., Olivieri G., Pollio A., Monti D.M. Identification of a potential microalgal strain for thermo resistant antioxidants production. AlgaEurope Conference France (Paris, France, December 3-5, 2019)

EXPERIENCE IN FOREIGN LABORATORIES

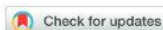
Visiting period at TNW faculty, UNIVERSITY OF TWENTE, The Netherlands, from February 4th 2019 to June 6th 2019 and from February 17th 2020 to March 12th 2020. The work was carried out in Sustainable Process technology research group under supervision of Prof.dr.ir. D.W.F. Brillman

EXPERIENCE IN INDUSTRY

Visiting period at ATlbiotech s.r.l., Castel Baronia (Av), Italy, from August 1st 2019 to October 31st 2019 and from August 1st 2020 to October 31st 2020. The work was carried out under supervision of Ing. Domenico Liotto.



RESEARCH ARTICLE

View Article Online
View Journal | View IssueCite this: *Inorg. Chem. Front.*, 2018, 5, 2921

C-Glycosylation in platinum-based agents: a viable strategy to improve cytotoxicity and selectivity†

Maria Elena Cucciolito,^{a,b} Ferdinando De Luca Bossa,^a Roberto Esposito,^b Giarita Ferraro,^a Alfonso Iadecni,^{a,b} Ganna Petruk,^a Luigi D'Elia,^a Claudia Romanetti,^a Serena Traboni,^a Angela Tuzi,^a Daria Maria Monti,^a Antonello Merlino^{a,b} and Francesco Ruffo^{a,b}

Novel coordinatively saturated platinum(II) compounds bearing C-linked carbohydrates were synthesized and characterized. The complexes exhibit bipyramidal trigonal geometry with a bidentate nitrogen ligand and ethylene in the equatorial plane. The axial positions are occupied by a halide ligand X and a D-galactose or D-glucose derivative, linked either via C1 or C6. The compounds were designed for evaluation of the biological activity because they combine the steady coordinative saturation, the beneficial action of the modular sugar moiety and the organometallic nature of the Pt-sugar linkage, which is expected to be stable in the biological media, until the target is reached. The newly synthesized molecules were stable in mixed DMSO/aqueous solvents, able to bind DNA *in vitro* and exhibited a selective cytotoxic activity on cancer cells through apoptosis activation.

Received 8th July 2018,
Accepted 29th September 2018
DOI: 10.1039/c8qj00664d
rsc.li/frontiers-inorganic

Introduction

An important application of coordination chemistry is the design of metal complexes with biological activity. The availability of metals in several oxidation states and geometries, along with the tunability of the ligands, results in a great diversity of action, both as drugs and diagnostic tools.¹ Following the serendipitous discovery of the anticancer properties of cisplatin (*cis*-PtCl₂(NH₃)₂, *cis*-diamminedichloroplatinum(II)) by Rosenberg in 1965² and its introduction into clinics, several studies have been carried out to improve its performance and reduce its numerous side effects.^{3–7} Thus, hundreds of Pt-based drugs have been prepared and characterized.⁸ Among these, a second generation of Pt containing anticancer drugs, comprising carboplatin (*cis*-diammine(cyclobutane-1,1-dicarboxylate-*O,O'*)platinum(II)) and oxaliplatin (ethane-dioate (1*R*,2*R*)-1,2-cyclohexanediamineplatinum(II)), reaches clinical practice. Both these cisplatin analogues act using a mechanism of action comparable to that of cisplatin: upon diffusion into the intracellular environment, they are transformed into a

positively charged species, able to irreversibly bind DNA, thus inhibiting its replication and transcription. Similarly, they share common undesired side effects.⁸

Today, the interest of the scientific community is directed towards the discovery of new complexes with safer mechanisms of action, capable of addressing the target by maintaining the integrity of the healthy cells.^{9–22} In this context, it is known that several cancer cells significantly increase carbohydrate uptake,^{23,24} to sustain growth and proliferation ("Warburg effect"). Therefore, they overexpress many glycosyl receptors and transporters. This is the basis of the design of drugs based on glycoconjugation.^{25–34} A recent study demonstrated that a glucose-platinum conjugate preferentially accumulates in cancer cells,³⁵ through a glucose-transporter-mediated cellular uptake mechanism, and not *via* passive diffusion.

At the same time, carbohydrates are also excellent chiral³⁶ building blocks for ligands^{37,38} since they are widespread in nature and in biological systems,³⁹ where they serve as energy storage units and assist in cellular recognition.^{27,40–43} It is worth noting that sugar conjugation to Pt complexes may improve the metal-based drug water solubility and biocompatibility.

Up to now, a wide variety of metal complexes with carbohydrate-derived ligands has been investigated for potential applications as therapeutic agents.^{25–34} Within this emerging area, our research group has recently⁴⁴ focused its attention on a novel class of cationic five-coordinate^{45–47} platinum(II) complexes (Fig. 1).

These compounds, which present a nitrogen heterocycle coordinating fragment linked to a glucoside residue, are more

^aDipartimento di Scienze Chimiche, Università di Napoli Federico II, Complesso Universitario di Monte S. Angelo, via Cintia 21-80126, Napoli, Italy. E-mail: antonello.merlino@unina.it, ruffo@unina.it

^bConsorzio Interuniversitario di Reattività Chimica e Catalisi, via Celso Ulpiani 27, 70126 Bari, Italy

† Electronic supplementary information (ESI) available. CCDC 1851051. For ESI and crystallographic data in CIF or other electronic format see DOI: 10.1039/c8qj00664d

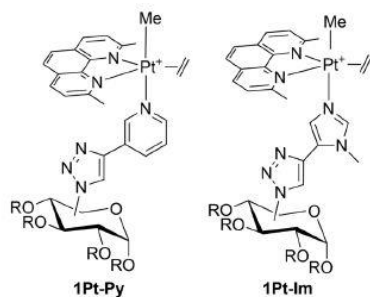


Fig. 1 The five-coordinate Pt(II) compounds containing a heterocycle linked to a glucoside residue.

active than cisplatin, but they are still scarcely selective. Furthermore, the complexes exhibit similar toxicity, thus suggesting that the active species could somehow have lost the sugar portion before reaching the target cell. This hypothesis is in line with the in-solution data demonstrating that the neutral sugar ligand could be replaced by coordinating solvents, such as DMSO⁴⁴ or even water.

Considering these observations, and with the aim of improving the performance of the five-coordinate Pt complexes, the present study was undertaken to prepare compounds in which glycoconjugation is realized through a direct link between platinum and a carbon atom of the carbohydrate residue (Fig. 2). The expectation is that the inertness of the Pt-C bond towards hydrolysis may preserve the integrity of the whole complexes up to the target. In this case, the axial positions are occupied by a halide ligand X and a D-galactose (gal) or D-glucose (glu), resulting in the families of complexes **1gal₁-X**/**1glu₁-X** and **1gal₀-X**. A deprotected form was also prepared by hydrolysis of the acetyl groups (**1gal₁-ldcp**). The molecules were stable in mixed DMSO/aqueous solvents, able to bind DNA *in vitro* and exhibited a selective cytotoxic activity on cancer cells through apoptosis activation.

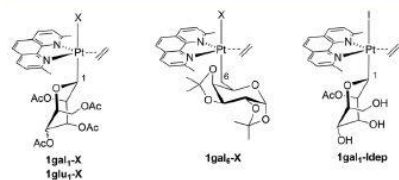


Fig. 2 The five-coordinate Pt(II) compounds containing C-linked carbohydrates (X = halide).

Results and discussion

Synthesis of the complexes

Scheme 1 describes the synthetic chemistry within this work.

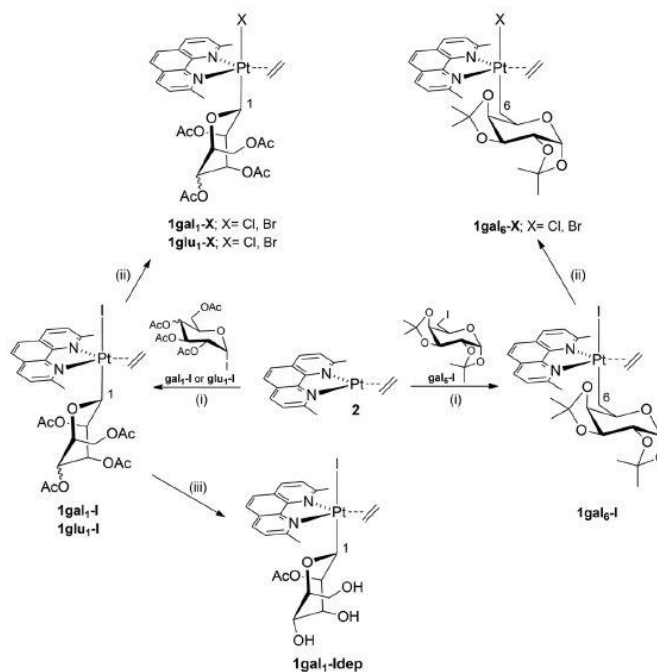
Complexes of type 1 share the trigonal bipyramidal arrangement with the *N,N*-bidentate ligand and the alkene in the plane, and a halide and the sugar residue (galactosyl, gal or glucosyl, glu) in the axial position. The stabilization of the structure is ensured by the simultaneous presence of 2,9-dimethyl-1,10-phenanthroline (dmphen),^{48,49} and of ethylene, which was selected to avoid the formation of undesired geometrical isomers. The complexes differ regarding the position of the sugar residue linked to Pt: C1 (**1gal₁-X**/**1glu₁-X**) or C6 (**1gal₀-X**), and, within the same subclass, for the nature of the halide X.

The synthetic approach involves the initial oxidative addition (paths i) of a 1-iodo-D-pyranose (**gal₁-I** or **glu₁-I**) or 6-iodo-D-galactose derivative (**gal₀-I**) to the platinum(0) precursor [Pt(dmphen)(ethylene)] (2), which yields the five-coordinate complexes **1gal₁-I**/**1glu₁-I** and **1gal₀-I**, respectively. Representative portions of the ¹H NMR spectra of **1gal₁-I** and **1gal₀-I** are reported in Fig. 3 (the proton and carbon spectra of all the complexes are reported in the ESI†).

The non-equivalent olefin protons are observed in the range between 2.2 and 3.5 ppm with characteristic coupling to ¹⁹⁵Pt. As expected, the position is largely shifted to low frequencies compared to free ethylene, because of the intense π -backdonation in the Pt-olefin bond.^{50,51} According to previous studies,⁵² the signals at higher δ can be attributed to the olefin protons facing the halide. Also, protons H1 or H6 (not shown) are shifted to low frequency, according to their position on a carbon directly bound to platinum in a five-coordinate geometry.

The pattern of the sugar protons in both **1gal₁-I** as well as in **1glu₁-I** reveals important aspects related to the stereochemical outcome of the reaction. In fact, the expected set of couplings typical of the ⁴C₁ chair is replaced by that of its alternative ¹C₄ arrangement. This evidence indicates that the reaction proceeds with chair inversion, as found in another work related to iridium complexes.⁵³ Accordingly, the metal is likely to occupy the α -position, in the stereochemical environment described in Scheme 1.

Single crystals of **1gal₀-I** appropriate for a diffractometric study were obtained by slow evaporation of a dichloromethane/hexane mixture. The compound crystallizes in the *P2₁2₁2₁* space group with a single molecule in the independent unit. The molecular structure in the ORTEP view is reported in Fig. 4. In the complex, the Pt atom adopts a fairly regular trigonal bipyramidal geometry with dmphen and olefin ligands in the equatorial plane. The axial positions are occupied by the iodine atom and the C6 atom of the D-galactose derivative. A small deviation of the ax-pt-ax angle from 180° is observed, probably due to the steric encumbrance of the galactose derivative. The normal chair conformation of the pyranose ring is hampered by the fusion of the two dioxolane rings and a distorted half-boat conformation is assumed. The two dioxo-



Scheme 1 Synthesis of the complexes: (i) toluene, RT; (ii) +AgX (X = Cl or Br), DCM, RT; (iii) KOH (5%), MeOH, RT.

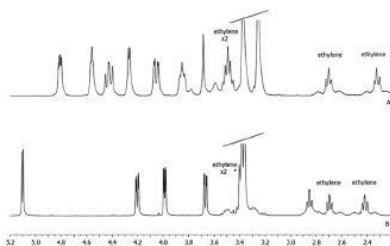


Fig. 3 Representative portions of the ^1H NMR spectra of **1gal₁-1** (A) and **1gal₆-1** (B) (CDCl_3 , 400 MHz).

lane rings exhibit a slightly distorted envelope conformation with O3 and C3 at the flap. The bidentate nitrogen ligand is planar, and its medium plane is slightly sloping (15.30°) compared to the coordination plane defined by N1/N2/C27/C28/Pt1 atoms (Fig. 5A). Crystal packing is stabilized by van der Waals interactions and π - π stacking interactions between the dmphen rings (Fig. 5B).

The platinum(II) complexes containing the other halides were prepared through an exchange by employing the different solubilities of the silver halides (path ii in Scheme 1). The NMR spectra of these compounds show all the distinctive signals previously discussed. The signals of the ethylene protons facing the halide progressively shift at lower frequencies moving through I, Br, Cl.

The complex **1gal₁-1** was also transformed into the corresponding deprotected form, **1gal₁-Iddep** (path iii in Scheme 1), to compare the biological effects of the protected hydroxyl groups with those of the deprotected ones, since deprotection can significantly affect the solubility properties and the mem-

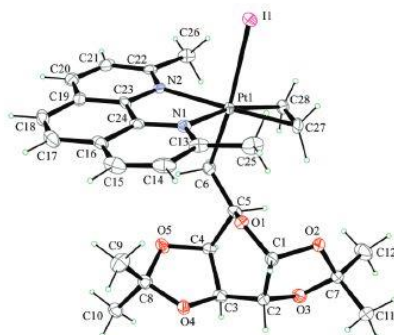


Fig. 4 ORTEP view of **1gal_L-I** with a thermal ellipsoid drawn at a 30% probability level. Selected bond lengths (Å) and angles (°): Pt–N1 = 2.210(5), Pt–N2 = 2.219(5), Pt–C27 = 2.056(7), Pt–C28 = 2.075(7), Pt–C6 = 2.063(6), Pt–I1 = 2.7535(5), C27–C28 = 1.42.

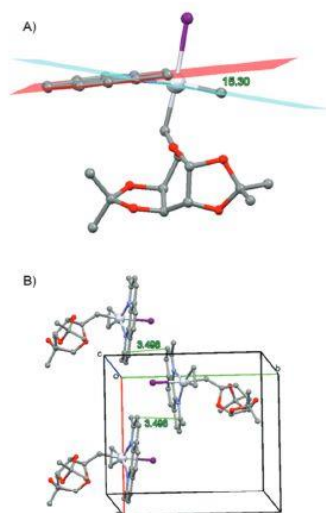


Fig. 5 (A) Angle between the bidentate ligand plane and the coordination plane. (B) Partial packing due to π - π stacking interactions. H atoms are not shown for clarity.

brane permeability of the Pt complexes. Deprotection was carried out in methanol with a catalytic amount of KOH (5% in moles). Surprisingly, it did not affect the acetyl group on the C2 of the sugar residue, whose residual signal (0.95 ppm) in the ^1H NMR spectrum is at a low frequency, compared to the typical position (2–2.5 ppm). This shift may be a consequence of an interaction with the aromatic portion of the bidentate ligand, which also stabilizes the acetyl fragment.

In-solution stabilities of the newly synthesized compounds

The stability of the compounds **1gal_L-I**, **1gal_D-I** and **1glu_L-I** in DMSO, in 10% DMSO/90% PBS at pH 7.4 and in 10% DMSO/0.05 M ammonium acetate pH 7.5 was monitored using electronic absorption spectroscopy. The spectra in DMSO showed an absorption peak at about 278 nm, accompanied by a smaller “shoulder” at about 300 nm. The time-evolution UV-vis spectra for **1gal_L-I**, **1gal_D-I** and **1glu_L-I** at room temperature are reported in Fig. 6.

Inspection of these spectra suggests a high stability of the analyzed compounds under the investigated experimental conditions. The compounds were stable for 24 h in 100% DMSO, whereas they experienced a change of their structure upon 7 days incubation in this coordinating solvent.

In contrast, the compounds appeared highly stable in mixed solvents since the spectra of the three compounds remained completely unchanged over 7 days incubation.

Cytotoxicity studies

To assess the cytotoxic effect of the newly synthesized Pt compounds, a couple of cell lines, immortalized and tumorigenic, was chosen. Immortalized murine fibroblast BALB/c-3T3 cells were used as normal cells and BALB/c-3T3 transformed with SV40 virus (SVT2) were used as cancer cells. Cells were incubated for 48 h with increasing concentrations of the compounds (from 1 to 10 $\mu\text{g mL}^{-1}$). Then, cell viability was measured using a MTT assay, in which the functionality of mitochondria is evaluated. In Fig. 7, the dose-response curves are reported, and the corresponding IC_{50} values, which represent the amount of drug able to induce 50% of cell death, are summarized in Table 1.

The results clearly show that all **gal** complexes were more toxic towards the cancer cell line than towards the immortalized cells. Surprisingly, **1gal_L-X** was the class of compounds endowed with higher selectivity, even though **1gal_L-X** compounds were still selective. No selectivity was observed instead with **1glu_L-X** compounds. It has to be noted that all drugs were more toxic towards cancer cells with respect to cisplatin alone (Table 1). The IC_{50} values of the deprotected form (**1gal_L-Idep**) showed a higher toxicity with respect to the protected one on both cell lines, and no selectivity was observed.

As is well known that GLUT11, a sugar transporter, is highly overexpressed in many tumor types, we analyzed its involvement in **1gal_L-I** cytotoxicity, using quercetin as glucose transporter inhibitor. Indeed, quercetin is known to be a potent inhibitor for GLUT1, -3, and -4.^{34,35} In this regard, pre-

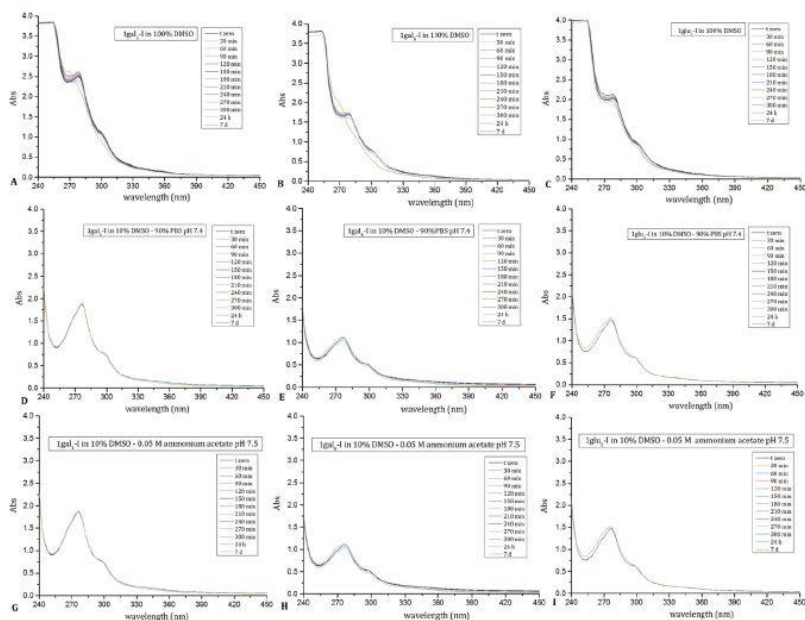


Fig. 6 Time course UV-vis spectra of 5×10^{-5} M **1gal₁-I**, **1gal₄-I** and **1glu₁-I** in 100% DMSO (A)–(C) 10% DMSO/90% PBS at pH 7.4 (D)–(F) and 10% DMSO/0.05 M ammonium acetate pH 7.5 (G)–(I).

liminary experiments were performed to assess the non-lethal quercetin concentration, which was found to be $3 \mu\text{M}$ (data not shown). Then, both cell lines were exposed to different concentrations of **1gal₁-I** in the presence or absence of $3 \mu\text{M}$ quercetin for 48 h. As shown in Fig. 8, no difference in cell viability was observed in the presence or in the absence of quercetin on immortalized fibroblasts. Interestingly, **1gal₁-I** was less toxic to cancer cells when incubated in the presence of quercetin. This difference was particularly evident when the compound was tested at $1 \mu\text{g mL}^{-1}$ (88 vs. 62% of cell viability, $p < 0.05$). This result suggested the possible involvement of a glucose transporter in **1gal₁-I** endocytosis.

Then, the mechanism of action of **1gal₁-I** was analyzed by measuring, on both cell lines, the intracellular ROS levels and the phosphorylation level of p38 (as markers of oxidative stress), I κ B- α (marker of inflammation), LDH release (marker of necrosis) and mitochondrial potential and pro-caspase-3 levels (as markers for apoptosis). Cells were incubated with $4 \mu\text{g mL}^{-1}$ of **1gal₁-I** as this concentration represents the IC_{50} value for cancer cells.

As shown in Fig. 9A, on immortalized cells, a significant increase in ROS levels was observed after 24 h, whereas on cancer cells, a small but significant increase was found after 30 min incubation.

The increase in ROS levels was constant up to 6 h, and then decreased over time. After 48 h incubation, no alteration in p38 level was observed for immortalized cells, whereas a significant increase was observed with SVT2 cells (Fig. 9B). When the mitochondrial potential ($\Delta\psi_{\text{m}}$) was measured after 4–6–24–48 h (Fig. 9C), we found a strong decrease in cancer cells and a strong increase in immortalized cells after 48 h incubation. We hypothesized that in immortalized cells the source of ROS was mitochondrial. This increase has been related to a pro-inflammatory state;⁵⁶ thus, we analyzed the I κ B- α level after 48 h incubation. As shown in Fig. 9E, no alteration in the I κ B- α level was observed on immortalized cells, whereas a strong decrease was observed in cancer cells. Taken together, our data indicate that, in immortalized cells, an increase in ROS levels, due to an alteration in mitochondrial potential, is counteracted by the antioxidant system of the cell, and no

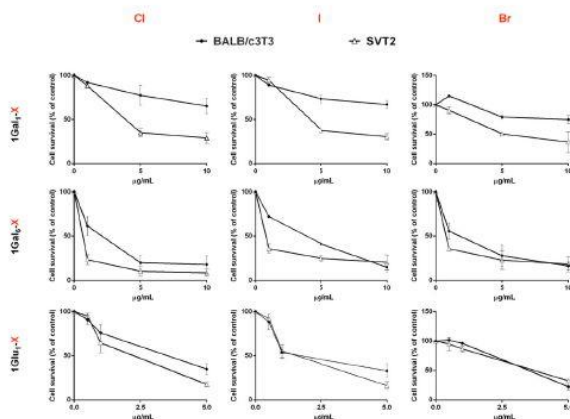


Fig. 7 Toxicity of new platinum complexes on fibroblasts. BALB/c-3T3 (full circles) and SVT2 (empty triangles) cells were incubated with increasing amounts of 1gal₁-X, 1gal₆-X and 1glu₁-X for 48 hours.

Table 1 IC₅₀ values (µg mL⁻¹) obtained for Pt-derived drugs, on BALB/c-3T3 and SVT2 cells after 48 h incubation

Cell line	1gal ₁ -Cl	1gal ₁ -I	1gal ₁ -Br	1gal ₆ -Cl	1gal ₆ -I	1gal ₆ -Br	1glu ₁ -Cl	1glu ₁ -I	1glu ₁ -Br	1gal ₁ -idep	cis-Pt
BALB/c-3T3	15.2 ± 0.3	19 ± 1.1	22 ± 2	2.45 ± 0.07	3.95 ± 0.07	2.1 ± 0.3	3.6 ± 0.5	1.2 ± 0.6	3.5 ± 0.14	2.8 ± 0.4	72 ± 14
SVT2	3.9 ± 0.3	4.0 ± 0.3	5.3 ± 0.4	0.65 ± 0.07	0.8 ± 0.14	0.80 ± 0.01	2.6 ± 0.5	1.5 ± 0.2	3.6 ± 0.1	2.4 ± 0.15	58 ± 2

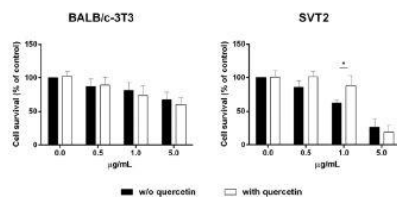


Fig. 8 Glucose transporter dependent cytotoxicity of 1gal₁-1 on fibroblasts. Cells were incubated with increasing amounts of each drug in the absence (black bars) or in the presence (white bars) of 3 µM quercetin. Cell viability was assessed using the MTT assay after 48 h incubation. Values are given as mean ± SD. * Indicates $p < 0.05$, between cells incubated in the absence or in the presence of quercetin.

alteration in phospho-p38 levels was observed. On the other hand, on cancer cells, an early increase in ROS levels will activate the oxidative stress pathway (increase in phospho-p38 level), the pro-inflammatory state and will finally lead to cell death, as suggested by $\Delta\psi_m$ decrease. To understand which cell death was activated, we measured the LDH release and the

apoptotic marker caspase-3. No release of the cytosolic enzyme was observed at any concentration analyzed (data not shown), whereas a strong decrease in pro-caspase-3 level was observed only in cancer cells (Fig. 9D).

Interaction with DNA monitored by ethidium bromide displacement fluorescence assay and by circular dichroism spectroscopy

To clarify the mechanism of action of the analyzed compounds, their interaction with DNA was evaluated. The interactions of the selected Pt compounds with sperm salmon double strand DNA (ssDNA) were investigated by the ethidium bromide (EtBr) displacement fluorescence assay (FID), which allows evaluating the DNA binding ability of small molecules, and by circular dichroism. EtBr is a double helix intercalator that is luminescent when it interacts with DNA. When it is displaced from the double helix by another molecule and it is free in solution, its emission is quenched. The relative fluorescence of EtBr in the presence of increasing amounts of 1glu₁-1, 1gal₆-1 and 1gal₁-1 in 0.05 M ammonium acetate at pH 7.5 is reported in Fig. 10. The emission intensity of the ssDNA-EtBr complex is quenched by the addition of Pt compounds, thus implying that they interact with ssDNA. The com-

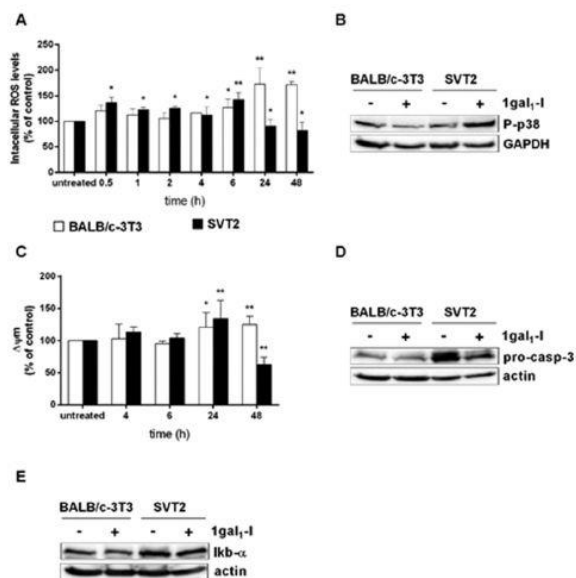


Fig. 9 Mechanism of action of **1gal₁-I** on fibroblasts. BALB/c-3T3 (white bars) or SVT2 (black bars) cells were incubated with $4 \mu\text{g mL}^{-1}$ of **1gal₁-I** for different lengths of time. (A) Time-dependent changes in ROS levels detected with a 2',7'-dichlorodihydrofluorescein diacetate probe and expressed as the fluorescence intensity percentage of the control (%). (B) Western blotting of the phosphorylation level of p38 (upper panel) after 48 h of incubation with **1gal₁-I**. Glyceraldehyde-3-phosphate dehydrogenase (lower panel) was used as an internal standard. (C) Time-dependent changes in the mitochondrial membrane potential ($\Delta\psi_m$) were determined using cationic lipophilic dye tetramethylrhodamine ethyl ester staining and expressed as the TMRE fluorescence intensity over control (%). (D) and (E) Cell extracts were subjected to western blotting analysis using anti pro-caspase-3 ((D) upper panel) or I κ B- α ((E) upper panel); actin was used as the loading control ((D) and (E) lower panels). In (A) and (C), data shown are the means \pm S.D. of three independent experiments and * indicates $p < 0.05$; ** indicates $p < 0.01$ with respect to untreated cells.

pounds with the galactose ligand, **1gal₆-I** and **1gal₁-I**, show greater DNA affinity than **1glu₁-I**, since they induce a stronger fluorescence quenching. A comparison of the present data with those previously reported for five-coordinate Pt(II) compounds containing heterocycles linked to glucoside residues indicates that the newly synthesized compounds have a lower affinity for ssDNA than the compounds that have been previously published.¹⁴

The interaction between ssDNA and the analyzed compounds was also investigated by collecting the CD spectra of the nucleic acid in the presence of **1gal₁-I**, **1gal₆-I** and **1glu₁-I** at two different Pt:DNA molar ratios (Fig. 11). When the spectra of ssDNA are compared to those of the DNA complexes with **1gal₁-I**, **1gal₆-I** and **1glu₁-I**, a slight variation of CD intensity is found, while the spectra profiles remain unchanged. These data are compatible with a change in the DNA helicity and base stacking following the Pt-double helix interaction.

Interestingly, when DNA was incubated with **1gal₆-I** at the 2:1 Pt to DNA molar ratio, a significant increase of the CD signal was detected.

Altogether, fluorescence and circular dichroism spectroscopy data clearly indicate that the compounds interact with DNA, with **1gal₆-I** that has the highest affinity for the double helix among the analyzed Pt compounds.

Experimental

Materials and methods

All solvents and reagents were purchased from Sigma-Aldrich and were used without further purification. All NMR spectra were recorded using a 400 Bruker Avance Ultrashield™ or a 500 Varian Innova spectrometer at 298 K. Chemical shifts were given in parts per million (ppm, δ), referenced to the solvent

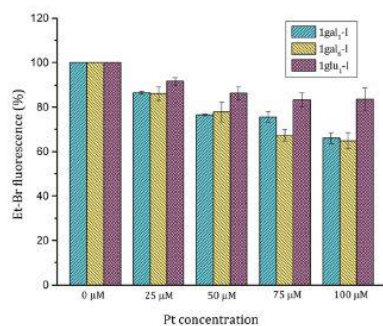


Fig. 10 Relative ethidium bromide fluorescence in the presence of increasing amounts of Pt compounds **1gal₁-I**, **1gal₆-I** and **1glu₁-I**.

peak of CDCl_3 (^1H NMR δ 7.26, ^{13}C NMR δ 77), $(\text{CD}_3)_2\text{CO}$ (^1H NMR δ 2.05 ppm, ^{13}C NMR δ 29.8 ppm and $\delta = 206.3$). Coupling constants were quoted in Hz (J). ^1H NMR and ^{13}C NMR splitting patterns were designated as singlet (s), doublet (d), triplet (t), quartet (q), double doublet (dd), double triplet (dt), and double AB quartet (dABq). Splitting patterns that

could not be interpreted or easily visualized were designated as multiplet (m). Peracetylated 1-iodo-D-glucose,^{57,58} 1-iodo-D-galactose,^{57,58} and bis(acetal)-6-iodo-D-galactose⁵⁹ were prepared according to published methods.

Synthesis of the complexes

A suspension of $[\text{Pt}(\text{COD})_2]$ (0.300 g, 0.728 mmol) in dry toluene (3 mL) was put in an ice bath under an ethylene atmosphere and vigorously stirred. 2,9-Dimethyl-1,10-phenanthroline (dmphen) (0.182 g, 0.874 mmol) was added in small aliquots, leading to the formation of the red trigonal planar species $[\text{Pt}(\text{dmphen})(\text{ethylene})]$. After 10 minutes, the mother liquors were removed, and the complex was washed with dry toluene (2×1 mL). A solution of the appropriate iododerivative (0.810 mmol) in dry toluene (2 mL) was added to the red suspension and the reaction mixture was stirred at room temperature for 30 minutes (for **1gal₁-I** or **1glu₁-I**) or overnight (for **1gal₆-I**), respectively. The product was washed with toluene (2 mL) and hexane (3×3 mL), and then dried under vacuum. The solid was solved in the minimum volume of dichloromethane, filtered on Florisil®, and crystallized with diethyl ether. Mother liquors were removed, and the white solid was dried under vacuum.

The complexes with the other halides were prepared by treating the appropriate iodo-complex (0.100 mmol) in DCM (4 mL) with an excess of AgX ($\text{X} = \text{Cl}, \text{Br}$). After 3 hours of stirring, the suspension was filtered, and the volume of the

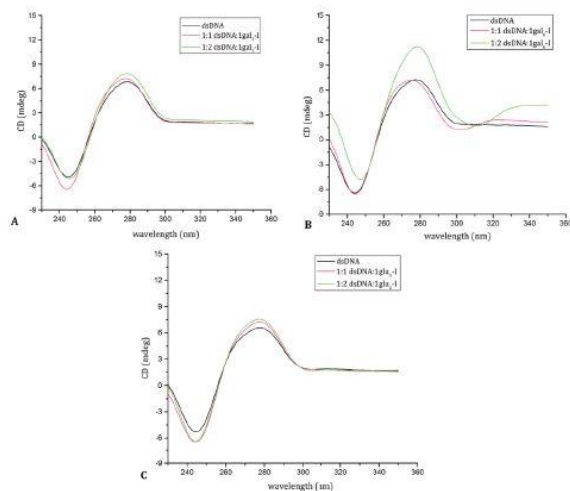


Fig. 11 CD spectra of DNA (200 μM in 0.01 M ammonium acetate buffer, pH 7.5) in the presence of **1glu₁-I** (A), **1gal₆-I** (B) and **1gal₁-I** (C) 1:1 and 1:2 DNA to metal molar ratios.

solvent was reduced under vacuum. The addition of diethyl ether yielded the product as a microcrystalline solid in nearly quantitative yield.

1gal₆-I. ¹H NMR (400 MHz, CDCl₃) δ 8.28 (d, 1H), 8.27 (d, 1H), 7.81 (s, 2H), 7.73 (d, 2H), 5.13 (d, H1, ²J_{H1-H2} = 5.2 Hz, 1H), 4.23 (dd, H3, ³J_{H3-H4} = 7.8, ³J_{H3-H2} = 2.3 Hz, 1H), 4.01 (dd, H2, 1H), 3.69 (dd, H4, ³J_{H4-H3} = 1.9 Hz, 1H), 3.42 (app d, C₂H₄, ²J_{F₆-H} = 84 Hz, 2H), 3.41 (s, 3H, Me-dmpfen), 3.39 (s, 3H, Me-dmpfen), 2.88 (dt, H5, ³J_{H5-H6} = ³J_{H5-H6'} = 6.9 Hz, 1H), 2.72 (dt, ²J_{F₆-H} = 65 Hz, 1H, C₂H₄), 2.44 (dt, ²J_{F₆-H} = 63 Hz, 1H, C₂H₄), 1.18 (s, 3H, Me), 1.11 (s, 3H, Me), 1.09 (s, 3H, Me), 0.94 (s, 3H, Me), 1.08 (dABq, H6 and H6', ³J_{H6-H6'} = 10.8 Hz, 2H). ¹³C NMR (100 MHz, 298 K, CDCl₃): δ 162–125 (aromatics), 108.2, 107.7, 96.4, (1C hidden by the solvent), 72.8, 71.0, 69.9, 29.2 (×2), 29.0 (×2), ¹J_{F₆-C} = 340 Hz), 25.7, 25.6, 24.7, 24.4, 12.8 (¹J_{F₆-C} = 690 Hz). Anal. calcd (found): (C₂₈H₃₃IN₂O₃PT): C, 41.95 (41.80); H, 4.40 (4.49); N, 3.49 (3.38).

1gal₆-Br. ¹H NMR (400 MHz, CDCl₃) δ 8.27 (d, 2H), 7.81 (s, 2H), 7.73 (d, 2H), 5.0 (s, H1, ²J_{H1-H2} = 5.2 Hz, 1H), 4.20 (d, H3, ³J_{H3-H4} = 7.7, 1H), 4.01 (d, H2, 1H), 3.69 (d, H4, 1H), 3.40 (s, 3H, Me-dmpfen), 3.38 (s, 3H, Me-dmpfen), 3.20 (app d, C₂H₄, ²J_{F₆-H} = 84 Hz, 2H), 2.89 (t, H5, ³J_{H5-H6} = ³J_{H5-H6'} = 6.8 Hz, 1H), 2.67 (dt, ²J_{F₆-H} = 63 Hz, 1H, C₂H₄), 2.41 (dt, ²J_{F₆-H} = 62 Hz, 1H, C₂H₄), 1.15 (s, 3H, Me), 1.08 (s, 3H, Me), 1.07 (s, 3H, Me), 0.94 (s, 3H, Me), 1.0 (partially overlapped m, H6 and H6', 2H). ¹³C NMR (100 MHz, 298 K, CDCl₃): δ 162–125 (aromatics), 108.2, 107.5, 96.4, 77 (hidden by the solvent), 72.9, 71.1, 70.0, 66.3, 30.2 (×2), ¹J_{F₆-C} = 368 Hz), 28.6 (×2), 25.6, 24.7, 24.4, 24.1, 7.1 (¹J_{F₆-C} = 703 Hz). Anal. calcd (found): (C₂₈H₃₃BrN₂O₃PT): C, 44.57 (44.77); H, 4.68 (4.59); N, 3.71 (3.74).

1gal₆-Cl. ¹H NMR (400 MHz, CDCl₃) δ 8.28 (d, 2H), 7.81 (s, 2H), 7.73 (d, 2H), 5.1 (s, H1, ²J_{H1-H2} = 5.0 Hz, 1H), 4.21 (dd, H3, ³J_{H3-H4} = 7.5, ³J_{H3-H2} = 2.2 Hz, 1H), 3.99 (dd, H2, 1H), 3.69 (d, H4 1H), 3.41 (s, 3H, Me-dmpfen), 3.39 (s, 3H, Me-dmpfen), 3.09 (app d, C₂H₄, ²J_{F₆-H} = 82 Hz, 2H), 2.92 (t, H5, ³J_{H5-H6} = ³J_{H5-H6'} = 7.0 Hz, 1H), 2.66 (dt, ²J_{F₆-H} = 62 Hz, 1H, C₂H₄), 2.42 (dt, ²J_{F₆-H} = 62 Hz, 1H, C₂H₄), 1.15 (s, 3H, Me), 1.09 (s, 3H, Me), 1.05 (s, 3H, Me), 0.98 (s, 3H, Me), 1.0 (partially overlapped m, H6 and H6'). ¹³C NMR (100 MHz, 298 K, CDCl₃): δ 162–125 (aromatics), 108.2, 107.5, 96.4, 77 (hidden by the solvent), 73.0, 71.1, 70.0, 66.6, 30.9 (2C, ¹J_{F₆-C} = 379 Hz), 28.4 (×2), 25.7 (×2), 24.7, 24.4, 3.5 (¹J_{F₆-C} = 712 Hz). Anal. calcd (found): (C₂₈H₃₃ClN₂O₃PT): C, 47.36 (47.46); H, 4.97 (5.05); N, 3.94 (3.83).

1gal₆-I. ¹H NMR (400 MHz, CDCl₃) δ 8.33 (d, 1H), 8.29 (d, 1H), 7.85 (dABq, 2H), 7.78 (d, 1H), 7.74 (d, 1H), 4.81 (dd, H4, ³J_{H3-H4} = 3.6 Hz, ³J_{H4-H3} = 6.8 Hz, 1H), 4.56 (t, H3, ³J_{H3-H3} = 3.7 Hz, 1H), 4.42 (dd, H6, ³J_{H6-H6'} = 10.1 Hz, ³J_{H6-H6'} = 12.2 Hz, 1H), 4.27 (d, H2, 1H), 4.05 (dd, H6', ³J_{H6-H6'} = 2.5 Hz, 1H), 3.85 (m, H5, 1H), 3.68 (s, H1, ²J_{F₆-H} = 76 Hz, 1H), 3.49 (t, C₂H₄, ²J_{F₆-H} = 80 Hz, 2H), 3.37 (s, Me-dmpfen, 3H), 3.25 (s, Me-dmpfen, 3H), 2.70 (m, C₂H₄, ²J_{F₆-H} = 68 Hz, 1H), 2.33 (m, C₂H₄, ²J_{F₆-H} = 63 Hz, 1H), 2.14 (s, Me, 3H), 2.03 (s, Me, 3H), 1.88 (s, Me, 3H), 0.82 (s, Me, 3H). ¹³C NMR (100 MHz, 298 K, CDCl₃): δ 170.8, 169.5, 168.7 (×2), 163–124 (aromatics), 74.6, 72.2, 66.9, 65.7, 59.5, 50.2 (¹J_{F₆-C} = 867 Hz), 31.3 (¹J_{F₆-C} = 362 Hz), 30.5

(¹J_{F₆-C} = 360 Hz), 29.2, 28.8, 20.9 (×2), 20.5, 19.7. Anal. calcd (found): (C₃₀H₃₃IN₂O₃PT): C, 40.50 (40.34); H, 3.97 (3.92); N, 3.15 (3.21).

1gal₆-Br. ¹H NMR (400 MHz, CDCl₃) δ 8.32 (d, 1H), 8.29 (d, 1H), 7.84 (dABq, 2H), 7.78 (d, 1H), 7.74 (d, 1H), 4.82 (dd, H4, ³J_{H3-H4} = 3.5 Hz, ³J_{H4-H3} = 6.9 Hz, 1H), 4.57 (t, H3, ³J_{H3-H3} = 3.6 Hz, 1H), 4.45 (dd, H6, ³J_{H6-H6'} = 10.0 Hz, ³J_{H6-H6'} = 12.2 Hz, 1H), 4.27 (d, H2, 1H), 4.05 (dd, H6', ³J_{H6-H6'} = 2.5 Hz, 1H), 3.85 (m, H5 and H1, ²J_{F₆-H} = 74 Hz, 2H), 3.38 (s, Me-dmpfen, 3H), 3.30 (t, C₂H₄, 2H), 3.26 (s, Me-dmpfen, 3H), 2.70 (m, C₂H₄, ²J_{F₆-H} = 65 Hz, 1H), 2.32 (m, C₂H₄, ²J_{F₆-H} = 60 Hz, 1H), 2.14 (s, Me, 3H), 2.04 (s, Me, 3H), 1.88 (s, Me, 3H), 0.78 (s, Me, 3H). ¹³C NMR (100 MHz, 298 K, CDCl₃): δ 170.8, 169.5, 168.7, 168.6, 163–125 (aromatics), 74.7, 72.2, 66.8, 65.7, 59.6, 46.4 (¹J_{F₆-C} = 888 Hz), 32.7 (¹J_{F₆-C} = 367 Hz), 32.0 (¹J_{F₆-C} = 367 Hz), 28.8, 28.3, 20.9 (×2), 20.6, 19.7. Anal. calcd (found): (C₃₀H₃₃BrN₂O₃PT): C, 42.76 (42.93); H, 4.19 (4.15); N, 3.32 (3.26).

1gal₆-Cl. ¹H NMR (400 MHz, CDCl₃) δ 8.33 (d, 1H), 8.29 (d, 1H), 7.85 (dABq, 2H), 7.78 (d, 1H), 7.74 (d, 1H), 4.81 (dd, H4, ³J_{H3-H4} = 3.5 Hz, ³J_{H4-H3} = 6.9 Hz, 1H), 4.57 (t, H3, ³J_{H3-H3} = 3.5 Hz, 1H), 4.47 (dd, H6, ³J_{H6-H6'} = 10.2 Hz, ³J_{H6-H6'} = 12.2 Hz, 1H), 4.29 (d, H2, 1H), 4.07 (dd, H6', ³J_{H6-H6'} = 2.7 Hz, 1H), 3.94 (s, H1, ²J_{F₆-H} = 74 Hz, 1H), 3.86 (m, H5, 2H), 3.39 (s, Me-dmpfen, 3H), 3.26 (s, Me-dmpfen, 3H), 3.18 (t, C₂H₄, ²J_{F₆-H} = 79 Hz, 2H), 2.70 (m, C₂H₄, ²J_{F₆-H} = 63 Hz, 1H), 2.32 (m, C₂H₄, ²J_{F₆-H} = 62 Hz, 1H), 2.15 (s, Me, 3H), 2.05 (s, Me, 3H), 1.88 (s, Me, 3H), 0.75 (s, Me, 3H). ¹³C NMR (100 MHz, 298 K, CDCl₃): δ 170.9, 169.5, 168.7, 168.6, 163–125 (aromatics), 74.8, 72.1, 66.8, 65.7, 59.6, 46.6 (¹J_{F₆-C} = 169 Hz), 33.4 (¹J_{F₆-C} = 370 Hz), 32.8 (¹J_{F₆-C} = 368 Hz), 28.6, 28.0, 20.9 (×2), 20.6, 19.6. Anal. calcd (found): (C₃₀H₃₃ClN₂O₃PT): C, 45.14 (45.07); H, 4.42 (4.48); N, 3.51 (3.62).

1gal₆-Idep. ¹H NMR (400 MHz, CDCl₃) δ 8.60 (d, 1H), 8.52 (d, 1H), 8.08 (dABq, 2H), 7.96 (d, 1H), 7.94 (d, 1H), 4.20 (d, H2, ³J_{H2-H3} = 3.7 Hz, 1H), 4.11 (s, H1, ²J_{F₆-H} = 80 Hz, 2H), 3.85 (m, H5, 1H), 3.61 (m, H6, 1H), 3.51 (m, H4 and H6', 2H), 3.40 (s, Me-dmpfen, 3H), 3.29 (s, Me-dmpfen, 3H), 3.29 (m, C₂H₄, 2H), 3.16 (m, H3, 1H), 2.79 (m, C₂H₄, ²J_{F₆-H} = 68 Hz, 1H), 2.41 (m, C₂H₄, ²J_{F₆-H} = 64 Hz, 1H), 0.95 (s, Me, 3H). ¹³C NMR (100 MHz, 298 K, acetone-d₆): δ 169.7, 163–127 (aromatics), 78.8 (×2), 69.1, 66.7, 60.0, 51.7 (¹J_{F₆-C} = 835 Hz), (4C hidden by the solvent), 20.3. Anal. calcd (found): (C₂₃H₂₅IN₂O₃PT): C, 37.76 (37.61); H, 3.83 (3.90); N, 3.67 (3.75).

1glu₁-I. ¹H NMR (400 MHz, CDCl₃) δ 8.33 (d, 1H), 8.31 (d, 1H), 7.87 (dABq, 2H), 7.79 (d, 1H), 7.77 (d, 1H), 4.65 (dd, H4, ³J_{H3-H4} = 4.4 Hz, ³J_{H4-H3} = 6.5 Hz, 1H), 4.29 (dd, H3, ³J_{H3-H3} = 3.5 Hz, 1H), 4.15 (d, H2, 1H), 3.87 (s, H1, ²J_{F₆-H} = 76 Hz, 1H), 3.83 (dd, H6, ³J_{H6-H6'} = 5.9 Hz, ³J_{H6-H6'} = 12.0 Hz, 1H), 3.71 (dd, H6', ³J_{H6-H6'} = 3.9 Hz, 1H), 3.49 (app d, C₂H₄, ²J_{F₆-H} = 76 Hz, 2H), 3.43 (m, H5, 1H), 3.40 (s, Me-dmpfen, 3H), 3.31 (s, Me-dmpfen, 3H), 2.69 (m, C₂H₄, ²J_{F₆-H} = 71 Hz, 1H), 2.39 (m, C₂H₄, ²J_{F₆-H} = 64 Hz, 1H), 2.05 (s, Me, 3H), 1.94 (s, Me, 3H), 1.82 (s, Me, 3H), 1.10 (s, Me, 3H). ¹³C NMR (100 MHz, 298 K, CDCl₃): δ 170.6, 169.3, 168.9, 168.8, 162–125 (aromatics), 74.2, 71.4, 70.5, 68.2, 61.9, 53.4 (¹J_{F₆-C} = 859 Hz), 31.2 (¹J_{F₆-C} = 364 Hz), 30.8 (¹J_{F₆-C} = 366 Hz), 29.3, 29.1, 20.8 (×2), 20.7, 20.0.

Anal. calcd (found): (C₃₀H₃₅IN₂O₉Pt): C, 40.50 (40.34); H, 3.97 (3.86); N, 3.15 (3.09).

1glu-Br. ¹H NMR (400 MHz, CDCl₃) δ 8.33 (d, 1H), 8.31 (d, 1H), 7.86 (dABq, 2H), 7.79 (d, 1H), 7.77 (d, 1H), 4.68 (dd, H4, ³J_{H3-H4} = 4.5 Hz, ²J_{H4-H5} = 6.7 Hz, 1H), 4.31 (dd, H3, ²J_{H2-H3} = 3.2 Hz, 1H), 4.18 (d, H2, 1H), 4.02 (s, H1, ²J_{Pt-H} = 82 Hz, 1H), 3.86 (dd, H6, ³J_{H5-H6} = 5.9 Hz, ²J_{H6-H6'} = 11.9 Hz, 1H), 3.76 (dd, H6', ³J_{H5-H6'} = 4.2 Hz, 1H), 3.46 (m, H5, 1H), 3.42 (s, Me-dmphen, 3H), 3.32 (s, Me-dmphen, 3H), 3.30 (app d, C₂H₄, ²J_{Pt-H} = 71 Hz, 2H), 2.70 (m, C₂H₄, ²J_{Pt-H} = 71 Hz, 1H), 2.38 (m, C₂H₄, ²J_{Pt-H} = 62 Hz, 1H), 2.06 (s, Me, 3H), 1.95 (s, Me, 3H), 1.82 (s, Me, 3H), 1.04 (s, Me, 3H). ¹³C NMR (100 MHz, 298 K, CDCl₃): δ 170.6, 169.3, 168.8 (×2), 163–125 (aromatics), 74.5, 71.4, 70.6, 68.2, 61.9, 49.8 (²J_{Pt-C} = 883 Hz), 32.6 (¹J_{Pt-C} = 362 Hz), 32.3 (¹J_{Pt-C} = 360 Hz), 28.7, 28.6, 20.7 (×2), 20.6, 19.9. Anal. calcd (found): (C₂₆H₃₅BrN₂O₉Pt): C, 42.76 (42.92); H, 4.19 (4.21); N, 3.32 (3.27).

1glu-Cl. ¹H NMR (400 MHz, CDCl₃) δ 8.34 (d, 1H), 8.32 (d, 1H), 7.86 (dABq, 2H), 7.79 (d, 1H), 7.77 (d, 1H), 4.70 (dd, H4, ³J_{H3-H4} = 4.7 Hz, ²J_{H4-H5} = 6.6 Hz, 1H), 4.32 (dd, H3, ²J_{H2-H3} = 2.8 Hz, 1H), 4.19 (d, H2, 1H), 4.10 (s, H1, ²J_{Pt-H} = 81 Hz, 1H), 3.89 (dd, H6, ³J_{H5-H6} = 5.9 Hz, ²J_{H6-H6'} = 11.8 Hz, 1H), 3.80 (dd, H6', ³J_{H5-H6'} = 4.0 Hz, 1H), 3.48 (m, H5, 1H), 3.43 (s, Me-dmphen, 3H), 3.32 (s, Me-dmphen, 3H), 3.18 (app d, C₂H₄, ²J_{Pt-H} = 75 Hz, 2H), 2.71 (m, C₂H₄, ²J_{Pt-H} = 66 Hz, 1H), 2.40 (m, C₂H₄, ²J_{Pt-H} = 64 Hz, 1H), 2.07 (s, Me, 3H), 1.96 (s, Me, 3H), 1.83 (s, Me, 3H), 0.99 (s, Me, 3H). ¹³C NMR (100 MHz, 298 K, CDCl₃): δ 170.7, 169.3, 168.9, 168.8, 162–125 (aromatics), 74.6, 71.3, 70.5, 68.1, 61.9, 47.3 (²J_{Pt-C} = 885 Hz), 33.3 (¹J_{Pt-C} = 376 Hz), 33.0 (¹J_{Pt-C} = 374 Hz), 28.6, 28.4, 20.8 (×2), 20.5, 19.9. Anal. calcd (found): (C₃₀H₃₅ClN₂O₉Pt): C, 45.14 (45.03); H, 4.42 (4.30); N, 3.51 (3.67).

X-ray crystallography

Single crystals of **1gal-I** suitable for X-ray diffraction studies were obtained under the slow evaporation of a dichloromethane/hexane solution. Data were measured at 173 K using a Bruker-Nonius KappaCCD four-circle diffractometer endowed with Oxford Cryostream 700 apparatus and graphite monochromator (radiation MoKα = 0.71073 Å). Reduction of data and semiempirical absorption correction was done using the SADABS program.⁶⁰ Structure was solved using direct methods (SIR97 program⁶¹) and refined by the full-matrix least-squares method on *F*² using the SHELXL-2016/6 program⁶² with the aid of the program WinGX.⁶³ Anisotropic parameters were used for non-H atoms. Ethylene hydrogen atoms were located in different Fourier maps and freely refined with an isotropic thermal parameter *U*_{iso}(H) equal to 1.2*U*_{eq} of the carrier atom. All the other H atoms were generated stereochemically and refined accordingly to the riding model with C–H distances in the range 0.95–1.00 Å and *U*_{iso}(H) equal to 1.2*U*_{eq} of the carrier atom (1.5*U*_{eq} for C_{meq}). Details on crystal and refinement data are reported in Table 2. The figures were generated using ORTEP-3⁶⁴ and Mercury CSD 3.9⁶⁵ programs.

Table 2 Crystal data and structure refinement for **1gal-I**

Empirical formula	C ₃₀ H ₃₅ IN ₂ O ₉ Pt
Formula weight	798.54
Temperature	298(2) K
Wavelength	0.71073 Å
Crystal system, space group	Orthorhombic, <i>P</i> 2 ₁ 2 ₁ 2 ₁
Unit cell dimensions	<i>a</i> = 11.3000(10) Å, <i>α</i> = 90° <i>b</i> = 12.8040(11) Å, <i>β</i> = 90° <i>c</i> = 19.8560(16) Å, <i>γ</i> = 90°
Volume	2872.9(4) Å ³
Z, calculated density	4, 1.846 Mg m ⁻³
Absorption coefficient	5.997 mm ⁻¹
<i>F</i> (000)	1540
Crystal size	0.40 × 0.10 × 0.01 mm
Theta range for data collection	2.051 to 27.504°
Reflections collected/unique	10 728/6027 [<i>R</i> (int) = 0.0332]
Data/restraints/parameters	6027/0/340
Goodness-of-fit on <i>F</i> ²	1.105
Final <i>R</i> indices [<i>I</i> > 2σ(<i>I</i>)]	<i>R</i> ₁ = 0.0408, <i>wR</i> ₂ = 0.1037
<i>R</i> indices (all data)	<i>R</i> ₁ = 0.0514, <i>wR</i> ₂ = 0.1204
Absolute structural parameter	0.047(7)
Largest diff. peak and hole	0.903 and −1.242 e Å ⁻³

Crystallographic data for **1gal-I** were deposited in the Cambridge Crystallographic Data Centre with the deposition number CCDC 1851105.[†]

Stability of selected Pt compounds in aqueous solutions

The in-solution stability of selected Pt compounds (**1gal-I**, **1gal-I** and **1glu-I**) was monitored using UV-vis absorption spectroscopy using a Varian Cary 5000 UV-vis-NIR spectrophotometer and the following parameters: wavelength range: 240–700 nm, data pitch: 1 nm, scanning speed: 600 nm min⁻¹, quartz cuvette with 1 cm path length. The compounds were prepared with a concentration of 5 × 10⁻⁵ M in 100% DMSO, 10% DMSO/90% PBS (v/v), 10% DMSO/0.05 M ammonium acetate pH 7.5, 10% DMSO/0.01 M sodium citrate pH 5.1, 10% DMSO/0.05 M sodium acetate pH 5.5, and 10% DMSO/0.01 M sodium acetate pH 4.4.

Cell culture and MTT assay

Murine BALB/c-3T3 and SVT2 fibroblasts were obtained from ATCC and cultured in Dulbecco's modified Eagle's medium (DMEM) (Sigma-Aldrich, St Louis, MO, USA), supplemented with 10% foetal bovine serum (HyClone), 2 mM L-glutamine and antibiotics, all from Sigma-Aldrich, under a 5% CO₂ humidified atmosphere at 37 °C. For the dose-response experiments, cells were seeded in 96-well plates at a density of 2.5 × 10⁵ cells per well. 24 h after seeding, increasing concentrations of compounds were added to the cells (0.5–20 μg mL⁻¹). Cell viability was assessed by the MTT (3-(4,5-dimethylthiazol-2-yl)-2,5-diphenyltetrazolium bromide) assay after 48 h, as described by Ferraro *et al.*⁶⁶ For the GLUT inhibitor mediated cytotoxicity assay, 24 h after seeding, the cells were treated with 0.5–1.5 μg mL⁻¹ of **1gal-I** in the presence or absence of 3 μM quercetin. Quercetin alone was used as the control. After 48 h incubation, the MTT assay was performed. Cell survival was expressed as the percentage of viable cells in the presence of the compound

under test compared to the controls. Two groups of cells were used as the controls, *i.e.* untreated cells and cells supplemented with identical volumes of DMSO. Each sample was tested in three independent analyses, each carried out in triplicate.

Analysis of the mechanism of action

ROS levels were measured as described in Petruk *et al.*⁶⁷ Briefly, the cells were incubated with $4 \mu\text{g mL}^{-1}$ of **1gal₁-1**, for different times (0–48 h) and then incubated with 2',7'-dichlorodihydrofluorescein diacetate (DCFDA, Sigma-Aldrich). Fluorescence intensity was measured using a PerkinElmer LS50 spectrofluorometer (525 nm emission wavelength, 488 nm excitation wavelength, 300 nm min^{-1} scanning speed and 5 nm slit width for both excitation and emission). ROS production was expressed as a percentage of DCF fluorescence intensity of the sample under test, with respect to the untreated sample. Each value was assessed by three independent experiments, each with three determinations. Significance was determined by the Student's *t*-test. The mitochondrial membrane potential ($\Delta\psi_m$) was measured as described by Monti *et al.*⁶⁸ Cells were plated at a density of 2×10^4 cells per well and after 24 h were treated as described above. At the end of the treatment, the cells were incubated with 200 nM of the cationic lipophilic dye tetramethylrhodamine ethyl ester (TMRE) for 20 min at 37 °C. Then, the cells were gently washed with 0.2% BSA in PBS three times and the fluorescence was measured in a microplate reader with peak $\lambda(\text{ex})/\lambda(\text{em}) = 549/575 \text{ nm}$. Each value is the mean of three independent experiments, each with three determinations. Significance was determined by the Student's *t*-test. For western blotting analyses, cells were treated as described above. After 48 h of incubation, cell lysates were analysed by western blotting performed as reported by Galano *et al.* Antibodies for phospho-p38, pro-caspase-3, and I κ B- α were purchased from Cell Signal Technology (Danvers, MA, USA). To normalize the protein intensity levels, a specific antibody against internal standards was used, *i.e.* anti-GAPDH (Thermo Fisher, Rockford, IL, USA) or anti-actin (Sigma-Aldrich). The chemiluminescence detection system (SuperSignal® West Pico) was purchased from Thermo Fischer.

The occurrence of necrosis was determined by measuring the release of lactate dehydrogenase (LDH) in the culture medium using the LDH-based *in vitro* toxicology assay kit (Sigma-Aldrich).

Interaction with DNA

The interaction of selected Pt compounds (**1gal₁-1**, **1gal₆-1** and **1glu₁-1**) with sperm salmon double strand DNA (ssDNA) was studied using fluorescence spectroscopy. A fluorescence quenching assay of the DNA-ethidium bromide (EtBr) complex was performed using a Spectrofluorometer (HORIBA Fluoromax 4) equipped with 1.0 cm quartz cells and a thermostat bath. ssDNA was incubated with EtBr in 0.05 M ammonium acetate at pH 7.5 at a DNA:EtBr molar ratio of 50:1 for 30 min at room temperature. Then, the fluorescence quenching of this complex was evaluated by adding to it

increasing amounts of Pt compounds dissolved in DMSO ($30 \times 10^{-3} \text{ M}$). Samples were equilibrated for 5 min. In control experiments, it has been verified that the EtBr efficiently binds ssDNA and that the addition of DMSO to DNA-EtBr does not change the fluorescence spectra of this complex. Quenching was followed using an excitation wavelength of 545 nm. The interaction of Pt compounds with DNA was also investigated by circular dichroism spectroscopy. Circular dichroism experiments were performed on a Jasco J-810 spectropolarimeter at 25 °C. Spectra were collected on samples of ssDNA incubated with **1gal₁-1**, **1gal₆-1** and **1glu₁-1** for 24 h in different molar ratios (1:1, 1:2) in 0.01 M ammonium acetate pH 7.5. CD spectra were compared with those collected using ligand-free ssDNA. Quartz cells with a path length of 0.1 cm were used in the far-UV region from 230 to 350 nm. Each spectrum was obtained averaging three scans and subtracting contributions from the corresponding references. Other experimental settings were: 50 nm min^{-1} scan speed, 2.0 nm bandwidth, 1.0 nm resolution, 50 mdg sensitivity and 4 s response.

Conclusions

Here, we have reported the convenient synthesis and the characterization of the biological activity of a new class of five-coordinate complexes of Pt(II) glycosylated with glucose and galactose through either C1 or C6. These molecules have been studied to verify any beneficial effects of both the coordinative saturation and the Pt–C linkage in the recognition of tumorigenic cells. The results of the biological assays have pleasingly revealed that the complexes are indeed selective. This attitude may originate from the active involvement of the sugar receptors overexpressed by the tumor cells. The study of the interaction with the DNA was in line with the results, showing that, within the C-glycosylated compounds studied in this work, greater activity and selectivity coincide with a higher binding affinity. Overall, the results are a robust demonstration that the glycosylation of Pt compounds through a Pt–C linkage can be a very effective strategy for the destruction of cancer cells, while preserving the survival of the healthy ones.

Conflicts of interest

There are no conflicts to declare.

Acknowledgements

FR acknowledges the MIUR for the financial support (PRIN2015 – Prot. 20154X9ATP).

Notes and references

- 1 I. Romero-Cancelón, M. Mos and P. J. Sadler, *J. Med. Chem.*, 2015, **58**, 7874–7880.

- 2 B. Rosenberg, L. Vancamp, J. E. Trosko and V. H. Mansour, *Nature*, 1969, **222**, 385.
- 3 M. A. Fuertes, C. Alonso and J. M. Pérez, *Chem. Rev.*, 2003, **103**, 645–662.
- 4 B. L. Stocker and J. O. Hoberg, *Organometallics*, 2006, **25**, 4537–4541.
- 5 P. C. A. Bruijninx and P. J. Sadler, *Curr. Opin. Chem. Biol.*, 2008, **12**, 197–206.
- 6 V. Hellberg, I. Wallin, S. Eriksson, E. Hernlund, E. Jerremalm, M. Berndtsson, S. Eksborg, E. S. J. Arnér, M. Shoshan, H. Ehrsson and G. Laurell, *J. Natl. Cancer Inst.*, 2009, **101**, 37–47.
- 7 S. Amptoulach and N. Tsavaris, *Chemother. Res. Pract.*, 2011, **2011**, 5.
- 8 R. Oun, Y. E. Moussa and N. J. Wheate, *Dalton Trans.*, 2018, **47**, 6645–6653.
- 9 T. C. Johnstone, K. Suntharalingam and S. J. Lippard, *Chem. Rev.*, 2016, **116**, 3436–3486.
- 10 M. A. Medrano, M. Morais, V. F. C. Ferreira, J. D. G. Correia, A. Paulo, I. Santos, C. Navarro-Ranninger, A. A. Valdes, A. Casini, F. Mendes and A. G. Quiroga, *Eur. J. Inorg. Chem.*, 2017, 1835–1840.
- 11 E. Bauer, X. Domingo, C. Balcells, I. H. Polat, M. Crespo, J. Quirante, J. Badia, L. Baldoma, M. Font-Bardia and M. Cascante, *Dalton Trans.*, 2017, **46**, 14973–14987.
- 12 R. G. Kenny, S. W. Chuah, A. Crawford and C. J. Marmion, *Eur. J. Inorg. Chem.*, 2017, 1596–1612.
- 13 E. Gabano, M. Ravera, I. Zanellato, S. Tinello, A. Gallina, B. Rangone, V. Gandin, C. Marzano, M. G. Bottone and D. Osella, *Dalton Trans.*, 2017, **46**, 14174–14185.
- 14 B. J. Pages, K. B. Garbutcheon-Singh and J. R. Aldrich-Wright, *Eur. J. Inorg. Chem.*, 2017, 1613–1624.
- 15 M. Á. Martínez, M. P. Carranza, A. Massaguer, L. Santos, J. A. Organero, C. Aliende, R. de Llorens, I. Ng-Choi, L. Feliu, M. Planas, A. M. Rodríguez, B. R. Manzano, G. Espino and F. A. Jalón, *Inorg. Chem.*, 2017, **56**, 13679–13696.
- 16 M. Yang and U. Bierbach, *Eur. J. Inorg. Chem.*, 2017, 1561–1572.
- 17 N. Muhammad, N. Sadia, C. Zhu, C. Luo, Z. Guo and X. Wang, *Chem. Commun.*, 2017, 53, 9971–9974.
- 18 Y. N. Nosova, L. S. Foteeva, I. V. Zenin, T. I. Fetisov, K. I. Kirsanov, M. G. Yakubovskaya, T. A. Antonenko, V. A. Tafencko, L. A. Aslanov, A. A. Lobas, M. V. Gorshkov, M. Galanski, B. K. Keppler, A. R. Timerbaev, E. R. Milaeva and A. A. Nazarov, *Eur. J. Inorg. Chem.*, 2017, 1785–1791.
- 19 P. Zhang and P. J. Sadler, *Eur. J. Inorg. Chem.*, 2017, 1541–1548.
- 20 S. Q. Yap, C. F. Chin, A. H. Hong Thng, Y. Y. Pang, H. K. Ho and W. H. Ang, *ChemMedChem*, 2017, **12**, 300–311.
- 21 N. S. Sommerfeld, D. Strohhofer, K. Cseh, S. Theiner, M. A. Jakupec, G. Koellensperger, M. Galanski and B. K. Keppler, *Eur. J. Inorg. Chem.*, 2017, 4049–4054.
- 22 S. D'Errico, N. Borbone, V. Piccialli, E. Di Gennaro, A. Zotti, A. Budillon, C. Vitagliano, I. Piccialli and G. Oliviero, *Eur. J. Org. Chem.*, 2017, 4935–4947.
- 23 M. B. Calvo, A. Figueroa, E. G. Pulido, R. G. Campelo and L. A. Aparicio, *Int. J. Endocrinol.*, 2010, **2010**, 14.
- 24 L. Szablewski, *Biochim. Biophys. Acta*, 2013, **1835**, 164–169.
- 25 Y. Chen, M. J. Heeg, P. G. Braunschweiger, W. Xie and P. G. Wang, *Angew. Chem., Int. Ed.*, 1999, **38**, 1768–1769.
- 26 Y. Mikata, Y. Shinohara, K. Yoneda, Y. Nakamura, I. Brudzińska, T. Tanase, T. Kitayama, R. Takagi, T. Okamoto, I. Kinoshita, M. Doe, C. Orvig and S. Yano, *Bioorg. Med. Chem. Lett.*, 2001, **11**, 3045–3047.
- 27 M. Gottschaldt and U. S. Schubert, *Chem. – Eur. J.*, 2009, **15**, 1548–1557.
- 28 J. Möker, U. Salge-Bartels and J. Thiem, *J. Carbohydr. Chem.*, 2012, **31**, 702–710.
- 29 S. Yano, H. Ohi, M. Ashizaki, M. Obata, Y. Mikata, R. Tanaka, T. Nishioka, I. Kinoshita, Y. Sugai, I. Okura, S. i. Ogura, J. A. Czaplewski, M. Gottschaldt, U. S. Schubert, T. Funabiki, K. Morimoto and M. Nakai, *Chem. Biodiversity*, 2012, **9**, 1903–1915.
- 30 P. Liu, Y. Lu, X. Gao, R. Liu, D. Zhang-Negrierie, Y. Shi, Y. Wang, S. Wang and Q. Gao, *Chem. Commun.*, 2013, **49**, 2421–2423.
- 31 J. Ma, Q. Wang, X. Yang, W. Hao, Z. Huang, J. Zhang, X. Wang and P. G. Wang, *Dalton Trans.*, 2016, **45**, 11830–11838.
- 32 Q. Wang, Z. Huang, J. Ma, X. Lu, L. Zhang, X. Wang and P. George Wang, *Dalton Trans.*, 2016, **45**, 10366–10374.
- 33 M. Wu, H. Li, R. Liu, X. Gao, M. Zhang, P. Liu, Z. Fu, J. Yang, D. Zhang-Negrierie and Q. Gao, *Eur. J. Med. Chem.*, 2016, **110**, 32–42.
- 34 R. Liu, H. Li, X. Gao, Q. Mi, H. Zhao and Q. Gao, *Biochem. Biophys. Res. Commun.*, 2017, **487**, 34–40.
- 35 M. Patra, T. C. Johnstone, K. Suntharalingam and S. J. Lippard, *Angew. Chem., Int. Ed.*, 2016, **55**, 2550–2554.
- 36 Y. Wang, H. Huang, Q. Zhang and P. Zhang, *Dalton Trans.*, 2018, **47**, 4017–4026.
- 37 V. Benessere, R. Del Litto, A. De Roma and F. Ruffo, *Coord. Chem. Rev.*, 2010, **254**, 390–401.
- 38 V. Benessere, M. Lega and F. Ruffo, *J. Organomet. Chem.*, 2014, **771**, 105–116.
- 39 C. De Castro, R. Lanzetta, S. Leone, M. Parrilli and A. Molinaro, *Carbohydr. Res.*, 2013, **370**, 9–12.
- 40 T. Tsubomura, S. Yano, K. Kobayashi, T. Sakurai and S. Yoshikawa, *J. Chem. Soc., Chem. Commun.*, 1986, 459–460, DOI: 10.1039/C39860000459.
- 41 T. Tsubomura, M. Ogawa, S. Yano, K. Kobayashi, T. Sakurai and S. Yoshikawa, *Inorg. Chem.*, 1990, **29**, 2622–2626.
- 42 S. Hanessian and J. Wang, *Can. J. Chem.*, 1993, **71**, 886–895.
- 43 S. Yano and Y. Mikata, *Bull. Chem. Soc. Jpn.*, 2002, **75**, 2097–2113.
- 44 M. E. Cucciolioto, A. D'Amora, G. De Feo, G. Ferraro, A. Giorgio, G. Petruk, D. M. Monti, A. Merlino and F. Ruffo, *Inorg. Chem.*, 2018, **57**, 3133–3143.

- 45 P. Carpinelli, S. Bartolucci and F. Ruffo, *Anti-Cancer Drug Des.*, 1995, **10**, 43–49.
- 46 M. Bigioni, P. Ganis, A. Panunzi, F. Ruffo, C. Salvatore and A. Vito, *Eur. J. Inorg. Chem.*, 2000, 1717–1721.
- 47 S. A. De Pascali, D. Migoni, P. Papadia, A. Muscella, S. Marsigliante, A. Ciccarese and F. P. Fanizzi, *Dalton Trans.*, 2006, 5077–5087, DOI: 10.1039/B610945D.
- 48 F. P. Fanizzi, L. Maresca, G. Natile, M. Lanfranchi, A. Tiripicchio and G. Pacchioni, *J. Chem. Soc., Chem. Commun.*, 1992, 333–335, DOI: 10.1039/C39920000333.
- 49 M. E. Cucciolito, V. De Felice, G. Roviello and F. Ruffo, *Eur. J. Inorg. Chem.*, 2011, 457–469.
- 50 L. Calvanese, M. E. Cucciolito, A. D'Amora, G. D'Auria, A. Esposito, R. Esposito, L. Falcigno and F. Ruffo, *Eur. J. Inorg. Chem.*, 2015, **2015**, 4068–4075.
- 51 R. Esposito, L. Calvanese, M. E. Cucciolito, G. D'Auria, L. Falcigno, V. Fiorini, P. Pezzella, G. Roviello, S. Stagni, G. Talarico and F. Ruffo, *Organometallics*, 2017, **36**, 384–390.
- 52 M. L. Ferrara, I. Orabona, F. Ruffo and V. De Felice, *J. Organomet. Chem.*, 1996, **519**, 75–82.
- 53 E. M. Pelczar, C. Munro-Leighton and M. R. Gagné, *Organometallics*, 2009, **28**, 663–665.
- 54 J. C. Vera, A. M. Reyes, F. V. Velásquez, C. I. Rivas, R. H. Zhang, P. Strobel, J. C. Slebe, J. Núñez-Alarcón and D. W. Golde, *Biochemistry*, 2001, **40**, 777–790.
- 55 X. Gao, S. Liu, Y. Shi, Z. Huang, Y. Mi, Q. Mi, J. Yang and Q. Gao, *Eur. J. Med. Chem.*, 2017, **125**, 372–384.
- 56 I. Diebold, J. K. Hennigs, K. Miyagawa, C. G. Li, N. P. Nickel, M. Kaschwich, A. Cao, L. Wang, S. Reddy, P.-I. Chen, K. Nakahira, M. A. A. Alcazar, R. K. Hopper, L. Ji, B. J. Feldman and M. Rabinovitch, *Cell Metab.*, 2015, **21**, 596–608.
- 57 M. Adinolfi, A. Iadonisi, A. Ravidà and M. Schiattarella, *Tetrahedron Lett.*, 2003, **44**, 7863–7866.
- 58 M. Giordano and A. Iadonisi, *Eur. J. Org. Chem.*, 2013, 125–131.
- 59 S. Traboni, E. Bedini and A. Iadonisi, *ChemistrySelect*, 2018, **3**, 1616–1622.
- 60 Bruker-Nonius, SADABS, Delft, the Netherlands, 2002.
- 61 A. Altomare, M. C. Burla, M. Camalli, G. L. Cascarano, C. Giacovazzo, A. Guagliardi, A. G. G. Moliterni, G. Polidori and R. Spagna, *J. Appl. Crystallogr.*, 1999, **32**, 115–119.
- 62 G. Sheldrick, *Acta Crystallogr., Sect. C: Struct. Chem.*, 2015, **71**, 3–8.
- 63 L. Farrugia, *J. Appl. Crystallogr.*, 2012, **45**, 849–854.
- 64 L. Farrugia, *J. Appl. Crystallogr.*, 1997, **30**, 565.
- 65 C. F. Macrae, I. J. Bruno, J. A. Chisholm, P. R. Edgington, P. McCabe, E. Pidcock, L. Rodriguez-Monge, R. Taylor, J. van de Streek and P. A. Wood, *J. Appl. Crystallogr.*, 2008, **41**, 466–470.
- 66 G. Ferraro, D. M. Monti, A. Amoresano, N. Pontillo, G. Petruk, F. Pane, M. A. Cinellu and A. Merlino, *Chem. Commun.*, 2016, **52**, 9518–9521.
- 67 G. Petruk, A. Raiola, R. Del Giudice, A. Barone, L. Frusciantè, M. M. Rigano and D. M. Monti, *J. Photochem. Photobiol., B*, 2016, **163**, 284–289.
- 68 D. M. Monti, G. Ferraro, G. Petruk, L. Maiore, F. Pane, A. Amoresano, M. A. Cinellu and A. Merlino, *Dalton Trans.*, 2017, **46**, 15354–15362.

Encapsulation of the Dinuclear Trithiolato-Bridged Arene Ruthenium Complex Diruthenium-1 in an Apoferritin Nanocage: Structure and Cytotoxicity

Ganna Petruk,^[a] Daria Maria Monti,^[a] Giarita Ferraro,^[a] Andrea Pica,^[b] Luigi D'Elia,^[a] Francesca Pane,^[a] Angela Amoresano,^[a] Julien Furrer,^[c] Konrad Kowalski,^[d] and Antonello Merlino^{*[a]}

The effects of encapsulating the cytotoxic dinuclear trithiolato-bridged arene ruthenium complex $[(\eta^6\text{-}p\text{-MeC}_6\text{H}_4\text{P}r)_2\text{Ru}_2(\mu\text{-}5\text{-}p\text{-C}_6\text{H}_4\text{tBu})_2\text{Cl}]$ (DiRu-1) within the apoferritin (Aft) nanocage were investigated. The DiRu-1-Aft nanocarrier was characterized by UV/Vis spectroscopy, ICP-MS, CD and X-ray crystallography. In contrast to previously reported Au- and Pt-based drug-loaded Aft carriers, we found no evidence of direct interactions between DiRu-1 and Aft. DiRu-1-Aft is cytotoxic toward immortalized murine BALB/c-3T3 fibroblasts transformed with

SV40 virus (SVT2) and human epidermoid carcinoma A431 malignant cells, and exhibits moderate selectivity for these cancer cells over normal BALB/c-3T3 cells. DiRu-1-Aft triggers the production of reactive oxygen species, depolarization of mitochondrial membrane potential, and induces cell death via p53-mediated apoptosis. Comparison between our data and previous results suggests that the presence of specific interactions between a metal-based drug and Aft within the protein cage is not essential for drug encapsulation.

Introduction

Protein-based assemblies have attracted wide attention because of their physicochemical properties and their potential applications in various fields, such as catalysis, coordination chemistry, imaging, and medicine.^[1] In this context, protein cages have been used as reaction vessels to form inorganic nanoparticles or as carriers for drugs.^[1–4] Among the proteins used to form nanoparticles, ferritin (Ft), which consists of 24 subunits that assemble into a robust cage with octahedral (432) symmetry (outside diameter \approx 12–13 nm, inside diameter \approx 7–8 nm), has appeared as one of the most promising.^[5] The physiological function of Ft is to store up to 4500 iron atoms inside the cavity, thereby preventing cytosolic and serum iron from forming cell-destructive reactive oxygen species (ROS). Mammalian Fts are heteropolymers formed by the assembly of two distinct chains, denoted as H-chain and L-chain, which

have different functions. The H-chain is a ferroxidase enzyme, whereas the L-chain, which lacks enzymatic activity, contains the residues that bind the iron ions and is responsible for iron storage.

Apoferritin (Aft) has been widely used as a protein cage to entrap metal-based drugs, as it can be reversibly dissociated and reassembled upon pH variation. Adducts formed upon encapsulation of drugs within Aft cages have the advantage of enhanced selectivity for tumor cells,^[6] because H- and L-chains as well as H/L heteropolymers can be recognized by surface receptors that are overexpressed by various tumor cell lines.^[7,8]

Recently, cisplatin,^[9–13] carboplatin,^[11–14] a bimetallic cytotoxic gold-platinum compound (4PF₆),^[15] and cytotoxic gold(III) compounds, namely Auoxo3 ($[\text{Au}_2(\text{bipy}^{\text{Me}})_2(\mu\text{-O})_2][\text{PF}_6]_2$, where $\text{bipy}^{\text{Me}} = 6\text{-methyl-}2,2\text{-bipyridine}$),^[9] Auoxo4 ($[\text{Au}_2(\text{bipy}^{\text{Me}})_2(\mu\text{-O})_2][\text{PF}_6]_2$, where $\text{bipy}^{\text{Me}} = 6\text{-neopentyl-}2,2\text{-bipyridine}$) and Au₂phen ($[\text{Au}_2(\text{phen})_2(\mu\text{-O})_2][\text{PF}_6]_2$, where $\text{phen}^{\text{Me}} = 2,9\text{-dimethyl-}1,10\text{-phenanthroline}$),^[16] have been successfully encapsulated within the horse spleen Aft nanocage. X-ray diffraction analysis shows that cisplatin and carboplatin bind the Aft chain close to the imidazole rings of His132, and His132 and His49, respectively.^[13,14] On the other hand, gold compounds degrade upon encapsulation within the cage, and gold(I) ions bind the side chains of Cys126, Cys48, His49, His132, and His147, with a preference for Cys126.^[6–16] Incorporation of Auoxo3 inside the cage also leads to the formation of gold nanoparticles.^[6] These protein adducts are cytotoxic toward various human malignant cells (HeLa, MCF-7, and HepG2) and, at least in some cases, moderately selective.^[6] However, the inclusion of the compounds within the cage decreases their activity.^[6–16]

[a] Dr. G. Petruk, Dr. D. M. Monti, Dr. G. Ferraro, L. D'Elia, Dr. F. Pane, Prof. A. Amoresano, Prof. A. Merlino
Department of Chemical Sciences, University of Naples Federico II, Complesso Universitario di Monte Sant'Angelo, via Cinthia 21, 80126, Naples (Italy)
E-mail: antonello.merlino@unina.it

[b] Dr. A. Pica
EMBL, CS 90181, 71 Av des Martyrs, 38009 Grenoble (38) (France)

[c] Prof. J. Furrer
Department of Chemistry and Biochemistry, University of Bern, Freiestrasse 3, 3012 Bern (Switzerland)

[d] Prof. K. Kowalski
Department of Organic Chemistry, Faculty of Chemistry, University of Łódź, Tamka 12, 91-403 (Poland)

Supporting information and the ORCID identification number(s) for the author(s) of this article can be found under:
<https://doi.org/10.1002/cmdc.201800805>.

Ruthenium compounds play an important role in the search for antitumor metallodrug alternatives to cisplatin and Pt-based drugs.^[17–21] Among the ruthenium compounds of medicinal interest, arene ruthenium(II) complexes have been widely investigated because of their well-balanced lipophilic/hydrophilic character, which allows these molecules to cross the cell membrane.^[23–26] The family of dinuclear trithiolato complexes of the general type $[(\text{arene})_2\text{Ru}_2(\text{SR})_3]^+$ is a promising class of anticancer arene ruthenium compounds. The most active member of this family is $[(\eta^6\text{-}p\text{-Me-C}_6\text{H}_4\text{Pr})_2\text{Ru}_2(\mu\text{-}S\text{-}p\text{-C}_6\text{H}_4\text{tBu})_3\text{Cl}]$, termed diruthenium-1 or DiRu-1 (Figure 1).^[27] This

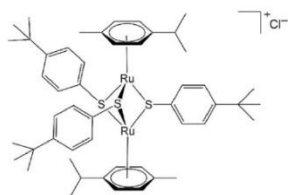


Figure 1. Structure of DiRu-1.

compound is very toxic in vitro toward hepatocellular carcinoma (HepG2 cells), estrogen-responsive breast adenocarcinoma (MCF-7 cells) and BT549 cells, triple-negative breast adenocarcinoma (MDA-MB-231 cells), human ovarian cancer (A2780 cells), and the cisplatin-resistant cell line A2780cis, with IC_{50} values in the low nanomolar range.^[28–31] Recent in vivo studies^[27,32, 33] have demonstrated that these complexes have potential as anticancer drugs, especially DiRu-1, which significantly prolongs the survival of tumor-bearing mice.^[33] Dinuclear trithiolato complexes $[(\text{arene})_2\text{Ru}_2(\text{SR})_3]^+$ are also promising antiparasitic compounds, as they are able to inhibit the apicomplexan parasite *Toxoplasma gondii* grown in human foreskin fibroblast host cells.^[34] Interestingly, DiRu-1 and in general dinuclear trithiolato complexes $[(\text{arene})_2\text{Ru}_2(\text{SR})_3]^+$ are very stable in aqueous solution^[35] and are inert toward ligand substitution.^[36] The results of the recent in vivo study suggest that increasing the aqueous solubility of DiRu-1 and its selectivity for cancer cells could significantly increase the efficacy of this promising ruthenium-based anticancer agent.^[27] The concept of using protein-based assemblies that are able to entrap DiRu-1 has therefore appeared as a logical follow-up to these studies.

Herein we describe the preparation of the nanocomposite formed upon encapsulation of DiRu-1 within horse spleen Aft (DiRu-1-encapsulated Aft), the structural characterization of this system, and its in vitro anticancer activity against human epidermoid carcinoma (A431) and immortalized murine fibroblast BALB/c-3T3 cells transformed with SV40 virus (SVT2). Interestingly, DiRu-1 does not directly coordinate to Aft, but is trapped in the bulk of the protein cage. The drug-loaded protein is cytotoxic toward cancer cells and is moderately selective for malignant cells over immortalized cells, as determined by the results obtained using A431, SVT2, and BALB/c-3T3 cell

lines. When DiRu-1 is encapsulated within the Aft cage, its cytotoxicity is 4- to 7-fold lower than that of its free form on A431, SVT2, and BALB/c-3T3 cell lines, in line with the results obtained with Au- and Pt-based drug-loaded Afts, for which a specific interaction between the compounds and protein residues within the cage is present. These findings suggest that direct interactions between a metal-based drug and the ferritin nanocage are not essential for metallodrug encapsulation.

Results and Discussion

Preparation and characterization of DiRu-1-encapsulated Aft

The encapsulation of ruthenium compounds within protein cages has been only scarcely investigated thus far.^[37,38] Feng and co-workers prepared composites of apoferritin with hydrophobic ruthenium(II) polypyridyl complexes, $\text{Ru}(\text{bpy})_2\text{dppz}^{2+}$ and $\text{Ru}(\text{phen})_2\text{dppz}^{2+}$ ($\text{bpy} = 2,2'$ -bipyridine, $\text{phen} = 1,10$ -phenanthroline, and $\text{dppz} = \text{dipyridophenazine}$), in order to improve the solubility of Ru-loaded luminescent molecules,^[39] while Ueno and co-workers encapsulated Ru-containing CO-releasing molecules to improve their delivery properties and to decrease the rate of the rapid exchange reactions of metal ligands.^[37]

The dissociation of Aft at acid or alkaline pH followed by reassembly at neutral pH provides a facile route for preparing metal-based drug-loaded Aft cages. DiRu-1 was encapsulated within an Aft cage by using a protocol originally described by Huang et al.,^[10] and which we used to incorporate both Pt- and Au-based anticancer agents within the Aft cage.^[6,15] Briefly, the Ft nanocage is dissociated into subunits at pH 13.0 by adding NaOH up to a final concentration of 0.1 M, and then reconstituted in the presence of DiRu-1 at pH 7.4 (using 1.0 M sodium phosphate buffer). The nanocomposite is purified from unfolded Ft chains, iron salts, and excess unencapsulated DiRu-1 by dialysis using Centricon filters. It was previously shown that a homogenous sample can be obtained using this procedure.^[13] The amount of DiRu-1-encapsulated Ft that is recovered after the encapsulation and purification processes is about 10% of the theoretical value.

To confirm DiRu-1 encapsulation within the inner cavity of Aft, the amount of Ru in DiRu-1-encapsulated Aft solutions was examined by inductively coupled plasma mass spectrometry (ICP-MS). Results indicate that the sample presents an average protein chain to Ru ratio of about 1:3 (3.3 ± 0.7), that is, an average of about 72 Ru atoms per cage, which would correspond to 36 molecules of DiRu-1 per cage. This result is similar to that obtained by Feng et al., who found 30–40 molecules of $[\text{Ru}(\text{phen})_2\text{dppz}^{2+}]$ within the horse spleen Aft cage.^[39] Ueno and co-workers identified 48 ± 2 Ru atoms within the recombinant L-chain apoferritin from horse liver complexed with the CO-releasing molecule CORM-2.^[37]

The characterization of DiRu-1-encapsulated Aft and the comparison with Aft were carried out by recording UV/Vis absorption and circular dichroism (CD) spectra (Figures 2 A,B). The UV/Vis spectrum of DiRu-1-encapsulated Aft presents a broad

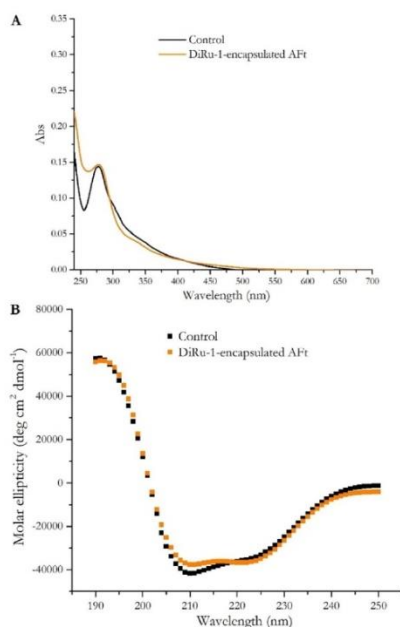


Figure 2. A) UV/Vis spectra of DiRu-1-encapsulated Aft and Aft alone as control. Measurements were recorded at a protein concentration of 0.25 mg mL⁻¹ in 10 mM sodium phosphate buffer, pH 7.4. B) Far-UV CD spectra of DiRu-1-encapsulated Aft and Aft alone as control; in this experiment, protein concentration was 0.05 mg mL⁻¹ in 10 mM sodium phosphate buffer, pH 7.4.

intense absorption signal in the 250–300 nm range, distinctly separated from the background signal of the control. This region is characteristic of the interactions between proteins and several metal-based drugs.^[11,40] These spectral variations were not observed upon mixing DiRu-1 with the untreated holo form of ferritin (this sample was named DiRu-1 + Ft) at pH 7.4 (Supporting Information Figure S1).

DiRu-1-encapsulated Aft is very stable in aqueous solution, as it can be conserved for weeks without visible precipitation.

The far-UV CD spectrum of DiRu-1-encapsulated Aft presents a positive peak at 192 nm and negative peaks of α -helix at 208 nm and 222 nm in very good agreement with those observed for the control. CD data indicate that 71% of the residues of the entire cage are involved in the formation of α helices/turns, consistent with the value obtained with the CD spectra of the wild-type protein (72%) and the crystal structure of Aft used as control (74%) (PDB ID: 5ERK).^[13] This suggests that the structure of Aft in the drug-loaded Aft is preserved,

as the secondary structure content in the adduct is similar to that observed for Aft (Figure 2B). Thermal denaturation analysis carried out by following the CD signal intensity at 222 nm at increasing temperature from 25 °C to 90 °C indicates that DiRu-1-encapsulated Aft is thermostable, as it is not fully denatured at 90 °C (Supporting Information Figure S2).

X-ray structure of DiRu-1-encapsulated Aft

To obtain more evidence on the encapsulation of DiRu-1 within the protein shell and to verify the integrity of the nanocage structure, the X-ray structure of DiRu-1-encapsulated Aft was determined at 1.43 Å resolution, using the molecular replacement method and the PDB coordinates of Aft deposited under PDB ID: 5ERK^[13] as starting model. The structure was refined to $R=0.174$ and $R_{free}=0.191$ (Figure 3). In this respect, it should be noted that X-ray crystallography is the best way to characterize the structure of the Ft-metallo-drug adducts, as recognized by other authors.^[41]

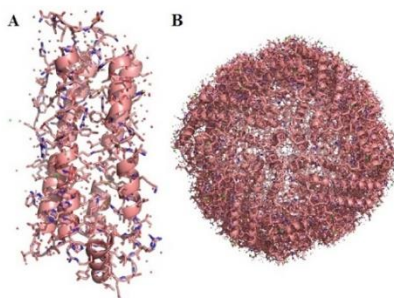


Figure 3. A) Structure of the single chain and B) the 24-mer DiRu-1-encapsulated Aft. The asymmetric unit of the crystal contains one single chain, whereas the 24-mer is generated by crystal symmetry.

The superimposition of the structure of DiRu-1-encapsulated Aft structure with the structure of Aft results in root-mean-square deviation (RMSD) values of 0.09 Å for C α atoms, indicating that the presence of DiRu-1 inside the cage does not significantly alter the overall structure of the protein. This demonstrates that the size of the cage is not altered by the presence of DiRu-1.

Analysis of the electron-density map reveals that Ru atoms are not directly bound to any protein residue side chains in the structure of DiRu-1-encapsulated Aft. Examples of the good quality of the electron-density maps corresponding to different regions of the protein are reported in Supporting Information Figure S3. These findings suggest that DiRu-1 is trapped within the cage and that only weak interactions (such as long-range electrostatic interactions) between DiRu-1 and Aft are present. This result is in line with the low reactivity of

DiRu-1 toward model proteins, i.e., hen egg white lysozyme and bovine pancreatic ribonuclease (unpublished data), and with published data indicating that DiRu-1 is inert toward all the amino acids, with the exception of cysteines, for which DiRu-1 promotes oxidation of the sulfur atom.^[31,35,36] Similar results were obtained with three hexacationic arene ruthenium metallaprisms and several human proteins. No covalent adducts are formed between the proteins and the metallaprisms, and only electrostatic interactions have been observed.^[42]

It is likely that DiRu-1 remains intact during encapsulation, as the compound is stable under the experimental conditions used for the encapsulation protocol (Supporting Information Figure S4), in agreement with previous structural stability data collected at both acidic and basic pH values.^[34]

To further confirm the presence of Ru atoms within the crystals of DiRu-1-encapsulated Aft, ICP-MS measurements were performed. Similar experiments were performed by Rompel and co-workers to verify the presence of KP1019 in human serum albumin–KP1019 crystals^[43] and also suggested in recent protocols for the determination of the X-ray structures of the adducts formed in the reaction between proteins and metallo-drugs.^[44,45] Crystals of Aft and of DiRu-1-encapsulated Aft were extensively washed with the reservoir solution and then dissolved in 20 μL of milli-Q water. These solutions were analyzed by ICP-MS; the data indicate that Aft crystals contained an undetectable amount of Ru, whereas the solution with DiRu-1-encapsulated Aft crystals contained a significant amount of Ru (37 ng). Altogether, these findings unambiguously demonstrate that DiRu-1 was successfully encapsulated within the Aft cage, that the structure of the protein in DiRu-1-encapsulated Aft is undistinguishable from Aft alone, and that DiRu-1 does not coordinate to the protein, but is trapped in the bulk.

To determine if the presence of DiRu-1 within the cage alters the flexibility of the protein chain, a comparative B-factor analysis of the structures of DiRu-1-encapsulated Aft and Aft was carried out. To avoid any bias due to differences in crystallization conditions, crystal solvent content, quality of the X-ray diffraction data, absorbed dose, resolution and packing contacts, relative B-factors (B_{relative})^[46] see the Experimental Section for further details) were used. Results of this analysis, reported in Figure 4, indicate that the nanocomposite and Aft used as control have similar B_{relative} versus residue number trend, with small differences observed for the N- and C-terminal tails.

Biological activity

The biological activity of DiRu-1-encapsulated Aft was tested on various cell lines. Two cancer cell lines, that is, immortalized murine fibroblast BALB/c-3T3 cells transformed with SV40 virus (SVT2) and human epidermoid carcinoma A431, and one immortalized cell line (BALB/c-3T3 cells) were incubated with increasing amounts of DiRu-1-encapsulated Aft (0.15–3 μM) and DiRu-1 (0.05–0.2 μM) for 48 h. Cell viability, evaluated by MTT assay,^[47] is reported as a function of DiRu-1 concentration in Figure 5. The results clearly indicate that tumor cells are much more sensitive to DiRu-1-encapsulated Aft than the immortal-

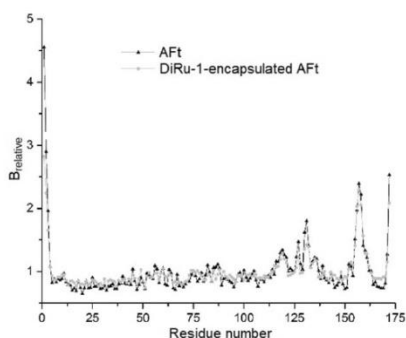


Figure 4. Relative B-factors (B_{relative}) versus residue number trend in DiRu-1-encapsulated Aft and Aft used as control (PDB ID: 5ERK). B_{relative} is defined in the Experimental Section.

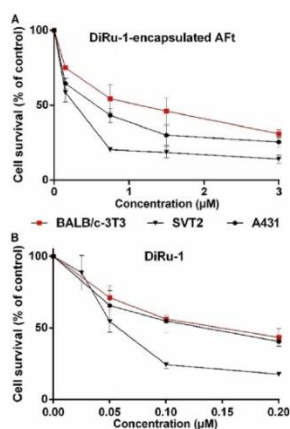


Figure 5. Effect of A) DiRu-1-encapsulated Aft and B) DiRu-1 on the survival of A431 (●), SVT2 (▼) and BALB/c-3T3 (■) cells. Cells were incubated with increasing amounts of DiRu-1-encapsulated Aft (0.15–3 μM) or DiRu-1 (0.05–0.2 μM) for 48 h. At the end of incubation, cell viability was assessed by MTT assay^[47] as described in the Experimental Section. Data are the mean \pm SD of three independent analyses, each carried out in triplicate.

ized cells and that free DiRu-1 is more toxic than the drug-loaded Aft for all cell lines analyzed. Aft does not show significant toxicity on any of the cell lines (data not shown).

The IC_{50} values of DiRu-1 and DiRu-1-encapsulated Aft, which correspond to the drug concentration able to inhibit cell growth by 50%, are reported in Table 1. These data indicate that the nanocomposite has a moderate selectivity for

Table 1. IC₅₀ values calculated based on the concentration of DiRu-1, for DiRu-1 and DiRu-1-encapsulated Aft on BALB/c-3T3, SVT2, and A431 cell lines.

Cell line	IC ₅₀ (nM) (48 h)	
	DiRu-1-encapsulated Aft ^d	DiRu-1
BALB/c-3T3	1230 ± 240	165 ± 31
SVT2	380 ± 90	56 ± 10
A431	640 ± 70	157 ± 26

[a] These values were calculated by considering the average value of Ru atoms encapsulated within Aft.

cancer cells relative to BALB/c-3T3 with a selectivity index (SI) of 3.2 in the case of SVT2 cells and 1.9 in the case of A431 (DiRu-1 has SI values of 2.9 and 1.0, respectively). The results also indicate that the presence of the cage decreases the toxicity of the drug to 4- to 7-fold, in good agreement with the decrease in cytotoxicity observed for the Au- and Pt-based drug-loaded Afts, which are characterized by specific interactions between the metal and protein residues within the cages.^[6,15,16] In this respect, it should be noted that the inclusion of a drug within an Aft nanocage is beneficial for the pharmacological properties, despite the cytotoxicity of the drug being lower within the protein cage. In fact, cytotoxicity is not the only essential requirement for an anticancer agent. Rather, the encapsulation of a drug within Aft improves its biocompatibility and its stability.

Clearly, the nanocarrier protects DiRu-1 and more generally metal compounds from being reduced by, for example, gluta-

thione, as described earlier,^[35] and prevents reaction with other biomolecules, thereby decreasing their toxicity. Keeping metalodrugs intact in the circulatory system and releasing them in a timely manner at the target site are crucial features for a metal-based drug carrier.^[11] Finally, it is possible to improve the already good selectivity of DiRu-1-encapsulated Aft by modifying the Ft surface, by introducing RGD motifs^[46] or folic acid.^[49] These features indicate that Aft is a good carrier for metal-based drugs, although it decreases the cytotoxicity of the anticancer compounds.

Cell death mechanism

The SVT2 cell line and its parental immortalized BALB/c-3T3 cell line were used for further investigations on the molecular mechanisms behind the selective anticancer activity of DiRu-1 and DiRu-1-encapsulated Aft. The concentrations used in the experiments were those of the IC₅₀ values obtained on SVT2 cells. The aim was to evaluate which toxic effect could be observed on immortalized cells when using the amount of drugs required to kill 50% of cancer cells.

It has been reported that DiRu-1 triggers the production of ROS in MCF-7 cells.^[28] Therefore, oxidative stress was evaluated by measuring intracellular ROS in cells incubated with DiRu-1 or DiRu-1-encapsulated Aft for various periods of time (Figure 6A,B). Interestingly, no significant increase in ROS levels was observed on immortalized cells with either DiRu-1 or DiRu-1-encapsulated Aft (Figure 6A). On the other hand, cancer cells were more sensitive to oxidative stress, as an in-

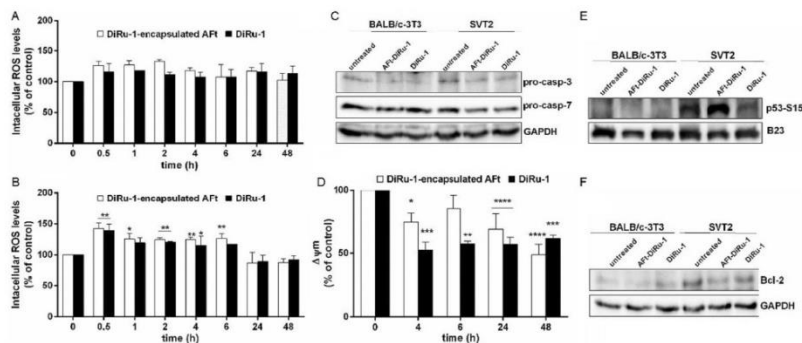


Figure 6. Effects of DiRu-1 and DiRu-1-encapsulated Aft on BALB/c-3T3 and SVT2 cells. For all experiments, cells were incubated with 56 nM DiRu-1 and 380 nM DiRu-1-encapsulated Aft (Aft-DiRu-1 in this figure), and results are reported as the mean \pm SD from experiments carried out in triplicate. A), B) ROS levels were detected between 0.5 and 48 h by measuring the emission of 2',7'-dichlorofluorescein diacetate (DCFH-DA); its emission intensity is expressed as the percent fluorescence intensity relative to control, as previously described.^[16] C) Western blot analysis was performed after 48 h incubation, using anti-pro-caspase-3 and anti-pro-caspase-7, which recognize the inactivated form of the proteins. Glycereraldehyde-3-phosphate dehydrogenase (GAPDH) was used as the loading control. D) Mitochondrial membrane potential was determined over 4–48 h using tetramethylrhodamine ethyl ester (TMRE) staining and is expressed as percentage relative to control, as previously described.^[16] E), F) Western blot analysis performed on nuclear (E) and cytosolic (F) proteins obtained from cells after 48 h incubation; p53-P-Ser15 was quantified by densitometric analysis and normalized with respect to B23 (nucleus); Bcl-2 levels were quantified with respect to GAPDH (cytosol). In the histograms, the white bars refer to cells incubated with DiRu-1-encapsulated Aft, and black bars to cells incubated with DiRu-1; * $p < 0.05$, ** $p < 0.01$, *** $p < 0.005$, **** $p < 0.001$ with respect to untreated cells.

crease in ROS levels (about 40%, $p < 0.01$) was observed after 30 min incubation with both drugs (Figure 6B). The ROS amount was constant up to 6 h incubation, and then decreased over time, in agreement with recent findings with DiRu-1.^[28]

We then investigated the type of cell death induced by DiRu-1 and DiRu-1-encapsulated Aft, distinguishing between apoptosis (the predominant type of programmed cell death) or necrosis. DiRu-1 is known to effect both apoptosis and necrosis in MCF-7 cells.^[28] To determine whether, in our experimental system, both pathways were activated, the release of the cytosolic enzyme lactate dehydrogenase (LDH), which is a marker of necrosis, and the decrease in the pro-caspase-3 and -7 levels, which are markers of apoptosis, were evaluated. After 48 h incubation, no LDH release was observed in the media of immortalized and cancer cell lines incubated with the two drugs (data not shown). In contrast, a decrease in both pro-caspase-3 and -7 levels was observed only in cancer cells treated with either DiRu-1 or DiRu-1-encapsulated Aft (Figure 6C). The apoptotic event in cancer cells was confirmed by the decrease in the mitochondrial membrane potential ($\Delta\psi_m$) (Figure 6D).

Our results suggest that DiRu-1 and DiRu-1-encapsulated Aft mainly trigger apoptosis in SVT2 cells and that this event could be a direct effect of increased ROS levels. This is a valuable result because apoptosis (programmed cell death) by a designed metallodrug is preferred against necrosis.

To further confirm this cell death mechanism, we subsequently analyzed the phosphorylation level of p53-Ser15 (herein termed p53-P-Ser15) in nuclei and the level of Bcl-2 in the cytosol. It is well established that in response to an apoptotic stimulus, the nuclear protein p53 is phosphorylated on Ser15 or on Ser20, thus inhibiting the expression of Bcl-2. Xu and co-workers^[50] and Zhao et al.^[51] have shown mitochondrial dysfunction and an increase in p53 levels in cells treated with Ru-based anticancer agents.

As shown in Figures 6E,F, no changes in p53-P-Ser15 and in Bcl-2 levels were observed on immortalized cells. On the other hand, in cancer cells incubated with DiRu-1-encapsulated Aft, a 3-fold increase in p53-P-Ser15 level was observed, together with a related significant decrease in Bcl-2 levels (about 50%). No significant alterations in p53-P-Ser15 levels were observed in cells exposed to the free drug, although a small decrease in the levels of Bcl-2 was observed. Overall, our data suggest that both DiRu-1 and DiRu-1-encapsulated Aft induce SVT2 cell death via ROS generation and apoptosis, with DiRu-1-encapsulated Aft that significantly alters the p53-P-Ser15 levels. These data indicate that although DiRu-1 and DiRu-1-encapsulated Aft induce the same mechanism of cell death (apoptosis), there are differences in their induced cell death pathways, suggesting that Ft plays a role in the mechanism of action of the DiRu-1-loaded system.

Conclusions

DiRu-1 is a dimetallic compound that is very toxic toward hepatocellular carcinoma (HepG2 cells), estrogen-responsive breast

adenocarcinoma (MCF-7 cells), and triple-negative breast adenocarcinoma (MDA-MB-231 cells).^[28–31] In this study, DiRu-1 was successfully encapsulated within the Aft nanocage by taking advantage of the reversible dissociation and reassembly characteristics of the protein at different pH values. Each Aft nanocage contains about 72 atoms of Ru within its inner cavity, which correspond to 36 molecules of DiRu-1. These molecules are trapped within the cage without specific interactions with protein residue side chains. Considering the amount of Ru atoms encapsulated within Aft, the cytotoxicity of the drug-loaded protein was compared with that of the free compound. DiRu-1-encapsulated Aft is 4- to 7-fold less toxic than DiRu-1, in line with the loss of activity observed for Pt- and Au-based complexes that have been encapsulated within the Aft cage^[15,16,52] via direct interactions with protein residues within the cage. Our findings indicate that the protein cage decreases the cytotoxicity of the drug independently of the formation of direct interactions between the drug and Aft residues within the protein cage. This is clearly in contrast to the common belief that direct binding of metal compounds to protein residue side chains is associated with drug sequestration that negatively affects the biological activity of the drug. These data suggest that it could be possible to build new nanocomposites by modifying the Ft sequence in order to directly coordinate metal-based drugs. This should assure the trapping of the metal compound within the cage. Most importantly, our results indicate that the presence of specific interactions between a metal-based drug and Aft within the protein cage is not essential for drug encapsulation.

Although the Ft cage decreases the cytotoxicity of DiRu-1, it is a suitable vehicle for its delivery and in general for the delivery of metal-based drugs. Indeed, DiRu-1-encapsulated Aft is still highly cytotoxic toward the investigated tumor cell lines and moderately selective, as it is more toxic toward SVT2 (and A431) cells rather than toward SVT2 parental counterpart BALB/c-3T3 cells. Furthermore, DiRu-1-encapsulated Aft is stable and is expected to be highly biocompatible. Finally, the protein cage protects the metallic compound from the attack of reducing agents^[53] and other molecules in the bloodstream and decreases the natural tendency of the compound to precipitate.

Although we have not studied the mechanism of release of DiRu-1 from DiRu-1-encapsulated Aft, we expect that the action of DiRu-1-encapsulated Aft could be associated with the release of the drug in the acidic endosome compartment,^[53,54] as it is well known that lowering the pH to the highly acidic range leads to the release of the content of the Aft cage.^[51,53] DiRu-1-encapsulated Aft induces cancer cell death via ROS production, depolarization of mitochondrial potential, and finally apoptosis (accumulation of nuclear p53-P-Ser15). Interestingly, a different mechanism seems operative in the case of DiRu-1, as accumulation of nuclear p53-P-Ser15 is not observed when the free compound is added to SVT2 cells.

Experimental Section

Sample preparation and spectroscopic and spectrometric characterization of DiRu-1-encapsulated Aft

Holo-horse spleen ferritin (Ft) was purchased from Sigma (code F4503, about 90% L-chain) and used without further purification. DiRu-1 was synthesized according to published procedures.^{36,38} DiRu-1-encapsulated Aft was prepared following our published protocol.⁶⁰ Briefly, the ferritin cage was disassembled at pH 13 by adding 1.0 M NaOH and DiRu-1 was added to Ft at a protein chain to Ru complex molar ratio of 1:20. After 60 min, the pH was adjusted to 7.4 with sodium phosphate buffer (1.0 M). Finally, the resulting solution was ultra-filtered and dialyzed (10 kDa MW cutoff) against 10.0 mM sodium phosphate buffer (pH 7.4). DiRu-1-encapsulated Aft was stored at 4 °C for later use. The same experiment was repeated for Aft used as control.

Ru concentrations within DiRu-1-encapsulated Aft were determined by using an ICP-MS (Agilent 7700 ICP-MS instrument from Agilent Technologies). A standard curve for Ru atom was obtained by using DiRu-1 standard solutions (in 5% HNO₃) at four different concentrations (1, 10, 50, and 100 µg L⁻¹). Protein adduct concentration was evaluated using the BCA method.¹⁶⁴

Absorption spectra of DiRu-1-encapsulated Aft and of the control were registered on a Jasco V650 UV/Vis spectrophotometer at room temperature and pressure in 10 mM sodium phosphate buffer pH 7.4, using the protein at a concentration of 0.25 mg mL⁻¹, with a scan range of 240–700 nm, a scan speed of 200 nm min⁻¹ and a data pitch of 1 nm. The same spectra were registered using a sample of untreated Ft and of ferritin mixed with DiRu-1 (DiRu-1 + Ft) in 1:20 protein to metal ratio at pH 7.4 (10.0 mM sodium phosphate buffer) and then dialyzed.

The circular dichroism (CD) spectra of DiRu-1-encapsulated Aft and of the control were recorded by using a Jasco V815 spectropolarimeter thermostated with a Peltier system. The system was calibrated using (1S)-(+)-10-camphorsulfonic acid ($\epsilon = 34.5 \text{ M cm}^{-1}$ at 285 nm, molar ellipticity = 2.36 M cm^{-1} at 295 nm). Thermal denaturation of DiRu-1-encapsulated Aft was monitored by following the change in ellipticity at 222 nm over the temperature range of 25–90 °C, with a scan rate of 1.0 °C min⁻¹. All the spectra of DiRu-1-encapsulated Aft were acquired in the 190–250 nm range using a protein concentration of 0.05 mg mL⁻¹ in 10 mM sodium phosphate pH 7.4 with a 0.1 cm path length, and the following experimental conditions: band width 2 nm, scan speed 50 nm min⁻¹, data pitch 1 nm, and response time 4 s. Spectra were averaged from three scans. Spectra deconvolutions were carried out using BestSel (<http://bestsel.elte.hu>).¹⁵⁷

Crystallization, X-ray diffraction data collection, structure resolution and refinement of DiRu-1-encapsulated Aft

DiRu-1-encapsulated Aft was crystallized by the hanging-drop vapor diffusion method at 298 K using 5 mg mL⁻¹ protein adduct. Drops were prepared by mixing 1 µL of a protein solution with an equal amount of the precipitant solution (0.6–0.8 M (NH₄)₂SO₄, 0.1 M Tris-HCl pH 7.7, 50 mM CdSO₄), as described previously.^{6,14}

X-ray diffraction data on these crystals were first collected at the CNR Institute of Biostructure and Bioimages, Naples, Italy, and then recollected at higher resolution at ESRF synchrotron in Grenoble, France. Data frames were indexed and scaled using HKL2000¹⁵² or AutoProc.¹⁵⁸ The structure was solved by molecular replacement

method with Phaser¹⁵⁹ using the coordinates of the protein extracted from PDB ID: SERK¹³ as starting model. Atomic positions and individual B-factors were refined using Refmac 5.7¹⁶⁰ and auto-Buster.¹⁶¹ Refinement statistics are reported in Supporting Information Table S1.

To verify the presence of Ru atoms within the DiRu-1-encapsulated Aft crystals, ICP-MS data were collected. In particular, crystals of the control and DiRu-1-encapsulated Aft were extensively washed with the reservoir solution and then dissolved in 20 µL of milli-Q water. Data indicate that the solution with crystals of the control contained an undetectable amount of Ru, whereas that containing crystals of DiRu-1-encapsulated Aft contained 37 ng of Ru.

Comparison of the relative B-factors (B_{relative}) of DiRu-1-encapsulated Aft and Aft was performed by calculating B_{relative} as the ratio between B-factor of the α carbon atom of each residue and the average B-factor of the α carbon atoms of the whole molecule. The structure of Aft deposited in the RCSB Protein Data Bank (PDB ID: SERK) was used as control.¹³

Cell culture and cell growth inhibition

Human A431, murine BALB/c-3T3, and SVT2 fibroblasts were obtained from ATCC and were maintained in culture as previously described.⁶² For dose-response experiments, cells were seeded in 96-well plates at a density of 2.5×10^3 cells per well; 24 h after seeding, increasing amounts of DiRu-1-encapsulated Aft (0.15–3 µM) or DiRu-1 (0.05–0.2 µM) were added to the cells for 48 h. Cell viability was then assessed by MTT [3-(4,5-dimethylthiazol-2-yl)-2,5-diphenyltetrazolium bromide] assay,¹⁶¹ as described by Ferraro et al.²⁹ Cell survival was expressed as the percentage of viable cells in the presence of test compound relative to controls. Two groups of cells were used as controls: untreated cells and cells supplemented with identical volumes of buffer. Each sample was tested in three independent analyses, each carried out in triplicate.

The selectivity index (SI) was calculated as follows: $SI = (IC_{50} \text{ of DiRu-1-encapsulated Aft in a normal cell line}) / (IC_{50} \text{ of DiRu-1-encapsulated Aft in cancer cell lines})$. SI indicates the cytotoxic selectivity (i.e., safety) of a cytotoxic compound against cancer cells versus normal cells.

Measurement of intracellular ROS and mitochondrial membrane potential

To estimate intracellular reactive oxygen species (ROS) production and mitochondrial membrane potential, the procedure described by Monti et al. was followed.¹¹⁶ The concentrations used in these experiments were based on the IC_{50} values obtained for SVT2 cells (DiRu-1 concentration: 56 nM for DiRu-1 and 380 nM for DiRu-1-encapsulated Aft).

Western blot analysis

Cells were plated at a density of 2×10^4 cells cm⁻² in complete medium for 24 h and then treated as described above. Nuclear pellet was obtained after extracting cytosolic proteins with 0.1% Triton in PBS in the presence of protease and phosphatase inhibitors. Nuclear lysate was obtained by suspending the pellet in RIPA buffer (150 mM NaCl, 1% NP-40, 0.1% SDS, protease inhibitors in 50 mM Tris-HCl pH 8.0). Lysates (100 µg of proteins) were analyzed by western blotting performed as previously described.¹¹⁶ Anti-p53-P-Ser15, pro-caspase-3, pro-caspase-7, Bcl-2, GAPDH were ob-

tained from Cell Signal Technology (Danvers, MA, USA). Anti-B23 and the chemiluminescence detection system (SuperSignal® West Pico) were obtained from ThermoFisher, Rockford, IL, USA.

Acknowledgements

The authors thank Alessia Ruggiero and Luigi Vitagliano (CNR Institute of Biostructures and Biomages, Napoli, Italy) for their help with the transport of DiRu-1-encapsulated Aft crystals to ESRE.

Conflict of interest

The authors declare no conflict of interest.

Keywords: anticancer · diruthenium · drug delivery · ferritin · protein cages

- [1] B. Maity, K. Fujita, T. Ueno, *Curr. Opin. Chem. Biol.* **2015**, *25*, 88–97.
- [2] B. Maity, A. Abe, T. Ueno, *Nat. Commun.* **2017**, *8*, 14820.
- [3] B. Maity, K. Fukumori, S. Abe, T. Ueno, *Chem. Commun.* **2016**, *52*, 5463–5466.
- [4] S. Abe, B. Maity, T. Ueno, *Chem. Commun.* **2016**, *52*, 6496–6512.
- [5] S. C. Andrews, P. Arosio, W. Botke, J. F. Briat, M. Vonclari, P. M. Harrison, J. P. Laulhere, S. Levi, S. Lobreaux, S. J. Yewdall, *J. Inorg. Biochem.* **1992**, *47*, 161–174.
- [6] G. Ferraro, D. M. Monti, A. Amoresano, N. Pontillo, G. Petruk, F. Pane, M. A. Cinellu, A. Merlino, *Chem. Commun.* **2016**, *52*, 9518–9521.
- [7] L. Zhang, L. Li, A. Di Penta, U. Carmona, F. Yang, R. Schops, M. Brandsch, J. L. Zugaza, M. Knez, *Adv. Healthcare Mater.* **2015**, *4*, 1305–1310.
- [8] M. Uchida, M. L. Flenniken, M. Allen, D. A. Willits, B. E. Crowley, S. Brumfield, A. F. Willis, L. Jackiw, M. Jutila, M. J. Young, T. Douglas, *J. Am. Chem. Soc.* **2006**, *128*, 16626–16633.
- [9] B. Zhu, L. Huang, H. Q. Huang, *Comp. Biochem. Physiol. C* **2012**, *156*, 95–103.
- [10] X. T. Ji, L. Huang, H. Q. Huang, *J. Proteomics* **2012**, *75*, 3145–3157.
- [11] R. M. Xing, X. Y. Wang, C. L. Zhang, Y. M. Zhang, Q. Wang, Z. Yang, Z. J. Guo, *J. Inorg. Biochem.* **2009**, *103*, 1039–1044.
- [12] G. Ferraro, S. Ciambellotti, L. Messori, A. Merlino, *Inorg. Chem.* **2017**, *56*, 9064–9070.
- [13] N. Pontillo, F. Pane, L. Messori, A. Amoresano, A. Merlino, *Chem. Commun.* **2016**, *52*, 4136–4139.
- [14] N. Pontillo, G. Ferraro, H. H. R. Hellivell, A. Amoresano, A. Merlino, *ACS Med. Chem. Lett.* **2017**, *8*, 433–437.
- [15] G. Ferraro, G. Petruk, L. Maiore, F. Pane, A. Amoresano, M. A. Cinellu, D. M. Monti, A. Merlino, *Int. J. Biol. Macromol.* **2018**, *115*, 1116–1121.
- [16] D. M. Monti, G. Ferraro, G. Petruk, L. Maiore, F. Pane, A. Amoresano, M. A. Cinellu, A. Merlino, *Dalton Trans.* **2017**, *46*, 15354–15362.
- [17] C. S. Allardayce, P. J. Dyson, *Platinum Met. Rev.* **2001**, *45*, 62–69.
- [18] E. Alessio, *Eur. J. Inorg. Chem.* **2017**, 1549–1560.
- [19] I. Bratsos, S. Jedner, T. Gianferrara, E. Alessio, *Chimia* **2007**, *61*, 692–697.
- [20] E. Alessio, G. Mestroni, A. Bergamo, G. Sava, *Curr. Top. Med. Chem.* **2004**, *4*, 1525–1535.
- [21] E. Alessio, E. Iengo, B. Serli, G. Mestroni, G. Sava, *J. Inorg. Biochem.* **2001**, *86*, 21.
- [22] A. Merlino, *Coord. Chem. Rev.* **2016**, *326*, 111–134.
- [23] G. Süss-Fink, *Dalton Trans.* **2010**, *39*, 1673–1688.
- [24] D. Stibal, T. Riedel, P. J. Dyson, G. Süss-Fink, B. Therrien, *Inorg. Chim. Acta* **2016**, *444*, 51–55.
- [25] P. Nowak-Silwinska, J. R. van Beijnum, A. Casini, A. A. Nazarov, G. Wag-nieres, H. van den Bergh, P. J. Dyson, A. W. Griffioen, *J. Med. Chem.* **2011**, *54*, 3895–3902.
- [26] W. H. Ang, E. Daldini, C. Scolaro, R. Scopelliti, L. Juillerat-Jeanerret, P. J. Dyson, *Inorg. Chem.* **2006**, *45*, 9006–9013.
- [27] J. Furrer, G. Süss-Fink, *Coord. Chem. Rev.* **2016**, *309*, 36–50.
- [28] A. Koceva-Chyla, K. Matczak, P. Hliskz, K. Durka, K. Kochel, G. Süss-Fink, J. Furrer, K. Kowalski, *ChemMedChem* **2016**, *11*, 2171–2187.
- [29] A. F. Ibaio, M. Gras, B. Therrien, G. Süss-Fink, O. Zava, P. J. Dyson, *Eur. J. Inorg. Chem.* **2012**, 1531–1535.
- [30] M. Gras, B. Therrien, G. Süss-Fink, O. Zava, P. J. Dyson, *Dalton Trans.* **2010**, *39*, 10305–10313.
- [31] F. Giannini, J. Furrer, A. F. Ibaio, G. Süss-Fink, B. Therrien, O. Zava, M. Baquie, P. J. Dyson, P. Stepnicka, *J. Biol. Inorg. Chem.* **2012**, *17*, 951–960.
- [32] D. Muthná, P. Tomšik, R. Havelék, R. Kohlerová, V. Kaslingam, E. Cermaková, D. Stibal, M. Rezacová, G. Süss-Fink, *Anti-Cancer Drugs* **2016**, *27*, 643–650.
- [33] P. Tomšik, D. Muthná, M. Rezacová, S. Micuda, J. Cmielova, M. Hroch, R. Endlicher, Z. Cervinkova, E. Rudolf, S. Hann, D. Stibal, B. Therrien, G. Süss-Fink, *J. Organomet. Chem.* **2015**, *782*, 42–51.
- [34] D. Stibal, L. Geiser, G. Süss-Fink, J. Furrer, *RSC Adv.* **2016**, *6*, 38332–38341.
- [35] F. Giannini, G. Süss-Fink, J. Furrer, *Inorg. Chem.* **2011**, *50*, 10552–10554.
- [36] A. P. Basto, J. Müller, R. Rubbiani, D. Stibal, F. Giannini, G. Süss-Fink, V. Balmer, A. Hemphill, G. Gasser, J. Furrer, *Antimicrob. Agents Chemother.* **2017**, *61*, e01031-17.
- [37] K. Fujita, Y. Tanaka, T. Sho, S. Ozeki, S. Abe, T. Hikage, T. Kuchimaru, S. Kizaka-Kondoh, T. Ueno, *J. Am. Chem. Soc.* **2014**, *136*, 16902–16908.
- [38] Y. Takezawa, P. Bockmann, N. Sugii, Z. Wang, S. Abe, T. Murakami, T. Hikage, G. Erker, Y. Watanabe, S. Kitagawa, T. Ueno, *Dalton Trans.* **2011**, *40*, 2190–2195.
- [39] X. Li, Y. J. Zhang, H. Chen, J. Sun, F. D. Feng, *ACS Appl. Mater. Interfaces* **2016**, *8*, 22756–22761.
- [40] G. Ferraro, A. Pica, I. R. Krauss, F. Pane, A. Amoresano, A. Merlino, *J. Biol. Inorg. Chem.* **2016**, *21*, 433–442.
- [41] G. Tosi, D. Belletti, F. Pederzoli, B. Ruzzi, *Expert Opin. Drug Delivery* **2016**, *13*, 1341–1343.
- [42] L. E. H. Paul, B. Therrien, J. Furrer, *Org. Biomol. Chem.* **2015**, *13*, 946–953.
- [43] A. Bijelic, S. Theiner, B. K. Keppler, A. Rompel, *J. Med. Chem.* **2016**, *59*, 5894–5903.
- [44] I. R. Krauss, G. Ferraro, A. Pica, J. A. Marquez, J. R. Hellivell, A. Merlino, *Metallomics* **2017**, *9*, 1534–1547.
- [45] K. B. Handing, E. Niedzialkowska, I. G. Shabalin, M. L. Kuhn, H. P. Zheng, W. Minor, *Nat. Protoc.* **2018**, *13*, 1062–1090.
- [46] A. Merlino, I. R. Krauss, I. Castellano, E. De Vendittis, B. Rossi, M. Conte, A. Vergara, F. Sica, *J. Struct. Biol.* **2010**, *172*, 343–352.
- [47] J. C. Stockert, A. Blazquez-Castro, M. Canete, R. W. Horobin, A. Villanueva, *Acta Histochem.* **2012**, *114*, 785–796.
- [48] Z. Zhen, W. Tang, H. Chen, X. Lin, T. Todd, G. Wang, T. Cowger, X. Chen, J. Xie, *ACS Nano* **2013**, *7*, 4830–4837.
- [49] S. Khashanian, R. Rafipour, E. Mahdavian, K. Mansouri, *Artif. Cells Nanomed. Biotechnol.* **2018**, *1*–8.
- [50] Y. Chen, M. Y. Qin, L. Wang, H. Chao, L. N. Ji, A. L. Xu, *Biochimie* **2013**, *95*, 2050–2059.
- [51] Z. N. Zhao, Z. D. Luo, Q. Wu, W. J. Zheng, Y. X. Feng, T. F. Chen, *Dalton Trans.* **2014**, *43*, 17017–17028.
- [52] Z. Otwinowski, W. Minor, *Macromol. Crystallogr. Pt. A* **1997**, *276*, 307–326.
- [53] G. Ferraro, A. Pica, G. Petruk, F. Pane, A. Amoresano, A. Cilibrizzi, R. Vilar, D. M. Monti, A. Merlino, *Nanomedicine* **2018**, DOI: <https://doi.org/10.2217/nmm-2018-0259>.
- [54] I. Blazkova, H. V. Nguyen, S. Dostalova, P. Kopel, M. Stanislavjevic, M. Vuculovicova, M. Stiborova, T. Eckschlager, R. Kizek, V. Adam, *Int. J. Mol. Sci.* **2013**, *14*, 13391–13402.
- [55] F. Chérloux, C. M. Thomas, T. Monnier, G. Süss-Fink, *Polyhedron* **2003**, *22*, 543–548.
- [56] P. K. Smith, R. I. Krohn, G. T. Hermanson, A. K. Mallia, F. H. Gartner, M. D. Provenzano, E. K. Fujimoto, N. M. Goeke, B. J. Olson, D. C. Klenk, *Anal. Biochem.* **1985**, *150*, 76–85.
- [57] A. Miconai, F. Wien, L. Kerna, Y. H. Lee, Y. Goto, M. Regfriers, J. Kardos, *Proc. Natl. Acad. Sci. USA* **2015**, *112*, E3095–E3103.
- [58] C. Vonrhein, C. Flensburg, P. Keller, A. Shaffr, O. Smart, W. Paciorek, T. Womack, G. Bricogne, *Acta Crystallogr. Sect. D* **2011**, *67*, 293–302.
- [59] A. J. McCoy, R. W. Grosse-Kunstleve, P. D. Adams, M. D. Winn, L. C. Storoni, R. J. Read, *J. Appl. Crystallogr.* **2007**, *40*, 658–674.

- [60] G. N. Murshudov, P. Skubak, A. A. Lebedev, N. S. Pannu, R. A. Steiner, R. A. Nicholls, M. D. Winn, F. Long, A. A. Vagin, *Acta Crystallogr. Sect. D* **2011**, *67*, 355–367.
- [61] G. Bricogne, E. Blanc, M. Brandl, C. Flensburg, P. Keller, W. Paciorek, P. Roversi, A. Sharff, O. S. Smart, C. Vonrhein, T. O. Womack (2017), *BUSTER* version 2.11.2, Global Phasing Ltd., Cambridge (UK).
- [62] R. Del Giudice, G. Petruk, A. Raiola, A. Barone, D. M. Monti, M. M. Rigano, *J. Sci. Food Agric.* **2017**, *97*, 1616–1623.

Manuscript received: December 18, 2018
Revised manuscript received: January 21, 2019
Accepted manuscript online: January 23, 2019
Version of record online: February 11, 2019

Green Compressed Fluid Technologies To Extract Antioxidants and Lipids from *Galdieria phlegrea* in a Biorefinery Approach

Paola Imbimbo, Monica Bueno, Luigi D'Elia, Antonino Pollio, Elena Ibañez, Giuseppe Olivieri,* and Daria Maria Monti*



Cite This: ACS Sustainable Chem. Eng. 2020, 8, 2939–2947



Read Online

ACCESS |

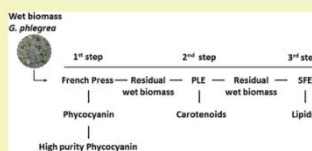
Metrics & More

Article Recommendations

Supporting Information

ABSTRACT: A green cascade approach was used to recover phycocyanins, carotenoids and lipids from *Galdieria phlegrea*. Phycocyanin extraction was performed by high pressure homogenization and purified by ultrafiltration, whereas carotenoids were obtained by a pressurized liquid extraction and lipids by supercritical fluid extraction. The second step of this innovative, green, and cost-effective procedure is able to improve the recovery of zeaxanthin and β -carotene up to 40%, without affecting the quality of compounds and avoiding the use of organic solvents and the drying processes. The isolated carotenoids were active as antioxidants, as clearly shown by their protective activity on a cell-based model. The lipid yield was increased by 12% with respect to conventional methods.

KEYWORDS: phycocyanin, carotenoids, lipids, compressed fluid technologies, biorefinery, microalgae, *Galdieria phlegrea*



INTRODUCTION

Microalgae are a continuous and reliable source of safe natural and high-value products, such as soluble proteins, polyunsaturated fatty acids, and pigments. Phycocyanins (PCs) are blue colored, highly fluorescent, and water-soluble proteins, synthesized in cyanobacteria and red algae. PCs, as the other phycobiliproteins, are antenna pigments that can improve the photosynthetic efficiency of microalgae. Because of their brilliant color, PCs are commonly used in cosmetic and food industry.¹ They are also endowed with therapeutic properties such as antioxidant, anti-inflammatory, hepato-protective, and antitumoral activity.² Among pigments, carotenoids function as accessory pigments in a light-harvesting photosystem during photosynthesis,³ and they are also important for their antioxidant function, as they deactivate free radicals, thus preventing cell damages. In the last decades, carotenoids have attracted great interest because of their beneficial effect on human health. The demand of carotenoids is rapidly growing: the global carotenoid market was estimated to be ~1.24 billion USD in 2016 and is projected to increase to ~1.53 billion USD by 2021, at a compound annual growth rate of 3.78% from 2016 to 2021.⁴ To date, commercially available carotenoids are generally synthetic because they are more stable than natural ones as they are formulated to minimize oxidation or isomerization.⁵ However, the emulsified preparations of synthetic carotenoids show high toxicity, carcinogenicity, and teratogenicity properties, thus generating criticism among health-conscious consumers.^{5,6} With microalgae being good producers of many pigments, the extraction of carotenoids from these microorganisms would be very competitive in the market and would have a huge economic impact.⁷ Microalgae

can accumulate also significant amount of lipids (from 1 to 70%),⁸ depending on the strain and the culture conditions.⁹ Lipids can be employed as feedstock for nutraceutical, pharmaceutical, foods, and biofuel industries. To date, the bioenergy market has the lowest value. This is due to the fact that biogas, bioethanol, and biodiesel have a selling price of 0.2 € m⁻³, 0.4 € kg⁻¹, and 0.5 € L⁻¹ respectively, a price that still exceeds their high downstream process costs (20.5 € m⁻³, 33.34 € kg⁻¹, and 25.56 g € L⁻¹, respectively).¹⁰ Thus, an improvement in efficient, cost-effective, and green extraction techniques to produce high-quality compounds is needed. In this context, microalgae are an excellent source of molecules endowed with biological activity. Notably, the design of a suitable integrated biorefinery platform can efficiently extract target compounds in a cascade approach and, in accordance with the green chemistry principles, is still a challenge. Among all the innovative techniques, compressed fluid extractions are considered the most competitive ones because they may fulfill this criteria.¹¹ In this context, pressurized liquid extraction (PLE) and supercritical fluid extraction (SFE) are the most widely employed as they could be based on the use of the same system; so they would represent process intensification. PLE and SFE are innovative techniques that use pressurized solvents at an elevated temperature and pressure to extract molecules. Moreover, the extraction performance is enhanced

Received: December 16, 2019

Revised: January 27, 2020

Published: January 31, 2020



as compared to those techniques carried out at near room temperature and atmospheric pressure.^{11–13}

In the present work, we set up a cascade approach to recover high value bioproducts from *Galdieria phlegrea*, a unicellular thermo-acidophilic red alga. The experimental strategy is reported in Figure 1. Starting from the previously established

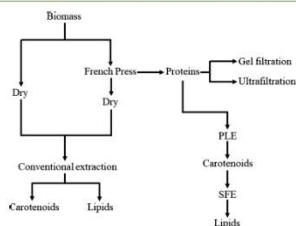


Figure 1. Schematic representation of the extraction strategy.

technique used to disrupt cells and extract PCs,¹⁴ an optimization of the isolation of PC was carried out. Then, the residual wet biomass was used to extract two different bioproducts in two sequential steps: carotenoids by using PLE and finally lipids by SFE. The bioactivity of the extracted carotenoids obtained by PLE was validated on a cell-based model, using human immortalized keratinocytes and compared to the bioactivity of the commercial molecules.

MATERIALS AND METHODS

Reagents. High performance liquid chromatography (HPLC)-grade acetone and methanol were from VWR (Barcelona, Spain). Antibodies were from Cell Signal Technology (Danvers, MA, USA). All the other reagents and standards were from Sigma-Aldrich (Madrid, Spain).

Microalgal Strain and Culture Conditions. *G. phlegrea* (strain 009) was provided from the Algal Collection of the University Federico II (ACUF, <http://www.acuf.net>). Cells were grown in autotrophic conditions in photobioreactors, as described in Imbimbo et al.¹⁴

PC Extraction and Purification. After harvesting the biomass by centrifugation at 1200g for 30 min at room temperature, cells were suspended in 50 mM sodium acetate pH 5.5.¹⁵ Cell disruption was performed by high-pressure (French Press). Two consecutive cycles, each at 2 kbar, were performed to disrupt the biomass. The cell lysate was obtained by centrifugation at 5000g at 4 °C for 30 min, and proteins were recovered in the supernatant, whereas the residual biomass was used for further extractions. To purify PC, two single step purification techniques were used in parallel: gel-filtration and ultrafiltration.

The size-exclusion chromatography was performed by using a Sephadex G-75 fine equilibrated in 50 mM sodium acetate pH 5.5. The ultrafiltration was performed by using 100 kDa molecular weight cut off membranes, and the process was performed at room temperature. At the end of the purification, the permeate was discarded and the retentate was collected. The grade of purity of PC was calculated by measuring the ratio A_{620nm}/A_{380nm} .

Storage of Biomass. The residual wet biomass, after protein extraction, was stored at -80 °C. To avoid that the storage conditions would affect the results, extraction of carotenoids was performed after 72 h.

Conventional Carotenoid Extraction. Carotenoids were extracted using the method of Reyes et al.¹⁶ Briefly, 200 mg of lyophilized biomass was mixed with 20 mL of HPLC-grade acetone

containing 0.1% (w/v) butylate hydroxytoluene, and the mixture was shaken for 24 h in a thermostatic shaker at 500 rpm and 20 °C. Then, the sample was centrifuged at 4 °C for 10 min at 5000g. The supernatant was collected, and the solvent was removed under N_2 stream. The extracts were weighted and stored in the dark at -20 °C.

Conventional Lipid Extraction. Total lipid extraction was performed according to the Axelsson and Gentil method.¹⁷ Freeze-dried microalgae biomass (25 mg) was mixed with 8 mL of chloroform/methanol 2:1 (v/v). Then, 2 mL of NaCl 0.73% (w/v) was added and mixed again. The sample was centrifuged at 350g for 5 min at room temperature, allowing the separation of the two phases. The lower layer was removed and collected. The solvent was removed under N_2 stream. The extracts were weighted and stored in the dark at -20 °C.

Compressed Fluid Extraction Processes. All high pressure extractions were performed in a homemade compressed fluid extractor coupled to a PU-2080 HPLC pump from Jasco (Tokyo, Japan). This equipment can be employed to carry out both PLE and SFE. To this purpose, 2 g of wet algal biomass (the equivalent of 200 mg of dried biomass) were mixed with silica gel of 150 Å (S150) pore size with a particle size of 200–425 mesh. The required amount of this silica gel was added as an adsorbent till a static paste was obtained.¹⁸ Silica prevents the paste draining in the equipment pipeline when loading in the extraction cell and improves the solute recovery.¹⁸ The mixture was added into a stainless-steel extraction cell sandwiched between glass wool to prevent clogging problems. Extractions were carried out in triplicate in two sequential steps, decreasing the polarity of the solvents, in order to exhaust the microalgae biomass of relevant extractable compounds. PLE was performed at a static extraction mode at 100 bar, 50 °C for 30 min using pure ethanol as a solvent. The extracts were collected in glass vials, dried under N_2 stream, and then weighed and stored at -20 °C in the dark. Subsequently, the residue of the previous extraction was used as a raw material for the next step. SFE was carried out in the same apparatus, using pure CO_2 as a solvent. The extraction was performed at 350 bar, 60 °C for 100 min. The CO_2 flow rate was set up at 5 mL/min. Pressure was controlled by using a back pressure regulator. The extracts were collected in glass vials, dried under N_2 stream, and then weighed and stored at -20 °C in the dark. A schematic representation of the used apparatus is reported in Figure S1 (Supporting Information).

Total Carotenoid Determination. The total carotenoid content was determined spectrophotometrically as described by Gilbert-López et al.¹⁹ The extracts from PLE were dissolved in pure methanol in a concentration ranging from 0.05 to 5 mg/mL. A standard calibration curve of β -carotene (from 5 to 200 μ g/mL) was used to calculate the concentration of total carotenoids. The absorbance of samples was recorded at 470 nm. The total carotenoid content was expressed as the ratio of mg of carotenoids and g of the extract. The carotenoid yield was expressed as mg of carotenoids extracted per g of dry biomass. Analyses was carried out in triplicate.

Carotenoid Characterization by HPLC–DAD–MS. Carotenoids were characterized by HPLC–DAD using the method described by Castro-Puyana et al.²⁰ with some modifications. HPLC analyses were performed using an Agilent 1100 series liquid chromatograph (Santa Clara, CA, USA) equipped with a diode-array detector and using a YMC-C₃₀ reversed-phase column (250 mm \times 4.6 mm inner diameter, 5 μ m particle size; YMC Europe, Scherneck, Germany) and a precolumn YMC-C₃₀ (10 mm \times 4 mm i.d., 5 μ m). The mobile phase was a mixture of methanol–MTBE–water (90:7:3, v/v/v) (solvent A) and methanol–MTBE (10:90, v/v) (solvent B). Carotenoids were eluted according to the following gradient: 0 min, 0% B; 20 min, 30% B; 35 min, 50% B; 45 min, 80% B; 50 min, 100% B; 60 min, 100% B; 62 min, 0% B. The flow rate was 0.8 mL/min while the injection volume was 10 μ L. The detection was performed at 280, 450, and 660 nm, although the spectra from 240 to 770 nm were recorded using the DAD (peak width >0.1 min (2 s) and slit 4 nm). The instrument was controlled by LC Chem Station 3D Software Rev. B.04.03 from Agilent. Extracts were dissolved in pure methanol in a concentration ranging from 1 to 10 mg/mL to 10 and

Table 1. Comparison in PC Recovery after Gel Filtration and Ultrafiltration^a

technique used	initial PC (mg/g _{biomass})	PC recovery (%)	PC concentration (mg/mL)	purity grade (Abs ₂₅₀ /Abs ₂₈₀)
gel-filtration	98 ± 1.4	78 ± 8	0.19 ± 0.01	5 ± 0.2
ultrafiltration	98 ± 1.4	80 ± 7	13 ± 1.4 ^b	5 ± 1

^aPC was determined spectrophotometrically. Data shown are means ± S.D. of three independent experiments. ^b*p* < 0.05 with respect to gel filtration.

Table 2. Comparison between Conventional Extraction Performed on Raw Biomass and Biomass Post French Press Extraction and PLE Extraction after French Press in Terms of Extracted Carotenoids^a

sample	carotenoid yield (mg/g _{biomass})	carotenoid content (mg/g _{extract})	zeaxanthin (mg/g _{extract})	β-carotene (mg/g _{extract})
raw biomass	62 ± 2	222 ± 24	2.7 ± 0.3	22 ± 4
post French press (conventional extraction)	100 ± 5 ^b	362 ± 24 ^b	33.4 ± 3.7 ^b	320 ± 76 ^c
post French press (PLE)	89 ± 6	911 ± 23 ^{b,c}	48 ± 5 ^{b,d}	436 ± 60 ^c

^aData shown are means ± S.D. of three independent experiments. ^b*p* < 0.05 with respect to raw biomass. ^c*p* < 0.005 with respect to conventional extraction after PC recovery. ^d*p* < 0.05 with respect to conventional extraction after PC recovery. ^e*p* < 0.005 with respect to raw biomass.

filtered through 0.45 μm nylon filters before HPLC analysis. Each dilution was injected in triplicate. For calibration plots, different concentrations of zeaxanthin (from 3.9 to 62.5 μg/mL) and of β-carotene (from 31.3 to 1000 μg/mL) were analyzed in duplicate as described in Gallego et al.²¹ The same instrument was directly coupled at the exit of the DAD to an Agilent ion trap 6320 mass spectrometer (Agilent Technologies) via an atmospheric pressure chemical ionization interface. Analyses were conducted under the positive ionization mode using the parameters described elsewhere.²¹ This time extracts were dissolved in pure methanol in concentrations between 10 and 20 mg/mL and injected in duplicate. Automatic tandem mass spectrometry (MS/MS) analyses were also performed fragmenting the two highest precursor ions.

ABTS Assay. The antioxidant activity of the lipophilic extract was evaluated by ABTS assay (2,2'-azino-bis[3-ethylbenzothiazoline-6-sulfonic acid]). The colorimetric assay is based on the reduction of the ABTS[•] radical by the antioxidant molecules present in the sample. The radical is produced by the reaction of a 7 mM ABTS solution mixed with 2.45 mM of potassium persulfate conducted for 16 h at room temperature in the dark. The mixture is then diluted in deionized water to obtain an absorbance of 0.7 ± 0.02 at 734 nm. The lipophilic extract in different concentrations was allowed to react with ABTS for 7 min in the dark, and the absorbance was measured at 734 nm again. Trolox (6-hydroxy-2,5,7,8-tetramethylchromane-2-carboxylic acid) was used as a standard to obtain a calibration curve. Each extract was analyzed three times in triplicate.

Cell Culture and Cytotoxicity Assay. Human immortalized keratinocytes (HaCaT) were from Innoprot (Biscay, Spain), whereas immortalized murine fibroblasts (BALB/c 3T3) were from ATCC (Manassas, Virginia). Cells were cultured in 10% fetal bovine serum in Dulbecco's modified Eagle's medium, in the presence of 1% antibiotics and 2 mM L-glutamine, in a 5% CO₂ humidified atmosphere at 37 °C. HaCaT cells were seeded in 96-well plates at a density of 2 × 10³ cells/well and BALB/c 3T3 at a density of 3 × 10³ cells/well. Approximately 24 h after seeding, increasing concentrations of the lipophilic extract (from 10 to 100 μg/mL) were added to the cells for different lengths of time. At the end of each experimental point, cell viability was measured by the MTT assay, as described by Arciello et al.²² Cell survival was expressed as the percentage of viable cells in the presence of the lipophilic extract compared to control cells (represented by the average obtained between untreated cells and cells supplemented with the highest concentration of buffer). Each sample was tested in three independent analyses, each carried out in triplicates.

DCFDA Assay. The antioxidant effect of the lipophilic extract (50 μg/mL) was measured by determining the intracellular ROS levels. The protocol used by Del Giudice et al. was followed,²³ with some modifications. Briefly, HaCaT cells were exposed for different lengths of time to the extract under test and then irradiated by UVA light for

10 min (100 J/cm²). Fluorescence intensity of the fluorescent probe (2',7'-dichlorofluorescein, DCF) was measured at an emission wavelength of 525 nm and an excitation wavelength of 488 nm using a Perkin-Elmer LSS0 spectrofluorimeter (Shelton, CT, USA). Emission spectra were acquired at a scanning speed of 300 nm/min, with 5 slit width both for excitation and emission. ROS production was expressed as a percentage of DCF fluorescence intensity of the sample under test, compared to the untreated sample. Three independent experiments were carried out, each one with three determinations.

Determination of Lipid Peroxidation Levels. The levels of lipid peroxidation were determined by using the thiobarbituric acid reactive substances (TBARS) assay according to the protocol proposed by Petruk et al.²⁴ Briefly, HaCaT cells were preincubated for 15 and 30 min with the lipophilic extract and then irradiated by UVA light for 10 min (100 J/cm²). Cells were detached by trypsin and centrifuged at 1000g for 10 min, 5 × 10⁵ cells were resuspended in 0.67% thiobarbituric acid (TBA), and an equal volume of 20% trichloroacetic acid was added. Samples were then heated at 95 °C for 30 min, incubated on ice for 10 min, and centrifuged at 3000g for 5 min, at 4 °C. TBA reacts with the oxidative degradation products of lipids in samples, yielding red complexes that absorb at 532 nm. Lipid peroxidation levels were expressed as a percentage of absorbance at 532 nm of the sample under test, compared to the untreated sample. Three independent experiments were carried out, each one with three determinations.

Western Blot Analysis. HaCaT cells were seeded at a density of 3 × 10⁵ cells/cm² in a complete medium for 24 h and then treated with 50 μg/mL of the lipophilic extract for different lengths of time. To analyze Nrf-2 expression levels, nuclear and cytosolic lysates were prepared as follows. Cells were detached by trypsin and centrifuged at 1000g for 10 min. Pellets were resuspended in lysis buffer (0.5% Triton X-100 in PBS pH 7.4) containing protease and phosphatase inhibitors. After 20 min incubation on ice, samples were centrifuged at 1200g for 5 min at 4 °C. The supernatants were removed and collected as cytosolic lysates. The residual pellets were washed in the same buffer and resuspended in RIPA buffer (50 mM Tris-HCl pH 7.4, 1% NP-40, 0.25% Na deoxycholate, 150 mM NaCl, 1 mM EDTA) completed with protease and phosphatase inhibitors. After 20 min incubation on ice, vortexing every 5 min, samples were centrifuged at 14,000g for 30 min at 4 °C. The supernatants were collected as nuclear lysates. The concentration of samples was determined by the Bradford assay, and the samples were analyzed by sodium dodecyl sulfate-polyacrylamide gel electrophoresis and western blot analysis. To normalize protein intensity levels, antibodies against β-actin and B23 were used. The chemiluminescence detection system was from Bio-Rad (Hercules, CA, USA).

Statistical Analysis. Experimental data results were analyzed by ANOVA, and means were compared by Tukey's HSD (SPSS statics

Table 3. Pigments Detected in *G. phlegrea* Extracts

peak	identification	RT (min)	UV-vis max, nm	[M + H] ⁺ m/z	MS/MS main fragments detected
1	carotenoid	13.706	450, 475	664.3	607.5, 551.5, 495.4
2	hydroxychlorophyll <i>a</i>	15.062	430, 663	910.1	893.0, 631.8, 614.5
3	chlorophyll-type	15.696	426, 665	940.7	629.4, 661.4, 907.7, 852.7, 574.4
4	zeaxanthin ^a	17.926	428, 450, 476	569.6	551.5
5	chlorophyll <i>a</i> ^a	19.092	432, 664	894.0	615.4, 583.3
6	chlorophyll <i>a</i> '	20.523	430, 665	894.1	615.6
7	carotenoid	21.453	445, 471		
8	carotenoid	24.772	450, 476	584.7	564.8
9	pheophytin <i>a</i>	30.425	408, 666	872.1	594.0, 683.3, 535.5
10	pheophytin <i>a</i> '	31.681	408, 666	871.9	593.8
11	β -carotene ^a	33.685	450, 475	537.7	
12	carotenoid	35.591	446, 472	592.8	533.4

^aIdentification corroborated by comparison with commercial standards; RT: retention time.

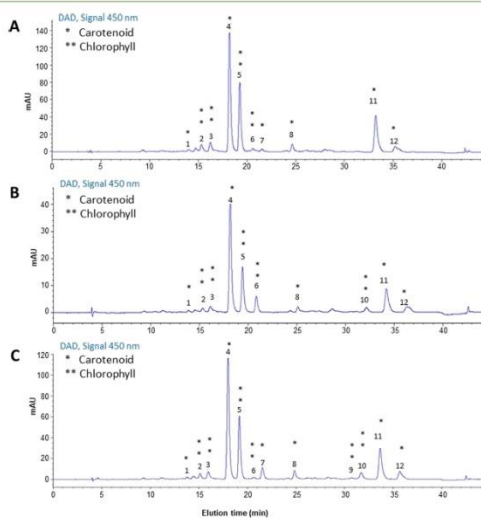


Figure 2. Representative HPLC–DAD chromatograms of carotenoids extracted from *G. phlegrea*. (A) Conventional extraction of raw biomass; (B) conventional extraction of the residual biomass after PC extraction; (C) PLE extraction of the residual biomass after PC extraction. * indicates carotenoids and ** indicates chlorophylls. Peak numbers and their identification are reported in Table 3.

V15 IBM, New York, United States). The value of $p \leq 0.05$ was considered statistically significant, figured by alphabetical letters along means in tables.

RESULTS AND DISCUSSION

Optimization of PC Purification. We recently set up a procedure to disrupt *G. phlegrea* biomass by using a conventional high-pressure procedure. PC was then easily recovered from the supernatant by a single purification step, that is, gel filtration.¹⁴ However, from an economic point of view, the size exclusion chromatography is not feasible, as it is difficult to be scaled-up. Thus, we optimized PC purification by using ultrafiltration and compared the results with those

Table 4. Comparison between Conventional Extractions Performed on Raw Biomass and Biomass Post French Press Extraction and SFE Extraction after French Press in Terms of Extracted Lipids^a

sample	lipid yield (mg/g _{biomass})
raw biomass (conventional extraction)	110 ± 3
post French press (conventional extraction)	164 ± 6 ^b
post French press (SFE)	184 ± 5 ^b

^aData shown are means ± S.D. of three independent experiment. ^b $p < 0.05$.

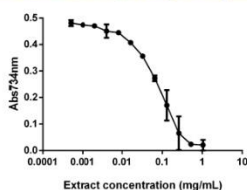


Figure 3. ABTS assay on carotenoids extracted from *G. phlegrea*. ABTS scavenging activity of different concentrations of the lipophilic extract (mg/mL) obtained by PLE from *G. phlegrea*. Data shown are means \pm S.D. of three independent experiments.

previously obtained. As shown in Table 1, both the ultrafiltration technique and gel filtration allow obtaining a PC with a high purity grade. It is known that a purity grade ≤ 0.7 is indicative of a food grade, between 0.7 and 3.9 is of reagent grade, and ≥ 4.0 of analytical grade.²⁵ As for the yield, about 80% PC was obtained with both techniques. However, the protein concentration was much higher when ultrafiltration was used, as 13 mg/mL of PC was obtained with respect to 0.19 mg/mL of gel filtration.

Total Carotenoid Extraction. Starting from the residual wet biomass after PC extraction, carotenoid extraction was performed by using the PLE technology. In order to compare the carotenoid extraction after PLE, a conventional acetone extraction was performed in parallel on dried raw biomass and on the dried residual biomass after PC extraction, as schematized in Figure 1. Usually, one of the mechanisms employed to break cell wall is freeze-drying the biomass, which is a high energy-consuming treatment and causes rapid loss and degradation of carotenoids, thus affecting the bioactivity of the desired compounds.^{26,27} The results of the extractions are reported in Table 2. The carotenoid yield is expressed as mg of carotenoids extracted per g of dry biomass. It is interesting to notice that the conventional extraction allowed obtaining 62 mg of carotenoids from the raw biomass, whereas about 100 mg was recovered starting from the disrupted biomass. Thus, a significant increase ($p < 0.05$) in total carotenoid extraction was observed when the disrupted biomass was used. When PLE was employed on residual wet biomass, about 90 mg of carotenoids was obtained. Noteworthy, although the PLE did not increase the extraction yield with respect to the

conventional method, the time needed to obtain carotenoids significantly decreased from 24 h to 30 min. In addition, no organic solvents were used, thus suggesting that this technology is green and very effective. In terms of total carotenoid content, the high-pressure procedure allowed obtaining a purer extract. In fact, as shown in Table 2, the conventional extraction allowed an increase in the carotenoid content up to 63% when the disrupted biomass was used instead of the raw one ($p < 0.05$). Surprisingly, PLE allowed a further increase of 250% in the total carotenoid content when compared to the conventional extraction technique on the disrupted biomass ($p < 0.005$) and 400% on the raw biomass ($p < 0.05$).

Carotenoid Characterization by HPLC–DAD–MS.

Carotenoids obtained by the PLE technique were analyzed by high-performance liquid chromatography coupled to the diode array detector and mass spectrometry detector (HPLC–DAD–MS) in order to collect more information about the specific pigments (carotenoids and chlorophylls). When possible, a tentative identification was accomplished by combining the information provided by UV–vis spectra from DAD, $[M + H]^+$, and MS/MS fragmentation patterns from the mass spectrometry detector and bibliographic search (Table 3). Chromatographic profiles shown in Figure 2 revealed that the extract obtained by PLE with ethanol is the one with the highest number of pigments.

Peaks numbers 4, 5, and 11 stood out as the most relevant ones, and they could be tentatively identified as zeaxanthin, chlorophyll *a*, and β -carotene, respectively. These pigments were also present in the pressurized liquid extracts obtained with ethanol from other microalgae (*Neochloris oleoabundans*²⁰ and *Porphyridium cruentum*²¹). Protonated ions of these compounds were detected (m/z 569.6 $[M + H]^+$ for zeaxanthin, m/z 894.0 $[M + H]^+$ for chlorophyll *a* and m/z 537.7 $[M + H]^+$ for β -carotene), along with fragment ions of zeaxanthin and chlorophyll *a* produced by the loss of a water molecule (m/z 551.5 $[M + H - H_2O]^+$) or phytol group (m/z 615.4 $[M + H - C_{20}H_{43}]^+$), respectively. Furthermore, the identification of these three compounds was corroborated by the injection of commercial standards.

Other minor chlorophylls, peaks 2 and 9 were tentatively assigned as hydroxychlorophyll *a*²⁰ and pheophytin *a*¹¹ because of their UV–vis UV and MS/MS spectra, showing the particular loss of a phytol group. Peaks number 6 and 10 have been tentatively identified as chlorophyll *a'* and

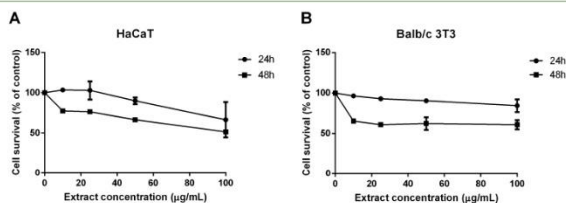


Figure 4. Effect of the lipophilic extract on the viability of HaCaT and BALB/c 3T3 cells. Dose–response curves of HaCaT (A) and BALB/c 3T3 (B) cells after 24 h (black circles) and 48 h (black squares) incubation with increasing concentrations of lipophilic extracts obtained by PLE (10–100 $\mu\text{g/mL}$). Cell viability was assessed by the MTT assay, and cell survival expressed as percentage of viable cells in the presence of the lipophilic extract under test, with respect to control cells grown in the absence of the extract. Data shown are means \pm S.D. of three independent experiments.

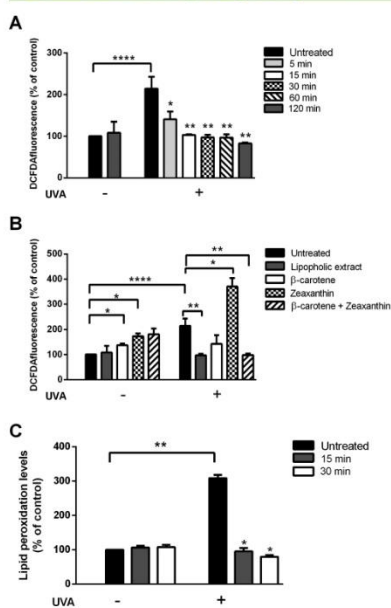


Figure 5. Antioxidant effect of the lipophilic extract from *G. phlegrea* on stressed HaCaT cells. Cells were preincubated in the presence of 50 $\mu\text{g}/\text{mL}$ lipophilic extract from different lengths of time, prior to be irradiated by UVA (100 J/cm^2). (A) Determination of intracellular ROS levels by DCFDA assay. Cells were incubated for 5 min (light grey bars), 15 min (white bars), 30 min (black-squared bars), 60 min (dashed bars), or 120 min (dark grey bars) with the lipophilic extract in the absence (-) or in the presence (+) of UVA. Black bars are referred to untreated cells. For each experimental condition, ROS production was measured and a percentage of the ratio between ROS production in treated cells and ROS production in untreated cells was calculated and reported in the graph. (B) Comparison of the protective effect of the lipophilic extract with commercial antioxidants by the DCFDA assay. Cells were incubated for 30 min prior to UVA exposure. Black bars are referred to untreated cells in the absence (-) or in the presence (+) of UVA. Grey bars are referred to cells incubated with 50 $\mu\text{g}/\text{mL}$ lipophilic extract; white bars are referred to cells incubated with 24 $\mu\text{g}/\text{mL}$ β -carotene; black squared bars are referred to cells incubated with 2.4 $\mu\text{g}/\text{mL}$ zeaxanthin; and dashed bars are referred to cells incubated with both β -carotene and zeaxanthin. (C) Analysis of lipid peroxidation levels evaluated by TBARS assay. Cells were preincubated with the lipophilic extract for 15 (grey bars) or 30 min (white bars) before UVA irradiation. Values are expressed as % with respect to control (i.e. untreated) cells. For each experimental condition, lipid peroxidation levels were measured, and a percentage of the ratio between lipid peroxidation levels in treated cells and lipid peroxidation levels in untreated cells was calculated and reported in the graph. Data shown are means \pm S.D. of three independent experiment. * indicates $p < 0.05$, ** indicates $p < 0.005$, and **** indicates $p < 0.0001$.

pheophytin a' in concordance with their spectra, similar to those of chlorophyll a and pheophytin a but presenting longer retention times. Peak number 3 presented the characteristic absorbance spectrum of chlorophylls and therefore have been designed as chlorophyll-type.

The rest of the minor peaks in the chromatogram presented the characteristic absorbance spectrum of carotenoids. With the exception of peak number 7, that could not be detected in MS due to the lack of enough ionization efficiency, the rest of carotenoids were characterized in terms of $[M + H]^+$, and many fragments from MS/MS were detected. However, a tentative identification was not possible. On the other hand, it is not the first time that peak number 12 has been reported. This carotenoid with the UV-vis spectrum with maximums at 446 and 472 nm was previously mentioned in gas expanded liquid extracts obtained with 75% of ethanol from the microalga *Scenedesmus obliquus*.²⁸ In conclusion, the pigment analysis revealed β -carotene and zeaxanthin as the two main carotenoids in all extracts in agreement with Marquardt,²⁹ but with a different *Galdieria* species (*G. sulphuraria*).

In addition, a method based on HPLC-DAD was employed to quantify the amount of zeaxanthin and β -carotene. To fit the calibration curves prepared with the commercial standards of both pigments, the samples analyzed were diluted in pure methanol at different concentrations: 10 mg/mL for the conventional extraction starting from raw biomass and 1 mg/mL for the two extracts obtained after French press. Quantification results are reported in Table 2. As expected, PLE improved the amount of both pigments. Moreover, the increase obtained was surprisingly interesting: up to 40% in comparison with the ones obtained by conventional extraction and to about 2000 times with respect to the raw biomass.

Total Lipid Extraction. To further improve the biorefinery design, after the PLE extraction a lipid extraction was carried out using supercritical CO_2 (ScCO_2). Notably, both PLE and SFE were performed on the same apparatus, without the need to recover the biomass from the extraction cell after carotenoid extraction. In particular, after PLE, CO_2 was injected in the extraction cell to push out ethanol-containing carotenoids. Afterward, pressure was increased to the super critical point, and lipids were extracted (Figure S1). As a benchmark, conventional chloroform/methanol extraction was carried out on raw dried biomass and on the residual dried biomass after PC extraction. Results of the extractions are reported in Table 4. The ScCO_2 extraction allowed obtaining the same amount of lipids that those by conventional extraction, avoiding the use of an organic solvent. This result was quite surprising, as the lipids extracted are the third class of molecules obtained in a biorefinery approach. When compared with our previous results,¹⁴ we found a lower recovery in lipid yield, but this could be due to a different extraction method used.

Evaluation of Biocompatibility and Antioxidant Activity of Lipophilic Extract Obtained by PLE Extraction on Eukaryotic Cells. To verify if the carotenoids extracted by the PLE technique were biologically active and safe for humans, their in vitro antioxidant activity, along with their biocompatibility on eukaryotic cells, was tested. The results of the in vitro ABTS colorimetric assay are shown in Figure 3 and clearly indicate that the lipophilic extract is endowed with a significant antioxidant activity. Its IC_{50} value, that is, the concentration of the extract that can inhibit 50% of the radical, is 50 $\mu\text{g}/\text{mL}$. This result is much lower than those reported in the literature, as the IC_{50} value here obtained is

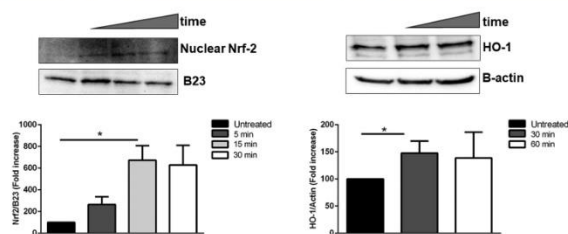


Figure 6. Effect of the lipophilic extract on Nrf-2 activation on HaCaT cells. Cells were incubated with 50 $\mu\text{g}/\text{mL}$ lipophilic extract obtained by the PLE technique for different lengths of time and then nuclear (A) or cytosolic (B) proteins were analyzed by western blotting. (A) Western blot analysis of nuclear Nrf-2 after 5 min (dark grey bar), 15 min (light grey bar), and 30 min (white bar) incubation. Nuclear Nrf-2 and B23 were quantified by densitometric analysis. The ratio between Nrf-2 and B23 of each treated sample was then related to the ratio Nrf-2/B23 of untreated cells, considered as 100%. (B) Western blot analysis of cytosolic HO-1 was performed after incubation with 50 $\mu\text{g}/\text{mL}$ of the extract for 30 min (dark grey bar) and 60 min (white bar). HO-1 and β -actin were quantified by densitometric analysis, and the ratio HO-1/ β -actin of each treated sample was then related to the ratio HO-1/ β -actin of untreated cells, considered as 100%. Data shown are means \pm S.D. of three independent experiments. * indicates $p < 0.05$ with respect to control cells.

about 1600 times lower than others reported with different microalgae.³⁰ The biocompatibility of the extract was tested by a time-course and dose–response test on immortalized murine fibroblasts (BALB/c 3T3) and immortalized human keratinocytes (HaCaT). Cell viability was assessed by the tetrazolium salt colorimetric (MTT) assay, and cell survival was expressed as the percentage of viable cells in the presence of the extract compared to that of control samples. As shown in Figure 4A,B, after 48 h, cell viability was not affected up to 50 $\mu\text{g}/\text{mL}$, while at the highest concentration tested (100 $\mu\text{g}/\text{mL}$), a 50% reduction of cell viability was observed.

Protective Effect of the Lipophilic Extract against Oxidative Stress on HaCaT Cells. As the lipophilic extract obtained by PLE contains antioxidants, the potential protective effect against oxidative stress was analyzed on a cell-based model. As a cell system, we chose immortalized keratinocytes as they are normally present in the outermost layer of the skin and UVA radiations as a source of stress. Cells were treated with 50 $\mu\text{g}/\text{mL}$ extracts for different lengths of time (from 5 to 120 min), and then oxidative stress was induced by UVA irradiation (100 J/cm^2). Immediately after irradiation, ROS levels were measured by using $\text{H}_2\text{DCF-DA}$ as a probe. For each set of experiments, untreated cells were used as a control. Under physiological conditions (i.e., in the case of untreated cells), a physiological release of ROS is observed (100%). As shown in Figure 5A, no effect on ROS levels was observed when cells were incubated with the extract for 120 min (grey bars), whereas UVA treatment significantly increased DCF fluorescence intensity (black bars). Interestingly, pretreatment of cells with the lipophilic extract, prior to UVA exposure, resulted in an inhibition of ROS production, which was clear already after 5 min of pretreatment. We then performed a comparison between the antioxidant activity of the total lipophilic extract obtained by PLE and commercial β -carotene and zeaxanthin, the two most abundant species identified in the extract. On the basis of the quantification data reported in Table 2, we calculated that, when the lipophilic extract was tested at 50 $\mu\text{g}/\text{mL}$, the amount of β -carotene corresponded to 24 $\mu\text{g}/\text{mL}$ and that of zeaxanthin to 2.4 $\mu\text{g}/\text{mL}$. Thus, HaCaT cells were preincubated for 30 min with either: 50 $\mu\text{g}/\text{mL}$ of lipophilic extract; 24 $\mu\text{g}/\text{mL}$ of β -carotene; 2.4 $\mu\text{g}/\text{mL}$ of

zeaxanthin; a mixture of both carotenoids. At the end of incubation, oxidative stress was induced as previously mentioned. Alteration of ROS levels was measured by using $\text{H}_2\text{DCF-DA}$. As shown in Figure 5B, a significant increase in ROS production was observed when cells were incubated with commercial β -carotene (white bars) or zeaxanthin (black squared bars), also in the absence of any UVA exposure. Interestingly, only the mixture of both commercial carotenoids (dashed bars), as well as the lipophilic extract (grey bars), were able to counteract oxidative stress in a similar way. The protective effect of the lipophilic extract was also confirmed by analyzing the lipid peroxidation levels. To this purpose, TBARS were measured and related to lipid peroxidation levels. A significant increase in lipid peroxidation levels was observed after UVA treatment, but, notably, this effect was abolished when cells were pretreated with the lipophilic extract, either after 15 or 30 min preincubation (grey and white bars, respectively). Treatment of cells with the lipophilic extract did not alter significantly lipid peroxidation levels (Figure 5C).

Nrf-2 Regulates the Antioxidant Activity of the Lipophilic Extract. To understand the molecular mechanism responsible for the protective effect of the lipophilic extract, the involvement of the transcription factor Nrf-2 was analyzed. Under normal physiological conditions, Nrf-2 is associated with Keap-1, which retains Nrf-2 in the cytosol and directs it to the proteasomal degradation. Upon either oxidative stress induction and/or in the presence of antioxidants, Keap-1 dissociates from Nrf-2, which is translocated to the nucleus where it binds to antioxidant responsive elements sequences and activates the transcription of several phase-II detoxifying enzymes.³¹ Thus, we incubated HaCaT cells in the presence of the lipophilic extract for different length of time (from 5 to 30 min), and lysates were analyzed by western blot analysis, using Nrf-2 antibody. As shown in Figure 6A, an increase in nuclear Nrf-2 was observed after 15 min of incubation. The activation of Nrf-2 was further confirmed by analyzing the translation level of the heme oxygenase-1 (HO-1) by western blot analysis. HO-1 is a ubiquitous and redox-sensitive inducible stress protein that degrades heme to CO, iron, and biliverdin.³² The importance of this protein in physiological and

pathological states is underlined by the versatility of HO-1 inducers and the protective effects attributed to heme oxygenase products in conditions that are associated with moderate or severe cellular stress. Thus, HaCaT cells were incubated for 30 and 60 min, and lysates were analyzed by western blot analysis, using a HO-1 antibody. As shown in Figure 6B, an increase in HO-1 levels was observed after 30 min of incubation.

CONCLUSIONS

One of the aims of green chemistry is to preserve the natural environment, promoting a better use of resources and limiting the negative influence of human involvement, such as the use of procedures that require the use of toxic solvents.³³ Compared to conventional extractions, this innovative green biorefinery approach is able to extract, in cascade, three different bioactive compounds from the microalga *G. phlegrea*. In combination, the described process allows achieving higher yields of PC, carotenoids, and lipids using Generally Recognized As Safe (GRAS) solvents, in shorter time and with less solvent consumption. Here, we demonstrated that PLE using ethanol has a high potential to extract carotenoids from *G. phlegrea*. Moreover, as *G. phlegrea* is an eukaryotic microalga, it possesses a robust cell wall, which prevents the release of intracellular products. The idea of breaking the biomass by high pressure homogenization allowed to isolate PC and helped the subsequent release of carotenoids. Both final products, PC, and carotenoids were biologically active in terms of antioxidant activity.¹⁴ These results will open the way to the idea of commercializing carotenoids from microalgae for cosmeceutical applications. In conclusion, this work will help to achieve a complete valorization of the *G. phlegrea* microalga biomass. The results can then contribute to increase the revenue streams of the process, in order to compensate the large cultivation and downstream cost for biomass production and, finally, turn positive the economic balance of the microalga biorefinery. Furthermore, they contribute to develop a green process which can also increase the social acceptance of industrial microalgal products.

ASSOCIATED CONTENT

Supporting Information

The Supporting Information is available free of charge at <https://pubs.acs.org/doi/10.1021/acssuschemeng.9b07505>.

Schematic representation of the equipment employed for compressed fluid extractions (PDF)

AUTHOR INFORMATION

Corresponding Authors

Giuseppe Olivieri – Bioprocess Engineering Group, Wageningen University and Research, 6700AA Wageningen, The Netherlands; Department of Chemical, Materials and Industrial Engineering, University of Naples Federico II, 80125 Naples, Italy; Email: giuseppe.olivieri@wur.nl

Daria Maria Monti – Department of Chemical Sciences, University of Naples Federico II, 80126 Naples, Italy; orcid.org/0000-0002-1136-0576; Email: mdmonti@unina.it

Authors

Paola Imbimo – Department of Chemical Sciences, University of Naples Federico II, 80126 Naples, Italy

Monica Bueno – Laboratory of Foodomics, Institute of Food Science Research, CIAL, CSIC, 28049 Madrid, Spain

Luigi D'Elia – Department of Chemical Sciences, University of Naples Federico II, 80126 Naples, Italy

Antonino Pollio – Department of Biology, University of Naples Federico II, 80126 Naples, Italy

Elena Ibañez – Laboratory of Foodomics, Institute of Food Science Research, CIAL, CSIC, 28049 Madrid, Spain

Complete contact information is available at: <https://pubs.acs.org/10.1021/acssuschemeng.9b07505>

Notes

The authors declare no competing financial interest.

ACKNOWLEDGMENTS

M.B. acknowledges MINECO for the "Juan de La Cierva-Formación" postdoctoral grant FJCI-2016-30902. This research was financed under projects ABACUS (Algae for a Biomass Applied to the production of added value compounds—funded by the Bio Based Industries Joint Undertaking under the European Union's Horizon 2020 research and innovation programme under grant agreement no. 745668) and AGL2017-89417-R (MINECO, Spain).

REFERENCES

- (1) Santiago-Santos, M. C.; Ponce-Noyola, T.; Olvera-Ramírez, R.; Ortega-López, J.; Cañizares-Villanueva, R. O. Extraction and Purification of Phycocyanin from *Calothrix* Sp. *Process Biochem.* **2004**, *39*, 2047–2052.
- (2) Basha, O. M.; Hafez, R. A.; El-Ayouty, Y. M.; Mahrous, K. F.; Baredy, M. H.; Salama, A. M. C. Phycocyanin Inhibits Cell Proliferation and May Induce Apoptosis in Human HepG2 Cells. *Egypt. J. Immunol.* **2008**, *15*, 161–167.
- (3) Jin, E. S.; Melis, A. Microalgal Biotechnology: Carotenoid Production by the Green Algae *Dunaliella Salina*. *Biotechnol. Bioprocess Eng.* **2003**, *8*, 331–337.
- (4) Sathasivam, R.; Ki, J.-S. A Review of the Biological Activities of Microalgal Carotenoids and Their Potential Use in Healthcare and Cosmetic Industries. *Mar. Drugs* **2018**, *16*, 26.
- (5) Nagarajan, J.; Ramanan, R. N.; Raghunandan, M. E.; Galanakis, C. M.; Krishnamurthy, N. P. *Carotenoids*; Elsevier Inc.: Chapter 8, 2017.
- (6) Blomhoff, R. Vitamin A and Carotenoid Toxicity. *Food Nutr. Bull. Suppl.* **2001**, *22*, 320–334.
- (7) Ambati, R. R.; Gogisetty, D.; Aswathanarayana, R. G.; Ravi, S.; Bikkina, P. N.; Bo, L.; Yuepeng, S. Industrial Potential of Carotenoid Pigments from Microalgae: Current Trends and Future Prospects. *Crit. Rev. Food Sci. Nutr.* **2019**, *59*, 1880–1902.
- (8) Spolaore, P.; Joannis-Cassan, C.; Duran, E.; Isambert, A. Commercial Applications of Microalgae. *J. Biosci. Bioeng.* **2006**, *101*, 87–96.
- (9) Pruvost, J.; Van Vooren, G.; Le Gouic, B.; Couzinet-Mossion, A.; Legrand, J. Systematic Investigation of Biomass and Lipid Productivity by Microalgae in Photobioreactors for Biodiesel Application. *Bioresour. Technol.* **2011**, *102*, 150–158.
- (10) Barsanti, L.; Gualtieri, P. Is Exploitation of Microalgae Economically and Energetically Sustainable? *Algal Res.* **2018**, *31*, 107–115.
- (11) Gallego, R.; Bueno, M.; Herrero, M. Sub- and Supercritical Fluid Extraction of Bioactive Compounds from Plants, Food-by-Products, Seaweeds and Microalgae – An Update. *TrAC, Trends Anal. Chem.* **2019**, *116*, 198–213.
- (12) Camel, V. Recent Extraction Techniques for Solid Matrices - Supercritical Fluid Extraction, Pressurized Fluid Extraction and Microwave-Assisted Extraction: Their Potential and Pitfalls. *Analyst* **2001**, *126*, 1182–1193.

- (13) Mubarak, M.; Shaiba, A.; Suchithra, T. V. A Review on the Extraction of Lipid from Microalgae for Biodiesel Production. *Algal Res.* **2015**, *7*, 117–123.
- (14) Imbimbo, P.; Romanucci, V.; Pollio, A.; Fontanarosa, C.; Amoresano, A.; Zarrelli, A.; Olivieri, G.; Monti, D. M. A Cascade Extraction of Active Phycocyanin and Fatty Acids from *Galdieria Phlegrea*. *Appl. Microbiol. Biotechnol.* **2019**, *103*, 9455–9464.
- (15) Wu, H.-L.; Wang, G.-H.; Xiang, W.-Z.; Li, T.; He, H. Stability and Antioxidant Activity of Food-Grade Phycocyanin Isolated from *Spirulina platensis*. *Int. J. Food Prop.* **2016**, *19*, 2349–2362.
- (16) José, M.; Reyes, F. A.; Mendiola, J. A.; Iba, E. Astaxanthin Extraction from *Haematococcus Pluvialis* Using CO₂-Expanded Ethanol. *J. Supercrit. Fluids* **2014**, *92*, 75–83.
- (17) Axelsson, M.; Gentili, F. A Single-Step Method for Rapid Extraction of Total Lipids from Green Microalgae. *PLoS One* **2014**, *9*, No. e89643.
- (18) Reyes, F. A.; Mendiola, J. A.; Suárez-Alvarez, S.; Ibañez, E.; Del Valle, J. M. Adsorbent-Assisted Supercritical CO₂ Extraction of Carotenoids from *Neochloris Oleoabundans* Paste. *J. Supercrit. Fluids* **2016**, *112*, 7–13.
- (19) Gilbert-López, B.; Mendiola, J. A.; Fontecha, J.; Van Den Broek, L. A. M.; Sijtsma, L.; Cifuentes, A.; Herrero, M.; Ibañez, E. Downstream Processing of *Isochrysis Galbana*: A Step towards Microalgal Biorefinery. *Green Chem.* **2015**, *17*, 4599–4609.
- (20) Castro-Puyana, M.; Herrero, M.; Urreta, I.; Mendiola, J. A.; Cifuentes, A.; Ibañez, E.; Suárez-Alvarez, S. Optimization of Clean Extraction Methods to Isolate Carotenoids from the Microalga *Neochloris Oleoabundans* and Subsequent Chemical Characterization Using Liquid Chromatography Tandem Mass Spectrometry. *Anal. Bioanal. Chem.* **2013**, *405*, 4607–4616.
- (21) Gallego, R.; Martínez, M.; Cifuentes, A.; Ibañez, E.; Herrero, M. Development of a Green Downstream Process for the Valorization of Porphyrinoid Cruentum Biomass. *Molecules* **2019**, *24*, 1564.
- (22) Arciello, A.; De Marco, N.; Del Giudice, R.; Guglielmi, F.; Pucci, P.; Relini, A.; Monti, D. M.; Piccoli, R. Insights into the Fate of the N-Terminal Amyloidogenic Polypeptide of ApoA-I in Cultured Target Cells. *J. Cell. Mol. Med.* **2011**, *15*, 2652–2663.
- (23) Del Giudice, R.; Petruk, G.; Raiola, A.; Barone, A.; Monti, D. M.; Rigano, M. M. Carotenoids in Fresh and Processed Tomato (*Solanum Lycopersicum*) Fruits Protect Cells from Oxidative Stress Injury. *J. Sci. Food Agric.* **2017**, *97*, 1616–1623.
- (24) Petruk, G.; Raiola, A.; Del Giudice, R.; Barone, A.; Fruscante, L.; Rigano, M. M.; Monti, D. M. An Ascorbic Acid-Enriched Tomato Genotype to Fight UVA-Induced Oxidative Stress in Normal Human Keratinocytes. *J. Photochem. Photobiol., B* **2016**, *163*, 284–289.
- (25) Fernández-Rojas, B.; Hernández-Juárez, J.; Pedraza-Chaverri, J. Nutraceutical Properties of Phycocyanin. *J. Funct. Foods* **2014**, *11*, 375–392.
- (26) Mcmillan, J. R.; Watson, I. A.; Ali, M.; Jaafar, W. Evaluation and Comparison of Algal Cell Disruption Methods: Microwave, Waterbath, Blender, Ultrasonic and Laser Treatment. *Appl. Energy* **2013**, *103*, 128–134.
- (27) Papaioannou, E.; Roukas, T.; Liakopoulou-Kyriakides, M. Effect of Biomass Pre-Treatment and Solvent Extraction on β -Carotene and Lycopene Recovery from *Blakeslea Trispora* Cells. *Prep. Biochem. Biotechnol.* **2008**, *38*, 246–256.
- (28) Gilbert-López, B.; Mendiola, J. A.; van den Broek, L. A. M.; Houweling-Tan, B.; Sijtsma, L.; Cifuentes, A.; Herrero, M.; Ibañez, E. Green Compressed Fluid Technologies for Downstream Processing of *Scenedesmus Obliquus* in a Biorefinery Approach. *Algal Res.* **2017**, *24*, 111–121.
- (29) Marquardt, J. Effects of Carotenoid-Depletion on the Photosynthetic Apparatus of a *Galdieria Sulphuraria* (Rhodophyta) Strain That Retains Its Photosynthetic Apparatus in the Dark. *J. Plant Physiol.* **1998**, *152*, 372–380.
- (30) Peraman, M.; Nachimuthu, S. Identification and Quantification of Fucoxanthin in Selected Carotenoid-Producing Marine Microalgae and Evaluation for Their Chemotherapeutic Potential. *Pharmacogn. Mag.* **2019**, *15*, 243–249.
- (31) Ma, Q. Role of Nrf2 in Oxidative Stress and Toxicity. *Annu. Rev. Pharmacol. Toxicol.* **2013**, *53*, 401.
- (32) Balogun, E.; Hoque, M.; Gong, P.; Killeen, E.; Green, C. J.; Foresti, R.; Alam, J.; Motterlini, R. Curcumin Activates the Haem Oxygenase-1 Gene via Regulation of Nrf2 and the Antioxidant-Responsive Element. *Biochem. J.* **2003**, *371*, 887–895.
- (33) Mustafa, A.; Turner, C. Analytica Chimica Acta Pressurized Liquid Extraction as a Green Approach in Food and Herbal Plants Extraction: A Review. *Anal. Chim. Acta* **2011**, *703*, 8–18.

Article

Autotrophic and Heterotrophic Growth Conditions Modify Biomolecule Production in the Microalga *Galdieria sulphuraria* (Cyanidiophyceae, Rhodophyta)

Roberto Barone ^{1,*}, Lorenzo De Napoli ², Luciano Mayol ², Marina Paolucci ^{3,4,*}, Maria Grazia Volpe ⁴, Luigi D'Elia ⁵, Antonino Pollio ⁵, Marco Guida ⁵, Edvige Gambino ⁵, Federica Carraturo ⁵, Roberta Marra ¹, Francesco Vinale ^{6,7}, Sheridan Lois Woo ^{2,7,*} and Matteo Lorito ^{1,7}

¹ Department of Agricultural Science, University of Naples Federico II, Via Università, Portici, 80138 Naples, Italy; robmarra@unina.it (R.M.); matteo.lorito@unina.it (M.L.)

² Department of Pharmacy, University of Naples Federico II, Via D. Montesano, 80138 Naples, Italy; lorenzo.denapoli@unina.it (L.D.N.); luciano.mayol@unina.it (L.M.)

³ Department of Science and Technologies (DST), University of Sannio, 82100 Benevento, Italy

⁴ Institute of Food Sciences, National Research Council (ISA-CNR), Via Roma 64, 83100 Avellino, Italy; mgvolpe@isa.cnr.it

⁵ Department of Biology, University of Naples Federico II, Via Cinthia, 80138 Naples, Italy; luigi.delia@unina.it (L.D.); antonino.pollo@unina.it (A.P.); marco.guida@unina.it (M.G.); ed.gambino@gmail.com (E.G.); federica.carraturo@unina.it (F.C.)

⁶ Department of Veterinary Medicine and Animal Production, University of Naples Federico II, Via Federico Delpino, 80138 Naples, Italy; frvinale@unina.it

⁷ IPSP-CNR-Via Università-Portici, 80138 Naples, Italy

* Correspondence: robbaron@unina.it (R.B.); paolucci@unisannio.it (M.P.); woo@unina.it (S.L.W.); Tel.: +39-081-2534544 (R.B.); +39-0824-305126 (M.P.); +39-081-2539010 (S.L.W.)

Received: 26 February 2020; Accepted: 17 March 2020; Published: 18 March 2020



Abstract: Algae have multiple similarities with fungi, with both belonging to the *Thallophyte*, a polyphyletic group of non-mobile organisms grouped together on the basis of similar characteristics, but not sharing a common ancestor. The main difference between algae and fungi is noted in their metabolism. In fact, although algae have chlorophyll-bearing thalloids and are autotrophic organisms, fungi lack chlorophyll and are heterotrophic, not able to synthesize their own nutrients. However, our studies have shown that the extremophilic microalga *Galdieria sulphuraria* (GS) can also grow very well in heterotrophic conditions like fungi. This study was carried out using several approaches such as scanning electron microscope (SEM), gas chromatography/mass spectrometry (GC/MS), and infrared spectrophotometry (ATR-FTIR). Results showed that the GS, strain ACUF 064, cultured in autotrophic (AGS) and heterotrophic (HGS) conditions, produced different biomolecules. In particular, when grown in HGS, the algae (i) was 30% larger, with an increase in carbon mass that was 20% greater than AGS; (ii) produced higher quantities of stearic acid, oleic acid, monounsaturated fatty acids (MUFAs), and ergosterol; (iii) produced lower quantities of fatty acid methyl esters (FAMES) such as methyl palmylate, and methyl linoleate, saturated fatty acids (SFAs), and polyunsaturated fatty acids (PUFAs). ATR-FTIR and principal component analysis (PCA) statistical analysis confirmed that the macromolecular content of HGS was significantly different from AGS. The ability to produce different macromolecules by changing the trophic conditions may represent an interesting strategy to induce microalgae to produce different biomolecules that can find applications in several fields such as food, feed, nutraceutical, or energy production.

Keywords: *Galdieria sulphuraria*; microalga; fungi; autothrophy; heterotrophy; fatty acids; ATR-FTIR

1. Introduction

Microalgae are unicellular organisms commonly found in fresh and marine waters. They are very similar to fungi [1], both are morphologically undifferentiated and included in the group of *Thallophytes*. However, the main difference is that algae require light, contain chlorophyll, and are autotrophs. Members are characterized by a high biodiversity whose potential, in terms of the production of high value biological molecules, is yet to be explored and exploited [2]. Microalgae cultivation can provide diverse essential nutrients, including carbohydrates, proteins, and lipids, as well as pigments, vitamins, bioactive compounds, and antioxidants [3,4]; substances that can be utilized in nutraceuticals, pharmaceuticals, biofuels, health supplements, and the cosmetic industry. Furthermore, microalgae cultivation provides a potential strategy to produce an alternative food source for both humans and animals. This feature, plus the ability of microalgae to grow more rapidly than vascular plants, satisfies the need for large-scale, cost-effective, high nutritional value production [5]. Therefore, microalgae represent an interesting resource in the biotechnology field, as they are able to quickly reach a high level of biomass and produce a large quantity of fatty acids (FAs) such as palmitic acid (C16:0), myristic acid (C14:0), monounsaturated (MUFAs), polyunsaturated FAs (PUFAs), and fatty acid methyl esters (FAMES), molecules extremely interesting for commercial applications. Microalgae also produce pharmacologically active molecules with immunomodulatory, anti-inflammatory, antihypercholesterolemic, antioxidant, anticancer, and antidiabetic properties [6–8]. The metabolic flexibility of microalgae allows them to grow in both autotrophic and heterotrophic conditions [9]. The benefit trade-offs are diverse for algae, whereby the autotrophic growing condition is preferred from an efficiency point of view, but it provides a limited growth of biomass, whereas the biomass obtained under heterotrophic growing conditions is greater, but requires additional external carbon sources that are energetically expensive [10,11]. The heterotrophic cultivation of *Chlorella vulgaris*, the oldest microalgae exploited for commercial application, has demonstrated higher biomass yields than the autotrophic cultivation, with higher lipid productivity [12].

Galdieria sulphuraria (GS; Cyanidiophyceae, Rhodophyta) is an ancient extremophilic unicellular red microalga capable of growing in hot springs at low pH [13,14] all around the world. It shows optimal growth conditions at pH 1.5 and temperatures in the range of 35–45 °C, extreme growth conditions that prevent bacterial contamination, one of the major problems faced with large scale microalgae cultivation [15,16]. Moreover, GS is able to grow photoautotrophically, heterotrophically, and mixotrophically, but to date, not much is known about the morphological and biochemical changes induced by the different growing conditions or the effect on the production of different biomolecules by the microalgae. It has been noted that heterotrophic growth of GS leads to cytological changes in the cell size, probably due to reduced chloroplast size and increased number of mitochondria, the organelles directly connected with nutrition [17]. GS exhibits a high metabolic flexibility that is matched by few other microorganisms, demonstrating the ability to thrive on more than 50 different carbon sources such as sugars, sugar alcohols, tricarboxylic-acid-cycle intermediates, and amino acids [18–21]. In addition, this genus has very high daily productivity of various bioactive compounds [15] and significant potential as a source of antioxidants and macronutrients, features that have driven interest towards conduct investigations on this Cyanidiophyceae for its potential biotechnological applications [22–25]. In the present study, a comparison was made on the growth and metabolism of GS cultured under both autotrophic and heterotrophic conditions, and the different biomolecules obtained under the different growing conditions were characterized and identified by using a combination of techniques: scanning electron microscope (SEM), gas chromatography/mass spectrometry (GC/MS), and infrared spectrophotometry (ATR-FTIR). The well-known, studied, and commercialized microalgae *Spirulina platensis* (Sp) was grown in autotrophic conditions and used in this study as a comparison species. The final aim of this investigation was to verify the possibility of directing or manipulating the metabolic flexibility of GS as a tool to induce the production of biomass and biomolecules that can be of interest to several important fields such as food, feed, nutraceutical, or energy production industries.

2. Results

2.1. Scanning Electron Microscopy

An increase in the cell dimension of GS grown in heterotrophic conditions with respect to the autotrophic conditions was detected by SEM analysis. The average cell size of heterotrophic (HGS) conditions was about 30% bigger than autotrophic (AGS) conditions (Figure 1). Moreover, AGS showed different element contents with respect to the heterotrophic conditions (Figure 2).

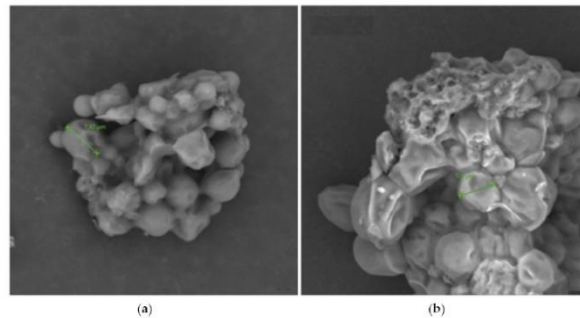


Figure 1. *Galdieria sulphuraria* strain ACUF 064 cultured in (a) heterotrophic (FOV: 62.5 μm , mode: 15kV-point, detector: BSD full) and (b) autotrophic conditions (FOV 39.5 μm , mode: 15kV-point, detector: BSD full).

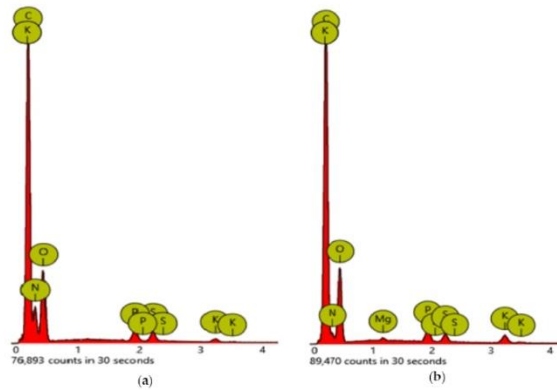


Figure 2. Different content of elements in *Galdieria sulphuraria* strain ACUF 064 cultured in heterotrophic (a) and autotrophic (b) conditions. Percentages are reported in Table 1.

Area values are reported in Table 1. A significant increase in carbon mass of 20% for the heterotrophic growth conditions was observed.

Table 1. Area values of different elements of *Galdieria sulphuraria* strain ACUF064 cultured in autotrophic (AGS) and heterotrophic (HGS) conditions.

Element Number	Element Symbol	Element Name	Atomic Conc. HGS	Weight Conc. HGS (%)	Atomic Conc. AGS	Weight Conc. AGS (%)
6	C	Carbon	63.81	57.16	51.79	46.03
8	O	Oxygen	23.74	28.33	21.20	25.11
7	N	Nitrogen	11.40	11.90	26.40	27.37
15	P	Phosphorus	0.38	0.89	0.24	0.55
19	K	Potassium	0.32	0.93	0.11	0.31
16	S	Sulfur	0.27	0.64	0.26	0.62
12	Mg	Magnesium	0.08	0.15	0.00	0.00

2.2. GC-MS Analysis

Fatty acid (FA) composition of *Galdieria sulphuraria* strain ACUF 064 cultivated in autotrophic (AGS) and heterotrophic (HGS) conditions and *Spirulina platensis* (Sp) for comparison are reported in Table 2.

Table 2. Comparison of the fatty acid composition of *G. sulphuraria* strain ACUF 064 cultivated in autotrophic (AGS) and heterotrophic (HGS) conditions, and to *Spirulina platensis* (Sp) grown in autotrophic conditions. Values are reported as mean values ($n = 3$) \pm SD, where SD is the standard deviation.

Molecular Formula	Peak	RT (min)	Compound	AGS	HGS	Sp
C8:0	1	7.53	Caprylic acid C8:0	0.060 \pm 0.01	-	0.04 \pm 0.03
C13:0	2	10.26	Tridecanoic acid	0.35 \pm 0.01	-	0.50 \pm 0.02
C14:0	3	11.28	Myristic acid C14:0	1.74 \pm 0.14 ^a	1.90 \pm 0.12 ^a	0.13 \pm 0.01 ^b
C14:1	4	12.41	Myristoleic acid C14:1	0.10 \pm 0.03	-	0.05 \pm 0.04
C15:0	5	12.54	Pentadecanoic acid C15:0	0.61 \pm 0.09 ^a	0.36 \pm 0.09 ^a	0.03 \pm 0.01 ^b
C16:0	6	14.28	Palmitic acid C16:0	27.19 \pm 0.12 ^b	21.15 \pm 0.31 ^c	22.51 \pm 0.27 ^a
C16:1	7	15.96	Palmitoleic acid C16:1	0.32 \pm 0.09 ^b	0.33 \pm 0.16 ^b	4.74 \pm 0.41 ^a
C17:0	8	16.50	Heptadecanoic acid C17:0	0.27 \pm 0.06 ^a	0.31 \pm 0.07 ^a	0.16 \pm 0.08 ^{ab}
C17:1	9	18.62	cis-10-Heptadecenoic acid	0.26 \pm 0.02 ^{ab}	0.21 \pm 0.08 ^b	0.32 \pm 0.04 ^a
C18:0	10	19.43	Stearic acid	1.04 \pm 0.11 ^b	2.96 \pm 0.06 ^a	0.72 \pm 0.11 ^c
C18:1 n9t	11	21.07	Elaidic acid	0.15 \pm 0.08 ^a	0.17 \pm 0.01 ^a	0.04 \pm 0.01 ^b
C18:1 n9c	12	21.82	Oleic acid	20.91 \pm 0.14 ^b	30.07 \pm 0.16 ^a	2.95 \pm 0.09 ^c
C18:3 n3	13	24.01	Linolenic acid	5.90 \pm 0.27 ^a	3.31 \pm 0.18 ^{ab}	0.10 \pm 0.03 ^c
C18:3 n6	14	25.58	γ -Linolenic acid	-	-	13.15 \pm 0.09
C18:2 n6c	15	26.13	Linoleic acid	18.91 \pm 0.13 ^a	14.31 \pm 0.62 ^{ab}	19.06 \pm 0.51 ^a
C20:0	16	28.25	Arachidic acid	0.05 \pm 0.01	0.10 \pm 0.07	0.04 \pm 0.01
C28H44O	17	28.47	Ergosterol	-	10.21 \pm 0.13 ^a	2.93 \pm 0.21 ^b
C20H40O	18	29.75	Phytol	15.34 \pm 0.14 ^b	6.05 \pm 0.09 ^c	16.07 \pm 0.76 ^b
C15H13N	19	30.01	4-methyl-2-phenylindole	-	7.01 \pm 0.03 ^a	2.86 \pm 0.04 ^b
C17H36	20	33.47	n-Heptadecene	5.72 \pm 0.35 ^b	-	12.92 \pm 0.47 ^a
C20:1	21	33.61	cis-11-Eicosenoic acid	0.26 \pm 0.11 ^b	0.53 \pm 0.02 ^a	0.01 \pm 0.01 ^c
C20:2	22	34.08	cis-11,14-Eicosadienoic acid	0.57 \pm 0.08 ^a	0.65 \pm 0.03 ^a	0.25 \pm 0.16 ^b
C20:3 n6	23	34.12	cis-8,11,14-Eicosatrienoic acid	-	-	0.28 \pm 0.07
C20:3 n3	24	35.03	cis-11,14,17-Eicosatrienoic acid	0.14 \pm 0.05	0.28 \pm 0.01	-
C24:1	25	35.97	Nervonic acid	0.11 \pm 0.02	0.09 \pm 0.01 ^{ab}	0.14 \pm 0.08 ^a
C19H34O2			Methyl linoleate	07.85 \pm 0.16 ^c	3.47 \pm 0.03 ^b	-
C17H34O2		N.P.A.	Methyl palmitate	11.41 \pm 0.73 ^a	6.21 \pm 0.03 ^b	4.01 \pm 0.62 ^b
C16H32O2			Hexadecanoic acid, methyl ester	9.47 \pm 0.49 ^a	-	6.23 \pm 0.31 ^b
			Σ -FAME	28.73 \pm 0.74 ^a	9.68 \pm 0.03 ^b	-
Σ -FATTY ACIDS			Σ -SFA	34.10 \pm 0.21 ^b	31.56 \pm 0.03 ^c	40.02 \pm 0.26 ^a
			Σ -MUFA	30.11 \pm 0.47 ^b	38.54 \pm 0.03 ^a	8.25 \pm 0.07 ^c
			Σ -PUFA	31.52 \pm 0.83 ^b	27.43 \pm 0.61 ^c	35.82 \pm 0.62 ^a

Organic compounds expressed as mean percentages of 100 mg of dry tissue weight. Values with different letters are significantly different ($p < 0.05$). N.P.A: naturally present in alga. See the Abbreviation section for the definitions of SFA, MUFA, and PUFA.

In the autotrophic conditions, higher levels of fatty acid methyl esters (FAMES) were present, especially methyl palmitate and methyl linoleate. Another compound present in higher quantities in AGS was phytol (PYT), an acyclic diterpenoid alcohol constituent of chlorophyll. The heterotrophic condition influenced the production of ergosterol, a phytosterol, stearic acid (SIA) and oleic acid, present in higher concentrations with respect to the autotrophic condition. Omega 3 long chain FAs, such as EPA, DHA, and arachidonic acid, were found neither in the autotrophic nor in the heterotrophic conditions.

2.3. ATR-FTIR

Mean FTIR spectra of GS strain ACUF 064 cultivated in autotrophic (AGS) and heterotrophic (HGS) conditions and Sp are shown in Figure 3. Each spectrum is the average of three raw spectra originating from five samples.

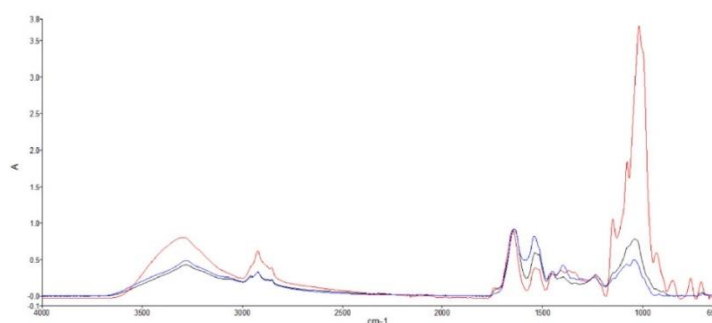


Figure 3. Infrared spectrophotometry (ATR-FTIR) spectra of *Galdieria sulphuraria* strain ACUF 064 cultured in autotrophic (—) and heterotrophic (---) conditions. (—) *Spirulina platensis*.

Each FTIR spectrum is formed by peaks arising from the infrared absorption of functional groups. The vibration intensity, reported as absorbance, is proportional to the relative abundance of organic molecules such as carbohydrates, lipids, and proteins. Table 3 reports FTIR peak assignments based on spectral values indicated in the current literature [26,27]. Although a certain degree of overlapping is present, macromolecules can be identified in relation to specific wavelength ranges [28]. Lipids can be identified in the range 3000–2800 and around 1740 cm^{-1} , proteins in the range 3600–3000 and around 1640 and 1540 cm^{-1} , and carbohydrates in the range 1174–950 cm^{-1} .

Table 3. Peak assignment of *Galdieria sulphuraria* strain ACUF 064 cultured in autotrophic (AGS) and heterotrophic (HGS) condition and *S. platensis*, based on the literature [26,27].

Spectral Ranges Analyzed with SIMCA	Peak Wavelength (cm ⁻¹)			Peak Assignment	Macromolecules
	AGS	HGS	Sp		
3600–3000		3298		$\nu(\text{N-H})$ stretching of amide A	Proteins
	3284		3282		
2999–2800			2959	$\nu_{\text{as}}(\text{CH}_2)$ and $\nu_{\text{s}}(\text{CH}_2)$ stretching	Lipids, triglycerides, fatty acids, carbohydrates
	2924	2924	2925		
	2854	2855			
1772–1712		1743		$\nu(\text{C=O})$ stretching of esters	Cellulose–fatty acids
1711–1576	1640	1646	1641	Amide I $\nu(\text{C=O})$ stretching	Proteins
1575–1478	1538	1537	1541	Amide II $\delta(\text{N-H})$ bending and $\nu(\text{C-N})$ stretching	Proteins
	1453	1453	1452	$\delta_{\text{as}}(\text{CH}_2)$ and $\delta_{\text{as}}(\text{CH}_3)$ bending of methyl	Proteins, lipids
1477–1175	1394	1411	1399	$\delta_{\text{s}}(\text{CH}_2)$ and $\delta_{\text{s}}(\text{CH}_3)$ bending of methyl; $\nu_{\text{s}}(\text{C-O})$ of COO^- groups; $\delta_{\text{s}}(\text{N(CH}_3)_3)$ bending of methyl	Proteins and lipids
		1368			
	1336				
			1388	Amide III	Proteins
	1236	1238	1240	$\nu_{\text{as}}(\text{P=O})$ stretching of phosphodiester	Nucleic acids and phospholipids
1174–950		1148		$\nu(\text{C-O-C})$	Carbohydrates (including glucose, fructose, glycogen, etc.), polysaccharides
		1077	1079		
		1039	1043		
		1018			
949–650	806	931	916	Fingerprint region	
	763	850	880		
	700	760	743		
		662			

The overlapping spectra reported in Figure 3 indicated how the intensity of the peaks corresponding to proteins, lipids, and carbohydrates was greater in HGS than in AGS and Sp, with the only exception of the peak around 1540 cm⁻¹, ascribable to N–H stretching of proteins, which was higher in Sp, followed by AGS. HGS was richer in polysaccharides and sugars compared to AGS and Sp, as indicated by the high absorbance in the range 1174–950 cm⁻¹. Polysaccharides in HGS were highlighted by the two peaks at 1148 and 1018 cm⁻¹, which were missing in AGS and Sp. Special attention should be devoted to the 950–650 cm⁻¹ region, also called the “fingerprint region”. In particular, HGS showed four different sharp absorption bands (931, 850, 760, 662 cm⁻¹) that represent a characteristic fingerprint of HGS, different from AGS and Sp that presented a very similar pattern in this region. A representative FTIR subtraction spectrum of HGS minus AGS highlights the differences in the concentration of macromolecules between autotrophic and heterotrophic conditions (Figure 4A). In order to quantify the different content of macromolecules such as lipids, carbohydrates, and proteins, the second derivative of the FTIR profiles was determined (Figure 4B).

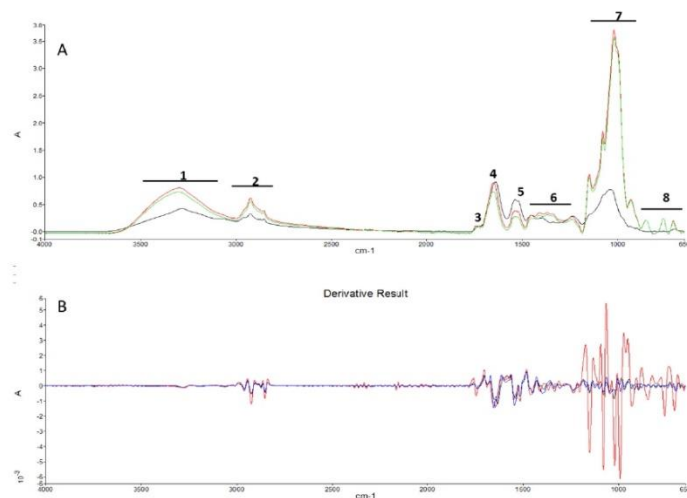


Figure 4. (A) Representative ATR-FTIR spectra of *Galdieria sulphuraria* strain ACUF 064 cultured in autotrophic (—) and heterotrophic (---) conditions and the subtraction spectrum (---). (B) Second derivatives of *Galdieria sulphuraria* strain ACUF 064 cultured in autotrophic (—) and heterotrophic (---) conditions. (---) *Spirulina platensis*.

To make a quantitative determination, the integration of the second derivative peaks was carried out according to Equation (2), reported in the Materials and Methods section. HGS compared to AGS showed a greater content of proteins, lipids, and carbohydrates of 91%, 57%, and 98%, respectively. The areas are reported in Table 4.

Table 4. Representative peak area relative to the second derivative subtraction spectrum between *Galdieria sulphuraria* grown in heterotrophic conditions and autotrophic conditions. In the first column, the FI-IR ranges are reported, as shown in Figure 4a. The subtraction area ($\Delta_{HGS-AGS}$) for each interval is expressed as the percentage of \log_{10} /total area.

Spectral Ranges (cm ⁻¹)			
FTIR	Start	End	$\Delta_{HGS-AGS}$
1	3600	3000	2.23 (18.63%)
2	2999	2800	1.16 (9.69%)
3	1772	1712	0.20 (1.67%)
4	1711	1576	1.62 (13.53%)
5	1575	1478	1.09 (9.11%)
6	1477	1175	1.78 (14.87%)
7	1174	950	2.60 (21.72%)
8	949	650	1.29 (10.78%)

FTIR spectra of HGS, AGS, and Sp were quite complex and required a multivariate statistical analysis for the data comparison. In this study, we used a chemometric approach based on the principal component analysis to analyze the whole spectral range and sub-ranges corresponding to specific

macromolecules as reported in Table 5. Data interpretation by means of SIMCA (soft independent modeling class algorithm) algorithm (Figure 5) confirmed the differences in macromolecules between the autotrophic and heterotrophic culture conditions.

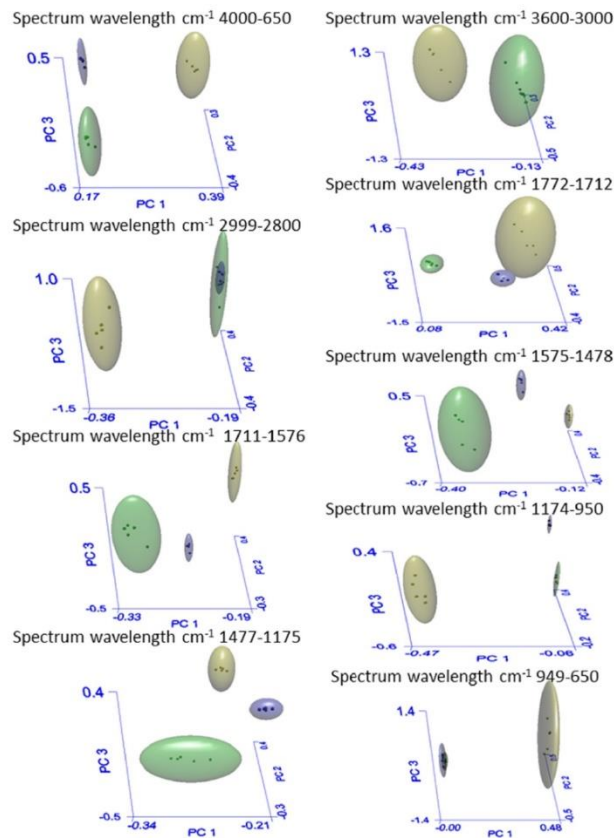


Figure 5. Three-dimensional principal component analysis score plot of *Caldieria sulphuraria* strain ACUF 064 cultivated in autotrophic (□) and heterotrophic conditions (■), plus *Spirulina platensis* in autotrophic conditions (▒). Data analysis was performed in the spectrum ranges reported in the rectangles above each plot.

The significant differences between the autotrophic and the heterotrophic conditions are demonstrated by the interclass distance (ID) reported in Table 5. The ID highlights the similarities between AGS and Sp (Sp-AGS), as well as the differences between them and HGS (AGS-HGS, HGS-Sp).

The higher the ID value, the greater the difference. It is reported that a distance value higher than 3 is indicative of well separated samples, and therefore belonging to different classes [29].

Table 5. Interclass distance, and recognition and rejection rates of *Galdieria sulphuraria* strain ACUF 064 cultivated in autotrophic conditions (AGS), heterotrophic conditions (HGS), and *Spirulina platensis* (Sp).

Spectrum Wavelength cm ⁻¹ 4000–650			
Groups	Recognition (%) ^a	Rejection (%) ^b	Interclass Distance ^c
AGS	100(5/5)	100(10/10)	AGS–HGS 26.2
HGS	100(5/5)	100(10/10)	HGS–Sp 36.3
Sp	100(5/5)	100(10/10)	Sp–AGS 12.2
Spectrum Wavelength cm ⁻¹ 3600–3000			
Groups	Recognition (%) ^a	Rejection (%) ^b	Interclass Distance ^c
AGS	100(5/5)	100(10/10)	AGS–HGS 21.9
HGS	100(5/5)	100(10/10)	HGS–Sp 21.2
Sp	100(5/5)	100(10/10)	Sp–AGS 6.56
Spectrum Wavelength cm ⁻¹ 2999–2800			
Groups	Recognition (%) ^a	Rejection (%) ^b	Interclass Distance ^c
AGS	100(5/5)	100(10/10)	AGS–HGS 24.8
HGS	100(5/5)	100(10/10)	HGS–Sp 23.9
Sp	100(5/5)	100(10/10)	Sp–AGS 4.94
Spectrum Wavelength cm ⁻¹ 1772–1712			
Groups	Recognition (%) ^a	Rejection (%) ^b	Interclass Distance ^c
AGS	100(5/5)	100(10/10)	AGS–HGS 15.3
HGS	100(5/5)	100(10/10)	HGS–Sp 14.2
Sp	100(5/5)	100(10/10)	Sp–AGS 6.5
Spectrum Wavelength cm ⁻¹ 1711–1576			
Groups	Recognition (%) ^a	Rejection (%) ^b	Interclass Distance ^c
AGS	100(5/5)	100(10/10)	AGS–HGS 15.4
HGS	100(5/5)	100(10/10)	HGS–Sp 36.5
Sp	100(5/5)	100(10/10)	Sp–AGS 20.8
Spectrum Wavelength cm ⁻¹ 1575–1478			
Groups	Recognition (%) ^a	Rejection (%) ^b	Interclass Distance ^c
AGS	100(5/5)	100(10/10)	AGS–HGS 15.5
HGS	100(5/5)	100(10/10)	HGS–Sp 24.2
Sp	100(5/5)	100(10/10)	Sp–AGS 21.7
Spectrum Wavelength cm ⁻¹ 1477–1175			
Groups	Recognition (%) ^a	Rejection (%) ^b	Interclass Distance ^c
AGS	100(5/5)	100(10/10)	AGS–HGS 22.5
HGS	100(5/5)	100(10/10)	HGS–Sp 14.7
Sp	100(5/5)	100(10/10)	Sp–AGS 17.7
Spectrum Wavelength cm ⁻¹ 1174–950			
Groups	Recognition (%) ^a	Rejection (%) ^b	Interclass Distance ^c
AGS	100(5/5)	100(10/10)	AGS–HGS 78.3
HGS	100(5/5)	100(10/10)	HGS–Sp 88.2
Sp	100(5/5)	100(10/10)	Sp–AGS 13.9
Spectrum Wavelength cm ⁻¹ 949–650			
Groups	Recognition (%) ^a	Rejection (%) ^b	Interclass Distance ^c
AGS	100(5/5)	100(10/10)	AGS–HGS 26.7
HGS	100(5/5)	100(10/10)	HGS–Sp 27.9
Sp	100(5/5)	100(10/10)	Sp–AGS 6.22

Notes: ^a Percentage of recognition in optimal model should be closer to 100% ; ^b percentage of rejection in optimal model should be closer to 100% ; ^c interclass distances (ID) should be as high as possible (minimum 3).

Figure 5 shows the 3D-PCA score plot generated by the SIMCA model. This multivariate analysis permits the visualization of the class separation among HGS, AGS, and Sp. The boundary ellipse (hyperboxes) defining each cluster represents a 95% confidence interval, and the points within each cluster represent the spectrum wavelengths of each sample in the three-dimensional space. Data analysis performed in smaller ranges of the spectrum (Table 5) revealed that there were significant differences among groups. The interclass distance clearly underlines the changes in GS as a consequence of the modification of the metabolism due to the growth conditions. In fact, although Sp and AGS are different microalgae species, both grown as autotrophs, they appeared to be extremely similar with an interclass distance ranging from a minimum of 4.94 (spectrum range 2999–2800 cm^{-1}) to a maximum of 21.7 (spectrum range 1575–1478 cm^{-1}), whereas HGS and AGS were found to be extremely different with a minimum inter-distance of 15.4 and a maximum of 78.3 (respectively for the intervals of 1711–1576 and 1174–950 cm^{-1}) due to the diverse metabolism imposed by the heterotrophic and autotrophic conditions.

3. Discussion

3.1. Scanning Electron Microscopy

According to the SEM analysis, the average size of GS cells grown in heterotrophic condition was about 30% greater than those cells produced in the autotrophic condition. This outcome is in agreement with Stadnichuk et al. [17] who reported an increase in the cell dimension of *Galdieria partita* grown in heterotrophic conditions with respect to the autotrophic conditions. Furthermore, the authors hypothesized that the outcome could be a result of D-glucose inhibition on the photosynthetic pigment apparatus. Interestingly, our findings noted a decrease in phytol (PYT) content, a constituent of chlorophyll, in HGS that could support this theory. Moreover, AGS exhibited different element contents with respect to the heterotrophic conditions, and there was a significant increase in carbon mass of 20% in the heterotrophic growth conditions.

3.2. GC-MS Analysis

AGS showed a different FA composition with respect to the HGS, whereby in the autotrophic conditions, higher levels of fatty acid methyl esters (FAMES) were present, especially for methyl palmitate, methyl linoleate, and hexadecanoic acid methyl ester with respect to the heterotrophic conditions. This outcome is quite interesting because it indicates the avoidance of the expensive phase of esterification that is necessary for the production of FAMES for their final application as biodiesel [30–32].

Another interesting compound present in higher quantities in AGS is phytol (PYT), an acyclic diterpenoid alcohol. Its presence is most likely related to the chlorophyll in the autotrophic form. PYT and its derivatives have a vast array of actions ranging from antimicrobial, anticancer, anti-inflammatory, and immune stimulant activities, to being a hair growth facilitator [33]. Furthermore, PYT is used as a precursor for the production of synthetic forms of vitamin E [34] and vitamin K [35], and therefore of great interest in pharmaceutical applications.

The condition of heterotrophy induced GS to produce higher levels of ergosterol, as observed in fungi [36] or phytosterol in plants, with many beneficial health effects for humans, including immunomodulatory, anti-inflammatory, neuromodulatory, antihypercholesterolemic, antioxidant, anticancer, and antidiabetic properties [37]. Ergosterol is also a biological precursor of vitamin D2 (ergocalciferol) [38], and exposure to ultraviolet light causes a photochemical reaction that activates the conversion of ergosterol to ergocalciferol. In addition, ergosterol is of great importance because it undergoes photolysis when exposed to UV light (280–320 nm) to yield provitamin D2 as one of the main products, which under thermal rearrangement, is spontaneously transformed into vitamin D2 [39]. Ergosterol and derivatives have shown a wide range of health-promoting properties, such as antioxidant, anti-inflammatory, and antihyperlipidemic activities [40]. Treatments with ergosterol

were able to significantly inhibit the proliferation of human epithelial type 2 (HEp-2) cells, a cell line originating from human laryngeal carcinoma, and the ergosterol derivatives were known to be a source of new potential antitumor or anti-angiogenesis chemotherapy agents [41]. Moreover, ergosterol derivatives have the ability to suppress lipopolysaccharide (LPS)-induced inflammatory responses of macrophages in vitro through the inhibition of highly proinflammatory cytokine (TNF- α) and cyclooxygenase-2 (COX-2) expression, as well as having a cytostatic effect on human colorectal adenocarcinoma cells [42]. Therefore, this molecule has promising multiple beneficial applications in the pharmacological field.

The heterotrophic condition was also found to influence the production of oleic acid, which was present in higher concentrations in comparison to the autotrophic condition. This is likely related to the increased cell dimensions of GS when cultured under heterotrophic conditions, and to the absence of chlorophyll a and phycocyanobilin biosynthesis, as previously observed by Stadniuchuk et al. [17]. Oleic acid is a MUFA that finds interesting applications in the field of nutrition because it has the ability to reduce low density lipoprotein cholesterol (LDL-cholesterol), and at the same time, to promote high density lipoprotein cholesterol (HDL-cholesterol) [43,44]. Although the production of the omega 3 long chain FAs, such as EPA, DHA, and arachidonic acid, fundamental constituents of the human and animal diet [45], have not been found either under autotrophic or heterotrophic conditions, it is interesting to note that the autotrophic condition is accompanied by a general increase in PUFA, and in particular in linoleic and linolenic acid, which respectively belong to the omega 6 and omega 3 series. This outcome may have important consequences in the field of animal nutrition, in particular for freshwater fish nutrition, as they are able to synthesize EPA, DHA, and arachidonic acid from linoleic and linolenic acids.

The GC-MS data also indicated the presence of a high percentage of stearic acid (STA) in HGS, whereas in Sp this SFA was found to be present in negligible quantities. Recent studies have shown that stearic acid has favorable effects on human health. In fact, diets in which STA has been added in high percentages were able to drastically reduce LDL-cholesterol. STA applications may thus be of great interest in the pharmacological and nutraceutical fields [46].

3.3. Infrared Spectrophotometry

FTIR spectra of biological samples reported the macromolecular composition on the basis of the infrared absorption of functional groups [47]. The vibration intensity, reported as absorbance, is proportional to the relative abundance of organic molecules such as carbohydrates, lipids, and proteins [48]. The FTIR spectra analysis of GS provides interesting information about the changes in the macromolecule composition induced by different growth conditions, confirming the usefulness of FTIR as a fast, non-disruptive method to identify macromolecules in microalgae [49,50]. The intensity of the peaks corresponding to proteins, lipids, and carbohydrates was greater in HGS than in AGS and Sp, with the only exception with the peak observed around 1540 cm^{-1} , which was higher in Sp and AGS, and was ascribable to N-H stretching of proteins. It is worth noting that Sp had a characteristic high content of proteins, as was also reported by Rafiquel et al. [51]. HGS was richer in polysaccharides and sugars when compared to AGS and Sp, as indicated by the high absorbance in the range 1174-950 cm^{-1} . Polysaccharides in HGS are highlighted by the two peaks at 1148 and 1018 cm^{-1} , which were similar to peaks that were present in *Chlorella vulgaris* by [52], but not present in AGS and Sp.

The different contents of macromolecules such as lipids, carbohydrates, and proteins, in AGS, HGS, and Sp, was confirmed by the evaluation of the second derivative of the FTIR profiles that revealed that HGS, in comparison to AGS, had a greater content of proteins, lipids, and carbohydrates at 91%, 57%, and 98%, respectively.

The significant differences between the autotrophic and the heterotrophic conditions were also demonstrated by the interclass distance (ID), whereby the ID highlights the similarities between AGS and Sp, plus their apparent differences to HGS with the higher ID values indicating a greater difference. It has been reported that a distance value higher than 3 is indicative of well-separated samples, which

confirms their difference [53]. The interclass distance is able to underline the changes in GS as a consequence of the modification of the metabolism. Thus, metabolic changes, from autotrophic to heterotrophic, have relevant effects on both morphological and chemical characteristics of GS.

4. Materials and Methods

4.1. Strain and Growth Medium

Galdieria sulphuraria (Galdieri) Merola n. 064 was obtained from the algal collection of the Department of Biology of the University of Naples Federico II (ACUF). A preliminary screening study of 43 strains showed that the strain 064 has the lowest doubling time in autotrophic and heterotrophic conditions. Modified Allen medium [54,55] (Table 6) was used for autotrophy growth, whereas the same medium supplemented with glycerol was used for heterotrophy growth. Modified Allen medium contained NaNO_3 as a nitrogen source. The standard concentration of the nitrate was 72 g L^{-1} . H_2SO_4 was adopted for fine setting of the initial pH at 1.5. The medium was autoclaved for 20 min before use.

Table 6. Composition of modified Allen medium (pH 1.5).

Components	g/L	Oligoelements	g/L
NaNO_3	1.7	$\text{MnCl}_2 \cdot 4\text{H}_2\text{O}$	0.02
$\text{MgSO}_4 \cdot 7\text{H}_2\text{O}$	0.3	$\text{CuSO}_4 \cdot 5\text{H}_2\text{O}$	0.0001
K_2HPO_4	0.6	$\text{CoCl}_2 \cdot \text{H}_2\text{O}$	0.00005
KH_2PO_4	0.3	$\text{Na}_2\text{MoO}_4 \cdot 2\text{H}_2\text{O}$	0.00005
$\text{CaCl}_2 \cdot 2\text{H}_2\text{O}$	0.02	ZnCl_2	0.00014
NaCl	0.05	H_2SO_4	0.30
$\text{FeSO}_4 \cdot 7\text{H}_2\text{O}$	0.1		

4.2. Growth Conditions

For microalgae culture (*Galdieria sulphuraria* in autotrophic conditions (AGS), *Galdieria sulphuraria* in heterotrophic conditions (HGS), and *Spirulina platensis* (Sp), pre-cultures of 50 mL inoculated from a single isolate picked from a solid plate were grown in 200 mL Erlenmeyer flasks housed in a climatic chamber (Gibertini, Italy) at $37 \pm 1 \text{ }^\circ\text{C}$. The chamber was equipped with daylight fluorescent lamps (Philips TLD 30 W/55) set at $150 \mu\text{E/m}^2 \text{ s}$ for 24/24. After 2 weeks, the pre-cultures were used to inoculate the photobioreactors. The growth was carried out in a cylindrical bubble column photobioreactor made of glass (0.04 m ID, 0.8 m high) with a 0.9 L working volume [56]. Air was sparged at the photobioreactor bottom by means of a porous ceramic diffuser at a volumetric flow rate ranging between 20 and 200 nl h^{-1} . Filters of $0.2 \mu\text{m}$ were used to sterilize air flow inlet and outlet. The photobioreactors were housed in a climate chamber (Solar Neon) at $37 \pm 1 \text{ }^\circ\text{C}$. The chamber was also equipped with fluorescent lamps (Philips TLD 30 W/55) for autotrophic conditions. Heterotrophic cultures were conducted in the dark. In order to sustain the autotrophic growth in optimal conditions in the photobioreactor for long periods, the concentration of salts in the modified Allen culture medium was doubled with respect to that reported in Table 6. The algal biomass was harvested at the end of the exponential phase. In order to remove the biomass from the culture medium, microalgae were centrifuged at 5000 rpm for 10 min in a centrifuge JA 14. The obtained biomass was stored at $-20 \text{ }^\circ\text{C}$, and the amounts of AGS and HGS obtained were 5.20 and 4.80 g L^{-1} of wet biomass and 1.50 and 1.43 g L^{-1} of dry biomass, respectively.

4.3. Scanning Electron Microscopy

Dried samples of AGS and HGS were analyzed by scanning electron microscopy (SEM) using the ThermoFisher microscope model Phenom Pro Desktop SEM, having an electron optical magnification range: 80–150,000x; a resolution $< 10 \text{ nm}$ (BSED) and $< 8 \text{ nm}$ (SED); digital zoom: max 12x; acceleration voltages: default 5 kV, 10 kV, and 15 kV; vacuum modes: charge reduction mode (low vacuum mode)—high vacuum mode; and detector: BSD.

4.4. Lipid Extraction

The microalgal biomass was lyophilized at -86°C , using a freeze-dryer (Lyovapor L200 Buchi) according to Lee et al. [57]. Total lipids were extracted from 1.0 g of dried biomass using a mixture of chloroform/methanol (2:1 v/v) according to Bligh et al. [58]. The FAMES naturally present in the microalgae (methyl linoleate, methyl palmitate, hexadecanoic acid, methyl ester) were obtained. The fatty acid methyl esters naturally present in the microalgae were extracted using Soxhlet extraction, without any previous transmethylation, and were analyzed by GC-MS. The Soxhlet extraction was implemented with 2 g of sample powder on a Soxhlet system HT (Foss Soxtec 1043) for 6 h of extraction process at 140°C , using hexane as solvent, followed by 30 min solvent rinse and 30 min solvent evaporation until the exhaustion of the oil contained in the microalgae. Only after Soxhlet extraction were the total lipids transmethylated to yield their corresponding fatty acid esters (FAMES) using 2 mL of 1% NaOH in MeOH, followed by heating at 55°C for 15 min at 55°C . Next, 4.0 mL of 5% methanolic HCl were added and again heated for 15 min at 55°C [59]. Finally, total FAMES were eluted by adding 2.0 mL of *n*-hexane to the reaction mixture described above. The total FAMES obtained were readily analyzed by GC-MS in order to determine the total saturated, monounsaturated and polyunsaturated fatty acids.

4.5. GC-MS Analysis

The *n*-hexane extracts were analyzed by GC-MS on an Agilent Technologies unit mod 6850—Series II, equipped with an auto sampler G45134 and an Agilent capillary column (DB-5 type, 0.18 mm ID, film 0.18 μm , length 20 m), using the Agilent Mass Selective Detector mod 5973. Helium was used as a carrier gas at a flow rate of 13.8 mL/min. The split ratio applied was 10:1. The injector temperature was 270°C . The gradient applied was as follows: an isotherm of 2 min at 60°C , a first ramp from 60 to 250°C for 20 min ($9.5^{\circ}\text{C}/\text{min}$), followed by a second ramp from 250 to 300°C for 10 min ($10^{\circ}\text{C}/\text{min}$). The temperature was then maintained at 300°C for 5 min. All the analyses were carried out in triplicate, a confidential interval of 95% and a coverage factor $K = 2$ were applied. The limit of detection by GC-MS was 1 μmole per injection. In each case, the peak area was plotted against the standards concentration to obtain a linear relationship. As standard, a 37 component fatty acid methyl ester (FAME) mixture purchased from Supelco (37 Component FAME Mix Supelco Inc., Bellefonte, PA, USA) was used. Ergosterol (95% pure, GC assay), phytol (97% pure, GC assay), *n*-heptadecene (98% pure, GC assay), and nevrionic acid (99% pure, GC assay) were purchased from Sigma (Sigma Aldrich, St. Louis, MO, USA). All the compounds utilized were analytical grade. Serial standard dilutions with hexane were made in triplicate to obtain concentrations of 15,000, 10,000, 5,000, 2,000, 1,000, 500, 200, 100, 50, and 25 $\mu\text{g}/\text{mL}$. A 1% lauric acid methyl ester (LAME, C12:0, Sigma-Aldrich) in hexane was prepared, and LAME equivalent to 5% of the total compounds was added to each dilution as an internal standard. The standard, the sample, and the internal standard solution as the compounds determination were carried out according to Lall et al. [60]. The identification of all the compounds was carried out by the interpretations of the mass spectra, in particular the analysis of fragment ions obtained, using the Nist Mass Spectral Library Program—version 2.0 software. The peak area of standards was plotted against the standard concentration to obtain a linear relationship. In particular, the coefficient of determination r^2 values obtained from the calibration curves were in the range between 0.98 and 0.99. Values of r^2 smaller than 0.98 were not accepted. Standard curves were in the same conditions of the sample analysis previously described. In each case, the peak area was plotted against the concentration to obtain a linear relationship. Specifically, the limit of detection (LOD), limit of quantification (LOQ), and r^2 values for each peak are reported in Table 7.

Table 7. Limit of detection (LOD), limit of quantification (LOQ), and coefficient of determination (r^2).

Peak	Area			Height		
	LOD (ng/mL)	LOQ (ng/mL)	r^2	LOD (ng/mL)	LOQ (ng/mL)	r^2
1	0.21	0.63	0.9994	0.36	1.11	0.9987
2	0.19	0.57	0.9978	0.26	0.86	0.9986
3	0.30	0.90	0.9819	0.18	0.62	0.9956
4	0.14	0.42	0.9973	0.24	0.79	0.9996
5	0.15	0.46	0.9983	0.23	0.78	0.9983
6	0.19	0.58	0.9967	0.65	2.08	0.9972
7	0.20	0.61	0.9978	0.47	1.50	0.9998
8	0.33	0.97	0.9977	0.40	1.33	0.9996
9	0.22	0.68	0.9972	0.46	1.35	0.9988
10	0.19	0.59	0.9951	0.31	1.01	0.9986
11	0.14	0.43	0.9894	0.43	1.27	0.9991
12	0.16	0.47	0.9978	0.24	0.83	0.9980
13	0.21	0.63	0.9965	0.27	0.85	0.9899
14	0.23	0.69	0.9994	0.37	1.16	0.9996
15	0.18	0.56	0.9989	0.72	2.36	0.9881
16	0.16	0.48	0.9976	0.23	0.75	0.9893
17	0.22	0.70	0.9995	0.41	1.38	0.9957
18	0.21	0.63	0.9945	0.43	1.43	0.9995
19	0.24	0.73	0.9971	0.37	1.25	0.9992
20	0.27	0.81	0.9996	0.27	0.83	0.9948
21	0.21	0.64	0.9961	0.38	1.24	0.9996
22	0.25	0.76	0.9897	0.34	1.11	0.9982
23	0.18	0.54	0.9979	0.41	1.35	0.9993
24	0.17	0.50	0.9987	0.43	1.39	0.9975
25	0.19	0.59	0.9919	0.56	1.85	0.9967

4.6. ATR-FTIR Analysis

Samples of AGS, HGS, and Sp were lyophilized and analyzed without any previous treatment and placed directly on the germanium piece of the infrared spectrometer with constant pressure applied (70 ± 2 psi). The FTIR spectra were recorded in the mid-IR region ($4000\text{--}650\text{ cm}^{-1}$) at resolutions of 4 cm^{-1} with 32 scans using the Perkin Elmer FTIR Frontier coupled with DTGS (deuterated tri-glycine sulfate) detector (Perkin-Elmer Inc., Norwalk, CT, USA). Air background spectra was recorded and subtracted before analysis. To test repeatability, analyses were performed in triplicate and average spectra were used. Five samples for each group were analyzed. Spectra were baseline corrected and normalized, then elaborated using Spectrum Assure ID software, purchased with the instrument.

4.7. Statistical Analysis

The parametric test of one-way analysis of variance (ANOVA) after confirmation of normality and homogeneity of variance was used. Significant differences between experimental groups were evaluated by Duncan's multiple range test. Significant differences were determined at the 0.05 level. Data were expressed as mean \pm standard error of mean. The analyses were carried out with the Statistica version 7.0 statistical package (Statsoft Inc., Tulsa, OK, USA).

FTIR spectra were analyzed by the Spectrum AssureID software (trademark of PerkinElmer, Inc. part number 0993 4516 Release E; publication date July 2006; Software Version 4.x). Assure ID employs the SIMCA algorithm (soft independent modeling class algorithm). Three classes were defined: AGS, HGS, and Sp. For cluster analysis, the spectral ranges (I) 3600–3000, (II) 2999–2800, (III) 1772–1712, (IV) 1711–1576, (V) 1575–1478, (VI) 1475–1175, (VII) 1174–950, and (VIII) 949–650 cm^{-1} were independently analyzed. Interclass distance between groups, recognition, and rejection rates of the samples were determined to evaluate the performance of the SIMCA model.

Second derivative was employed to obtain more specific identification of little and very close absorption peaks, which were not well-resolved in the original spectrum. According to the Beer–Lambert law, absorbance is expressed as follows:

$$A(\bar{\nu}) = \alpha(\bar{\nu})lc \quad (1)$$

where A is the wavenumber $\bar{\nu}$ -dependent absorbance, α is the wavenumber-dependent absorption coefficient, l is the optical pathlength (mainly determined by the section thickness), and c is the concentration. When Equation (1) is differentiated twice, the result is

$$\frac{d^2A(\bar{\nu})}{d\bar{\nu}^2} = \frac{d^2\alpha(\bar{\nu})}{d\bar{\nu}^2} lc \quad (2)$$

From Equation (2) it can be seen that quantitative information [61–63] can be obtained also from the second derivative spectra, as l and c are constant terms and are not affected by the differentiation.

5. Conclusions

The present study reports how it is possible to obtain different biomolecules from *G. sulphuraria* microalga by changing the culture conditions that influence the metabolic processes. This outcome expands our knowledge about the microalgae metabolism, and presents innovative strategies for developing biotechnological applications. In particular *G. sulphuraria*, due to its interchangeable and versatile metabolism, appears to be a very good candidate for the co-cultivation with fungi or other beneficial microbes for the production of bioactive molecules useful for purifying wastewater, generating biomass that represents a renewable and sustainable feedstock for biofuel, nutraceutical, pharmacological, food, or feed production [64]. Although there are still more investigations required regarding microalgae metabolic changes, our data can have significant repercussions for potential biotechnological applications in the food, animal feed, nutraceutical, pharmacological, and energy fields.

Author Contributions: M.P., S.L.W., and R.B. performed the infrared spectrophotometry experiments and edited the original draft of the manuscript; E.G., F.C., and M.G. participated in the analytical measures and in the elaboration of the data; M.G.V. performed the chemical determination by gas chromatography; L.D.N., L.M., and M.L. participated in the editing and review of the manuscript; L.D. and A.P. performed the microalgae growth in different metabolic conditions; F.V. and R.M. performed scanning electron microscopy, reviewed and edited the original draft, conceptualized the work, assisted with the data analysis, and discussed the results. All authors have read and agreed with the published version of the manuscript.

Funding: This research received no external funding.

Conflicts of Interest: The authors declare no conflict of interest.

Abbreviations: Scanning electron microscope (SEM), gas chromatography/mass spectrometry (GC/MS), infrared spectrophotometry (ATR-FTIR), fatty acids (FAs), monounsaturated fatty acids (MUFAs), fatty acid methyl esters (FAMEs), polyunsaturated fatty acids (PUFAs), *Galdieria sulphuraria* (GS), heterotrophic *Galdieria sulphuraria* (HGS), autotrophic *Galdieria sulphuraria* (AGS), *Spirulina platensis* (Sp), lipopolysaccharide (LPS), tumor necrosis factor (TNF), cyclooxygenase-2 (COX-2), eicosapentaenoic acid (EPA), docosahexaenoic acid (DHA), low density lipoprotein cholesterol (LDL), high density lipoprotein cholesterol (HDL), phytol (PYT), stearic acid (STA), lauric acid methyl ester (LAME), limit of detection (LOD), limit of quantification (LOQ), coefficient of determination (r^2).

References

1. Afonin, S.A.; Barinova, S.S.; Krassilov, V.A. A bloom of *Tympanocysta Balme* (green algae of zygematalean affinities) at the Permian–Triassic boundary. *Geodiversitas* **2001**, *23*, 481–487.
2. Sharma, N.K.; Rai, A.K. Biodiversity and biogeography of microalgae: Progress and pitfalls. *Environ. Rev.* **2011**, *19*, 1–15. [[CrossRef](#)]
3. Khan, M.I.; Shin, J.H.; Kim, J.D. The promising future of microalgae: Current status, challenges, and optimization of a sustainable and renewable industry for biofuels, feed, and other products. *Microb. Cell Fact.* **2018**, *17*, 36. [[CrossRef](#)] [[PubMed](#)]

4. de Freitas Coêlho, D.; Tundisi, L.L.; Cerqueira, K.S.; da Silva Rodrigues, J.R.; Mazzola, P.G.; Tambourgi, E.B.; de Souza, R.R. Microalgae: Cultivation Aspects and Bioactive Compounds. *Braz. Arch. Biol. Technol.* **2019**, *62*. [[CrossRef](#)]
5. Barkia, I.; Saari, N.; Schonna, R. Manning Microalgae for High-Value Products Towards Human Health and Nutrition. *Mar. Drugs* **2019**, *17*, E304. [[CrossRef](#)]
6. Ku, C.S.; Pham, T.X.; Park, Y.; Kim, B.; Shin, M.S.; Kang, I.; Lee, J. Edible blue-green algae reduce the production of pro-inflammatory cytokines by inhibiting NF- κ B pathway in macrophages and splenocytes. *BBA* **2013**, *1830*, 2981–2988. [[CrossRef](#)]
7. Pham, T.X.; Lee, Y.; Bae, M.; Hu, S.; Kang, H.; Kim, M.B.; Park, Y.K.; Lee, J.Y. Spirulina supplementation in a mouse model of diet-induced liver fibrosis reduced the pro-inflammatory response of splenocytes, reduced the pro-inflammatory response of splenocytes. *Br. J. Nutr.* **2019**, *121*, 748–755. [[CrossRef](#)] [[PubMed](#)]
8. Samuels, R.; Mani, U.V.; Iyer, U.M.; Nayak, U.S. Hypocholesterolemic effect of spirulina in patients with hyperlipidemic nephrotic syndrome. *J. Med. Food* **2002**, *5*, 91–96. [[CrossRef](#)]
9. Yang, C.; Hua, Q.; Shimizu, K. Energetics and carbon metabolism during growth of microalgal cells under photoautotrophic, mixotrophic and cyclic light-autotrophic/dark-heterotrophic conditions. *Biochem. Eng.* **2000**, *6*, 87–102. [[CrossRef](#)]
10. Kim, S.; Park, J.; Cho, Y.B.; Hwang, S.Y. Growth rate, organic carbon and nutrient removal rates of *Chlorella sorokiniana* in autotrophic, heterotrophic and mixotrophic conditions. *Bioresour. Technol.* **2013**, *144*, 8–13. [[CrossRef](#)]
11. Perez Garcia, O.; De Bashan, L.E.; Hernandez, J.P.; Bashan, Y. Efficiency of growth and nutrient uptake from wastewater by heterotrophic, autotrophic and mixotrophic cultivation of *Chlorella vulgaris* immobilized with Azospirillum brasilense. *J. Phycol.* **2010**, *46*, 800–812. [[CrossRef](#)]
12. Liang, Y.; Sarkany, N.; Cui, Y. Biomass and lipid productivities of *Chlorella vulgaris* under autotrophic, heterotrophic and mixotrophic growth conditions. *Biotechnol. Lett.* **2009**, *31*, 1043–1049. [[CrossRef](#)] [[PubMed](#)]
13. Yoon, H.S.; Ciniglia, C.; Wu, M.; Comeron, J.M.; Pinto, G.; Bhattacharya, D. Establishment of endolithic populations of extremophilic Cyanidiales (Rhodophyta). *BMC Evol. Biol.* **2006**, *6*, 78. [[CrossRef](#)] [[PubMed](#)]
14. Reeb, V.; Bhattacharya, D. The Thermo-Acidophilic Cyanidiophyceae (Cyanidiales). In *Red Algae in the Genomic Age, Cellular Origin, Life in Extreme Habitats and Astrobiology*; Seckbach, J., Chapman, D.J., Eds.; Springer: Dordrecht, The Netherlands, 2010; Volume 13, pp. 409–426.
15. da Silva, T.L.; Reis, A. Scale-up Problems for the Large Scale Production of Algae. In *Algal Biorefinery: An Integrated Approach*; Das, D., Ed.; Capital Publishing Company: Kolkata, West Bengal, India, 2015; pp. 125–149.
16. Graziani, G.; Schiavo, S.; Nicolai, M.A.; Buono, S.; Fogliano, V.; Pinto, G.; Pollio, A. Microalgae as human food: Chemical and nutritional characteristics of the thermo-acidophilic microalga *Galdieria sulphuraria*. *Food Funct.* **2013**, *4*, 144–152. [[CrossRef](#)]
17. Stadnichuk, I.N.; Rakhimberdieva, M.G.; Bolychevtseva, Y.V.; Yurina, N.P.; Karapetyan, N.V.; Selyakh, I.O. Inhibition by glucose of chlorophyll a and phycocyanobilin biosynthesis in the unicellular red alga *Galdieria partita* at the stage of coproporphyrinogen III formation. *Plant Sci.* **1998**, *1*, 11–23. [[CrossRef](#)]
18. Rigano, C.; Fuggi, A.; Di Martino Rigano, V.; Aliotta, G. Studies on utilization of 2-ketoglutarate, glutamate and other amino acids by the unicellular alga *Cyanidium caldarium*. *Arch. Microbiol.* **1976**, *107*, 133–138. [[CrossRef](#)]
19. Rigano, C.; Aliotta, G.; Rigano, V.D.; Fuggi, A.; Vona, V. Heterotrophic growth patterns in the unicellular alga *Cyanidium caldarium*. A possible role for threonine dehydrase. *Arch. Microbiol.* **1977**, *113*, 191–196. [[CrossRef](#)]
20. Gross, W.; Schnarrenberger, C. Purification and characterization of a galactose-1-phosphate: UDP-glucose uridylyltransferase from the red alga *Galdieria sulphuraria*. *Eur. J. Biochem.* **1995**, *234*, 258–263. [[CrossRef](#)]
21. Gross, W.; Lenze, D.; Nowitzki, U.; Weiske, J.; Schnarrenberger, C. Characterization, cloning, and evolutionary history of the chloroplast and cytosolic class I aldolases of the red alga *Galdieria sulphuraria*. *Gene* **1999**, *230*, 7–14. [[CrossRef](#)]
22. Chandra, R.; Iqbal, H.M.N.; Vishal, G.; Lee, H.S.; Nagra, S. Algal biorefinery: A sustainable approach to valorize algal-based biomass towards multiple product recovery. *Bioresour. Technol.* **2019**, *278*, 346–359. [[CrossRef](#)] [[PubMed](#)]

23. Dhivya, R.; Manimegalai, K. Preliminary Phytochemical Screening and GC- MS Profiling of Ethanol Flower Extract of *Calotropis gigantea* Linn. (Apocynaceae). *J. Pharmacogn. Phytochem.* **2013**, *2*, 28–32.
24. Russell, E.; Lewis Pharm, D. Current Concepts in Antifungal Pharmacology. *Mayo Clin. Proc.* **2011**, *86*, 805–817.
25. Montes D'Oca, M.G.; Viégas, C.V.; Lemões, J.S.; Miyasaki, K.E.; Morón-Villarreyes, J.A.; Primel, E.G.; Abreu, P.C. Production of FAMES from several microalgal lipidic extracts and direct transesterification of the *Chlorella pyrenoidosa*. *Biomass Bioenergy* **2011**, *35*, 1533–1538. [[CrossRef](#)]
26. Movasaghi, Z.; Rehman, S.; Rehman, I. Fourier transform infrared (FTIR) spectroscopy of biological tissues. *Appl. Spectrosc. Rev.* **2008**, *43*, 134–179. [[CrossRef](#)]
27. Malek, K.; Wood, B.R.; Bambery, K.R. FTIR imaging of tissues: Techniques and methods of analysis. In *Optical Spectroscopy and Computational Methods in Biology and Medicine*; Springer: Dordrecht, The Netherlands, 2013; pp. 419–473.
28. Hirschmugl, C.J.; Bayarri, Z.E.; Bunta, M.; Holt, J.B.; Giordano, M. Analysis of the nutritional status of algae by Fourier transform infrared chemical imaging. *Infrared Phys. Technol.* **2006**, *49*, 57–63. [[CrossRef](#)]
29. He, J.; Rodriguez-Saona, L.E.; Giusti, M.M. Mid infrared spectroscopy for juice authentications rapid differentiation of commercial juices. *J. Agric. Food Chem.* **2007**, *55*, 4443–4452. [[CrossRef](#)]
30. Jun, T.D.; Chao, W.; Yubin, M.; Chen, S.Z. Two-step in situ biodiesel production from microalgae with high free fatty acid content. *Bioresour. Technol.* **2013**, *136*, 8–15.
31. Anjai, P.A.; Singh, V.B.N. Biodiesel production by esterification of free fatty acid over sulfated zirconia. *Renew. Energy* **2013**, *51*, 227–233.
32. Olivieri, G.; Marzocchella, A.; Andreatti, R.; Pinto, G.; Folio, A. Biodiesel production from *Stichococcus* strains at laboratory scale. *J. Chem. Technol. Biot.* **2011**, *86*, 776–783. [[CrossRef](#)]
33. Islam, M.T.; de Alencar, M.V.; da Conceição Machado, K.; da Conceição Machado, K.; de Carvalho Melo-Cavalcante, A.A.; de Sousa, D.P.; de Freitas, R.M. Phytol in a pharma-medico-stance. *Chem. Biol. Interact* **2015**, *240*, 60–73. [[CrossRef](#)]
34. Netscher, T. Synthesis of vitamin E. *Vitam. Horm.* **2007**, *76*, 155–202. [[PubMed](#)]
35. Daines, A.M.; Payne, J.R.; Humphries, M.E.; Abell, A.D. The synthesis of naturally occurring Vitamin K and Vitamin K analogues. *Curr. Org. Chem.* **2003**, *7*, 1625–1634. [[CrossRef](#)]
36. Rodrigues, M.L. The Multifunctional Fungal Ergosterol. *mBio* **2018**, *9*, e01755-18. [[CrossRef](#)] [[PubMed](#)]
37. Luo, X.; Su, P.; Zhang, W. Advances in Microalgae-Derived Phytosterols for Functional Food and Pharmaceutical Applications. *Mar. Drugs* **2015**, *13*, 4231–4254. [[CrossRef](#)] [[PubMed](#)]
38. Sankaran, M.; Isabella, S.; Amaranth, K.S. Anti proliferative Potential of Ergosterol: A Unique Plant Sterol on Hep2 Cell Line. *Int. J. Pharm. Sci. Rev. Res.* **2017**, *5*, 1736–1742.
39. Kobori, K.; Yoshida, M.; Ohnishi-Kameyama, M.; Shinmoto, H. Ergosterol peroxide from an edible mushroom suppresses inflammatory responses in RAW264.7 macrophages and growth of HT29 colon adenocarcinoma cells. *Br. J. Pharmacol.* **2007**, *150*, 209–219. [[CrossRef](#)]
40. Kim, S.K.; Ta, Q.V. Potential beneficial effects of marine algal sterols on human health. *Food Nutr. Res.* **2011**, *64*, 191–198.
41. Shimizu, T.; Kawai, J.; Ouchi, K.; Kikuchi, H.; Osima, Y.; Hidemi, R. Agarol, an ergosterol derivative from *Agaricus blazei*, induces caspase-independent apoptosis in human cancer cells. *Int J Oncol.* **2016**, *48*, 1670–1678. [[CrossRef](#)]
42. Chen, S.; Yong, T.; Zhang, Y.; Su, J.; Jiao, C.; Xie, Y. Anti-tumor and anti-angiogenic Ergosterols from *Ganoderma lucidum*. *Front. Chem.* **2017**, *5*, 85. [[CrossRef](#)]
43. Allman-Farinelli, M.A.; Gomes, K.; Favaloro, E.J.; Petocz, P.A. Diet rich in high-oleic-acid sunflower oil favorably alters low-density lipoprotein cholesterol, triglycerides, and factor VII coagulant activity. *J. Am. Diet Assoc.* **2005**, *105*, 1071–1079. [[CrossRef](#)]
44. Saini, R.K.; Keum, Y.S. Omega-3 and omega-6 polyunsaturated fatty acids: Dietary sources, metabolism, and significance. A review. *Life Sci.* **2018**, *203*, 255–267. [[CrossRef](#)] [[PubMed](#)]
45. Tocher, D.R. Metabolism and Functions of Lipids and Fatty Acids in Teleost Fish. *Rev. Fish. Sci.* **2003**, *11*, 107–184. [[CrossRef](#)]
46. Hunter, J.E.; Zhang, J.; Kris-Etherton, P.M. Cardiovascular disease risk of dietary stearic acid compared with trans, other saturated, and unsaturated fatty acids: A systematic review. *Am. J. Clin. Nutr.* **2009**, *91*, 46–63. [[CrossRef](#)]

47. Baker, M.J.; Trevisan, J.; Bassan, P.; Bhargava, R.; Butler, H.J.; Dorling, K.M.; Fielden, P.M.; Fogarty, S.W.; Fullwood, N.J.; Heys, K.A.; et al. Using Fourier transform IR spectroscopy to analyze biological materials. *Nat. Protoc.* **2014**, *9*, 1771–1791. [[CrossRef](#)] [[PubMed](#)]
48. Corte, L.; Tiecco, M.; Roscini, L.; Germani, R.; Cardinali, G. FTIR analysis of the metabolomic stress response induced by N-alkyltropylium bromide surfactants in the yeasts *Saccharomyces cerevisiae* and *Candida albicans*. *Colloid. Surf. B Biointerfaces* **2014**, *116*, 761–771. [[CrossRef](#)]
49. Mayers, J.J.; Flynn, K.J.; Shields, R.J. Rapid determination of bulk microalgal biochemical composition by Fourier-Transform Infrared spectroscopy. *Bioresour. Technol.* **2013**, *148*, 215–220. [[CrossRef](#)]
50. Bartosova, A.; Blinova, L.; Gerulova, K. Characterisation of Polysaccharides and Lipids from Selected Green Algae Species by FTIR-ATR Spectroscopy. *Fac. Mater. Sci. Technol. Trnava Slovak Univ. Technol. Bratisl.* **2015**, *23*, 97–102. [[CrossRef](#)]
51. Rafiqul, I.M.; Jalal, K.C.A.; Alam, M.Z. Environmental Factors for Optimisation of Spirulina Biomass in Laboratory Culture. *Biotechnology* **2005**, *4*, 19–22.
52. Duygu, D. Fourier transform infrared (FTIR) spectroscopy for identification of *Chlorella vulgaris* Beijerinck 1890 and *Scenedesmus obliquus* (Turpin) Kützing 1833. *Afr. J. Biotechnol.* **2012**, *11*, 3817–3824.
53. Koo, T.K.; Da, P.; Li, M.Y. A Guideline of Selecting and Reporting Intraclass Correlation Coefficients for Reliability Research. *J. Chiropr. Med.* **2016**, *15*, 155–163. [[CrossRef](#)]
54. Allen, M.M.; Stanier, R.Y. Grow than division of some unicellular blue-greenalgae. *J. Gen. Microbiol.* **1968**, *51*, 199–202. [[CrossRef](#)] [[PubMed](#)]
55. De Luca, P.; Taddei, R. Crescita comparata di due forme di *Cyanidium caldarium* dei Campi Flegrei (Napoli) in presenza di diverse fonti di azoto. *Delpinoa* **1972**, *12*, 3–8.
56. Wang, S.K.; Stiles, A.R.; Guo, C.; Liu, C.Z. Microalgae cultivation in photobioreactors: An overview of light characteristics. *Eng. Life Sci.* **2014**, *14*, 550–559. [[CrossRef](#)]
57. Lee, J.Y.; Yoo, C.; Jun, S.Y.; Ahn, C.Y.; Oh, H.M. Comparison of several methods for effective lipid extraction from microalgae. *Bioresour. Technol.* **2010**, *101*, S75–S77. [[CrossRef](#)]
58. Bligh, E.G.; Dyer, W.J. A rapid method of total lipid extraction and purification. *Can. J. Biochem. Physiol.* **1959**, *37*, 911–917. [[CrossRef](#)]
59. Carreau, J.P.; Dubacq, J.P. Adaptation of a macro-scale method to the micro-scale for fatty acid methyl transesterification of biological lipid extracts. *J. Chromatogr. A* **1978**, *151*, 384–390. [[CrossRef](#)]
60. Lall, R.K.; Proctor, A.; Jain, V.P. A rapid, micro FAME preparation method for vegetable oil fatty acid analysis by gas chromatography. *J. Am. Oil Chem. Soc.* **2009**, *86*, 309–314. [[CrossRef](#)]
61. Rieppo, L.; Saarakkala, S.; Närhi, T.; Helminen, H.J.; Jurvelin, J.S.; Rieppo, J. Application of second derivative spectroscopy for increasing molecular specificity of fourier transform infrared spectroscopic imaging of articular cartilage. *Osteoarthr. Cartil.* **2012**, *20*, 451–459. [[CrossRef](#)]
62. Mach, H.; Thomson, J.A.; Middaugh, C.R. Quantitative analysis of protein mixtures by second derivative absorption spectroscopy. *Anal. Biochem.* **1989**, *181*, 79–85. [[CrossRef](#)]
63. Baldassarre, M.; Li, C.; Eremina, N.; Goormaghtigh, E.; Barth, A. Simultaneous Fitting of Absorption Spectra and Their Second Derivatives for an Improved Analysis of Protein Infrared Spectra. *Molecules* **2015**, *20*, 12599–12622. [[CrossRef](#)]
64. Wrede, D.; Taha, M.; Miranda, A.F.; Kadali, K.; Stevenscn, T.; Ball, A.S.; Mouradov, A. Co-Cultivation of Fungal and Microalgal Cells as an Efficient System for Harvesting Microalgal Cells, Lipid Production and Wastewater Treatment. *PLoS ONE* **2014**, *9*, e113497. [[CrossRef](#)] [[PubMed](#)]



Article

Synthesis and Biological Studies on Dinuclear Gold(I) Complexes with Di-(*N*-Heterocyclic Carbene) Ligands Functionalized with Carbohydrates

Federica Tresin ¹, Valentina Stoppa ¹, Marco Baron ¹ , Andrea Biffis ¹, Alfonso Annunziata ² , Luigi D'Elia ², Daria Maria Monti ² , Francesco Ruffo ² , Marco Roverso ¹, Paolo Sgarbossa ³ , Sara Bogialli ¹  and Cristina Tubaro ^{1,*} 

¹ Department of Chemical Sciences, University of Padova, via Marzolo 1, 35131 Padova, Italy; federica.tresin@unipd.it (F.T.); valentina.stoppa@studenti.unipd.it (V.S.); marco.baron@unipd.it (M.B.); andrea.biffis@unipd.it (A.B.); marco.roverso@unipd.it (M.R.); sara.bogialli@unipd.it (S.B.)

² Department of Chemical Sciences, University of Napoli Federico II, Complesso Universitario di Monte S. Angelo, via Cintia 21, 80126 Napoli, Italy; alfonso.annunziata@unina.it (A.A.); luigi.delia@unina.it (L.D.); mdmonti@unina.it (D.M.M.); ruffo@unina.it (F.R.)

³ Department of Industrial Engineering, University of Padova, via Marzolo 9, 35131 Padova, Italy; paolo.sgarbossa@unipd.it

* Correspondence: cristina.tubaro@unipd.it; Tel.: +39-049-8275655

Academic Editor: Michal Szostak

Received: 30 July 2020; Accepted: 19 August 2020; Published: 24 August 2020



Abstract: The design of novel metal complexes with *N*-heterocyclic carbene (NHC) ligands that display biological activity is an active research field in organometallic chemistry. One of the possible approaches consists of the use of NHC ligands functionalized with a carbohydrate moiety. Two novel Au(I)–Au(I) dinuclear complexes were synthesized; they present a neutral structure with one bridging diNHC ligand, having one or both heterocyclic rings decorated with a carbohydrate functionality. With the symmetric diNHC ligand, the dicationic dinuclear complex bearing two bridging diNHC ligands was also synthesized. The study was completed by analyzing the antiproliferative properties of these complexes, which were compared to the activity displayed by similar mononuclear Au(I) complexes and by the analogous bimetallic Au(I)–Au(I) complex not functionalized with carbohydrates.

Keywords: gold complexes; *N*-heterocyclic carbene; bidentate ligands; oxidative addition; cytotoxicity

1. Introduction

Cisplatin was used as an anticancer drug for many years, and it is still one of the most used ones, despite its numerous issues with drug resistance and side effects [1,2]. These issues require more research to find a valid transition metal-based alternative to cisplatin. In this regard, metal complexes with *N*-heterocyclic carbene ligands (NHC) [3–5] are attracting increasing attention from the bioinorganic scientific community; these complexes are especially interesting due to their high stability imparted by the strength of the M–NHC bond, such that it appears reasonable that the structure of these complexes remains unchanged and stable under physiological conditions [6–12].

In particular, the interest in gold-based drugs received great impulse from the discovery of the anti-cancer properties of Auranofin, originally used as an antiarthritic drug. Compared to cisplatin, Auranofin presents better activity against difficult to treat tumors, better selectivity, and less cell resistance [13,14]. As Auranofin presents a phosphine ligand, it is reasonable to assume that this ligand could be substituted with an NHC ligand, as NHCs are rapidly substituting phosphine ligands given the higher stability of the resulting complexes; furthermore, as for phosphine ligands, for NHC ones it

is also possible to easily and independently modify their steric and electronic properties [15]. This NHC versatility, obtained for example by simply changing the substituents on the nitrogen atoms of the heterocyclic ring, also allows a better fine-tuning of the lipophilic/hydrophilic balance of the molecule, thus enhancing the selectivity of the drug [16]. Many gold(I) and gold(III) complexes with NHC ligands show biological activity, and several reviews appeared on this topic in recent years [10,14,17].

The decoration of the carbene ligand with a carbohydrate can be of interest for a variety of reasons; sugars are abundant in nature and present an extremely varied structure, they can enhance the water solubility of the complex, and finally the presence of a sugar residue in the molecule can enhance the drug selectivity as a result of the increased carbohydrate uptake of cancer cells [18–23]. The bioactivity of mononuclear gold(I) complexes with carbohydrate-functionalized NHCs were recently studied by some of us [18]. In this manuscript, we report on the synthesis of dinuclear Au(I)–NHC complexes with incorporated acetylated glucopyranose moieties and on their antiproliferative activity. The performances of the dinuclear complexes, in terms of both activity and selectivity, were compared to their corresponding mononuclear counterparts and to dinuclear complexes not having carbohydrate-functionalized NHCs. Dinuclear Au(I) complexes with one or two bridging diNHC carbene ligands were reported to present anticancer properties, acting by inhibiting the thioredoxin reductase TrxR or by leading to mitochondria-induced apoptosis [24–31].

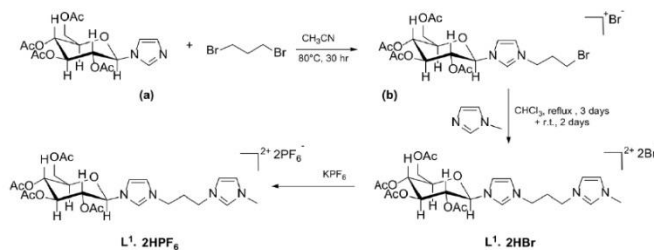
2. Results and Discussion

2.1. Synthesis of the Bis(Imidazolium) Salts

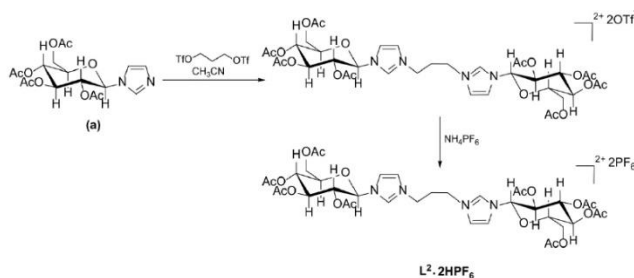
Compound **L¹-2HPF₆** was synthesized following a three-step process (Scheme 1), in which the carbohydrate-functionalized imidazole (**a**) [32] reacts with 1,3-dibromopropane to obtain the imidazolium salt (**b**). This reaction does not yield the bis(imidazolium) symmetric product, possibly due either to the limited nucleophilicity of the imidazole (**a**) or to the low reactivity of dibromopropane under the reaction conditions. In fact, by reacting product (**b**) with *N*-methylimidazole, compound **L¹-2HBr** can be isolated. The final Br[−]/PF₆[−] anion metathesis step is usually required to isolate an azolium salt more soluble in organic solvents, such as acetonitrile, and to prevent interferences of the counter anions during the synthesis of the Au(I) complexes, especially the dinuclear dicationic ones.

In order to obtain the symmetric bis(imidazolium) salt **L²-2HPF₆**, imidazole (**a**) was reacted with 1,3-propylenebistriflate, a substrate more activated than 1,3-dibromopropane for the nucleophilic substitution, following a procedure reported by Anneser et al. (Scheme 2) [33]. Also in this case, the final step is the anion metathesis.

Both **L¹-2HPF₆** and **L²-2HPF₆** were characterized by ¹H- and ¹³C[¹H]-NMR spectroscopy, as well as electrospray ionization mass spectrometry (ESI-MS), and both salts appear to be spectroscopically pure. In the case of compound **L¹-2HPF₆**, the acidic protons of the imidazole C2-H hydrogens give two signals in the ¹H-NMR spectrum at 8.72 and 8.73 ppm, indicating the lack of symmetry of the system. Conversely, the ¹H-NMR spectrum of symmetric **L²-2HPF₆** presents only one peak at 8.82 ppm. Anomerization processes were reported in the literature during the quaternization of the imidazole ring or during the synthesis of carbene complexes with carbohydrate functionalized NHC [34]. In both compounds, the signal relative to the anomeric proton, which is found around 5.7–5.8 ppm, has a coupling constant value of around 9 Hz. Comparing this ³J_{HH} value with data found in literature relative to the anomeric proton in glucopyranose rings, it is reasonable to state that the carbohydrate remains present in the β anomer form in both diazolium salts; the coupling constant of the same peak for the α anomer is, in fact, much lower, around 2–4 Hz [35].



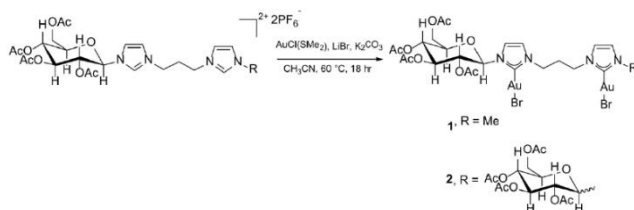
Scheme 1. Synthesis of the bis(imidazolium) salt $\text{L}^1 \cdot 2\text{HPF}_6$; (a) carbohydrate-functionalized imidazole; (b) imidazolium salt.



Scheme 2. Synthesis of the bis(imidazolium) salt $\text{L}^2 \cdot 2\text{HPF}_6$; (a) carbohydrate-functionalized imidazole.

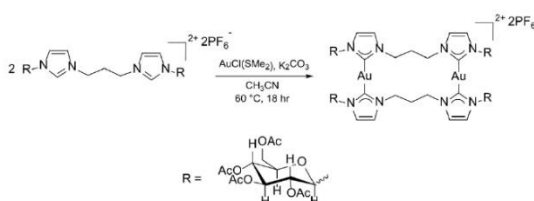
2.2. Synthesis of the $[\text{Au}_2\text{Br}_2\text{L}]$ Complexes

Compounds **1** and **2** were synthesized following a single-step procedure already reported in the literature [36] in which the proper bis(imidazolium) salt reacts with the gold precursor $\text{AuCl}(\text{SMe}_2)$ in the presence of LiBr and K_2CO_3 as a base to deprotonate the bis(imidazolium) salt. The addition of LiBr prevents the formation of the analogous chloro complexes $[\text{Au}_2\text{Cl}_2\text{L}]$; furthermore, it was reported by Nolan and co-workers that the anion which usually coordinates to gold(I) in the complexes is that of the starting azolium salt [37]. The neutral $[\text{Au}_2\text{Br}_2\text{L}]$ complexes (Scheme 3) were then characterized by ^1H - and $^{13}\text{C}\{^1\text{H}\}$ -NMR spectroscopy, as well as ESI-MS. In particular, an indication that the complexes formed is provided by the disappearance of the peak relative to the acidic C2-Hs, supporting the deprotonation of the diazolium salt. Further proof comes from the ^{13}C -NMR spectrum, in which the peak relative to the imidazole C2 is present at around 170–175 ppm, in the range of values found in the literature for carbene carbons coordinated to a gold(I) center *trans* to a bromide ligand [36,38]. In both complexes, the carbohydrate is present in the β anomeric form as suggested by the value (9 Hz) of the $^3J_{\text{H1H}}$ coupling constant of the anomeric proton in the glucopyranose ring [35]. From the ESI-MS spectra, the most prominent peaks are the $[\text{Au}_2\text{Br}_2\text{L}]^+$ (at m/z 993 and 1311 for compounds **1** and **2**, respectively) and the $[\text{Au}_2\text{Br}_2\text{LK}]^+$ cations (m/z 1113 and 1429 for compounds **1** and **2**, respectively).

Scheme 3. Synthesis of the dinuclear gold(I) complexes **1** and **2**.

2.3. Synthesis of the $[\text{Au}_2\text{L}_2](\text{PF}_6)_2$ Complexes

With this type of dicarbene ligand, in addition to the neutral complexes described in the previous section, it is possible to also isolate dinuclear dicationic complexes with the general formula $[\text{Au}_2\text{L}_2]^{2+}$ having two ligands bridging the two gold centers. Considering the asymmetric nature of the proligand **L**¹-**2HPF**₆, at least two configurational isomers can be isolated: one with the carbohydrate-imidazoles facing each other and one with each carbohydrate-NHC facing a methylimidazole-2-ylidene. Furthermore, we recently reported that, in similar $[\text{Au}_2\text{L}_2]^{2+}$ complexes with heteroditopic ligands, the number of possible products is also increased by the different conformations of the propylene linkers between the carbene units [39,40]. For this reason, we investigated only the reaction with the symmetric ligand **L**². Compound **3** was synthesized following the same procedure described for complex **2** but using a 1:1 **L**²-**2HPF**₆:AuCl(SMe₂) molar ratio and without adding LiBr to the reaction mixture (Scheme 4). Once again, the formation of the complex is supported by the disappearance in the ¹H-NMR spectrum of the peak associated to the C2-H on the imidazole rings. The stoichiometry of the complex was confirmed by high-resolution mass spectrometry measurements where a peak relative to the dicationic $[\text{Au}_2\text{L}_2]^{2+}$ fragment is present at 1033.2594 *m/z*. Another indication that this complex is cationic comes from the ¹³C[¹H]-NMR spectrum; the peak of the carbene carbon is found at 183.2 ppm, downfield shifted by ca. 10 ppm with respect to the signal observed in the corresponding neutral complex **2** (174.6 ppm). This chemical shift value is coherent with the values reported in literature for carbene carbons with another carbene carbon in *trans* position [41–45], and this geometry is frequently observed in cationic gold(I) complexes with two carbene ligands coordinated to the same metal center.

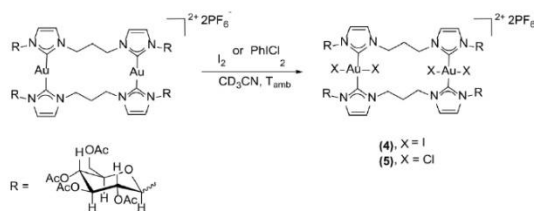
Scheme 4. Synthesis of the dinuclear gold(I) complex **3**.

2.4. Reactivity of the Gold(I) Complex **3** toward Oxidative Addition of Halogens

The reactivity of the gold(I) complex **3** in the oxidative addition of halogens to gold was investigated; the reactions were performed in an NMR tube at room temperature in deuterated acetonitrile as solvent, using a slight excess of oxidant (I_2 : $[\text{Au}] = 1.2:1$ and PhICl_2 : $[\text{Au}] = 1.5:1$) (Scheme 5). Many possible products can be obtained from the oxidative addition of halogens to dinuclear diNHC gold(I) complexes:

the fully oxidized gold(III)–gold(III) product, the mixed-valence gold(I)–gold(III) complex, and the gold(II)–gold(II) species (Figure 1) [46]. Therefore, the reactions were followed by recording $^1\text{H-NMR}$ spectra before the addition of the oxidant, immediately after, and three hours and 24 h later in order to monitor any possible changes in the product distribution. With both halogens, the dinuclear gold(III) complex was immediately formed, and no further evolution of the product was detected.

In both cases, the symmetry of the complex is maintained, as shown by the $^1\text{H-NMR}$ spectra which present only one set of peaks relative to the sugars and imidazole rings. This suggests that the two metal centers are equivalent and, therefore, present the same oxidation state. The $^{13}\text{C-NMR}$ spectra show more definite proof that the oxidation state of the gold centers changed from gold(I) to gold(III); the carbene carbons present, in fact, a peak at 145.6 ppm for complex 4 and 154.6 ppm for 5. These values of chemical shifts are 20–30 ppm lower than the value (δ 183.2 ppm) found for complex 3. This is usually explained taking into consideration the more pronounced Lewis acidic behavior of gold(III), causing an extended delocalization of the π electron density of the imidazole $\text{C}=\text{C}$ double bond toward the carbene carbon [47,48]. The difference between the $^{13}\text{C-NMR}$ carbene chemical shifts in 4 and 5 is ca. 10 ppm and is due to the different nature of the two halide ligands [46]. The definitive proof that both complexes are dinuclear gold(III) complexes comes from the high-resolution mass spectra; for both complexes, the most prominent signal is the one given by the $[\text{Au}_2\text{X}_4\text{L}_2]^{2+}$ ion, at m/z 1287.0697 for 4 and 1103.1974 for 5, both for monoisotopic peaks.



Scheme 5. Synthesis of the dinuclear Au(III) complexes by oxidative addition to 3.

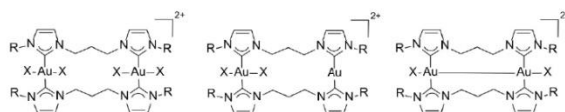


Figure 1. Possible products obtained from the oxidative addition of halogens to the dinuclear gold(I)–gold(I) complexes.

2.5. Biological Activity of the Gold(I) Complexes

The biological activity of the gold(I) complexes 1–3 and 6 was tested on different eukaryotic cell lines. Complex 6 (Figure 2), bearing only methyl groups as wingtip substituents, was chosen for the absence of any carbohydrate moiety as comparison.

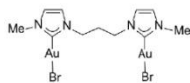


Figure 2. Structure of complex 6.

The assay was performed to study the importance of the functionalization with a carbohydrate moiety in determining the antiproliferative activity. We did not test the antiproliferative activity of gold(III) complexes **4** and **5**, as it is well known that similar dicationic gold(III) complexes easily undergo reduction to the corresponding gold(I) species in a physiological environment [26,48]. In particular, two cancer cell lines, A431 and SVT2, were tested in the presence of increasing amount of each compound. Immortalized cell lines, HaCaT and BALB/c-3T3, were analyzed as well to study the selectivity of the newly synthesized compounds. Cell viability was evaluated by the 3-(4,5-dimethylthiazol-2-yl)-2,5-diphenyltetrazolium bromide (MTT) assay and the results, after 48 h of incubation, are reported in Figure 3. All the complexes were cytotoxic on all cell lines analyzed, and they showed a dose-dependent toxicity. Interestingly, the analyzed compounds induced an increase in cell proliferation at very low concentration (5–10 $\mu\text{g/mL}$). The IC_{50} values, i.e., the complex concentration required to induce 50% of cell death, is reported in Table 1. Complex **3** was the compound with the lowest toxicity with respect to the other tested molecules.

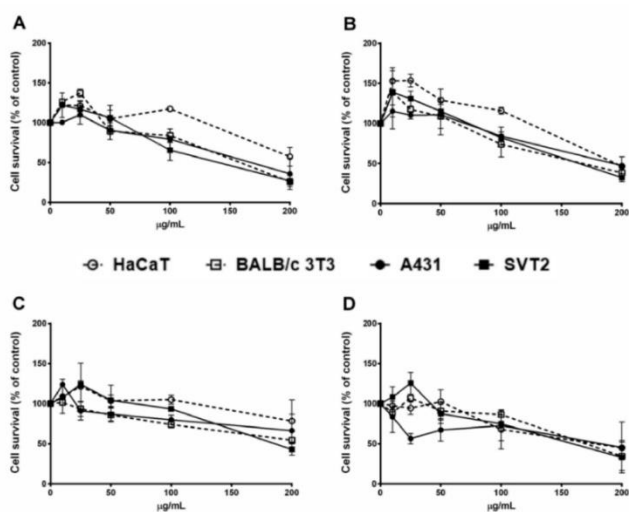


Figure 3. Effect of complexes **1**, **2**, **3**, and **6** on the survival of different cell lines. Immortalized human cells (HaCaT, dashed line with empty circles), immortalized murine cells (BALB/c-3T3, dashed line with empty squares), human epidermoid carcinoma (A431, black line with black circles), and murine fibroblast transformed with simian virus 40 (SV40) (SVT2, black line with black squares) were incubated with increasing amounts of each compound (10–200 $\mu\text{g/mL}$) for 48 h. Cell viability was assessed by 3-(4,5-dimethylthiazol-2-yl)-2,5-diphenyltetrazolium bromide (MTT) assay and expressed as described in the Section 3. **A**, complex **1**; **B**, complex **2**; **C**, complex **3**; **D**, complex **6**. Values are given as means \pm SD ($n \geq 3$).

Table 1. IC₅₀ values (μM) obtained for **1**, **2**, **3**, and **6** on HaCaT, BALB/c 3T3, A431, and SVT2 cells line after 48 h of incubation.

Cell Line	Complex 1	Complex 2	Complex 3	Complex 6
HaCaT	181 ± 8	>144	>85	240 ± 15
BALB/c 3T3	148 ± 15	108 ± 17	>85	241 ± 15
A431	162 ± 34	137 ± 5	>85	235 ± 16
SVT2	139 ± 12	118 ± 6	72 ± 15	207 ± 15

Even if the IC₅₀ values for the reported dinuclear complexes are very high (>100 μM), these results are not totally unexpected, as this inertness was also observed for the mononuclear complex [Au(magi)Cl] (magi = 1-methyl-3-(2,3,4,6-tetra-*O*-acetyl-β-*D*-glucopyranosyl)imidazole-2-ylidene) [18] and was attributed to the low mitochondrial penetration of the complex. Comparing the performances of complexes **1**, **2**, and **6**, it is evident that the introduction of a sugar in the carbene moiety only slightly improves the cytotoxic activity. Complex **3** shows lower IC₅₀ values than those of the neutral complex **2**, having the same diNHC ligand.

In general, halo-substituted neutral gold(I) complexes turn out to be less effective than their corresponding cationic bis(NHC) complexes. The lability of the Au–X (X = halogen) bond, compared to the relative inertness of the Au–NHC bonds, makes the halide derivatives less stable in biologically relevant conditions, favoring the occurrence of deactivation reactions by different cellular components. Another parameter that can explain the lower activity of the neutral gold(I) complexes is their lower solubility in water, which possibly reduces the drug uptake by cells [49]. Finally, the higher activity of complex **3** can be also attributed to its dicationic nature, which allows its classification as a delocalized lipophilic cation (DLC) [50]. Indeed, the difference in the mitochondrial membrane potential between cancerous and healthy cells could explain the higher penetration of DLCs into the mitochondrial membrane of tumor cells, which in turn would lead to cell apoptosis [51].

3. Materials and Methods

3.1. General Comments

All commercially available reagents (Sigma-Aldrich, Darmstadt, Germany) were used as received without additional purification steps. The reagents **a** [32], **b** [52], 1,3-propylenebistriflate [53], and complex **6** [36] were prepared according to literature procedures. The NMR spectra were recorded on a Bruker Avance 300 (Bruker, Billerica, MA, USA; 300.1 MHz for ¹H and 75.5 MHz for ¹³C) at 298 K unless otherwise stated; chemical shifts (δ) are reported in units of ppm relative to the residual solvent signals. ESI-MS analyses of compounds **L¹-2HPPF₆**, **L¹-2HPPF₆**, **1**, and **2** were performed using an LCQ-Duo (Thermo Fisher Scientific, Waltham, Massachusetts, USA) operating in positive ion mode; sample solutions were prepared by dissolving the compounds in acetonitrile and were directly infused into the ESI source by a syringe pump at 8 μL/min flow rate. The HRMS measures of complexes **3–5** were performed using a Q-Exactive hybrid quadrupole-Orbitrap™ mass spectrometer (Thermo Fisher Scientific). MS conditions were as follows: electrospray ionization in positive mode, resolution 70,000, automatic gain control (AGC) target 1 × 10⁶, max injection time of 50 ms, scan range 500–2000 amu, capillary voltage 3.5 kV and radiofrequency (RF) voltage 50 V, capillary temperature 320 °C and probe temperature 350 °C; nitrogen was used as sheath gas at 11 psi. Samples were prepared using acetonitrile as solvent and injected for analysis at a flow rate of 10 μL/min. Calibration was performed with a standard solution purchased from Thermo Fisher Scientific (Pierce®ESI positive Ion Calibration Solution). The software for analysis of MS data was Xcalibur 3.1 (Thermo Fisher Scientific). Elemental analyses were carried out by the microanalytical laboratory of Chemical Sciences Department (University of Padova) with a Thermo Scientific FLASH 2000 apparatus. The recorded NMR and ESI-MS spectra of the reported compounds can be found in the Supplementary Materials section.

In the characterization of the imidazolium salts and gold complexes, the following notation (Figure 4) was adopted for the sugar substituent:

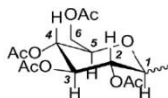


Figure 4. Numbering of the carbon atoms in the sugar substituent for NMR assignments.

3.2. Synthesis of the Bis(Imidazolium) Salts

3.2.1. Synthesis of the Bis(Imidazolium) Salt L¹-2HPF₆

Compound **b** (0.19 g, 0.32 mmol), *N*-methylimidazole (91 μ L, 1.14 mmol), and 10 mL of CHCl₃ were added to an Ace pressure tube. The solution was stirred at 65 °C for three days, then for two additional days at room temperature. The solvent was evaporated under reduced pressure to give a white solid. The solid product was dissolved in 5 mL of a saturated aqueous KPF₆ solution and left stirring overnight. The formation of an oil was observed. The oily residue was separated from the aqueous solution and dried under vacuum. The residue was treated with 20 mL of diethyl ether under stirring for three hours and the formation of a white solid was observed. The solid was isolated by filtration (yield 44%). ¹H-NMR (300 MHz, CD₃CN) δ 8.76 (s, 1H, NCHN-GluIm), 8.41 (s, 1H, NCHN-MeIm), 7.64 (s, 1H, GluIm), 7.47 (s, 1H, GluIm), 7.38 (m, 2H, MeIm), 5.74 (d, ³J = 9.0 Hz, 1H, 1-Glu), 5.50 (m, 1H, 3-Glu), 5.38–5.21 (m, 2H, 2,4-Glu), 4.32–4.18 (m, 3H, 5,6-Glu), 4.18–4.09 (m, 4H, NCH₂), 3.84 (s, 3H, CH₃-MeIm), 2.38 (quint, 2H, ³J = 7.2 Hz, 2H, CH₂), 2.07 (s, 3H, CH₃-Ac), 2.03 (s, 3H, CH₃-Ac), 1.99 (s, 3H, CH₃-Ac), 1.94 (s, 3H, CH₃-Ac). ¹³C[¹H]-NMR (75 MHz, CD₃CN) δ 171.16 (CO), 170.59 (CO), 170.48 (CO), 170.43 (CO), 136.91 (NCHN-GluIm), 136.31 (NCHN-MeIm), 124.78 (GluIm), 124.12 (GluIm), 123.01 (MeIm), 121.61 (MeIm), 85.28 (1-Glu), 75.56 (Glu), 72.13 (Glu), 71.87 (Glu), 67.97 (Glu), 62.08 (6-Glu), 47.64 (NCH₂), 46.76 (NCH₂), 36.67 (CH₃-MeIm), 30.46 (CH₂), 20.63 (CH₃-Ac), 20.56 (CH₃-Ac), 20.33 (CH₃-Ac). ESI-MS (positive ions, CH₃CN): *m/z* 667 [H₂L¹PF₆]⁺, 983 [H₂L²PF₆]⁺, 1479 [(H₂L¹)₂(PF₆)₃]⁺. Elemental analysis C₂₄H₃₄N₄O₉P₂F₁₂. Calculated: C, 35.48%; H, 4.22%; N, 6.90%. Found: C, 34.96%; H, 3.73%; N, 5.57%.

3.2.2. Synthesis of the Bis(Imidazolium) Salt L²-2HPF₆

Compound **a** (231 mg, 0.58 mmol) was dissolved in 50 mL of acetonitrile at 0 °C. A solution of 1,3-propylenebistriflate (98 mg, 0.29 mmol) in 7 mL of acetonitrile was prepared and added dropwise, over one hour, to the solution containing **a**. The resulting solution was warmed to room temperature and left stirring for 16 h. The solvent was removed and the obtained solid was dissolved in 5 mL of distilled water. A saturated aqueous NH₄PF₆ solution (5 mL) was added, and the final solution was left stirring for an hour until the formation of a white solid precipitate was observed. The solid was filtered, washed with distilled water, and then dried under reduced pressure (yield 48%). ¹H-NMR (300 MHz, CD₃CN) δ 8.82 (s, 2H, NCHN-Im), 7.67 (t, ³J = 1.9 Hz, 2H, Im), 7.50 (t, ³J = 1.9 Hz, 2H, Im), 5.78 (d, ³J = 9.0 Hz, 2H, 1-Glu), 5.52 (m, 2H, 3-Glu), 5.38–5.25 (m, 4H, 2,4-Glu), 4.28–4.22 (m, 6H, 5,6-Glu), 4.22–4.17 (m, 4H, NCH₂), 2.47–2.36 (m, 2H, CH₂), 2.05 (s, 6H, CH₃-Ac), 2.05 (s, 6H, CH₃-Ac), 2.01 (s, 6H, CH₃-Ac). ¹³C[¹H]-NMR (75 MHz, CD₃CN) δ 171.2 (CO), 170.6 (CO), 170.5 (CO), 136.5 (NCHN-Im), 124.2 (Im), 121.8 (Im), 85.4 (1-Glu), 75.7 (3-Glu), 72.2 (Glu), 71.9 (Glu), 68.0 (Glu), 62.1 (Glu), 47.6 (NCH₂), 30.4 (CH₂), 20.7 (CH₃-Ac), 20.7 (CH₃-Ac), 20.5 (CH₃-Ac). ESI-MS (positive ions, CH₃CN): *m/z* 983 [H₂L²PF₆]⁺, 507 [H₂L²-Glu]⁺, 419 [H₂L²]²⁺. Elemental analysis C₃₇H₅₀N₄O₁₈P₂F₁₂. Calculated: C, 39.37%; H, 4.46%; N, 4.96%. Found: C, 39.07%; H, 4.24%; N, 4.36%.

3.3. General Procedure for the Synthesis of Complexes [Au₂Br₂L]

The proper bis(imidazolium) salt (0.086 mmol), AuCl(SMe₂) (0.172 mmol), K₂CO₃ (1.89 mmol), LiBr (0.86 mmol), and 40 mL of acetonitrile were added to a round-bottom flask. The mixture was heated to 60 °C and left stirring for 18 h, then filtered on Celite to remove excess salts. The solvent was removed under reduced pressure. The solid was finally recrystallized with chloroform/*n*-hexane (for **1**) or acetonitrile/diethyl ether (for **2**), obtaining a white solid product which was filtered and dried under vacuum.

1. White solid, yield 59%. ¹H-NMR (300 MHz, CD₃CN) δ 7.43 (d, ³J = 2.1 Hz, 1H, GluIm), 7.29 (d, ³J = 2.1 Hz, 1H, GluIm), 7.20 (d, ³J = 1.9 Hz, 1H, MeIm), 7.17 (d, ³J = 1.9 Hz, 1H, MeIm), 6.12 (d, ³J = 8.9 Hz, 1H, 1-Glu), 5.52 (m, 1H, 3-Glu), 5.33–5.19 (m, 2H, 2,4-Glu), 4.27–4.17 (m, 3H, 5,6-Glu), 4.17–4.02 (m, 4H, NCH₂), 3.85 (s, 3H, CH₃-MeIm), 2.50–2.35 (m, 2H, CH₂), 2.06 (s, 3H, CH₃-Ac), 2.04 (s, 3H, CH₃-Ac), 1.98 (s, 3H, CH₃-Ac), 1.93 (s, 3H, CH₃-Ac). ¹³C[¹H]-NMR (75 MHz, CD₃CN) δ 175.07 (NCN-MeIm), 172.91 (NCN-GluIm), 171.27 (CO), 170.66 (CO), 170.58 (CO), 169.99 (CO), 123.93 (MeIm), 122.30 (GluIm), 120.73 (MeIm), 119.62 (GluIm), 86.64 (1-Glu), 75.13 (3-Glu), 72.64 (Glu), 72.24 (Glu), 68.51 (Glu), 62.34 (Glu), 48.31 (NCH₂), 47.50 (NCH₂), 38.75 (CH₃-MeIm), 30.96 (CH₂), 21.08 (CH₃-Ac), 20.95 (CH₃-Ac), 20.82 (CH₃-Ac), 20.75 (CH₃-Ac). ESI-MS (positive ions, CH₃CN): *m/z* 993 [Au₂L¹Br]⁺, 1113 [Au₂L¹Br₂K]⁺.

2. White solid, yield 89%. ¹H-NMR (300 MHz, CD₃CN) δ 7.45 (d, ³J = 2.0 Hz, 2H, Im), 7.30 (d, ³J = 2.0 Hz, 2H, Im), 6.14 (d, ³J = 8.9 Hz, 2H, 1-Glu), 5.54 (m, 2H, 3-Glu), 5.26 (m, 4H, 2,4-Glu), 4.34–4.18 (m, 6H, 5,6-Glu), 4.18–3.98 (m, 4H, NCH₂), 2.49–2.35 (m, 2H, CH₂), 2.06 (s, 6H, CH₃-Ac), 2.04 (s, 6H, CH₃-Ac), 1.98 (s, 6H, CH₃-Ac), 1.92 (s, 6H, CH₃-Ac). ¹³C[¹H]-NMR (75 MHz, CD₃CN) δ 174.64 (NCN-Im), 171.24 (CO), 170.65 (CO), 170.59 (CO), 170.01 (CO), 122.34 (Im), 119.67 (Im), 86.76 (1-Glu), 75.20 (Glu), 72.65 (Glu), 72.33 (Glu), 68.55 (Glu), 62.36 (6-Glu), 48.22 (NCH₂), 21.05 (CH₃-Ac), 20.97 (CH₃-Ac), 20.85 (CH₃-Ac), 20.78 (CH₃-Ac). ESI-MS (positive ions, CH₃CN): *m/z* 1311 [Au₂L²Br]⁺, 1429 [Au₂L²Br₂K]⁺.

3.4. Synthesis of the Complex [Au₂L²](PF₆)₂, **3**

The salt L²-2HPF₆ (76 mg, 0.067 mmol), AuCl(SMe₂) (20 mg, 0.067 mmol), K₂CO₃ (203 mg, 1.47 mmol), and 40 mL of acetonitrile were added to a round-bottom flask; the mixture was heated to 60 °C and left stirring for 18 h, then filtered on Celite to remove excess salts. The solvent was removed at reduced pressure. The residue was recrystallized with acetonitrile/diethyl ether, obtaining a white solid which was filtered and dried under vacuum (yield 69%). ¹H-NMR (300 MHz, CD₃CN) δ 7.58 (d, ³J = 1.9 Hz, 4H, Im), 7.42 (d, ³J = 1.9 Hz, 4H, Im), 6.08 (d, ³J = 8.9 Hz, 4H, 1-Glu), 5.63 (m, 4H, 3-Glu), 5.35 (m, 8H, 2,4-Glu), 4.47–4.31 (m, 8H, NCH₂), 4.31–4.13 (m, 12H, 5,6-Glu), 2.54–2.38 (m, 4H, CH₂), 2.05 (s, 12H, CH₃-Ac), 2.01 (s, 12H, CH₃-Ac), 2.01 (s, 12H, CH₃-Ac), 1.92 (s, 12H, CH₃-Ac). ¹³C[¹H]-NMR (75 MHz, CD₃CN) δ 183.17 (Im), 171.16 (CO), 170.73 (CO), 170.55 (CO), 170.09 (CO), 126.84 (Im), 123.80 (Im), 87.14 (1-Glu), 75.51 (Glu), 72.70 (Glu), 72.58 (Glu), 68.29 (Glu), 62.26 (Glu), 50.11 (NCH₂), 32.53 (CH₂), 21.04 (CH₃-Ac), 20.83 (CH₃-Ac), 20.80 (CH₃-Ac). HRMS (positive ions, monoisotopic peak): *m/z* 991.2506 [Au₂L²(-2CH₂CO)]²⁺ (calculated for C₇₀H₉₂Au₂N₈O₃₄²⁺ = 991.2518), 1012.2554 [Au₂L²(-CH₂CO)]²⁺ (calculated for C₇₂H₉₄Au₂N₈O₃₅²⁺ = 1012.2571), 1033.2594 [Au₂L²]²⁺ (calculated for C₇₄H₉₆Au₂N₈O₃₆²⁺ = 1033.2624).

3.5. Reactivity of Complex **3** in Halogen Oxidative Addition: Characterization of the Dinuclear Au(III) Complexes [Au₂L²X₄](PF₆)₂, **4** and **5**

Complex **3** was added to an NMR tube and dissolved in CD₃CN; the oxidant (I₂ or PhICl₂) was then added in a [I₂]/[Au] = 1.2 and [Cl₂]/[Au] = 1.5 ratio. NMR spectra were recorded before the addition of the oxidant, immediately after, and three hours and 24 hours later to monitor the reaction. In the case of the [Au₂L²Cl₄](PF₆)₂ complex, the product was isolated as a white solid by removal of the deuterated solvent and by treatment of the residue with diethyl ether to remove the coproduct of

the oxidant (PhI). These reactivity tests were run on NMR scale and, for this reason, the characterization of the complexes involved only NMR and MS analysis.

4. $^1\text{H-NMR}$ (300 MHz, CD_3CN) δ 7.77 (d, $^3J = 2.1$ Hz, 4H, Im), 7.62 (d, $^3J = 2.1$ Hz, 4H, Im), 5.90 (d, $^3J = 9.3$ Hz, 4H, 1-Glu), 5.66 (m, 4H, 3-Glu), 5.40 (m, 4H, 2-Glu), 5.24 (m, 4H, 4-Glu), 4.28–4.00 (m, 20H, 5,6-Glu and NCH_2), 2.66–2.43 (m, 4H, CH_2), 1.96 (s, 12H, $\text{CH}_3\text{-Ac}$), 1.94 (s, 12H, $\text{CH}_3\text{-Ac}$), 1.89 (s, 12H, $\text{CH}_3\text{-Ac}$). $^{13}\text{C}\{^1\text{H}\}\text{-NMR}$ (75 MHz, CD_3CN) δ 171.06 (CO), 171.01 (CO), 170.66 (CO), 170.64 (CO), 145.63 (NCN-Im), 126.58 (Im), 123.81 (Im), 85.81 (1-Glu), 75.96 (Glu), 72.69 (Glu), 72.29 (Glu), 68.11 (Glu), 62.43 (Glu), 50.02 (NCH_2), 30.45 (CH_2), 22.13 ($\text{CH}_3\text{-Ac}$), 20.96 ($\text{CH}_3\text{-Ac}$), 20.80 ($\text{CH}_3\text{-Ac}$), 20.75 ($\text{CH}_3\text{-Ac}$). HRMS (positive ions, monoisotopic peak): m/z 1160.1664 $[\text{Au}_2\text{L}_2\text{I}_2]^{2+}$ (calculated for $\text{C}_{74}\text{H}_{96}\text{Au}_2\text{I}_2\text{N}_8\text{O}_{36}^{2+} = 1160.1668$), 1287.0697 $[\text{Au}_2\text{L}_2\text{I}_4]^{2+}$ (calculated for $\text{C}_{74}\text{H}_{96}\text{Au}_2\text{I}_4\text{N}_8\text{O}_{36}^{2+} = 1287.0713$), 1266.0660 $[\text{Au}_2\text{L}_2\text{I}_4(-\text{CH}_2\text{CO})]^{2+}$ (calculated for $\text{C}_{72}\text{H}_{94}\text{Au}_2\text{I}_4\text{N}_8\text{O}_{35}^{2+} = 1266.0660$).

5. $^1\text{H-NMR}$ (300 MHz, CD_3CN) δ 7.84 (s, 4H, Im), 7.68 (s, 4H, Im), 6.39 (d, $^3J = 9.3$ Hz, 4H, 1-Glu), 5.80 (t, $^3J = 9.6$ Hz, 4H, 3-Glu), 5.45–5.19 (m, 8H, 2,4-Glu), 4.61–4.42 (m, 4H, NCH_2), 4.42–4.27 (m, 4H, NCH_2), 4.27–4.05 (m, 12H, 5,6-Glu), 2.71–2.48 (m, 4H, CH_2), 2.05 (s, 12H, $\text{CH}_3\text{-Ac}$), 2.01 (s, 12H, $\text{CH}_3\text{-Ac}$), 1.93 (s, 12H, $\text{CH}_3\text{-Ac}$), 1.90 (s, 12H, $\text{CH}_3\text{-Ac}$). $^{13}\text{C}\{^1\text{H}\}\text{-NMR}$ (75 MHz, CD_3CN) δ 171.37 (CO), 171.01 (CO), 170.66 (CO), 170.63 (CO), 154.57 (NCN-Im), 126.14 (Im), 122.99 (Im), 85.68 (1-Glu), 76.16 (Glu), 73.56 (Glu), 72.41 (Glu), 68.10 (Glu), 62.40 (6-Glu), 49.46 (NCH_2), 31.56 (CH_2), 21.50 ($\text{CH}_3\text{-Ac}$), 20.80 ($\text{CH}_3\text{-Ac}$), 20.76 ($\text{CH}_3\text{-Ac}$). HRMS (positive ions, monoisotopic peak): m/z 1033.2615 $[\text{Au}_2\text{L}_2\text{Cl}_2]^{2+}$ (calculated for $\text{C}_{74}\text{H}_{96}\text{Au}_2\text{Cl}_2\text{N}_8\text{O}_{36}^{2+} = 1033.2624$), 1103.1970 $[\text{Au}_2\text{L}_2\text{Cl}_4]^{2+}$ (calculated for $\text{C}_{74}\text{H}_{96}\text{Au}_2\text{Cl}_4\text{N}_8\text{O}_{36}^{2+} = 1103.2001$).

3.6. Cytotoxicity Assay

To assess the cytotoxicity of the compounds, both immortalized and tumorigenic cells were chosen. Immortalized human keratinocytes (HaCaT, from Innoprot, Derio, Spain), immortalized murine fibroblasts (BALB/c 3T3, from ATCC, Manassas, Vi, USA), human epidermoid carcinoma cells (A431, from ATCC), and BALB/c-3T3 transformed with simian virus 40 (SV40) (SVT2, from ATCC) were cultured in Dulbecco's modified Eagle's medium (DMEM) (Sigma-Aldrich, St Louis, MO, USA) supplemented with 10% fetal bovine serum (HyClone, Logan, UT, USA), 2 mM L-glutamine and antibiotics. Cells were grown in a 5% CO_2 humidified atmosphere at 37 °C and seeded in 96-well plates at a density of 2×10^3 cells per well. Cells were incubated with increasing concentrations of each compound (from 10 to 200 $\mu\text{g}\cdot\text{mL}^{-1}$). After 4 h of incubation, cell viability was measured using the MTT (3-(4,5-dimethylthiazol-2-yl)-2,5-diphenyltetrazolium bromide) assay, which measures mitochondrial functionality. Briefly, the MTT reagent was dissolved in DMEM in the absence of phenol red (Sigma-Aldrich) and added to the cells (0.5 $\text{mg}\cdot\text{mL}^{-1}$ final concentration). Following 4 h of incubation at 37 °C, the culture medium was removed and the resulting formazan salts were dissolved by adding isopropanol containing 0.01 $\text{mol}\cdot\text{L}^{-1}$ HCl (100 μL per well). Absorbance values were determined at 570 nm using an automatic plate reader (Microbeta Wallac 1420, PerkinElmer, Waltham, MA, USA).

4. Conclusions

In this work, we reported two novel diNHC precursors with one or both the heterocyclic rings functionalized with a carbohydrate moiety. The corresponding neutral complexes of the type $\text{Au}_2\text{Br}_2(\text{diNHC})$ and, with the symmetric ligand, also the dicationic complex $[\text{Au}_2(\text{diNHC})_2](\text{PF}_6)_2$ were synthesized. The antiproliferative properties of these complexes were investigated. Results suggest that the complexes appear rather inert and the introduction of a carbohydrate moiety does not significantly improve their performance. The investigation of the coordinating properties of the new ligands described in this work will be extended to other metal centers in the future.

Supplementary Materials: The following are available online at <http://www.mdpi.com/1420-3049/25/17/3850/s1>: NMR and ESI-MS spectra of the reported compounds.

Author Contributions: Conceptualization, C.T. and A.B.; methodology, C.T. and D.M.M.; validation, C.T., A.A., L.D., and D.M.M.; formal analysis, F.T., M.R., and P.S.; investigation, F.T., V.S., M.R., S.B., P.S., M.B., A.A., L.D., E.R., and D.M.M.; data curation, F.T., C.T., S.B., A.A., L.D., and D.M.M.; writing—original draft preparation, F.T., C.T., D.M.M., and F.R.; writing—review and editing, all authors; visualization, F.T.; supervision, C.T.; project administration, A.B.; funding acquisition, A.B. All authors read and agreed to the published version of the manuscript.

Funding: This research was funded by the Department of Chemical Sciences (University of Padova), grant number P-DISC #03BIRD2017-UNIPD.

Conflicts of Interest: The authors declare no conflict of interest. The funders had no role in the design of the study; in the collection, analyses, or interpretation of data; in the writing of the manuscript, or in the decision to publish the results.

References

1. Jamieson, E.R.; Lippard, S.J. Structure, Recognition, and Processing of Cisplatin–DNA Adducts. *Chem. Rev.* **1999**, *99*, 2467–2498. [[CrossRef](#)]
2. Ghosh, S. Cisplatin: The first metal based anticancer drug. *Bioorganic Chem.* **2019**, *88*, 102925. [[CrossRef](#)]
3. Diez-Gonzalez, S. *N-Heterocyclic Carbenes: From Laboratory Curiosities to Efficient Synthetic Tools*, 2nd ed.; RSC Catalysis Series; RSC: Cambridge, UK, 2017.
4. Hopkinson, M.N.; Richter, C.; Schedler, M.; Glorius, F. An overview of *N*-heterocyclic carbenes. *Nature* **2014**, *510*, 485–496. [[CrossRef](#)]
5. Huynh, H.V. *The Organometallic Chemistry of N-heterocyclic Carbenes*; John Wiley & Sons, Inc: Hoboken, NJ, USA, 2017.
6. Merics, L.; Albrecht, M. Beyond catalysis: *N*-heterocyclic carbene complexes as components for medicinal, luminescent, and functional materials applications. *Chem. Soc. Rev.* **2010**, *39*, 1903. [[CrossRef](#)]
7. Oehninger, L.; Rubbiani, R.; Ott, I. *N*-Heterocyclic carbene metal complexes in medicinal chemistry. *Dalton Trans.* **2013**, *42*, 3269–3284. [[CrossRef](#)]
8. Liu, W.; Gust, R. Update on metal *N*-heterocyclic carbene complexes as potential anti-tumor metallodrugs. *Co-ord. Chem. Rev.* **2016**, *329*, 191–213. [[CrossRef](#)]
9. Teyssot, M.-L.; Jarrousse, A.-S.; Manin, M.; Chevy, A.; Roche, S.; Norre, F.; Beaudoin, C.; Morel, L.; Boyer, D.; Mahiou, R.; et al. Metal-NHC complexes: A survey of anti-cancer properties. *Dalton Trans.* **2009**, 6894–6902. [[CrossRef](#)]
10. Mora, M.; Gimeno, M.C.; Visbal, R. Recent advances in gold–NHC complexes with biological properties. *Chem. Soc. Rev.* **2019**, *48*, 447–462. [[CrossRef](#)]
11. Tong, K.-C.; Hu, D.; Wan, P.-K.; Lok, C.-N.; Che, C.-M. Anti-cancer gold, platinum and iridium compounds with porphyrin and/or *N*-heterocyclic carbene ligand(s). *Adv. Inorg. Chem.* **2020**, *75*, 87–119. [[CrossRef](#)]
12. Ott, I. Metal *N*-heterocyclic carbene complexes in medicinal chemistry. *Adv. Inorg. Chem.* **2020**, *75*, 121–148. [[CrossRef](#)]
13. Marzano, C.; Gandin, V.; Folda, A.; Scutari, G.; Bindoli, A.; Rigobello, M.P. Inhibition of thioredoxin reductase by auranofin induces apoptosis in cisplatin-resistant human ovarian cancer cells. *Free. Radic. Biol. Med.* **2007**, *42*, 872–881. [[CrossRef](#)] [[PubMed](#)]
14. Porchia, M.; Pelli, M.; Marinelli, M.; Tisato, F.; Del Bello, F.; Santini, C. New insights in Au-NHCs complexes as anticancer agents. *Eur. J. Med. Chem.* **2018**, *146*, 709–746. [[CrossRef](#)] [[PubMed](#)]
15. Dominelli, B.; Correia, J.D.G.; Kühn, F.E. Medicinal Applications of Gold(I/III)-Based Complexes Bearing *N*-Heterocyclic Carbene and Phosphine Ligands. *J. Organomet. Chem.* **2018**, *866*, 153–164. [[CrossRef](#)]
16. Baker, M.V.; Barnard, P.J.; Berners-Price, S.J.; Brayshaw, S.K.; Hickey, J.L.; Skelton, B.W.; White, A.H. Synthesis and structural characterisation of linear Au(I) *N*-heterocyclic carbene complexes: New analogues of the Au(I) phosphine drug Auranofin. *J. Organomet. Chem.* **2005**, *690*, 5625–5635. [[CrossRef](#)]
17. Boselli, L.; Ader, I.; Carraz, M.; Hemmert, C.; Cuvillier, O.; Gornitzka, H. Synthesis, structures, and selective toxicity to cancer cells of gold(I) complexes involving *N*-heterocyclic carbene ligands. *Eur. J. Med. Chem.* **2014**, *85*, 87–94. [[CrossRef](#)] [[PubMed](#)]
18. Cucciolo, M.E.; Trinchillo, M.; Iannitti, R.; Palumbo, R.; Tesaro, D.; Tuzi, A.; Ruffo, F.; D'Amora, A. Sugar-Incorporated *N*-Heterocyclic-Carbene-Containing Gold(I) Complexes: Synthesis, Characterization, and Cytotoxic Evaluation. *Eur. J. Inorg. Chem.* **2017**, 4955–4961. [[CrossRef](#)]

19. Cucciolioto, M.E.; D'Amora, A.; De Feo, G.; Ferraro, G.; Giorgio, A.; Petruk, G.; Monti, D.M.; Merlino, A.; Ruffo, F. Five-Coordinate Platinum(II) Compounds Containing Sugar Ligands: Synthesis, Characterization, Cytotoxic Activity, and Interaction with Biological Macromolecules. *Inorg. Chem.* **2018**, *57*, 3133–3143. [CrossRef]
20. Cucciolioto, M.E.; Bossa, F.D.L.; Esposito, R.; Ferraro, G.; Iadonisi, A.; Petruk, G.; D'Elia, L.; Romanetti, C.; Traboni, S.; Tuzi, A.; et al. C-Glycosylation in platinum-based agents: A viable strategy to improve cytotoxicity and selectivity. *Inorg. Chem. Front.* **2018**, *5*, 2921–2933. [CrossRef]
21. Annunziata, A.; Cucciolioto, M.E.; Esposito, R.; Imbimbo, P.; Petruk, G.; Ferraro, G.; Pinto, V.; Tuzi, A.; Monti, D.M.; Merlino, A.; et al. A highly efficient and selective antitumor agent based on a glucoconjugated carbene platinum(II) complex. *Dalton Trans.* **2019**, *48*, 7794–7800. [CrossRef]
22. Zhao, W.; Ferro, V.; Baker, M.V. Carbohydrate–N-heterocyclic carbene metal complexes: Synthesis, catalysis and biological studies. *Coord. Chem. Rev.* **2017**, *339*, 1–16. [CrossRef]
23. Annunziata, A.; Amoresano, A.; Cucciolioto, M.E.; Esposito, R.; Ferraro, G.; Iacobucci, I.; Imbimbo, P.; Lucignano, R.; Melchiorre, M.; Monti, M.; et al. Pt(II) versus Pt(IV) in Carbene Glycoconjugate Antitumor Agents: Minimal Structural Variations and Great Performance Changes. *Inorg. Chem.* **2020**, *59*, 4002–4014. [CrossRef] [PubMed]
24. Barnard, P.J.; Baker, M.V.; Berners-Price, S.J.; Day, D. Mitochondrial permeability transition induced by dinuclear gold(I)–carbene complexes: Potential new antimetastatic antitumor agents. *J. Inorg. Biochem.* **2004**, *98*, 1642–1647. [CrossRef] [PubMed]
25. Zou, T.; Lum, C.T.; Lok, C.-N.; To, W.-P.; Low, K.-H.; Che, C.-M. A Binuclear Gold(I) Complex with Mixed Bridging Diphosphine and Bis(N-Heterocyclic Carbene) Ligands Shows Favorable Thiol Reactivity and Inhibits Tumor Growth and Angiogenesis In Vivo. *Angew. Chem. Int. Ed.* **2014**, *53*, 5810–5814. [CrossRef] [PubMed]
26. Baron, M.; Bellemin-Lapponnaz, S.; Tubaro, C.; Basato, M.; Bogiatti, S.; Dolmella, A. Synthesis and biological assays on cancer cells of dinuclear gold complexes with novel functionalised di(N-heterocyclic carbene) ligands. *J. Inorg. Biochem.* **2014**, *141*, 94–102. [CrossRef] [PubMed]
27. Bauer, E.B.; Bernd, M.A.; Schütz, M.; Oberkofler, J.; Pöthig, A.; Reich, R.M.; Kühn, F.E. Synthesis, characterization, and biological studies of multidentate gold(I) and gold(III) NHC complexes. *Dalton Trans.* **2019**, *48*, 16615–16625. [CrossRef]
28. Barnard, P.J.; Wedlock, L.E.; Baker, M.V.; Berners-Price, S.J.; Joyce, D.A.; Skelton, B.W.; Steer, J.H. Luminescence Studies of the Intracellular Distribution of a Dinuclear Gold(I) N-Heterocyclic Carbene Complex. *Angew. Chem. Int. Ed.* **2006**, *45*, 5966–5970. [CrossRef]
29. Wedlock, L.E.; Barnard, P.J.; Filipovska, A.; Skelton, B.W.; Berners-Price, S.J.; Baker, M.V. Dinuclear Au(I) N-heterocyclic carbene complexes derived from unsymmetrical azolium cyclophane salts: Potential probes for live cell imaging applications. *Dalton Trans.* **2016**, *45*, 12221–12236. [CrossRef]
30. Mullick, A.B.; Chang, Y.M.; Ghiviriga, I.; Abboud, K.A.; Tan, W.; Veige, A.S. Human cancerous and healthy cell cytotoxicity studies of a chiral μ -dicarbene–digold(II) metallamacrocyclic. *Dalton Trans.* **2013**, *42*, 7440. [CrossRef]
31. Rieb, J.; Dominelli, B.; Mayer, D.; Jandl, C.; Drechsel, J.; Heydenreuter, W.; Sieber, S.A.; Kühn, F.E. Influence of wing-tip substituents and reaction conditions on the structure, properties and cytotoxicity of Ag(I)– and Au(I)–bis(NHC) complexes. *Dalton Trans.* **2017**, *46*, 2722–2735. [CrossRef]
32. Smiataczowa, K.; Kosmalki, J.; Nowacki, A.; Czaja, M.; Warnke, Z. Proton-acceptor properties and capability for mutarotation of some glucosylamines in methanol. *Carbohydr. Res.* **2004**, *339*, 1439–1445. [CrossRef]
33. Anneser, M.R.; Haslinger, S.; Pöthig, A.; Cokoja, M.; Basset, J.-M.; Kühn, F.E. Synthesis and Characterization of an Iron Complex Bearing a Cyclic Tetra-N-heterocyclic Carbene Ligand: An Artificial Heme Analogue? *Inorg. Chem.* **2015**, *54*, 3797–3804. [CrossRef] [PubMed]
34. Scattolin, T.; Bortolamiol, E.; Rizzolio, F.; Demitri, N.; Visentin, F. Allyl palladium complexes bearing carbohydrate-based N-heterocyclic carbenes: Anticancer agents for selective and potent in vitro cytotoxicity. *Appl. Organomet. Chem.* **2020**, e5876. [CrossRef]
35. Govindaraju, V.; Young, K.; Maudsley, A.A. Proton NMR chemical shifts and coupling constants for brain metabolites. *NMR Biomed.* **2000**, *13*, 129–153. [CrossRef]

36. Baron, M.; Battistel, E.; Tubaro, C.; Biffis, A.; Armelao, L.; Rancan, M.; Graiff, C. Single-Step Synthesis of Dinuclear Neutral Gold(I) Complexes with Bridging Di(*N*-heterocyclic carbene) Ligands and Their Catalytic Performance in Cross Coupling Reactions and Alkyne Hydroamination. *Organometallics* **2018**, *37*, 4213–4223. [CrossRef]
37. Collado, A.; Suárez, A.G.; Martín, A.R.; Slawin, A.M.Z.; Nolan, S.P. Straightforward synthesis of [Au(NHC)X] (NHC = *N*-heterocyclic carbene, X = Cl, Br, I) complexes. *Chem. Commun.* **2013**, *49*, 5541–5543. [CrossRef]
38. Gil Rubio, J.; Cámara, V.; Bautista, D.; Vicente, J. Dinuclear Alkynyl Gold(I) Complexes Containing Bridging *N*-Heterocyclic Dicarbene Ligands: New Synthetic Routes and Luminescence. *Organometallics* **2012**, *31*, 5414–5426. [CrossRef]
39. Monticelli, M.; Baron, M.; Tubaro, C.; Bellemin-Laponnaz, S.; Graiff, C.; Bottaro, G.; Armelao, L.; Orian, L. Structural and Luminescent Properties of Homoleptic Silver(I), Gold(I), and Palladium(II) Complexes with nNHC-tzNHC Heteroditopic Carbene Ligands. *ACS Omega* **2019**, *4*, 4192–4205. [CrossRef]
40. Longhi, A.; Baron, M.; Rancan, M.; Bottaro, G.; Armelao, L.; Sgarbossa, P.; Tubaro, C. Possible Synthetic Approaches for Heterobimetallic Complexes by Using nNHC/tzNHC Heteroditopic Carbene Ligands. *Molecules* **2019**, *24*, 2305. [CrossRef]
41. Baron, M.; Tubaro, C.; Biffis, A.; Basato, M.; Graiff, C.; Poater, A.; Cavallo, L.; Armaroli, N.; Accorsi, G. Blue-Emitting Dinuclear *N*-heterocyclic Dicarbene Gold(I) Complex Featuring a Nearly Unit Quantum Yield. *Inorg. Chem.* **2012**, *51*, 1778–1784. [CrossRef]
42. Barnard, P.J.; Baker, M.V.; Berners-Price, S.J.; Skelton, B.W.; White, A.H. Dinuclear gold(I) complexes of bridging bidentate carbene ligands: Synthesis, structure and spectroscopic characterisation. *Dalton Trans.* **2004**, 1038–1047. [CrossRef]
43. Tubaro, C.; Baron, M.; Costante, M.; Basato, M.; Biffis, A.; Gennaro, A.; Isse, A.A.; Graiff, C.; Accorsi, G. Dinuclear gold(I) complexes with propylene bridged *N*-heterocyclic dicarbene ligands: Synthesis, structures, and trends in reactivities and properties. *Dalton Trans.* **2013**, *42*, 10952–10963. [CrossRef] [PubMed]
44. Hemmert, C.; Poteau, R.; Dominique, F.J.-B.D.; Ceroni, P.; Bergamini, G.; Gornitzka, H. Amide-Functionalized Bis(NHC) Systems: Anion Effect on Gold-Gold Interactions. *Eur. J. Inorg. Chem.* **2012**, 3892–3898. [CrossRef]
45. Cure, J.; Poteau, R.; Gerber, I.C.; Gornitzka, H.; Hemmert, C. Dimeric Gold Bis(carbene) Complexes by Transmetalation in Water. *Organometallics* **2012**, *31*, 619–626. [CrossRef]
46. Baron, M.; Tubaro, C.; Basato, M.; Isse, A.A.; Gennaro, A.; Cavallo, L.; Graiff, C.; Dolmella, A.; Falivene, L.; Caporaso, L. Insights into the Halogen Oxidative Addition Reaction to Dinuclear Gold(I) Di(NHC) Complexes. *Chem. - A Eur. J.* **2016**, *22*, 10211–10224. [CrossRef] [PubMed]
47. De Frémont, P.; Singh, R.; Stevens, E.D.; Petersen, J.L.; Nolan, S.P. Synthesis, Characterization and Reactivity of *N*-Heterocyclic Carbene Gold(III) Complexes. *Organometallics* **2007**, *26*, 1376–1385. [CrossRef]
48. Baron, M.; Tubaro, C.; Basato, M.; Biffis, A.; Natile, M.M.; Graiff, C. Dinuclear *N*-Heterocyclic Dicarbene Gold Complexes in I–III and III–III Oxidation States: Synthesis and Structural Analysis. *Organometallics* **2011**, *30*, 4607–4615. [CrossRef]
49. Zhang, C.; Hemmert, C.; Gornitzka, H.; Cuvillier, O.; Zhang, M.; Sun, R.W. Cationic and Neutral *N*-Heterocyclic Carbene Gold(I) Complexes: Cytotoxicity, NCI-60 Screening, Cellular Uptake, Inhibition of Mammalian Thioredoxin Reductase, and Reactive Oxygen Species Formation. *ChemMedChem* **2018**, *13*, 1218–1229. [CrossRef]
50. Ott, I. On the medicinal chemistry of gold complexes as anticancer drugs. *Coord. Chem. Rev.* **2009**, *253*, 1670–1681. [CrossRef]
51. Barnard, P.J.; Berners-Price, S.J. Targeting the mitochondrial cell death pathway with gold compounds. *Co-ord. Chem. Rev.* **2007**, *251*, 1889–1902. [CrossRef]
52. Zhou, Z.; Qiu, J.; Xie, L.; Du, F.; Xu, G.; Xie, Y.; Ling, Q. Synthesis of Chiral Imidazolium Salts from a Carbohydrate and Their Application in Pd-Catalyzed Suzuki–Miyaura Reaction. *Catal. Lett.* **2014**, *144*, 1911–1918. [CrossRef]
53. Salomon, M.F.; Salomon, R.G. The peroxide transfer reaction. *J. Am. Chem. Soc.* **1979**, *101*, 4290–4299. [CrossRef]

Sample Availability: Samples of the compounds are not available from the authors.



© 2020 by the authors. Licensee MDPI, Basel, Switzerland. This article is an open access article distributed under the terms and conditions of the Creative Commons Attribution (CC BY) license (<http://creativecommons.org/licenses/by/4.0/>).

Supplementary Information for

**Synthesis and Biological Studies on Dinuclear Gold(I)
Complexes with Di-(N-Heterocyclic Carbene) Ligands
Functionalized with Carbohydrates**

Federica Tresin ¹, Valentina Stoppa ¹, Marco Baron ¹, Andrea Biffis ¹, Alfonso Annunziata,² Luigi D'Elia ²,
Daria Maria Monti ², Francesco Ruffo ², Marco Roverso ¹, Paolo Sgarbossa ³, Sara Bogialli ¹, Cristina
Tubaro ^{1*}

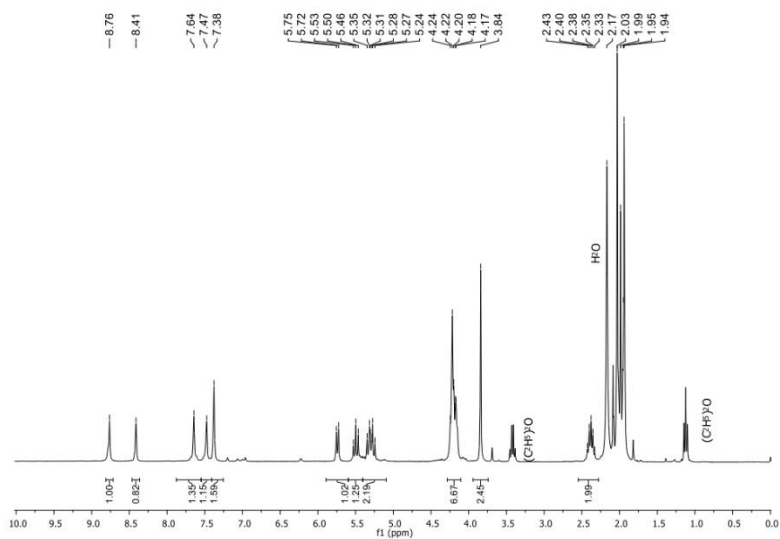
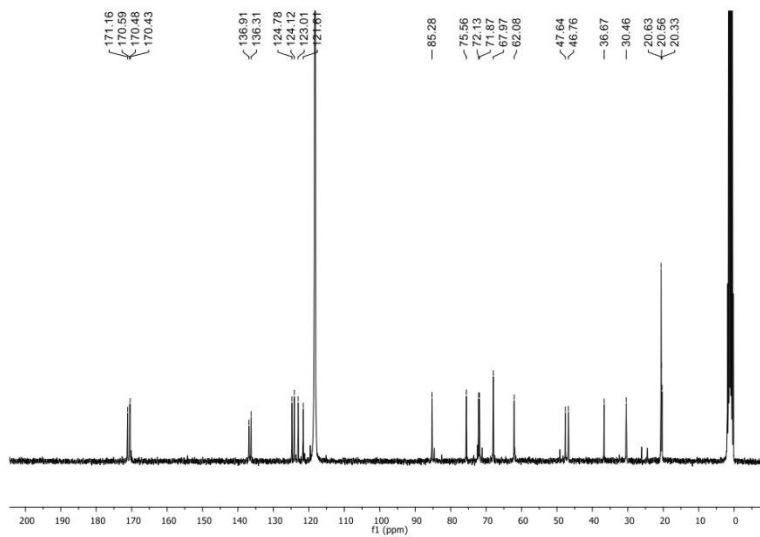
¹ Department of Chemical Sciences, University of Padova, via Marzolo 1, 35131 Padova (Italy).

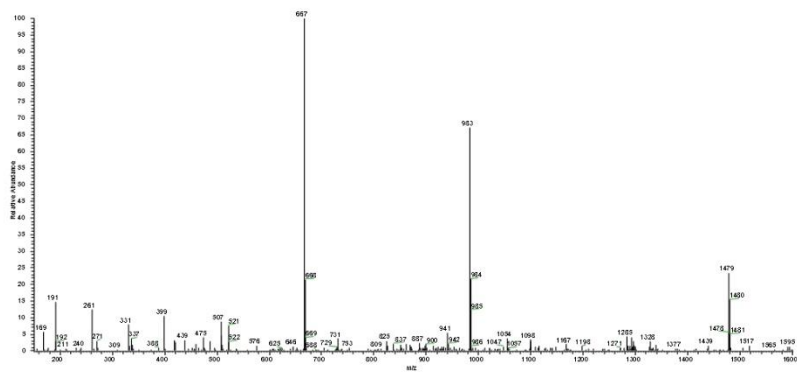
² Department of Chemical Sciences, University of Napoli Federico II, Complesso Universitario di Monte S. Angelo, via
Cintia 21, 80126 Napoli (Italy).

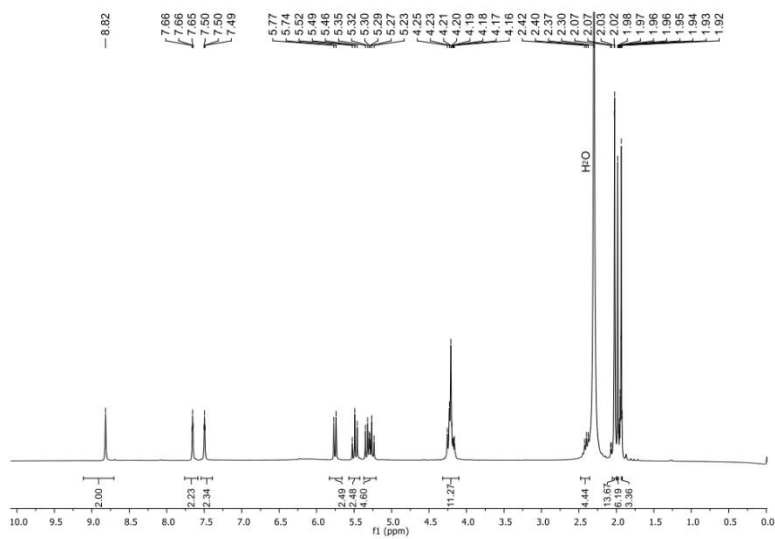
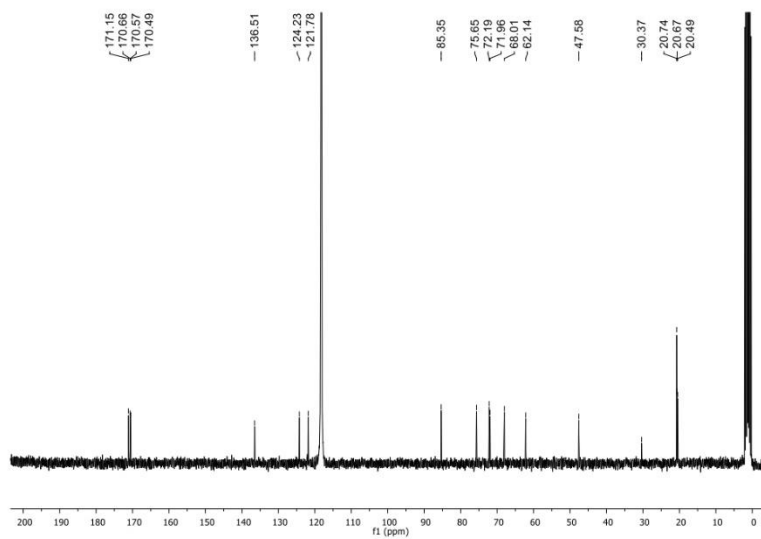
³ Department of Industrial Engineering, University of Padova, via Marzolo 9, 35131 Padova (Italy).

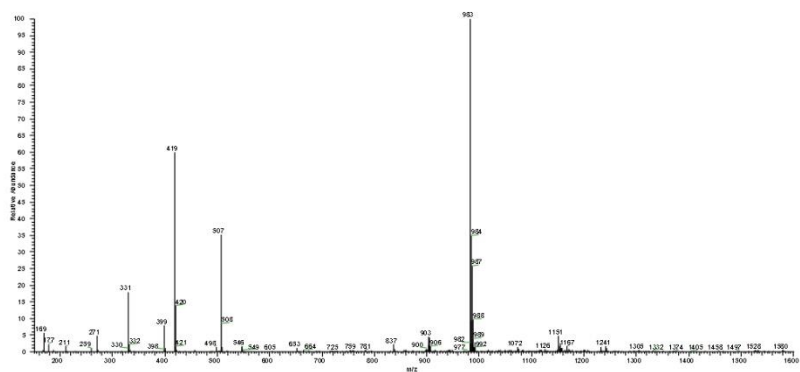
* Correspondence: cristina.tubaro@unipd.it; Tel.: +39-049-8275655 (C.T.).

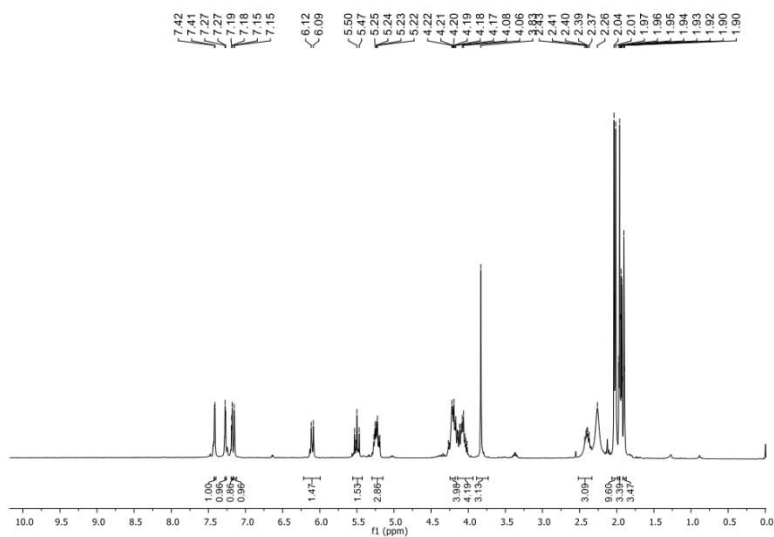
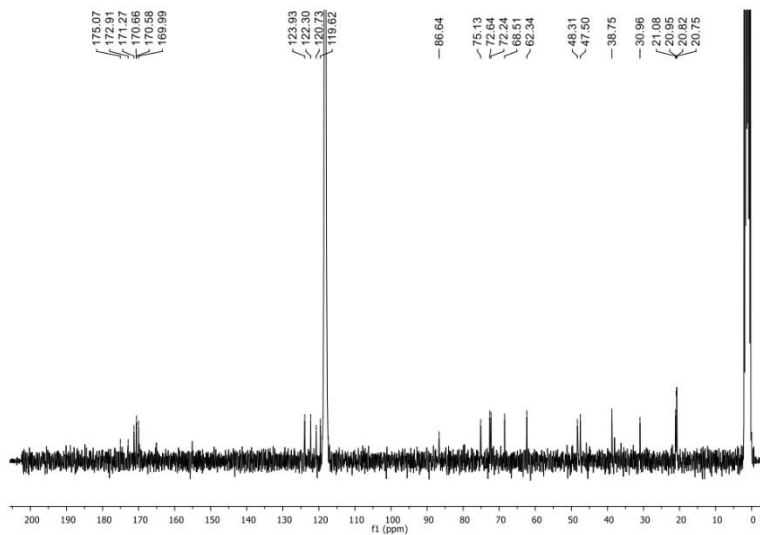
NMR Spectra and ESI-MS spectra for the new compounds

Figure S1: ¹H NMR spectra of L¹-2HPF₆ in CD₃CNFigure S2: ¹³C NMR spectra of L¹-2HPF₆ in CD₃CN

Figure S3: ESI-MS spectra of L¹-2HPF₆

Figure S4: ^1H NMR spectra of $\text{L}^2\text{-2HPF}_6$ in CD_3CN Figure S5: ^{13}C NMR spectra of $\text{L}^2\text{-2HPF}_6$ in CD_3CN

Figure S6: ESI-MS spectra of L²-2HPF₆

Figure S7: ^1H NMR spectra of complex **1** in CD_3CN Figure S8: ^{13}C NMR spectra of complex **1** in CD_3CN

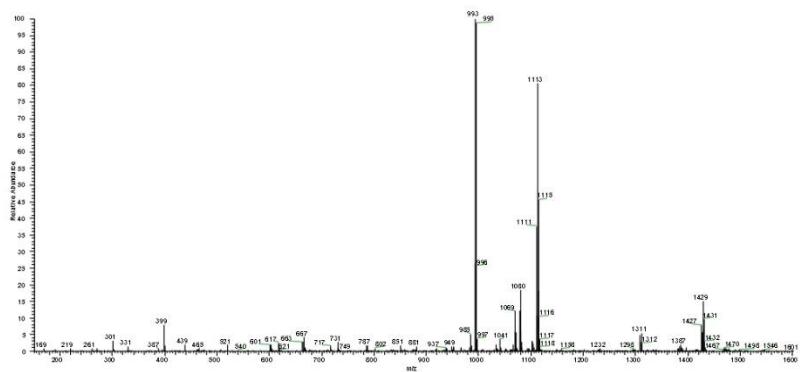
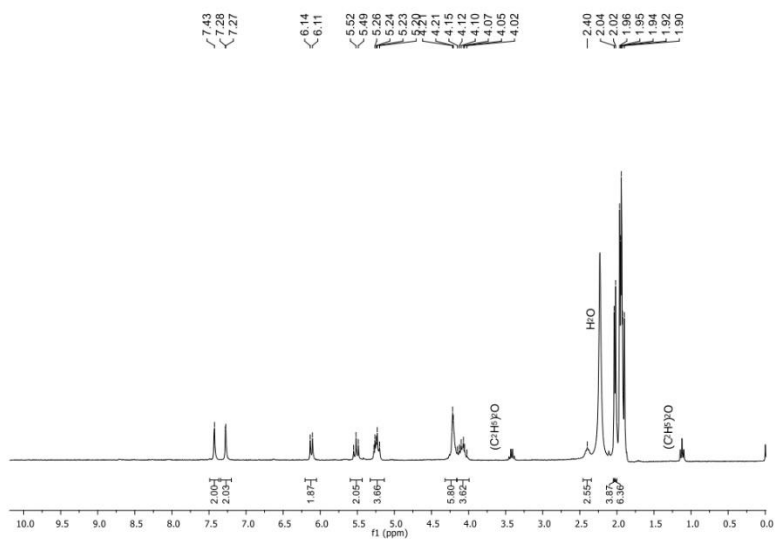
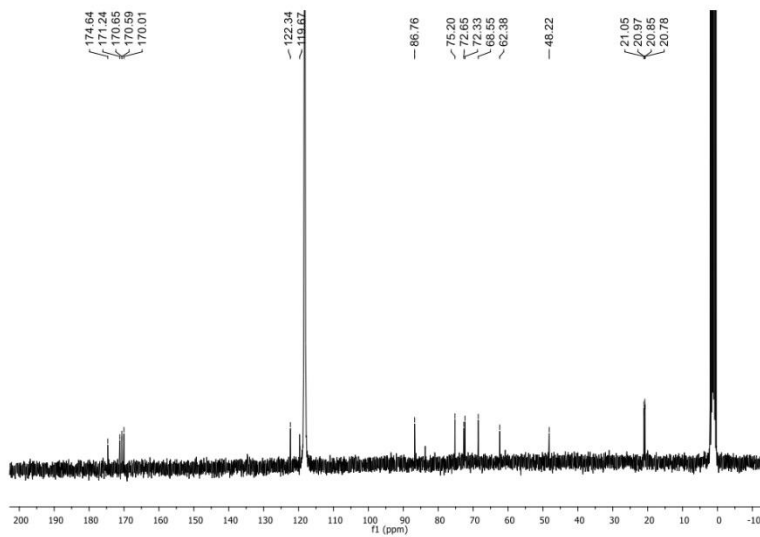


Figure S9: ESI-MS spectra of complex 1

Figure S10: ¹H NMR spectra of complex 2 in CD₃CNFigure S11: ¹³C NMR spectra of complex 2 in CD₃CN

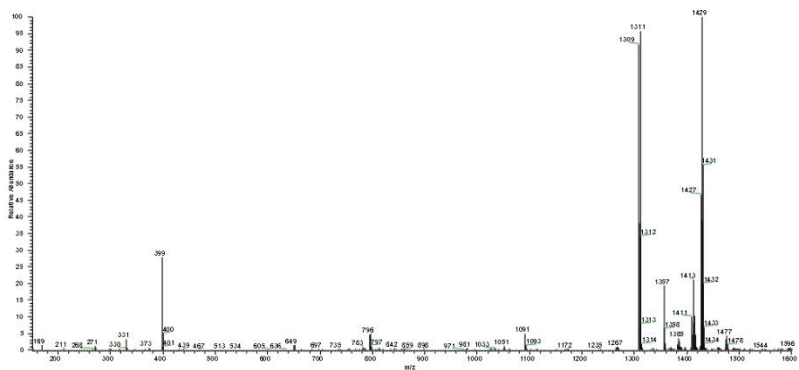
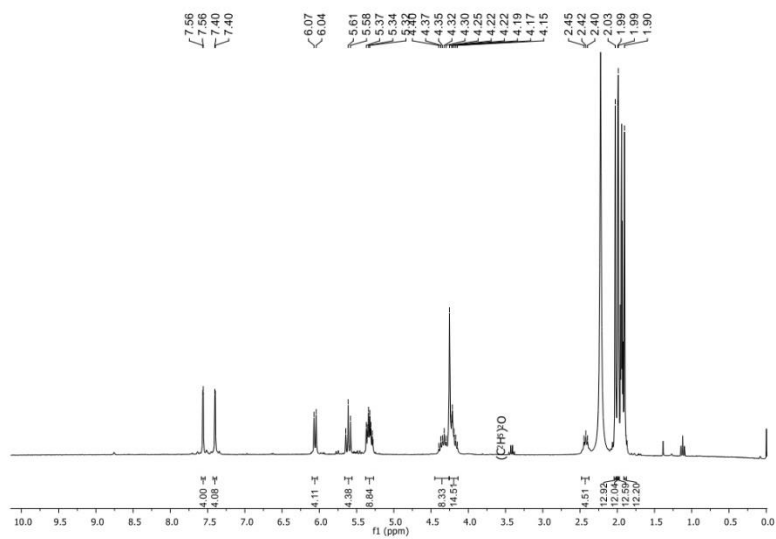
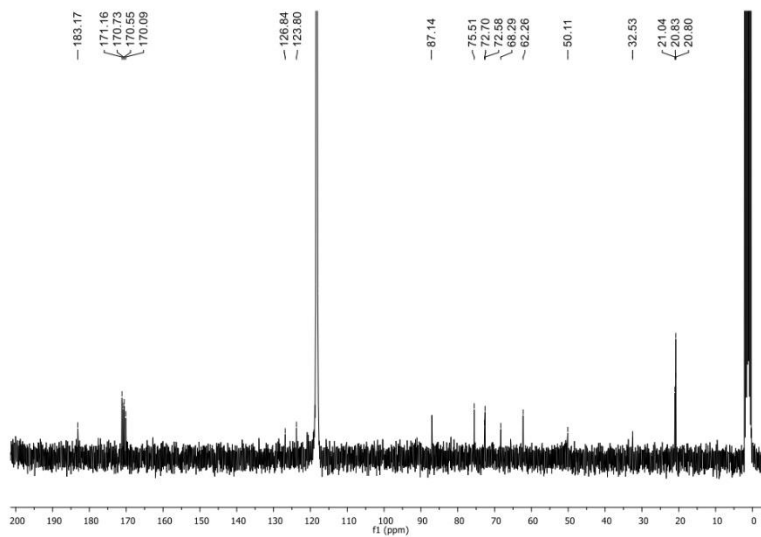
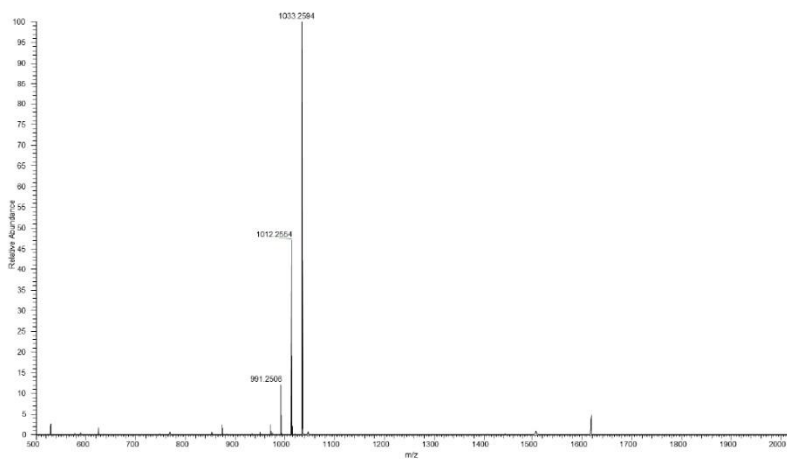
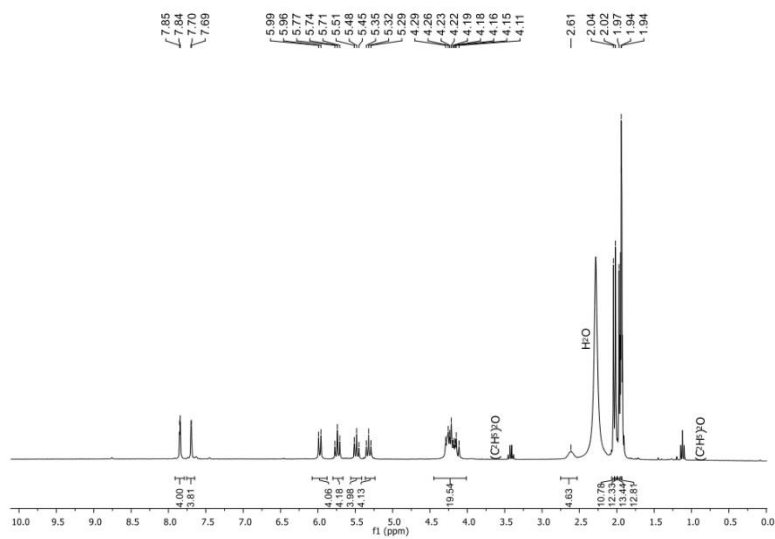
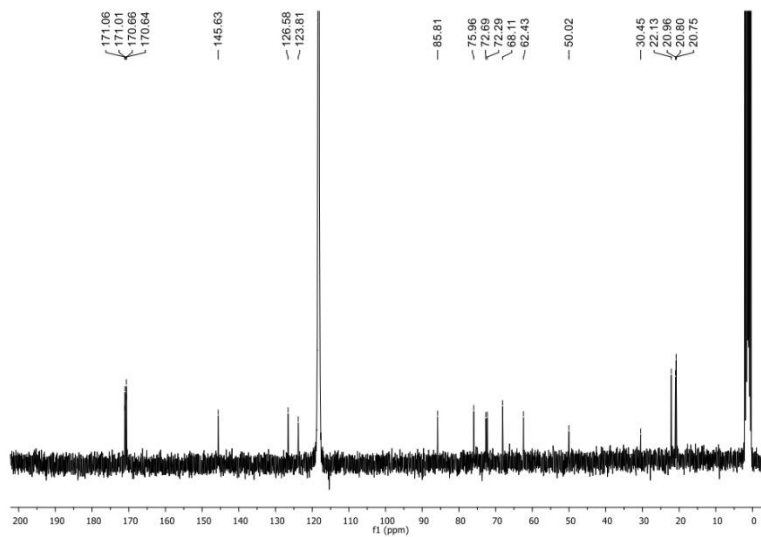


Figure S12: ESI-MS spectra of complex 2

Figure S13: ^1H NMR spectra of complex **3** in CD_3CN Figure S14: ^{13}C NMR spectra of complex **3** in CD_3CN

Figure S15: HRMS of complex 3 in CH₃CN

Figure S16: ^1H NMR spectra of complex **4** in CD_3CN Figure S17: ^{13}C NMR spectra of complex **4** in CD_3CN

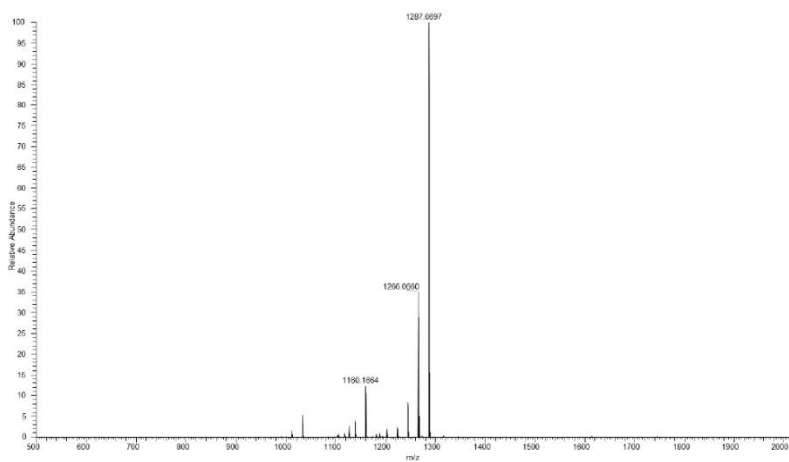
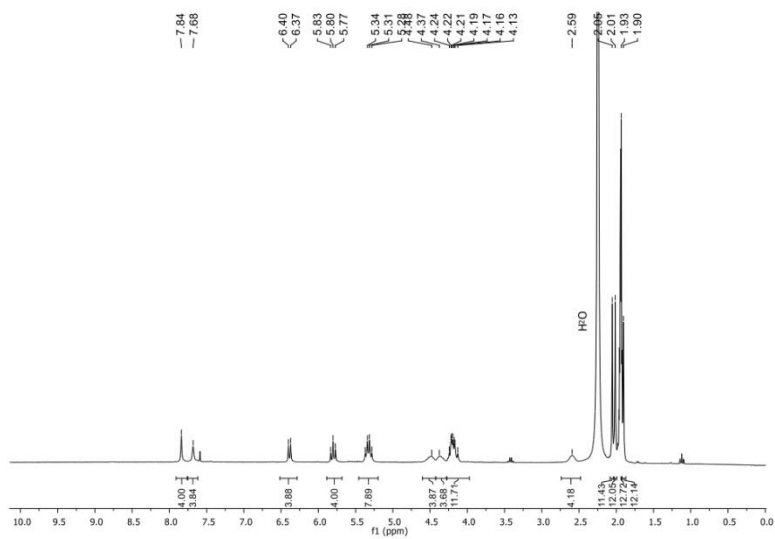
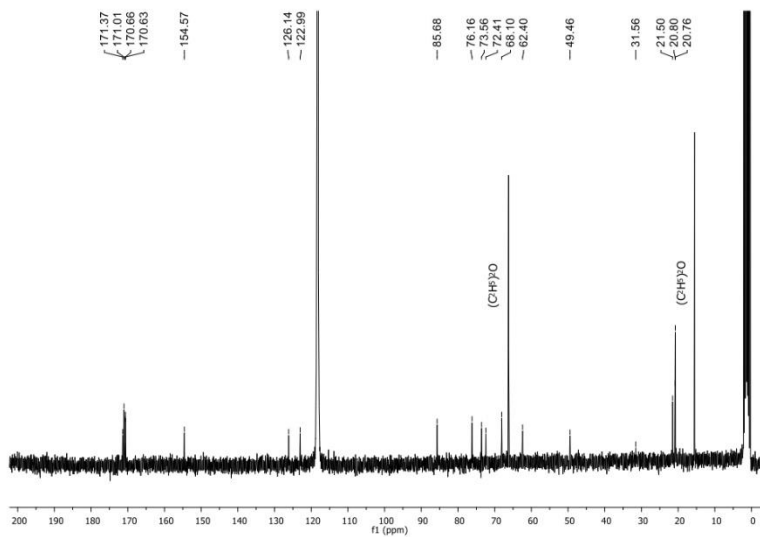
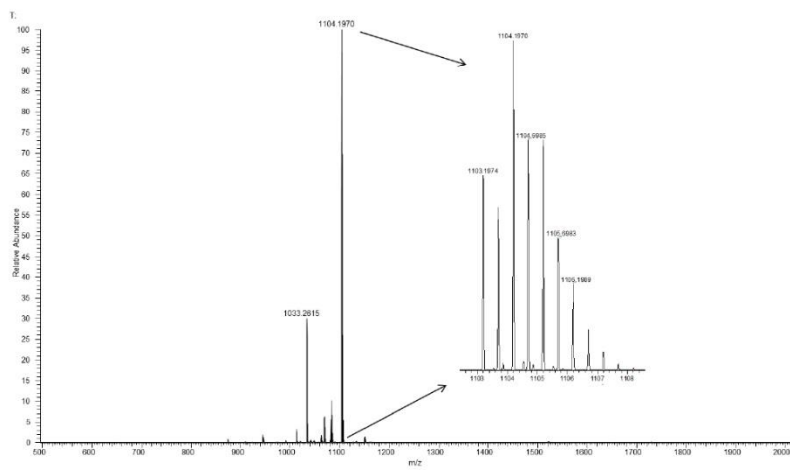


Figure S18: HRMS of complex 4 in CH₃CN

Figure S19: ^1H NMR spectra of complex 5 in CD_3CN Figure S20: ^{13}C NMR spectra of complex 5 in CD_3CN

Figure S21: HRMS of complex 5 in CH₃CN



Towards green extraction methods from microalgae learning from the classics

Paola Imbimbo¹ · Luigi D'Elia¹ · Davide Liberti¹ · Giuseppe Olivieri^{2,3} · Daria Maria Monti¹ Received: 13 May 2020 / Revised: 29 July 2020 / Accepted: 14 August 2020 / Published online: 22 September 2020
© Springer-Verlag GmbH Germany, part of Springer Nature 2020

Abstract

Microalgae started receiving attention as producers of third generation of biofuel, but they are rich in many bioactive compounds. Indeed, they produce many molecules endowed with benefic effects on human health which are highly requested in the market. Thus, it would be important to fractionate algal biomass into its several high-value compounds: this represents the basis of the microalgal biorefinery approach. Usually, conventional extraction methods have been used to extract a single class of molecules, with many side effects on the environment and on human health. The development of a green downstream platform could help in obtaining different class of molecules with high purity along with low environmental impact. This review is focused on technical advances that have been performed, from classic methods to the newest and green ones. Indeed, it is fundamental to set up new procedures that do not affect the biological activity of the extracted molecules. A comparative analysis has been performed among the conventional methods and the new extraction techniques, i.e., switchable solvents and microwave-assisted and compressed fluid extractions.

Keywords Microalgae · Green chemistry · Switchable solvents · Microwave-assisted extraction · Compressed fluid extraction · Lipids

Introduction

In the last years, high-value bioproducts extracted from microalgae achieved a foothold in the market (Pulz and Gross 2004). Compared with conventional crops, microalgae are considered a fast and continuous source of polyunsaturated fatty acids, carotenoids, and proteins, which exert beneficial effects on humans (Vega-López et al. 2004; Zhang et al. 2014). Despite microalgae representing a huge alternative to

conventional feedstocks, three main drawbacks limit their use at large scale: (i) cultivation, (ii) harvesting, and (iii) downstream costs (Günerken et al. 2015; Zhang et al. 2016; Youn et al. 2017; Gifuni et al. 2019).

The main problems related to cultivation are (i) costs associated to the control of growth parameters, especially the temperature, and (ii) risks related to contaminations (Wang et al. 2013; Molina et al. 2019). To control them, microalgae are generally grown in photobioreactors (PBRs), which allow also obtaining high productivity yields and keeping the cultures axenic (Benedetti et al. 2004; Liu et al. 2019). However, as PBRs are very expensive for industrial applications, microalgae are grown in open pond systems (OPS), which are uncontrolled outdoor systems and do not allow a good productivity. OPS have pros (i–iii) and cons (iv–vi), such as (i) a low initial investment (Narala et al. 2016); (ii) a low power demand (Chen et al. 2013); (iii) low operating and maintenance costs (González-Delgado and Kafarov 2011); (iv) high contamination risk (Banerjee and Ramaswamy 2017); (v) requirement of large areas of land (Norsker et al. 2011); and (vi) high water demand to overcome the poor light utilization (Yin et al. 2020). Moreover, cultivations performed in these systems are strongly influenced by weather and

✉ Giuseppe Olivieri
giuseppe.olivieri@wur.nl

✉ Daria Maria Monti
mdmonti@unina.it

¹ Department of Chemical Science, University of Naples Federico II, via Cinthia 4, 80126 Naples, Italy

² Bioprocess Engineering Group, Wageningen University and Research, Droevendaalsesteeg 1, 6700AA Wageningen, the Netherlands

³ Department of Chemical, Materials and Industrial Engineering, University of Naples Federico II, Piazzale Tecchio 80, 80125 Napoli, Italy

environmental conditions. Indeed, controlling the growth parameters, such as temperature, pH, and light intensity is still tricky and may affect the biomass productivity (Carvalho et al. 2006; Slegers et al. 2013; Koley et al. 2019). To face the contaminations, an optimization of highly selective environment is required. Among all the steps involved in the algal biomass production, the harvesting step represents the 20–30% of the overall costs (Rawat et al. 2011; Barros et al. 2015). Thus, the selection of the right technology to harvest the biomass is one of the key issues to make the microalgal exploitation cost-effective at large scale. The high costs are related to several factors, such as the high dilution of the culture that requires an intensive de-watering step; the density of the cells in the medium that is similar to the water density; and the negative charge of algal cells that implies an electrostatic repulsions among them, thus keeping cells in a stable disperse state (Zheng et al. 2012; Hu et al. 2014; Gayen et al. 2019). To date, the most common harvesting industrial procedures are centrifugation, flocculation, coagulation, and immobilization (Drexler and Yeh 2014; Fuad et al. 2018; Hidayah et al. 2019). These techniques present several disadvantages, not only for the elevated energy costs of each operation but also for the low separation efficiency (Danquah et al. 2009; Xu et al. 2010). For these reasons, the optimization of an efficient and economic harvesting procedure is still a challenge.

Another important issue to consider is the selection of the right extraction procedure to be employed. In fact, when extracting molecules from the biomass, one should choose a fully biocompatible buffer which will not alter the bioactivity of the extracted molecule. Currently, conventional extraction techniques involve the use of organic solvents, such as chloroform, acetone, methanol, and diethyl ether to be used in large amounts, for a long time and also the use of dry biomass as a starting material (Ghasemi Naghdi et al. 2016; Saini and Keum 2018; Zhang et al. 2019).

Recently, a new generation of extracting techniques, which do not require the involvement of toxic solvents, is being developed. Much effort has been done to set up green extraction procedures without using toxic solvents, thus minimizing environmental impact (Chemat et al. 2012; Armenta et al. 2019). Moreover, the new techniques allow to reduce the extraction time and to improve the extraction yields, without affecting the biological activity (Esquivel-Hernández et al. 2017; Dixon and Wilken 2018). To date, only few algae strains are considered suitable for the large-scale production (Brennan and Owende 2010; Kothari et al. 2017; De-Luca et al. 2019), such as *Spirulina*, *Chlorella*, *Dunaliella salina*, *Aphanizomenon flosaquae*, *Haematococcus pluvialis*, *Cryptothecodinium cohnii*, and *Shizochytrium* (García et al. 2017).

One way to reduce the overall costs of microalgal cultivation on a large-scale production is the valorization of different

microalgal biomass components (Lam et al. 2018; Chandra et al. 2019). In the last decades, the linear economy has given way to the circular economy, to promote a better use of resources by utilizing wastes and natural products as starting material, and to develop an integrated platform able to produce different bioproducts from biomasses (Bhalamurugan et al. 2018; Mathimani and Pugazhendhi 2019). In this context, microalgal biorefinery could be considered the most efficient and cost-effective approach to obtain different molecules, starting from the one endowed with the highest market value. This requires an appropriate selection of the extraction procedure to be employed. In this review, we will try to provide an overview on the different extraction techniques used for microalgae with a special focus on the improvements obtained.

Organic-solvent extraction techniques

The extraction step represents one of the main drawbacks in algae-based industries (Gifuni et al. 2019). Lipids and carotenoids are commonly recovered by using organic solvents, such as hexane, chloroform, acetone, methanol, and diethyl ether (Saini and Keum 2018). Conventional extractions usually require large amounts of organic solvent and long extraction times and they generally need dry biomass (Mansour et al. 2019; Sati et al. 2019). Moreover, a pretreatment step is often required before the extraction, thus increasing the overall costs (Alzate et al. 2012; Kadir et al. 2018). A brief description of the conventional methods, generally used to extract lipids, is reported, and the results obtained are summarized in Table 1.

The Folch method

The Folch method (Folch 1957) is one of the oldest methods employed for the extraction of lipids from microalgae and cyanobacteria. This procedure is fast and easy; however, it is less sensitive compared with the most recent procedures (Kumar et al. 2015). It requires chloroform and methanol as solvents, and it still represents one of the most used methods to estimate, spectrophotometrically, algal lipids. Banskota et al. (2019) extracted lipids from several microalgal strains. Extractions were performed starting from freeze-dried biomass using chloroform to methanol (2:1). They found that the method was able to extract from 30 to 40% (w/w of dry biomass) of lipids, with the exception of *Nannochloropsis granulata* in which the lipid content was $49.3 \pm 4.0\%$ (w/w of dry biomass). Authors demonstrated also that the lipid content was directly related to ORAC values (Banskota et al. 2019). Schipper et al. (2019) studied novel microalgal strains isolated from extreme desert environments: *Tetraselmis* sp.

Table 1 Different conventional extraction methods and their relative yields

Microalgal species	Extraction method	Solvent	Biomass	Lipid yield (%)	Reference
<i>N. oleoabundans</i>	Folch	Chloroform/methanol	Dry	31.8 ± 6.7	(Banskota et al. 2019)
<i>B. braunii</i>				41.1 ± 5.5	(Banskota et al. 2019)
<i>P. tricorutum</i>				44.8 ± 3.6	(Banskota et al. 2019)
<i>N. granulata</i>				49.3 ± 4.0	(Banskota et al. 2019)
<i>C. sorokiniana</i>				32.3 ± 2.4	(Banskota et al. 2019)
<i>P. aeruginosum</i>				30.9 ± 6.1	(Banskota et al. 2019)
<i>S. obliquus</i>				40.5 ± 7.8	(Banskota et al. 2019)
<i>Scenedesmus</i> sp.				36.3 ± 12.5	(Banskota et al. 2019)
<i>T. chui</i>				32.1 ± 5.5	(Banskota et al. 2019)
<i>T. subcordiformis</i> QUCCCM51				25.6 ± 0.9	(Banskota et al. 2019)
<i>P. maculatum</i> QUCCCM127				28.0 ± 2.0	(Banskota et al. 2019)
<i>N. oculata</i>				24.4	(Wei et al. 2014)
<i>T.subcordiformis</i>				22.2	(Wei et al. 2014)
<i>C. acidophila</i> LAFIC-004	Bligh and Dyer	Chloroform/methanol/water	Dry	54.6	(Souza et al. 2017)
<i>I. galbana</i>				25.3 ± 0.2	(Bonfanti et al. 2018)
<i>C. sorokiniana</i>				29.9	(Rasouli et al. 2018)
<i>M. capsulatus</i>				21.8	(Rasouli et al. 2018)
<i>C. vulgaris</i>		Chloroform/methanol		10.4	(Zullaikeh et al. 2019)
<i>G. phlegrea</i>	Soxhlet	Chloroform/methanol	Dry	79 ± 26	(Imbimbo et al. 2019)
<i>S. obliquus</i>				17.4 ± 0.4	(Wang et al. 2019)
<i>Chlorophyta</i> sp.		<i>n</i> -Hexane/ether		18.3 ± 0.4	(Yusuff 2019)
<i>C. gracilis</i>				12.3	(Kanda et al. 2020)
<i>P. carterae</i>		<i>n</i> -Hexane		7.5	(Kanda et al. 2020)
<i>C. vulgaris</i>		Heptane		57.5 ± 0.5	(Minyak et al. 2017)

and *Picochlorum* sp., characterized by their tolerance to high temperature and to high CO₂ concentrations. The species were isolated, and lipid extraction showed that the two novel strains contained significant amounts of lipids, up to 25.6 ± 0.9% and 28.0 ± 2.0% (w/w of dry biomass), for *Tetraselmis* sp. and *Picochlorum* sp., respectively. The method is very reliable as different authors reported the same extraction yield for the same strain (Danquah et al. 2009; Wei et al. 2014).

Bligh and Dyer

The Bligh and Dyer method (Bligh and Dyer 1959) is similar to Folch method. It allows for the extraction of lipids from homogenized cells, generally using a mixture of chloroform/methanol. It is a rapid and effective procedure, thus becoming a standard method for the lipid content determination in biological tissues (Iverson et al. 2001).

Souza and co-workers (Souza et al. 2017) studied the acidophilic microalga *Chlamydomonas acidophila* LAFIC-004 performing a lipid extraction by the Bligh and Dyer method

and obtained 54.6% (w/w of dry biomass) of lipids. Bonfanti et al. (2018) performed lipid extraction starting from *Isochrysis galbana*, with a 25.3 ± 0.2% (w/w of dry biomass) yield. Rasouli and co-workers (Rasouli et al. 2018) extracted about 30% of lipids from *Chlorella sorokiniana*, a value similar to that reported using the Folch method (Schipper et al. 2019), thus suggesting that all the methodologies are able to extract the same amount of lipids when the same strain and the same experimental procedure are followed.

Soxhlet extraction

Soxhlet extraction is a conventional procedure employed for the extraction of lipids and carotenoids. It is performed by using solvents at boiling temperature and ambient pressure, and even if it requires high amount of solvents and a long extraction time, it provides high yields and does not affect the bioactivity of the extracted molecules. We recently reported a Soxhlet extraction with chloroform to methanol (2:1) to obtain lipids from *Galdieria phlegrea* (Imbimbo et al. 2019).

This procedure allowed obtaining a recovery of $79 \pm 26\%$ (w/w of dry biomass) of lipids starting from the dried biomass (Imbimbo et al. 2019). Yusuff reported an oil extraction performed by Soxhlet from the green microalga *Chlorophyta* sp. The extraction was performed by using *n*-hexane to ether (4:1) mixture and allowed a yield of $18.3 \pm 0.4\%$ (w/w of dry biomass) (Yusuff 2019). Kanda and colleagues used two different microalgae strains to extract lipids: *Chaetoceros gracilis* and *Pleurochrysis carterae*. Extractions were performed by Soxhlet using pure *n*-hexane. This technique allowed achieving yields of 12.3% (w/w of dry biomass) for *C. gracilis* and 7.5% (w/w of dry biomass) for *P. carterae* (Kanda et al. 2020).

Green extraction techniques

Recently, the demand for greener, safer, and more natural products that do not require the involvement of toxic solvent increased. The development of green extraction procedures to recover valuable compounds from natural sources represents a significant advance. These eco-friendly techniques allow obtaining bioactive products by reducing or completely replacing toxic solvents, thus minimizing the environmental impact, in agreement with several Green Chemistry principles (Capello et al. 2007; Anastas and Eghbali 2010; Jeevan Kumar et al. 2017). Moreover, a reduction in the extraction time and an improvement in the extraction yields have been obtained. Nevertheless, only few innovative techniques succeeded so far.

Ionic liquids and switchable solvents

Ionic liquids (ILs) are organic solution of salts that can melt at mild temperature (< 100 °C). They are typically composed of a large number of inorganic or organic cations and are characterized by synthetic flexibility and thermal stability. Moreover, they are non-volatile and non-flammable (Vekariya 2017; Harris et al. 2018), being a good alternative to conventional solvents. They are generally employed for lipid extraction; however, to date, only limited papers are available in literature (Motlagh et al. 2019). One of the main drawbacks of ILs is the unrealistic application at industrial scale, due to their costs and the environmental impact (Zhang et al. 2008). Indeed, many ILs have been proved to be not harmful for humans, but their synthesis involves many steps that require expensive, toxic, and volatile reagents (Dominguez de Maria 2017; Harris et al. 2018; Singh and Savoy 2020). In recent years, a second generation of ILs has been developed: switchable solvents (SSs). First reported by Philipp Jessop et al. (2005), SSs are non-volatile liquids able to switch from hydrophobic to hydrophilic state and vice versa

in response to external stimuli, such as temperature or pH variation and/or the addition or removal of a gas (i.e., CO₂) (Al-Ameri and Al-Zuhair 2019; Do Yook et al. 2019). Theoretically, these SSs have many pros: (i) they allow performing cascade extractions of high-value molecules, (ii) it is possible to recover and reuse the solvent; thus, they are considered economically competitive and they require low energy consumption (iii); (iv) they are eco-friendly; (v) they are highly selective; and (vi) they enable extractions in a short time (Pollet et al. 2011; Jeevan Kumar et al. 2017; Clarke et al. 2018). For all these reasons, the second generation of SSs is considered green (Vanderveen et al. 2014; Jeevan Kumar et al. 2017). However, many cons have emerged with respect to solvent loss. This is mainly due to (i) the use of CO₂ in the switching process; (ii) the impossibility to completely remove the solvent from the residual biomass after the process; and (iii) the release of the solvent in water. To improve SS properties, functional groups may be incorporated into the structure during the chemical synthesis, with increase in production costs (Clarke et al. 2018). Nowadays, primary, secondary, and tertiary amines are among the most SSs (Schuur et al. 2019). Table 2 reports a comparison between the lipid yield extraction by using SSs and conventional methods.

Research on SSs is quite recent. In 2018, Cicci et al. (2018) used *N,N*-dimethyl-cyclohexylamine (DMCHA) on the wet biomass of *Scenedesmus dimorphus* to extract lipids. The lipid yield was 35.6% (w/w of dry biomass), about 1.2-fold more than the yield obtained by Gour and colleagues with a conventional method (Bligh and Dyer) (Gour et al. 2020). Nevertheless, the experimental procedure seemed to be able to extract similar amount of lipids independently from the strain. Indeed, the lipid yields obtained by Cicci et al. (2018) on *Scenedesmus dimorphus* can be compared with the lipid yield obtained by Samori et al. (2013) on *Tetraselmis suecica* (31.9%). Instead, Du et al. (2013) showed that *N*-ethylbutylamine (EBA) was able to extract lipids from *Desmodesmus* sp. with a yield of 16.8% (w/w of dry biomass), a value lower than that obtained by Samori and colleagues who used DMCHA (29.2%) (Samori et al. 2013). Indeed, the yield was higher than that obtained by the Bligh and Dyer method (Du et al. 2013; Samori et al. 2013). Probably, the tertiary amine DMCHA allows a better extraction of the lipid fraction from the biomass, as it is more hydrophobic than the secondary amine EBA. Afterwards, Du et al. (2018) showed that, starting from a stressed culture of *Neochloris oleoabundans*, EBA allowed to obtain an increase in the lipid yield, from 47.0 to 61.3% (w/w of dry biomass), only by increasing the number of extractions. In this case, authors found that EBA extracted about 4 times more lipids than the Bligh and Dyer method. It has to be noticed, however, that the switch back has not been reported in literature yet, so that the use of SSs is still far from being used in a biorefinery approach.

Table 2 Yields obtained with switchable solvent method from different microalgae

Microalgal species	Extraction method	Solvent	Biomass	Lipid yield (%)	Fold increase	Reference
<i>S. dimorphus</i> (UTEX 1237)	Switchable solvent	DMCHA	Wet	35.6 ± 1.9	1.2	(Cieci et al. 2018)
<i>S. dimorphus</i> (Sd12)	Bligh and Dyer	Chloroform/methanol/water	Dry	30.7		(Gour et al. 2020)
<i>N. gaditana</i>	Switchable solvent	DMCHA	Wet	57.9 ± 1.3	1.3	(Samori et al. 2013)
	Bligh and Dyer	Chloroform/methanol/water	Dry	45.1 ± 0.9		(Samori et al. 2013)
<i>T. suecica</i>	Switchable solvent	DMCHA	Wet	31.9 ± 1.5	1.3	(Samori et al. 2013)
	Bligh and Dyer	Chloroform/methanol/water	Dry	25.4 ± 2.6		(Samori et al. 2013)
<i>D. communis</i>	Switchable solvent	DMCHA	Wet	29.2 ± 0.9	1.6	(Samori et al. 2013)
	Bligh and Dyer	Chloroform/methanol/water	Dry	17.8 ± 0.1		(Samori et al. 2013)
<i>Desmodesmus</i> sp.	Switchable solvent	EBA	Wet	16.8 ± 0.5	1.3	(Du et al. 2013)
	Bligh and Dyer	Chloroform/methanol/water	Dry	12.8 ± 0.6		(Du et al. 2013)
<i>N. oleabundans</i>	Switchable solvent	EBA	Wet	47.0	1	(Du et al. 2017; Du et al. 2018)
	Bligh and Dyer	Chloroform/methanol/water	Dry	13.1		(Du et al. 2017; Du et al. 2018)
<i>Chlorella</i> sp.	Switchable solvent	EBA	Wet	12.3 ± 3.2	3.2*	(Al-Ameri and Al-Zuhair 2019)
					1.3**	
		DMCHA		13.3 ± 0.4	3.5*	(Al-Ameri and Al-Zuhair 2019)
					1.4**	
		Dipropylamine		7.0 ± 1.3		(Al-Ameri and Al-Zuhair 2019)
	Conventional	[Bmim][PF6]	Dry	3.8 ± 1.1		(Al-Ameri and Al-Zuhair 2019)
		<i>n</i> -Hexane		9.4 ± 0.7		(Al-Ameri and Al-Zuhair 2019)

*With respect to [Bmim][PF6]

**With respect to *n*-hexane

Microwave-assisted extraction

Microwave-assisted extraction (MAE) involves the use of microwaves to heat up the solvent in contact with the cell thus allowing to extract pigments, lipids, and other bioactive molecules (Jain et al. 2015). The heating is caused by two phenomena: dipole rotation and ionic conduction, which may happen individually or simultaneously (Tatke and Jaiswal 2011). MAE is generally performed in closed systems to avoid heating dissipation. By this way, the heating mechanism is targeted and selective, thus reducing the extraction time and improving the final yield. However, the main limitation of this method is the high temperature required that might affect the bioactivity of the extracted molecules. A study from Mahfud's group indicated that MAE was able to increase by almost 10 times the lipid extraction yield in *Spirulina platensis*, with respect to Soxhlet (Kalsum et al. 2019), when *n*-hexane was used as solvent. These and other results are reported in Table 3, with a comparison with conventional methods.

In the extraction processes using microwave, the use of a mixture of solvents may result in an increase of the yield. As an example, the mixture *n*-hexane/methanol is a non-polar solvent able to solve oils from the matrix cells of microalgae. On the other hand, methanol allows microalgae to absorb

more microwave energy with a consequent increase in microalgal disruption (Kalsum et al. 2019).

Krishnan and colleagues studied the importance of different ILs in the MAE extraction system on *Chlorella vulgaris*. Interestingly, they found that the extraction yield increased from 10.9 (Bligh and Dyer method) to 19.2% (w/w of dry biomass) when the 1-octyl-3-methylimidazolium acetate ([Omim][OAc]) was used (Krishnan et al. 2020). In general, they found that the polarity of the ILs and the electronegativity of the anions used played an important role in the type of lipids extracted: the higher the hydrophobicity of the anion used, the higher the extraction of non-polar compounds.

Recently, Zghaibi et al. (2019) found that it was possible to use MAE to extract lipids from *Nannochloropsis* sp. by using only 10% NaCl (6.9% yield). In particular, the lipid extraction yield was similar with respect to Soxhlet extraction (4.5%), and lower with respect to the Bligh and Dyer (18%). However, MAE fully replaced the use of organic and harmful solvents, and, noteworthy, a better quality of lipids was obtained (polyunsaturated fatty acids and omega-3) (Zghaibi et al. 2019). It has to be considered that water, which as a highly polar solvent, can absorb microwave energy, and NaCl can improve the dielectric loss responsible for converting microwave energy into heat. The result is a higher efficiency in PUFA recovery.

Table 3 Yields obtained with MAE method from different microalgae

Microalgal species	Extraction method	Solvent	Biomass	Operative parameters	Lipid yield (%)	Fold increase	Reference	
<i>S. platensis</i>	MAE	Methanol/ <i>n</i> -hexane	Dry	600 W; 40 min	12.5	9.6	(Kalsum et al. 2019)	
	Soxhlet	<i>n</i> -Hexane			1.3		(Kalsum et al. 2019)	
<i>C. vulgaris</i>	MAE	Chloroform/methanol/water [Omim][OAc] 2.5%		700 W; 10 min	19.2	1.8	(Krishnan et al. 2020)	
	Bligh and Dyer	Chloroform/methanol/water			10.9		(Krishnan et al. 2020)	
<i>Nannochloropsis</i> sp.	MAE	Water/sodium chloride 10%		800 W; 30 min	6.9	1.5*	(Zghaibi et al. 2019)	
	Soxhlet	<i>n</i> -hexane			4.5		0.38**	(Zghaibi et al. 2019)
	Bligh and Dyer	Chloroform/methanol/water			18			(Zghaibi et al. 2019)

*With respect to Soxhlet

**With respect to Bligh and Dyer

Compressed fluid extractions

Compressed fluid extractions are considered valuable green alternatives to conventional extractions. They include subcritical water extraction (SWE), pressurized liquid extraction (PLE), and supercritical fluid extraction (SFE). Solvents involved in PLE and SWE are maintained at a temperature above the boiling point and at a pressure high enough to keep fluids in their liquid states (Ramos et al. 2002). On the other hand, SFE operates at temperature and pressure above the critical point of the solvent selected (Herrero et al. 2013). These conditions allow for the increase of diffusivity of the solvent, thus improving the penetration of the solvent into the matrix (Phelps et al. 1996). Besides the differences between these techniques, they all require minimum amount of GRAS solvents to perform selective extraction of bioactive compounds, without affecting the bioactivity or the chemical structure (Herrero and Ibañez 2018). Unfortunately, they are still not diffused due to the high investment costs (Herrero and Ibañez 2018). So far, CO₂ is the most used solvent, especially in supercritical extractions (Goto et al. 2015). CO₂ is an economic, non-harmful, non-flammable, and recyclable solvent. Due to its thermodynamic properties, at supercritical conditions, CO₂ shows a high diffusivity and a high density that allow a better penetration into the matrix (Goto et al. 2015; Molino et al. 2020). However, supercritical CO₂ (ScCO₂) is limited to the extraction of non-polar or low polar compounds (Gilbert-López et al. 2015; Gallego et al. 2019). To overcome this problem, a low amount of co-solvent (e.g., ethanol) can be used to increase the CO₂ polarity.

According to this, Nobre and co-workers performed a lipid extraction starting from the dried biomass of *Nannochloropsis* sp. (NANNO-2) by using ScCO₂ in the presence and in the absence of a co-solvent (20% ethanol). Authors found that ScCO₂ combined with ethanol was able to increase lipid yield,

as 45% (w/w of dry biomass) of lipid yield was obtained with respect to 32% yield (w/w of dry biomass), in the absence of co-entrainer (Nobre et al. 2013). Moreover, Zullaikah et al. (2019) performed a lipid extraction from the wet raw biomass of *Chlorella vulgaris* by SWE. Besides the co-solvent, time and temperature may also affect the extraction yields. For this reason, experiments were performed in the presence or absence of co-solvents, at different temperatures and different time. In particular, chloroform, methanol, ethanol, ethyl acetate, and *n*-hexane were tested as co-solvents. Extractions were performed at 160 °C, 80 bar, at 160 °C, 180 °C and 200 °C, for 15 min, 30 min, 1 h, 3 h, and 5 h. All the results were then compared with conventional Bligh and Dyer extraction. The study revealed that SWE performed at 200 °C, 80 bar for 30 min, using ethyl acetate as co-solvent, gave the highest lipid yield (65.94%, w/w of dry biomass), while conventional chloroform/methanol extraction allowed for the obtaining of a lipid yield of 10.43% (w/w of dry biomass). Altenhofen da Silva and co-workers evaluated the effect of supercritical carbon dioxide (ScCO₂) on freeze-dried biomass of *Desmodium ssp.* *subspicatus*. Extractions were performed comparing two different pressures (20 and 30 MPa, that correspond to 200 and 300 bar, respectively) at 60 °C. Authors found out that a direct correlation was observed with pressure and lipid yield, as, at 30 MPa, 45% of lipids were recovered, a value which is almost the double of that obtained at 20 MPa or with Soxhlet (23% at and 20%, respectively) (Altenhofen et al. 2016).

Zimmerer et al. (2019) employed *Phaeodactylum tricornutum* dry biomass for lipid extraction. Cells were disrupted by ultrasonication prior the extraction with ScCO₂. Among the different pressures and temperatures tested, 90 °C and 621 bar were found to be the best conditions, as a 25% yield was obtained (w/w of dry biomass). As a reference, lipids were extracted by Folch method, using a mixture of

water, methanol, and chloroform. The lipid yield obtained by the conventional method was 28% (w/w of dry biomass). He and co-workers set up a process to obtain lipids from *Isochrysis* sp. dried biomass. Lipids were extracted by 3 cycles of 5 min each of PLE, at 103 bar, 80 °C, using two different solvents: *n*-hexane and ethanol. Soxhlet extraction (with hexane) and Folch method (with a mixture of chloroform/methanol/water) were performed to compare the extraction yields. PLE with *n*-hexane gave a higher yield (34.42 %) when compared with Soxhlet extraction performed with the same solvent (about 19% yield). However, PLE performed by using ethanol improved the process, as the lipid yield was 38.94% (w/w of dry biomass) (He et al. 2019).

We recently reported a process intensification to obtain three different high-value molecules in a biorefinery approach (Imbimbo et al. 2019). In particular, we improved lipid extraction as the third step of the cascade process. The extraction was performed using pure CO₂ as solvent, at 350 bar, 60 °C for 100 min starting from the wet biomass of *Galdieria phlegrea*. The yield was then compared with the one obtained by a conventional extraction performed with 0.37% NaCl in

chloroform/methanol (2:1) on dry biomass. SFE allowed for the obtaining of 18.4% yield (w/w of dry biomass), in comparison with 11% yield (w/w of dry biomass) obtained by the conventional extraction method (Imbimbo et al. 2020). All the extraction yields are reported in Table 4.

Conclusions

Microalgae represent a natural source of bioactive compounds to be used in pharmaceutical, nutraceutical, cosmetic, and food sectors. In particular, many hydrophobic molecules endowed with special biological activity can be extracted from microalgae and used. Of course, during extraction, many parameters have to be considered. An ideal extraction method should allow to operate at low costs and to preserve both the original characteristics of the isolated molecule and of the residual biomass. Green extraction techniques seem to combine environmentally friendly and cost-effective extractions. Most of them are economically and environmentally sustainable and non-toxic and can increase the selectivity and

Table 4 Yields obtained with compressed fluid extraction methods from different microalgae

Microalgal species	Extraction method	Solvent	Biomass	Lipid yield (%)	Fold increase	Reference
<i>Nannochloropsis</i> sp. (NANNO-2)	SFE	CO ₂	Dry	34	1.3*	(Nobre et al. 2013)
		CO ₂ + 20% ethanol		45		(Nobre et al. 2013)
	Soxhlet	<i>n</i> -Hexane		40.7		(Nobre et al. 2013)
		Ethanol		50.6		(Nobre et al. 2013)
		Chloroform/methanol/water		25.3		(Nobre et al. 2013)
<i>G. phlegrea</i>	SFE	CO ₂	Wet	18.4 ± 0.5	1.7	(Imbimbo et al. 2020)
	Conventional	Chloroform/methanol/sodium chloride	Dry	11 ± 0.3		(Imbimbo et al. 2020)
<i>C. vulgaris</i>	SWE	Water/ethyl acetate	Wet	65.9	6.3	(Zullaikah et al. 2019)
	Bligh and Dyer	Chloroform/methanol	Dry	10.4		(Zullaikah et al. 2019)
<i>D. subspicatus</i>	SFE	<i>n</i> -Hexane	Dry	45	2.3	(Altenhofen et al. 2016)
	Soxhlet	Chloroform/methanol/water		20		(Altenhofen et al. 2016)
<i>P. tricornutum</i>	SFE	CO ₂	Dry	25	0.9	(Zimmerer et al. 2019)
	Folch	Chloroform/methanol/water		28		(Zimmerer et al. 2019)
<i>Isochrysis</i> sp.	PLE	<i>n</i> -Hexane	Dry	34.41	1.4**	(He et al. 2019)
	PLE	Ethanol		38.94	1.8***	(He et al. 2019)
	Folch	Chloroform/methanol/water		25.36	1.5**	(He et al. 2019)
	Soxhlet	<i>n</i> -Hexane		19	2***	(He et al. 2019)

*With respect to SFE in absence of co-solvent

**With respect to Folch

***With respect to Soxhlet

extraction efficiency (Dominguez de María 2017; Häckl and Kunz 2018; Singh and Savoy 2020). However, all of them have pros and cons with respect to the industrial benchmark of extraction with organic solvent.

In particular, MAE is a green technique used to recover different thermo-stable molecules. Of course, this can be a problem in the case of thermolabile molecules as the experimental conditions used may affect the physical-chemical properties of the isolated molecules. Furthermore, the efficiency of the extraction is often lower with respect to organic solvents.

Compressed fluid extractions can represent an excellent alternative to recover thermolabile molecules. The major advantage resides in the possibility to recover and recycle the solvent. Furthermore, the solvent polarity can be tuned by combining the neutral CO₂ with polar co-solvents, such as ethanol or isopropanol. The major limitation of compressed fluid extractions is represented by its initial investment costs. Lab-scale tests seem efficient when achieving > 300-bar pressure, which is often economically unfeasible at industrial scale. In case of switchable solvents, solvent separation and recycle are the main advantage. Furthermore, the tunability of the polarity allows these solvents to extract both hydrophobic and hydrophilic molecules only by switching a chemical-physical factor. What is still a pending point for SSs is their effect on the residual biomass after the extraction. Unfortunately, there is still much effort to be done to use these solvents, as no evidence of their extraction abilities have been reported after the switch.

Generally speaking, one should keep in mind that microalgae can be used as an excellent source of bioactive molecules provided that a biorefinery approach has to be used. Thus, microalgae costs have to be paid by obtaining more than a class of molecules, starting from the one with the highest market value. So, if the biorefinery approach includes downstream processes able to fulfill the requirements of Green Chemistry, it will end up with a new and sustainable process. With respect to green extraction techniques of lipids and pigments, less is known on two important aspects: the residual amount of solvent in the biomass and, mainly, the effect of the extraction on the other molecules in the leftover spent biomass. This review provides a step further in the extraction knowledge that can help to valorize microalgae biomass by using innovative extraction techniques, which comply with the Green Chemistry principles.

References

- Al-Ameri M, Al-Zuhair S (2019) Using switchable solvents for enhanced, simultaneous microalgae oil extraction-reaction for biodiesel production. *Biochem Eng J* 141:217–224. <https://doi.org/10.1016/j.bej.2018.10.017>
- Altenhofen M, Barbosa H, Brito C, Arjonilla F, Bastos G, Guenter T (2016) Heterotrophic growth of green microalgae *Desmodesmus subspicatus* in ethanol distillation wastewater (vinasse) and lipid extraction with supercritical CO₂. *J Chem Technol Biotechnol* 92: 573–579. <https://doi.org/10.1002/jctb.5035>
- Alzate ME, Muñoz R, Rogalla F, Fdz-Polanco F, Pérez-Elvira SI (2012) Biochemical methane potential of microalgae: influence of substrate to inoculum ratio, biomass concentration and pretreatment. *Bioresour Technol* 123:488–494. <https://doi.org/10.1016/j.biortech.2012.06.113>
- Anastas P, Eghbali N (2010) Green chemistry: principles and practice. *Chem Soc Rev* 39:301–312. <https://doi.org/10.1039/b918763b>
- Armenta S, Garrigues S, Esteve-Turrillas FA, de la Guardia M (2019) Green extraction techniques in green analytical chemistry. *TrAC Trends Anal Chem* 116:248–253. <https://doi.org/10.1016/j.trac.2019.03.016>
- Banerjee S, Ramaswamy S (2017) Dynamic process model and economic analysis of microalgae cultivation in open raceway ponds. *Algal Res* 26:330–340. <https://doi.org/10.1016/j.algal.2017.08.011>
- Banskota AH, Sperker S, Stefanova R, McGinn PJ, O'Leary SJ (2019) Antioxidant properties and lipid composition of selected microalgae. *J Appl Phycol* 31:309–318. <https://doi.org/10.1007/s10811-018-1523-1>
- Barros AI, Gonçalves AL, Simões M, Pires JCM (2015) Harvesting techniques applied to microalgae: a review. *Renew Sust Energ Rev* 41: 1489–1500. <https://doi.org/10.1016/j.rser.2014.09.037>
- Benedetti S, Benvenuti F, Pagliarini S, Francogli S, Scoglio S, Canestrari F (2004) Antioxidant properties of a novel phycocyanin extract from the blue-green alga *Aphanizomenon flos-aquae*. *Life Sci* 75:2353–2362. <https://doi.org/10.1016/j.lfs.2004.06.004>
- Bhalamurugan GL, Valerie O, Mark L (2018) Valuable bioproducts obtained from microalgal biomass and their commercial applications: a review. *Environ Eng Res* 23:229–241. <https://doi.org/10.4491/ceer.2017.220>
- Bligh EG, Dyer WJ (1959) A rapid method of total lipid extraction and purification. *Can J Biochem Physiol* 37:911–917. <https://doi.org/10.1139/y59-099>
- Bonfanti C, Cardoso C, Afonso C, Matos J, Garcia T, Tanni S, Bandarra NM (2018) Potential of microalga *Isochrysis galbana*: bioactivity and bioaccessibility. *Algal Res* 29:242–248. <https://doi.org/10.1016/j.algal.2017.11.035>
- Brennan L, Owende P (2010) Biofuels from microalgae—a review of technologies for production, processing, and extractions of biofuels and co-products. *Renew Sust Energ Rev* 14:557–577. <https://doi.org/10.1016/j.rser.2009.10.009>
- Capello C, Fischer U, Hungerbühler K (2007) What is a green solvent? A comprehensive framework for the environmental assessment of solvents. *Green Chem* 9:927–934. <https://doi.org/10.1039/b617536h>
- Carvalho AP, Meireles A, Malcata FX (2006) Microalgal reactors: a review of enclosed system designs and performances. *Biotechnol Prog* 22:1490–1506. <https://doi.org/10.1021/bp060065r>
- Chandra R, Iqbal MN, Vishal G, Lee H, Nagra S (2019) Bioresource technology algal biorefinery: a sustainable approach to valorize algal-based biomass towards multiple product recovery. 278:346–359. <https://doi.org/10.1016/j.biortech.2019.01.104>
- Chemat F, Vian MA, Cravotto G (2012) Green extraction of natural products: concept and principles. *Int J Mol Sci* 13:8615–8627. <https://doi.org/10.3390/jms13078615>
- Chen Y, Wang J, Zhang W, Chen L, Gao L, Liu T (2013) Forced light/dark circulation operation of open pond for microalgae cultivation. *Biomass Bioenergy* 56:464–470. <https://doi.org/10.1016/j.biombioe.2013.05.034>

- Cicci A, Sed G, Jessop PG, Bravi M (2018) Circular extraction: an innovative use of switchable solvents for the biomass biorefinery. *Green Chem* 20:3908–3911. <https://doi.org/10.1039/c8gc01731j>
- Clarke CJ, Tu WC, Levers O, Bröhl A, Hallett JP (2018) Green and sustainable solvents in chemical processes. *Chem Rev* 118:747–800. <https://doi.org/10.1021/acs.chemrev.7b00571>
- Danquah MK, Gladman B, Moheimani N, Forde GM (2009) Microalgal growth characteristics and subsequent influence on dewatering efficiency. *Chem Eng J* 151:73–78. <https://doi.org/10.1016/j.cej.2009.01.047>
- De-Luca R, Bezzo F, Béchét Q, Bernard O (2019) Meteorological data-based optimal control strategy for microalgae cultivation in open pond systems. *Complexity* 2019:1–12. <https://doi.org/10.1155/2019/4363895>
- Dixon C, Wilken LR (2018) Green microalgae biomolecule separations and recovery. *Bioresour Bioprocess* 5. <https://doi.org/10.1186/s40643-018-0199-3>
- Do Yook S, Kim J, Woo HM, Um Y, Lee SM (2019) Efficient lipid extraction from the oleaginous yeast *Yarrowia lipolytica* using switchable solvents. *Renew Energy* 132:61–67. <https://doi.org/10.1016/j.renene.2018.07.129>
- Dominguez de María P (2017) Chapter 6-ionic liquids, switchable solvents, and eutectic mixtures. In: Pena-Pereira F, Tobiszewski MBT, TA of GS in SP (eds) The application of green solvents in separation processes. Elsevier, pp 139–154. <https://doi.org/10.1016/B978-0-12-805297-6.00006-1>
- Drexler ILC, Yeh DH (2014) Membrane applications for microalgae cultivation and harvesting: a review. *Rev Environ Sci Biotechnol* 13:487–504. <https://doi.org/10.1007/s11577-014-9350-6>
- Du Y, Schuur B, Samori C, Tagliavini E, Brilman DWF (2013) Secondary amines as switchable solvents for lipid extraction from non-broken microalgae. *Bioresour Technol* 149:253–260. <https://doi.org/10.1016/j.biortech.2013.09.039>
- Du Y, Schuur B, Brilman DWF (2017) Maximizing lipid yield in *Neochloris oleoabundans* algae extraction by stressing and using multiple extraction stages with N-ethylbutylamine as switchable solvent. *Ind Eng Chem Res* 56:8073–8080. <https://doi.org/10.1021/acs.iecr.7b01032>
- Du Y, Schuur B, Kersten SRA, Brilman DWF (2018) Multistage wet lipid extraction from fresh water stressed *Neochloris oleoabundans* slurry—Experiments and modelling. *Algal Res* 31:21–30. <https://doi.org/10.1016/j.algal.2018.01.001>
- Esquivel-Hernández DA, Ibarra-Garza IP, Rodríguez-Rodríguez J, Cuéllar-Bermúdez SP, Rostro-Alanis M d J, Alemán-Nava GS, García-Pérez JS, Parra-Saldívar R (2017) Green extraction technologies for high-value metabolites from algae: a review. *Biofuels* 10:1735–1753. <https://doi.org/10.1080/17513758.2017.13735>
- Folch J (1957) A simple method for the isolation and purification of total lipids from animal tissues. *J Biol Chem* 266:497–509
- Fuad N, Omar R, Kamarudin S, Harun R, Idris A, Wan WA (2018) Mass harvesting of marine microalgae using different techniques. *Food Bioprod Process* 112:169–184. <https://doi.org/10.1016/j.fbp.2018.10.006>
- Gallego R, Bueno M, Herrero M (2019) Sub- and supercritical fluid extraction of bioactive compounds from plants, food-by-products, seaweeds and microalgae—an update. *TrAC - Trends Anal Chem* 116:198–213. <https://doi.org/10.1016/j.trac.2019.04.030>
- García JL, de Vicente M, Galán B (2017) Microalgae, old sustainable food and fashion nutraceuticals. *Microb Biotechnol* 10:1017–1024. <https://doi.org/10.1111/1751-7915.12800>
- Gayen K, Bhowmick TK, Maity SK (Eds.) (2019) Sustainable downstream processing of microalgae for industrial application. CRC Press, Boca Raton
- Ghasemi Naghdi F, González González LM, Chan W, Schenk PM (2016) Minireview progress on lipid extraction from wet algal biomass for biodiesel production. *Microb Biotechnol* 9:718–726. <https://doi.org/10.1111/1751-7915.12360>
- Gifuni I, Pollio A, Safi C, Marzocchella A, Olivieri G (2019) Current bottlenecks and challenges of the microalgal biorefinery. *Trends Biotechnol* 37:242–252. <https://doi.org/10.1016/j.tibtech.2018.09.006>
- Gilbert-López B, Mendiola JA, Fontecha J, Van Den Broek LAM, Sijtsma L, Cifuentes A, Herrero M, Ibañez E (2015) Downstream processing of *Isochrysis galbana*: a step towards microalgal biorefinery. *Green Chem* 17:4599–4609. <https://doi.org/10.1039/c5gc01256b>
- González-Delgado Á-D, Kafarov V (2011) Biorefinery: issues. *CT&F - Ciencia, Tecnol y Futur* 4(4):5–22
- Goto M, Kanda H, Wahyudiono MS (2015) Extraction of carotenoids and lipids from algae by supercritical CO₂ and subcritical dimethyl ether. *J Supercrit Fluids* 96:245–251. <https://doi.org/10.1016/j.supflu.2014.10.003>
- Gour RS, Garlapati VK, Kant A (2020) Effect of salinity stress on lipid accumulation in *Scenedesmus* sp. and *Chlorella* sp.: feasibility of stepwise culturing. *Curr Microbiol*. <https://doi.org/10.1007/s00284-019-01860-z>
- Günerken E, D'Hondt E, Eppink MHM, García-González L, Elst K, Wijffels RH (2015) Cell disruption for microalgal biorefineries. *Biotechnol Adv* 33(2):243–260. <https://doi.org/10.1016/j.biotechadv.2015.01.008>
- Häckl K, Kunz W (2018) Some aspects of green solvents. *Comptes Rendus Chim* 21:572–580. <https://doi.org/10.1016/j.crci.2018.03.010>
- Harris J, Viner K, Champagne P, Jessop PG (2018) Advances in microalgal lipid extraction for biofuel production: a review. *Biofuels*. <https://doi.org/10.1080/17513758.2018.1511135>
- He Y, Huang Z, Zhong C, Guo Z, Chen B (2019) Biorefinery technology pressurized liquid extraction with ethanol as a green and efficient technology to lipid extraction of *Isochrysis* biomass. *Bioresour Technol* 293:122049. <https://doi.org/10.1016/j.biortech.2019.12.2049>
- Herrero M, Ibañez E (2018) Green extraction processes, biorefineries and sustainability: recovery of high added-value products from natural sources. *J Supercrit Fluids* 134:252–259. <https://doi.org/10.1016/j.supflu.2017.12.002>
- Herrero M, Castro-Puyana M, Mendiola JA, Ibañez E (2013) Compressed fluids for the extraction of bioactive compounds. *TrAC Trends Anal Chem* 43:67–83. <https://doi.org/10.1016/j.trac.2012.12.008>
- Hidayah N, Yasin M, Shafiqi NI, Ruslan NH, Raihana N, Sepian A, Said FM (2019) ScienceDirect the effect of microalgae harvesting on lipid for biodiesel production. *Mater Today Proc* 19:1582–1590. <https://doi.org/10.1016/j.matpr.2019.11.186>
- Hu Y, Guo C, Wang F, Wang S, Pan F, Liu C (2014) Improvement of microalgae harvesting by magnetic nanocomposites coated with polyethyleneimine. *Chem Eng J* 242:341–347. <https://doi.org/10.1016/j.cej.2013.12.066>
- Imbimbo P, Romanucci V, Pollio A, Fontanarosa C, Amoresano A, Zarelli A, Olivieri G, Monti DM (2019) A cascade extraction of active phycoyanin and fatty acids from *Galdieria phlegrea*. *Appl Microbiol Biotechnol* 103:9455–9464. <https://doi.org/10.1007/s00253-019-10154-0>
- Imbimbo P, Bueno M, D'Elia L, Pollio A, Ibañez E, Olivieri G, Monti DM (2020) Green compressed fluid technologies to extract antioxidants and lipids from *Galdieria phlegrea* in a biorefinery approach. *ACS Sustain Chem Eng* 8:2939–2947. <https://doi.org/10.1021/acscchemeng.9b07505>
- Iverson SJ, Lang SLC, Cooper MH (2001) Comparison of the bligh and dyer and folch methods for total lipid determination in a broad range of marine tissue. *Lipids* 36:1283–1287. <https://doi.org/10.1007/s11745-001-0843-0>

- Jeevan Kumar SP, Vijay Kumar G, Dash A, Scholz P, Banerjee R (2017) Sustainable green solvents and techniques for lipid extraction from microalgae: a review. *Algal Res* 21:138–147. <https://doi.org/10.1016/j.algal.2016.11.014>
- Jessop PG, Heldebrandt DJ, Li X, Eckert CA, Liotta CL (2005) Reversible nonpolar-to-polar solvent. *Green Chem* 436:1101–1102. <https://doi.org/10.1038/nature4361101a>
- Juin C, Chérourvrièr JR, Thiéry V, Gagez AL, Bérard JB, Joguet N, Kaas R, Cadoret JP, Picot L (2015) Microwave-assisted extraction of phycobiliproteins from *Porphyridium purpureum*. *Appl Biochem Biotechnol* 175:1–15. <https://doi.org/10.1007/s12010-014-1250-2>
- Kadir WNA, Lam MK, Uemura Y, Lim JW, Lee KT (2018) Harvesting and pre-treatment of microalgae cultivated in wastewater for biodiesel production: a review. *Energy Convers Manag* 171:1416–1429. <https://doi.org/10.1016/j.enconman.2018.06.074>
- Kalsum U, Kusuma HS, Roesyadi A, Mahfid M (2019) Lipid extraction from *Spirulina platensis* using microwave for biodiesel production. *Korean Chem Eng Res* 57:301–304. <https://doi.org/10.9713/ker.2019.57.2.301>
- Kanda H, Hoshino R, Murakami K, Wahyudiono ZQ, Goto M (2020) Lipid extraction from microalgae covered with biomineralized cell walls using liquefied dimethyl ether. *Fuel* 262:116590. <https://doi.org/10.1016/j.fuel.2019.116590>
- Koley S, Mathimani T, Bagchi SK, Sonkar S, Mallick N (2019) Microalgal biodiesel production at outdoor open and polyhouse raceway pond cultivations: a case study with *Scenedesmus accuminatus* using low-cost farm fertilizer medium. *Biomass Bioenergy* 120:156–165. <https://doi.org/10.1016/j.biombioe.2018.11.002>
- Kothari R, Pandey A, Ahmad S, Kumar A, Pathak VV, Tyagi VV (2017) Microalgal cultivation for value-added products: a critical environmental assessment. *Biochem Eng* 3:243
- Krishnan S, Ghani NA, Aminuddin NF, Quraishi KS, Azman NS, Cravotto G, Leveque JM (2020) Microwave-assisted lipid extraction from *Chlorella vulgaris* in water with 0.5%–2.5% of imidazolium based ionic liquid as additive. *Renew Energy* 149:244–252. <https://doi.org/10.1016/j.renene.2019.12.063>
- Kumar RR, Rao PH, Arumugam M (2015) Lipid extraction methods from microalgae: a comprehensive review. 2:1–9. <https://doi.org/10.3389/fenrg.2014.00061>
- Lam GP, Vermuë MH, Eppink MHM, Wijffels RH, Van Den Berg C (2018) Multi-product microalgal biorefineries: from concept towards reality. *Trends Biotechnol* 36:216–227. <https://doi.org/10.1016/j.tibtech.2017.10.011>
- Liu W, Chen Y, Wang J, Liu T (2019) Biomass productivity of *Scenedesmus dimorphus* (Chlorophyceae) was improved by using an open pond-photobioreactor hybrid system. *Eur J Phycol* 54:127–134. <https://doi.org/10.1080/09670262.2018.1519401>
- Mansour EA, Abo El-Enin SA, Hamed AS, Mahmoud HM (2019) Efficacy of extraction techniques and solvent polarity on lipid recovery from domestic wastewater microalgae. *Environ Nanotechnol Monit Manag* 12:100271. <https://doi.org/10.1016/j.enmm.2019.100271>
- Mathimani T, Pugazhendhi A (2019) Utilization of algae for biofuel, bio-products and bio-remediation. *Bioatal Agric Biotechnol* 17:326–330. <https://doi.org/10.1016/j.bcab.2018.12.007>
- Minyak P, Daripada A, Air M, Chlorella T (2017) Algae oil extraction from freshwater microalgae *Chlorella vulgaris*. *Malaysian J Anal Sci* 21:735–744. <https://doi.org/10.17576/mjas-2017-2103-23>
- Molina D, de Carvalho JC, Júnior AIM, Faulds C, Bertrand E, Soccol CR (2019) Biological contamination and its chemical control in microalgal mass cultures. *Appl Microbiol Biotechnol* 103:9345–9358. <https://doi.org/10.1007/s00253-019-10193-7>
- Molino A, Mehariya S, Di Sanzo G, Larocca V, Martino M, Leone GP, Marino T, Chianese S, Balducci R, Musmarra D (2020) Recent developments in supercritical fluid extraction of bioactive compounds from microalgae: role of key parameters, technological achievements and challenges. *J CO₂ Util* 36:196–209. <https://doi.org/10.1016/j.jcou.2019.11.014>
- Motlagh SR, Harun R, Biak DRA, Hussain SA, Ghani WAWAK, Khezri R, Wilfred CD, Elgharabawy AAM (2019) Screening of suitable ionic liquids as green solvents for extraction of ecosapentaenoic acid (EPA) from microalgal biomass using COSMO-RS model. *Molecules* 24:713. <https://doi.org/10.3390/molecules24040713>
- Namla RR, Garg S, Sharma KK, Thomas-Hall SR, Deme M, Li Y, Schenk PM (2016) Comparison of microalgal cultivation in photobioreactor, open raceway pond, and a two-stage hybrid system. *Front Energy Res* 4:1–10. <https://doi.org/10.3389/fenrg.2016.00029>
- Nobre BP, Villalobos F, Barragan BE, Oliveira AC, Batista AP, Marques PASS, Mendes RL, Sovová H, Palavra AF, Gouveia L (2013) A biorefinery from *Nannochloropsis* sp. microalgal cultivation of oils and pigments. Production of biohydrogen from the leftover biomass. *Bioresour Technol* 135:128–136. <https://doi.org/10.1016/j.biortech.2012.11.084>
- Norsker NH, Barbosa MJ, Vermuë MH, Wijffels RH (2011) Microalgal production—a close look at the economics. *Biotechnol Adv* 29(1):24–27. <https://doi.org/10.1016/j.biortechadv.2010.08.005>
- Phepels CL, Smart NG, Wai CM (1996) Past, present, and possible future applications of supercritical fluid extraction technology. *J Chem Educ* 73:1163–1168. <https://doi.org/10.1021/ed073p1163>
- Pollet P, Eckertab CA, Liotta CL (2011) Switchable solvents. *Chem Sci* 2:609–614. <https://doi.org/10.1039/c0sc00568a>
- Pulz O, Gross W (2004) Valuable products from biotechnology of microalgae. *Appl Microbiol Biotechnol* 65:635–648. <https://doi.org/10.1007/s00253-004-1647-x>
- Ramos L, Kristensen EM, Brinkman UAT (2002) Current use of pressurised liquid extraction and subcritical water extraction in environmental analysis. *J Chromatogr A* 975:3–29. [https://doi.org/10.1016/S0021-9673\(02\)01336-5](https://doi.org/10.1016/S0021-9673(02)01336-5)
- Rasouli Z, Valverde-Pérez B, D'Este M, De Francis D, Angelidaki I (2018) Nutrient recovery from industrial wastewater as single cell protein by a co-culture of green microalgae and methanotrophs. *Biochem Eng J* 134:129–135. <https://doi.org/10.1016/j.bej.2018.03.010>
- Rawat I, Kumar RR, Mutanda T, Bux F (2011) Dual role of microalgae: phycoremediation of domestic wastewater and biomass production for sustainable biofuels production. *Appl Energy* 88:3411–3424. <https://doi.org/10.1016/j.apenergy.2010.11.025>
- Saini RK, Keum Y (2018) Carotenoid extraction methods: a review of recent developments. *Food Chem* 240:90–103. <https://doi.org/10.1016/j.foodchem.2017.07.099>
- Samori C, López Barreiro D, Vet R, Pezzolesi L, Brilman DWF, Galletti P, Tagliavini E (2013) Effective lipid extraction from algae cultures using switchable solvents. *Green Chem* 15:353–356. <https://doi.org/10.1039/c2gc36730k>
- Sati H, Mitra M, Mishra S, Baredar P (2019) Microalgal lipid extraction strategies for biodiesel production: a review. *Algal Res* 38:101413. <https://doi.org/10.1016/j.algal.2019.101413>
- Schipper K, Al Muraikhi M, Alghasal GSHS, Saadaoui I, Bounnit T, Rasheed R, Dalgamouni T, Al Jabri HMSJ, Wijffels RH, Barbosa MJ (2019) Potential of novel desert microalgae and cyanobacteria for commercial applications and CO₂ sequestration. *J Appl Phycol* 31:2231–2243. <https://doi.org/10.1007/s10811-019-01763-3>
- Schuur B, Brouwer T, Smink D, Sprakel LMJ (2019) Green solvents for sustainable separation processes. *Curr Opin Green Sustain Chem* 18:57–65. <https://doi.org/10.1016/j.cogsc.2018.12.009>
- Singh SK, Savoy AW (2020) Ionic liquids synthesis and applications: an overview. *J Mol Liq* 297:112038. <https://doi.org/10.1016/j.molliq.2019.112038>

- Slegers PM, Löising MB, Wijffels RH, van Straten G, van Bostel AJB (2013) Scenario evaluation of open pond microalgae production. *Algal Res* 2:358–368. <https://doi.org/10.1016/j.algal.2013.05.001>
- Souza LS, Simioni C, Bouzon ZL, De Cassia R, Schneider S, Gressler P, Miotto MC, Rossi MJ, Rörig LR (2017) Morphological and ultrastructural characterization of the acidophilic and lipid-producer strain *Chlamydomonas acidophila* LAFIC-004 (*Chlorophyta*) under different culture conditions. 1385–1398. <https://doi.org/10.1007/s00709-016-1030-7>
- Tatke P, Jaiswal Y (2011) An overview of microwave assisted extraction and its applications in herbal drug research. *Res J Med Plant* 5:21–31. <https://doi.org/10.3923/rjmp.2011.21.31>
- Vanderveen JR, Durelle J, Jessop PG (2014) Design and evaluation of switchable-hydrophilicity solvents. *Green Chem* 16:1187–1197. <https://doi.org/10.1039/c3gc42164c>
- Vega-López S, Kaul N, Devaraj S, Cai RY, German B, Jialal I (2004) Supplementation with ω 3 polyunsaturated fatty acids and all-rac alpha-tocopherol alone and in combination failed to exert an anti-inflammatory effect in human volunteers. *Metabolism* 53:236–240. <https://doi.org/10.1016/j.metabol.2003.09.012>
- Vekariya RL (2017) A review of ionic liquids: applications towards catalytic organic transformations. *J Mol Liq* 227:44–60. <https://doi.org/10.1016/j.molliq.2016.11.123>
- Wang H, Zhang W, Chen L, Wang J, Liu T (2013) The contamination and control of biological pollutants in mass cultivation of microalgae. *Bioresour Technol* 128:745–750. <https://doi.org/10.1016/j.biortech.2012.10.158>
- Wang S, Yerkebulan M, Abomohra AEF, El-Khodary S, Wang Q, Souza LS, Simioni C, Bouzon ZL, Schneider RCS, Gressler P, Miotto MC, Rossi MJ, Rörig LR, Schipper K, Al Muraikhi M, Alghasal GSHS, Saadoui I, Bounnit T, Rasheed R, Dalgamouni T, Al Jabri HMSJ, Wijffels RH, Barbosa MJ, Yusuff AS, Wei L, Huang X, Huang Z (2019) Morphological and ultrastructural characterization of the acidophilic and lipid-producer strain *Chlamydomonas acidophila* LAFIC-004 (*Chlorophyta*) under different culture conditions. *J Appl Phycol* 31:121371–122243. <https://doi.org/10.1007/s10811-019-01763-3>
- Wei L, Huang X, Huang Z (2014) Temperature effects on lipid properties of microalgae *Tetraselmis subcordiformis* and *Nannochloropsis oculata* as biofuel resources. *Chin J Oceanol Limnol* 33:99–106. <https://doi.org/10.1007/s00343-015-3346-0>
- Xu L, Wang F, Li HZ, Hu ZM, Guo C, Liu CZ (2010) Development of an efficient electroflocculation technology integrated with dispersed-air flotation for harvesting microalgae. *J Chem Technol Biotechnol* 85: 1504–1507. <https://doi.org/10.1002/jctb.2457>
- Yin Z, Zhu L, Li S, Hu T, Chu R, Mo F, Hu D, Liu C, Li B (2020) A comprehensive review on cultivation and harvesting of microalgae for biodiesel production: environmental pollution control and future directions. *Bioresour Technol* 301:122804. <https://doi.org/10.1016/j.biortech.2020.122804>
- Youn S, Muk J, Keun Y, Oh Y (2017) Cell disruption and lipid extraction for microalgal biorefineries: a review. *Bioresour Technol* 244:1317–1328. <https://doi.org/10.1016/j.biortech.2017.06.038>
- Yusuff AS (2019) Environmental effects extraction, optimization, and characterization of oil from green microalgae *Chlorophyta* species. *Energy Sources, Part A Recover Util Environ Eff* 1–12. <https://doi.org/10.1080/15567036.2019.1676327>
- Zghaibi N, Omar R, Kamal SMM, Biak DRA, Harun R (2019) Microwave-assisted brine extraction for enhancement of the quantity and quality of lipid production from microalgae *Nannochloropsis* sp. *Molecules* 24:1–21. <https://doi.org/10.3390/molecules24193581>
- Zhang Y, Bakshi BR, Demessie ES (2008) Life cycle assessment of an ionic liquid versus molecular solvents and their applications. *Environ Sci Technol* 42:1724–1730. <https://doi.org/10.1021/es0713983>
- Zhang J, Sun Z, Sun P, Chen T, Chen F (2014) Microalgal carotenoids: beneficial effects and potential in human health. *Food Funct* 5:413–425. <https://doi.org/10.1039/c3fo60607d>
- Zhang T, Hu H, Wu Y, Zhuang L, Xu X (2016) Promising solutions to solve the bottlenecks in the large-scale cultivation of microalgae for biomass/bioenergy production. *Renew Sust Eng Rev* 60:1602–1614. <https://doi.org/10.1016/j.rser.2016.02.008>
- Zhang R, Pamiakov O, Grimi N, Lebodka N, Marchal L, Vorobiev E (2019) Emerging techniques for cell disruption and extraction of valuable bio-molecules of microalgae *Nannochloropsis* sp. *Bioprocess Biosyst Eng* 42:173–186. <https://doi.org/10.1007/s00449-018-2038-5>
- Zheng H, Gao Z, Yin J, Tang X, Ji X, Huang H (2012) Harvesting of microalgae by flocculation with poly (c-glutamic acid). *Bioresour Technol* 112:212–220. <https://doi.org/10.1016/j.biortech.2012.02.086>
- Zimmerer J, Pingin D, Hess SK, Koengeter T, Mecking S (2019) microalgae lipids in supercritical carbon dioxide †. *Green Chem* 21:2428–2435. <https://doi.org/10.1039/c9gc00312f>
- Zullaikah S, P MCJ, Yasmin M, Rachimoellah M, Wu D (2019) Lipids extraction from wet and unbroken microalgae *Chlorella vulgaris* using subcritical water. *Mater Sci Forum* 964:103–108. <https://doi.org/10.4028/www.scientific.net/MSF.964.103>

Publisher's note Springer Nature remains neutral with regard to jurisdictional claims in published maps and institutional affiliations.



OPEN *Thymus algeriensis* and *Thymus fontanesii* exert neuroprotective effect against chronic constriction injury-induced neuropathic pain in rats

Samar Rezq¹, Amira E. Alsemeh², Luigi D'Elia³, Assem M. El-Shazly⁴, Daria Maria Monti⁵, Mansour Sobeh^{5,6} & Mona F. Mahmoud^{1,6}

We have previously demonstrated that the *Thymus algeriensis* and *Thymus fontanesii* extracts have powerful anti-inflammatory, antipyretic, and analgesic effects against acute pain models. We profiled their chemical composition and found many phenolic acids, flavonoids, and phenolic diterpenes. In this work, we investigated their antioxidant properties on HaCaT cells exposed to UVA-induced oxidative stress and examined their effects against chronic neuropathic pain and the underlying mechanisms. Through a rat chronic constriction injury (CCI) model, we induced chronic neuropathic pain by placing 4 loose ligatures around the right sciatic nerve for 14 days. Thermal and mechanical hyperalgesia in addition to cold and dynamic allodynia were tested on the day before surgery and on the 7th and 14th post-surgery days. Key markers of the nitrosative and oxidative stresses, in addition to markers of inflammation, were measured at day 14 post surgery. Histopathological examination and immunostaining of both synaptophysin and caspase-3 of sciatic nerve and brain stem were also performed. Results of this study showed that *T. algeriensis* extract suppresses UVA oxidative stress in HaCaT cells via activation of the Nrf-2 pathway. Both extracts attenuated hyperalgesia and allodynia at 7- and 14-days post-surgery with more prominent effects at day 14 of surgery. Their protective effects against neuropathic pain were mediated by inhibiting NOX-1, iNOS, by increasing the enzyme activity of catalase, and inhibition of inflammatory mediators, NF- κ B, TNF- α , lipoxygenase, COX-2 enzymes, and PGE2. Furthermore, they improved deleterious structural changes of the brainstem and sciatic nerve. They also attenuated the increased caspase-3 and synaptophysin. The data indicate that both extracts have neuroprotective effects against chronic constriction injury-induced neuropathic pain. The observed protective effects are partially mediated through attenuation of oxidative and nitrosative stress and suppression of both neuroinflammation and neuronal apoptosis, suggesting substantial activities of both extracts in amelioration of painful peripheral neuropathy.

Neuropathic pain is usually considered as a chronic pain condition and its affects about 3–18% of the population¹. It is a serious neurological disease, resulting from the damage of a somatosensory nervous system, which consists of peripheral fibers (myelinated A β , A δ and unmyelinated C fibers) and central neurons². The etiology of neuropathic pain is diverse and includes physical injury, infection, metabolic or autoimmune disorders or any other condition that may result in a pathology of the nervous system. It is characterized by increased sensitivity to innocuous (allodynia) and noxious stimulation (hyperalgesia)³. Following the prolonged peripheral injury, profound central sensitization occurs⁴ and contributes to altered pain-related activity in neuropathic pain⁵.

¹Department of Pharmacology and Toxicology, Faculty of Pharmacy, Zagazig University, Zagazig 44519, Egypt. ²Department of Anatomy and Embryology, Faculty of Medicine, Zagazig University, Zagazig, Egypt. ³Department of Chemical Sciences, University of Naples Federico II, Complesso Universitario Monte Sant'Angelo, via Cinthia 4, 80126 Naples, Italy. ⁴Department of Pharmacognosy, Faculty of Pharmacy, Zagazig University, Zagazig 44519, Egypt. ⁵AgroBioSciences Research, Mohammed VI Polytechnic University, Lot 660–Hay MoulayRachid, 43150 Ben-Guerir, Morocco. ⁶email: mansour.sobeh@um6p.ma; mfabdelaziz@zu.edu.eg

There are many mechanisms underlying the pathogenesis of neuropathic pain, and ROS play an essential role in initiating and maintaining the pain. Peripheral nerve damage and cutaneous neurogenic inflammation elevated oxidative stress in the spinal cord with pain hypersensitivity as a consequence. Neural network is highly susceptible to ROS because of its increased lipid content. It was reported that CCI to the sciatic nerve lead to an increase of the endoneurial lipid peroxidation^{6,7}. It is also known that ROS accumulation in the spinal cord activates several inflammatory mediators such as cytokines and prostaglandins which enhance the neuronal excitability^{8,9}. In addition to the increase in peripheral nerves and spinal cord synaptic networks ectopic activity, the descending brain stem nociceptive circuits to the spinal cord are also activated, and play an essential role in pain-related behavior severity^{6,10}. We previously showed that oxidative stress is elevated in the brain stem as well as in sciatic nerve, and is responsible for several conditions such as allodynia, hyperalgesia, and inflammation that follow the CCI of the sciatic nerve^{6,10}. Moreover, we demonstrated that the centrally acting angiotensin receptor blocker, telmisartan had a favorable effect in improving the pain-related behavior in CCI compared to the peripherally acting one losartan¹¹. Therefore, studying the supraspinal mechanisms involved in neuropathic pain in the current study is equally important.

The current treatments for neuropathic pain repose mainly on tricyclic antidepressants (tricyclics or TCAs), nonsteroidal anti-inflammatory medicines (NSAIDs), anticonvulsants, and opioids; however, many patients do not respond to these conventional medications¹². They are also accompanied by side effects, such as sedation. So, understanding the mechanisms of action of effective alternative agents, endowed with analgesic properties is imperative to achieve ideal therapeutic efficacy.

Both *Thymus algeriensis* (TA) and *Thymus fontanesii* (TF), belong to the mint family Lamiaceae. They are widely distributed in Mediterranean basin. *T. algeriensis* is used in folk medicine to remedy respiratory problems (e.g., common cold), gastrointestinal disorders and prostate benign hypertrophy, and were also reported to abrogate miscarriage^{13–15}. On the other hand, *T. fontanesii* is used as food preservative and to treat some gastrointestinal diseases¹³. We previously reported that both extracts possess analgesic, antipyretic, antioxidant, and anti-inflammatory effects. Moreover, both extracts inhibit the inflammation pathway. Extracts contain several secondary metabolites, among them flavones and flavonols such as luteolin, apigenin and quercetin, and phenolic acids, such as rosmarinic, phloretic and caffeic acids and their derivatives¹³. Previous studies showed that flavonoids and phenolic acids are beneficial against different models of neuropathic pain^{10,14}. Interestingly, previous reports show that a number of *Thymus* species including TA exert acetylcholinesterase (AChE) inhibitory activities and hence they may be useful if used in different neurodegenerative disorders^{14,15}.

The current work was undertaken to investigate the antioxidant activities of extracts of both species, *T. fontanesii* and *T. algeriensis* on human immortalized keratinocytes and their possible mechanism of action. This study aimed also at evaluating these medicinal herb extracts for their anti-inflammatory and antinociceptive effects in rats with CCI-induced neuropathic pain model, elucidating the molecular mechanisms involved both on the peripheral (sciatic nerve) and supraspinal (brain stem) levels.

Materials and methods

Plant material and extracts preparation. Leaves of *Thymus fontanesii* Boiss. et Reut. and *Thymus algeriensis* Boiss. et Reut. were collected from Algeria. Voucher Specimens (TA-L10, TF-L11) were deposited at the herbarium of the Pharmacognosy Department, Faculty of Pharmacy, Zagazig University, Zagazig (Egypt). Plant collection coordinates, identification and extraction were performed according to Sobeh et al.¹³.

Cytotoxicity. All cell lines, with the exception of HaCaT cells (Innoprot, Berio, Spain), were from ATCC. Cells were cultured as previously described¹⁶. To evaluate the biocompatibility of the extracts, dose-response experiments were performed. 2.5×10^5 cells per well (96-well plates) were seeded 24 h prior adding the extracts (10–100 µg/mL). Cells were then kept in an incubator set at 37 °C and 5% CO₂ for 48 h, then, the MTT [3-(4,5-dimethylthiazol-2-yl)-2,5-diphenyltetrazolium bromide] assay has been used to analyze cell viability according to the method of Petruk et al.¹⁶. The cell viability is defined as follow: % Cell Viability = $100 \times A/A_0$.

Where A and A₀ corresponds to the viable cells in the presence of the extract and the negative control cells, respectively. The latter corresponds to untreated cells and cells incubated with buffer instead of extracts.

Determination of the antioxidant capacity using a cell-based model. The DCFDA (2',7'-dichlorofluorescein diacetate) assay was used to study the antioxidant activity of TA and TF extracts. HaCaT cells were seeded on plates at a density of 5×10^5 cells/cm². After incubation for 24 h, extracts were added to the plates at a concentration of 50 µg/mL and maintained for 120 min and then exposed to UVA radiations (100 J/cm²) to induce oxidative stress, as described before¹⁷. The HaCaT cells were then incubated with the probe (H₂-DCFDA, Sigma-Aldrich, 20 µM) and the procedure described in¹⁷ was followed. Reactive oxygen species (ROS) levels were expressed as the ratio between DCF (2',7'-dichlorofluorescein) fluorescence intensity determined for each sample, compared to the untreated cells.

Western blot (WB) analyses. The HaCaT cells were first seeded at a density of 2×10^4 cells/cm² and incubated for 24 h. At the end of the incubation, each extract was added at a concentration of 50 µg/ml, and then incubated for 15 or 30 min. The nuclear pellet was then obtained by centrifuging the cells and resuspending each pellet in RIPA buffer composed of 50 mM Tris-HCl pH8.0, 150 mM NaCl, 0.1% SDS, 1% NP-40, and proteases inhibitors. After centrifugation, 0.1 mg of the nuclear proteins (pellet) were used to conduct the WB analysis as previously described¹⁶. Specific antibodies (from Cell Signal Technology, Danvers, MA, USA) were used to detect the Nrf-2. The B-23 was used as internal standard (antibody from ThermoFisher, Rockford, IL, USA).

In vivo experiments. *Animals.* Male Wistar rats used for this study weighted 275–300 g. These laboratory rats that were obtained at the Faculty of Veterinary Medicine, Zagazig (Egypt) were housed in plastic cages at constant environmental conditions (22 °C with 50 ± 10% humidity, 12 h:12 h light–dark cycle). They had also a regular chow diet ad libitum and free access to water.

Experimental design. The Ethics Committee of the Faculty of Pharmacy (ECAH ZU) at the Zagazig University (Egypt) has approved the investigative protocols that were carried out in compliance with the recommendations of the Weatherall study (approval number: ZU-IACUC/3/E/115/2018) and conducted following the guidelines of the US National Institutes of Health on animal care and use. The Wistar rats were allocated, randomly and equally (n = 6), to eight groups. Group 1 includes control animals that received the vehicle. Group 2 is the sham operated group and received the vehicle. Group 3 includes CCI rats that received the vehicle. Groups 4–8 include CCI rats that received TA or TF at two concentrations (200 mg/kg and 400 mg/kg) or 30 mg/kg of pregabalin for rats that serves as positive control. Both plant extracts and the pregabalin were dissolved in dH₂O using as suspending agent, 10% w/v of the acacia gum and given by oral gavage (5 mL/kg) daily for the whole period of the experiment (2 weeks) starting from the 1st day following the neuropathic pain induction.

Neuropathic pain induction. The CCI to sciatic nerve was used to induce the neuropathic pain as previously reported¹¹. Briefly, following anesthesia with thiopental sodium (50 mg/kg, i.p.) the right sciatic nerve was exposed under aseptic conditions at the mid-thigh level beneath the gluteus and biceps femoris muscles. A common sciatic nerve segment (7-mm-long) proximal to the trifurcation was separated from the surrounding tissue. The CCI was then induced by placing four loose ligatures (4/0 silk suture) 1 mm apart around the nerve. The animals were returned to their cages following wound closure to recover.

Behavioral tests. Behavioral experiments were carried out by an experimenter who ignored the nature of the tests and was blinded to the different treatments.

Heat hyperalgesia. Heat hyperalgesia that refers also to the hot plate test was conducted to evaluate the thermal hyperalgesia according to the principal of Jain et al.¹⁸. Briefly, the rats were placed on a hot plate, maintained at a temperature of 52.5 °C ± 1.0 °C and the withdrawal latency to heat-induced nociceptive behavior was recorded with a cut-off time of 20 s.

Mechanical hyperalgesia (Pinprick test). As detailed in our recent study¹¹, a force was applied gently to the mid-plantar surface of the injured hind paw by bent gauge to avoid damaging the skin. Paw withdrawal duration (s) was recorded with a minimum value of 0.5 s (for the brief normal response) and a maximum value of 20 s.

Acetone drop test (paw cold allodynia). The response of each rat to cold allodynia was tested by spraying the injured paw with acetone (100 µl). Based on graded to a four-point scale the response was graded as follows: 0, no response; 1, quick withdrawal or flick of the paw; 2, prolonged withdrawal or repeated flicking; and 3, repeated flicking with licking of the paw. The test was repeated for three times with 5 min gap in between. The final score is the total of the individual scores. The minimum score was 0, while the maximum possible score was 9.

Paint-brush test (mechanical dynamic allodynia). A smooth paintbrush was used to produce a dynamic allodynic response by rubbing the plantar area of the injured paw five times with 5 s intervals and the number of withdrawals was recorded (between 0 and 5). The process was performed three times with a resting period of 5 min in between. A single cumulative score of the total number of withdrawals (in three tests) was calculated with a minimum value of 0 and maximum of 15¹¹. Biochemical analysis in sciatic nerve and brainstem tissue were done as before⁵, and the methods were detailed in the supplementary file.

Histopathological studies. Sciatic nerves and brains were extracted from animals (n = 6 each) and fixed in 10% of neutral buffered formalin (NBF) and mixed into paraffin; sections at a thickness of 5 µm were then obtained and mounted on glass slides. The sections were first deparaffinized by treatment with xylene and then stained with hematoxylin and eosin (H&E stain). Histopathological examination was performed as before¹⁹. Methods of osmic acid stain of sciatic nerve and immunohistochemical studies were done as before in Sobeh et al.⁵ and the methods were detailed in the supplementary file.

Statistical analysis. Biological replicates were analyzed in three independent replicates in *in-vitro* study. The used data are expressed as mean values ± SD. The significance point was fixed at 0.05 and the analysis were conducted using the Student's *t*-test. While in animal studies, data are expressed as the mean ± SEM. The data were subjected to one-way ANOVA or RM-ANOVA (repeated-measures analysis of variance). Differences among groups were determined by the Student's *t*-test and for the post hoc analysis, the Tukey multiple comparison was chosen. All analyses of the present study were performed using GraphPad Prism V. 6.01 (GraphPad Software, San Diego, CA). *p* < 0.05 is considered statistically significant.

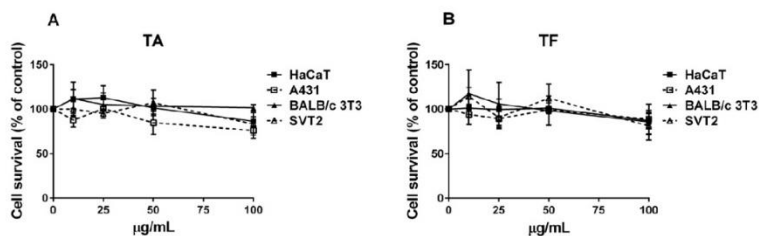


Figure 1. Immortalized and cancer cells viability after treatment for 48 h with increasing concentrations of *T. algeriensis* (TA) (A) and *T. fontanesii* (TF) (B) extracts (10–100 µg/mL). HaCaT (black squares), A431 (empty squares), BALB/c-3T3 (black triangles), and SVT2 (empty triangles) cells. Cell viability and cell survival were assessed according to method described in the section of materials and methods.

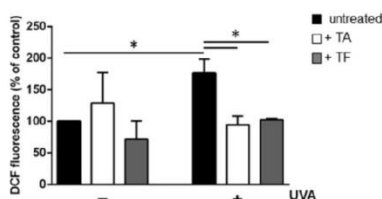


Figure 2. Antioxidant effect of TA and TF extracts (50 µg/mL) on UVA-stressed HaCaT cells. After 120 min of incubation with the *T. algeriensis* (TA) or *T. fontanesii* (TF) extracts, the HaCaT cells were stressed using the UVA (100 J/cm²). Untreated cells are reported as black bars. (-) indicates cells treated in the absence of stress. (+) indicates cells stressed by UVA. DCFDA assay was used to determine intracellular ROS levels. Statistical analysis was performed using one way-ANOVA, followed by Tukey post hoc test. Values are expressed as fold increase by comparing them with the control cells. *Indicates $p < 0.05$ compared to untreated cells.

Results

Cytotoxicity experiment. The cytotoxic activity of both extracts was evaluated on 4 cell lines, two cancer (A431 and SVT2 cells) and two immortalized (HaCaT and BALB/c-3T3 cells). After 48 h of cell incubation with increasing concentrations of each plant extract, the cytotoxic activity was measured, and the results are shown in Fig. 1. TA extract (Fig. 1A) was found to be fully biocompatible on both the immortalized cell lines tested and slightly toxic on cancer cells, but only at the highest concentration analyzed. TF extract showed the same activity on all the cell lines analyzed, with a very low toxicity at the highest concentration (100 µg/mL, Fig. 1B). Thus, 50 µg/mL of each extract were selected to test the protective effect against oxidative stress.

In vitro antioxidant activity. To analyze the potential antioxidant effects of TA and TF extracts in vitro, HaCaT cells were challenged with UVA irradiation (100 J/cm²). As expected, UVA induced about a two-fold augmentation in intracellular ROS contents in comparison with the control ($p < 0.05$) (Fig. 2). However, our results showed that the incubation of the cells with TA (white bars of Fig. 2) or TF (grey bars of Fig. 2) extracts before UVA exposure lead to no significant modification in ROS levels.

TA and TF extracts exert antioxidant effect by up-regulating Nrf2. To help understanding the likely molecular mechanisms involved in the antioxidant effects of TA and TF extracts in HaCaT, we studied the implication of the Nrf-2 (nuclear factor erythroid 2) transcription factor, a key regulator of cellular antioxidant defense system that is highly expressed in epithelial cells including keratinocytes³⁰. Kelch-like ECH-associated protein 1 (Keap-1) is normally associated to Nrf-2 to keep it in the cytoplasmic matrix and to direct it into the proteasome machinery for its degradation. Under stressful conditions, and/or in the presence of antioxidants, Keap-1, which is released from Nrf-2, translocates into the nucleus, and activates the transcription process of antioxidant genes that present in their promoter region, sequences named ARE (antioxidant responsive elements). As shown in Fig. 3, after incubation of the cells for 15 and 30 min with each extract, a significant increase in nuclear Nrf-2 levels was detected only after 15 min of incubation of the HaCaT cells with the TF extract.

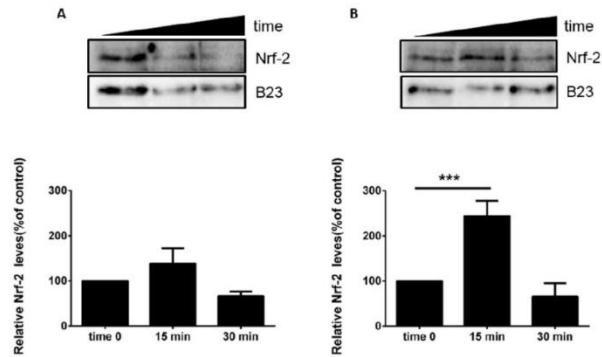


Figure 3. Effect of *T. algeriensis* (TA) and *T. fontanesii* (TF) extracts on the Nrf-2 levels of the HaCaT cells. After incubation of the HaCaT cells for 15 min (white bars) or 30 min (dark grey bars) with 50 µg/mL of either TA (A) or TB (B) extracts, nuclear proteins were extracted and used for Western blot analyses. The protein intensity levels were normalized to the internal standard (B-23) after being estimated by densitometric analysis. Statistical analysis was performed using one way-ANOVA, followed by Turkey's post hoc test. ***Corresponds to $p < 0.005$ compared to control cells.

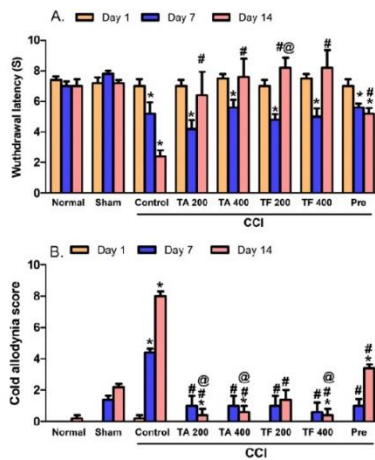


Figure 4. Effect of 200 and 400 mg/Kg of *T. algeriensis* (TA) and *T. fontanesii* (TF) extracts against (A): heat hyperalgesia and (B): cold allodynia in neuropathic pain rats induced by spinal nerve ligation. Results are expressed as mean \pm SE (n = 6). Statistical analysis was performed using RM-ANOVA, followed by Tukey post hoc test. The different symbols indicate the significance differences at $p < 0.05$ when compared with sham group (*), CCI group (#), and pregabalin group (Pre, @) at the different time points as indicated in the materials and methods section.

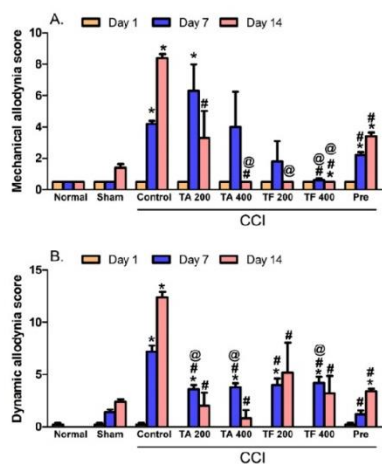


Figure 5. Effect of 200 and 400 mg/kg of *T. algerensis* (TA) and *T. fontanesii* (TF) extracts on (A): mechanical hyperalgesia score expressed as paw withdrawal and evaluated using the pin prick assay or (B): mechanical dynamic allodynia score (number of withdrawals) as evaluated in the neuropathic pain rats using the paint brush test. In response to the tip of the bent gauge needle, paw withdrawal duration in seconds (ranges from 0.5 s for the short normal response to a 20 s cut-off time), or the number of withdrawals (between 0 and 15) in a total of 15 experiments in response to a paint brush-induced stimulus were recorded and expressed as mean \pm SE ($n=6$). Statistical analysis was performed using RM-ANOVA, followed by Tukey post hoc test. The different symbols indicate the significance differences at $p < 0.05$ when compared with sham group (*), CCI group (#), and pregabalin group (Pre, @) at the different time points as indicated in the materials and methods section.

Effect of extracts on heat hyperalgesia and cold allodynia. Compared to the sham group, cold allodynia and heat hyperalgesia signs were observed in rats exposed to CCI (Fig. 4A,B). These signs correspond to a time dependent decrease, cold allodynia scores and an increase in heat response latency time. Rats treated with 200 and 400 mg/kg of either TA or TF extracts revealed a restored heat response latency when measured at day 14 post CCI. Similarly, both extracts were able to restore normal cold allodynia responses starting day 7 post CCI. Noteworthy, for both cold and heat stimuli, the extracts showed superiority over the standard pregabalin drug, used for neuropathic pain, (Fig. 4).

Effects of extracts on mechanical hyperalgesia and mechanical dynamic allodynia. Compared to the sham group, an increase by 8.4- and 6-folds after 7 and 14 days, respectively, was observed in the withdrawal time of injured hind paw (Fig. 5A). This results in a significant increase in the mechanical hyperalgesia in CCI rats. This increase was attenuated or totally abolished when rats were given *T. algerensis* or *T. fontanesii* extract at all studied doses and the response was measured at day 14 post surgery (Fig. 5). As shown in Fig. 5B, CCI rats demonstrated higher dynamic allodynia (5 folds, $p < 0.001$) scoring when evaluated by paint brush assay at the 7th and 14th day post-surgery with regards to the sham group. On the other hand, both extracts time dependently attenuated the dynamic allodynia response (Fig. 5B) as the later effect was highly attenuated when assessed at day 7 and totally abolished when measured at day 14 post surgery. Interestingly, *T. fontanesii* extract (400 mg/kg) has a greater effect against mechanical allodynia at day 7, compared to both *T. algerensis* and pregabalin.

Histopathological changes. *Effect of extracts on structural variations in sciatic nerve.* Histopathological analysis of the sciatic nerve tissues from all groups was performed using H & E and osmic staining (Fig. 6). Microscopic examination of the sciatic nerve transverse sections of H&E from control and sham group (Fig. 6a,b) revealed normal morphological appearance which showed the perineurium surrounding the closely packed nerve fibers of the nerve fascicle. Myelinated nerve fibers (abbreviated as MNF) are derived from axoplasm bounded by white patches of myelin and nuclei of the neurolemmocytes that appear between the nerve fibers. One will see an occasional endoneurial blood vessel (Fig. 6c). CCI group revealed disorganized nerve fascicles. Most nerve fibers are dissociated and are separated from their protective covering (perineurium). In pregabalin

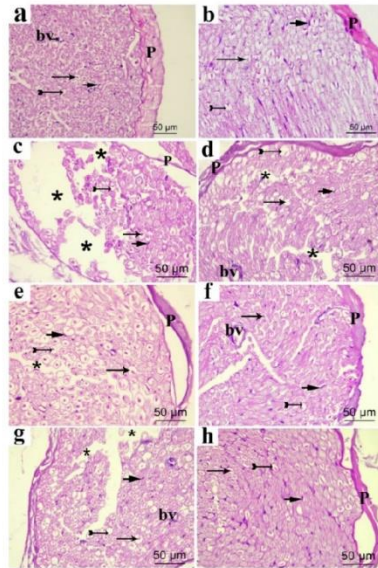


Figure 6. Representative photomicrographs of transverse sections of sciatic nerve in different experimental groups. (a) control group; (b) sham group; (c) CCI group; (d) pregabalin group; (e) TF (p.o., 200 mg/kg); (f) TF (p.o., 400 mg/kg); (g) TA (p.o., 200 mg/kg); (h) TA (p.o., 400 mg/kg). Arrow, bifid arrow, short arrow and asterisk illustrate axoplasm, area of dissolved myelin, Schwann cells nuclei and wide separation between the nerve fibers, respectively. (P) perineurium; (bv) blood vessel. Scale bar, 50 μm \times 400.

group and low doses of TF and TA groups (Fig. 6d,e,g), the nerve fascicle regained its normal form. However, the nerve fibers are still separated in some areas. By comparison, in the high-dose TF treated groups, apparently normal nerve fascicle consisted mainly of MNF and nuclei of the neurolemmocytes in endoneurial areas accompanied by minor differentiation in some few areas between the nerve fibers were seen (Fig. 6f). On the other hand, the high dose of TA restored the regular appearance of the nerve fascicle, which mostly consisted of neurolemmocytes nuclei and MNF in endoneurial areas without dissociation of the nerve fibers (Fig. 6h).

Osmic stain of sciatic nerve. Osmic staining of sciatic nerves of different studied groups are shown in Fig. 7. In control and sham group (Fig. 7A-a,b), the nerve fascicle is surrounded by connective tissue perineurium and contain transverse section of myelinated nerve fibers of various sizes. Myelin sheaths appear as well-preserved darkly brown stained structures, often rounded or elliptical with endoneurium in between. In CCI group, the nerve fascicle showed irregular faint stained myelin sheath in many nerve fibers giving them distorted appearance with wide separation in between the fibers is observed (Fig. 7A-c). In pregabalin, low dose of TF and TA, sciatic nerves are still showing irregular myelin sheath in some nerve fibers giving them distorted appearance with slight separation (Fig. 7A-d,e,g). In contrast, high doses of TF and TA revealed nearly normal myelinated nerve fibers which are formed of darkly stained myelin sheath (Fig. 7A-f,h). We also showed that in normal nerve group and sham group, the myelin area to fiber area ratios were statistically similar ($65.55 \pm 1.59\%$ and $62.64 \pm 1.60\%$, respectively). In contrast, in CCI group, the ratios of the myelin area to the fiber area were significantly decreased ($40.95 \pm 1.84\%$). Nonetheless, a significant increase in this ratio in pregabalin group ($48.87 \pm 1.36\%$), low dose TF group ($49.86 \pm 1.55\%$) and low dose TA group ($53.22 \pm 1.17\%$) was observed, they remain statistically different from the control. In contrary, in high dose TF group and high dose TA group, the myelin to the fiber areas ratio (60.98 ± 1.94 and $62 \pm 1.67\%$, respectively) revealed significant increase compared to low dose TF group, low dose TA group and pregabalin group and were not significantly different from the control group (Fig. 7B).

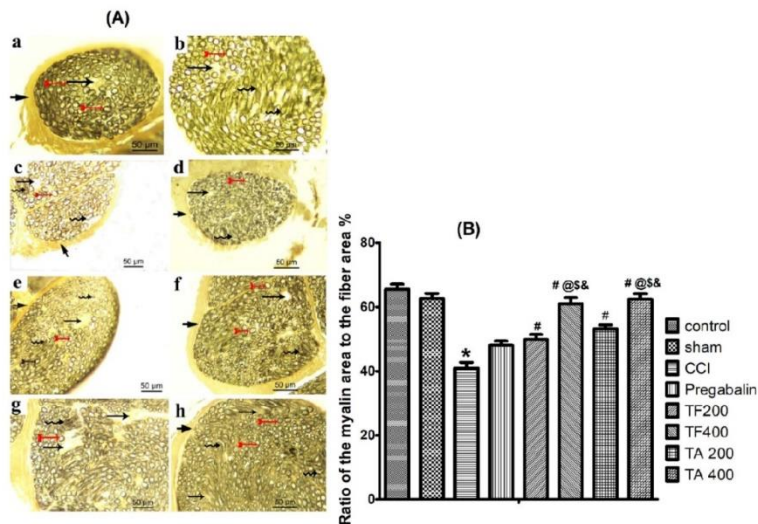


Figure 7. Representative Photomicrographs of osmic acid stained sciatic nerve transverse sections in (A): (a) normal group; (b) sham group; (c) CCI group; (d) pregabalin group; (e) TF (p.o., 200 mg/kg); (f) TF (p.o., 400 mg/kg); (g) TA (p.o., 200 mg/kg); (h) TA (p.o., 400 mg/kg). Arrow, arrowhead, bifid arrow, short arrow and wavy arrow show the usual concentric lamellar structure of myelin sheath, unmyelinated nerve fibers, and irregular concentric lamellar structure of myelin sheath, respectively. Scale bar, 50 $\mu\text{m} \times 400$. (B) Bar graph represents quantification of the ratio of myelin area to the fiber area %. Statistical analysis was performed using ANOVA one way, followed by post hoc testing by Tukey test. Values are set to mean \pm SE (n = 6). *Significant difference compared to the control group, $p < 0.05$; #Significant difference compared to the CCI group, $p < 0.05$; @Significant difference compared to the standard group, $p < 0.05$; \$Significant difference compared to the TF200 group, $p < 0.05$; &Significant difference compared to the TA200 group, $p < 0.05$.

Effect of extracts on structural changes of brain stem. Microscopic examination of the control groups of brain stem sections stained with the H&E stain (Fig. 8a) showed the gray matter with normal neuron having vesicular nuclei and basophilic cytoplasm containing Nissl bodies with prominent nuclei. Moreover, it was shown on the Fig. 8a that the acidophilic neuropil contains nuclei of normal neuroglia cells. The brainstem in sham group, is almost the same as control (Fig. 8b). The CCI group, on the other hand, showed degeneration of most neurons that had either shrunken vacuolated cytoplasm, with irregular and dark stained nuclei or pyknotic, small deeply stained nuclei with vacuolated cytoplasm. Glial cells with either lightly or deeply stained nuclei were seen. Perineurial glial cells have been shown to be closely related to some degenerated neurons (Fig. 8c). Most neuron were degenerated and have pyknotic nuclei in pregabalin group, and few neurons were normal (Fig. 8d). Low-dose administration of TF (Fig. 8e) and TA (Fig. 8g) showed partial restoration of degenerative neuronal changes, predominantly TF where some neurons were regular, and some were affected with either large rarified lightly stained cytoplasm and nuclei or shrunken cytoplasm. Meanwhile, high-dose administration of TF (Fig. 8f) and TA (Fig. 8h) restored most of the degenerative neuronal changes that were more prevalent with high-dose TA (h) where most neurons were normal and few neurons exhibited pyknotic, low, deeply stained nuclei (Fig. 8).

Immunohistochemical studies of brain stem. *Effect of extracts on caspase 3.* Using an antibody anti-caspase 3, we immunohistochemically analyzed the brain stem tissues in order to determine the apoptotic neurons within the different studied samples. The caspase-positive neurons had been expressed as dark brown staining in the cytoplasm. They were negatively expressed in the control group (Fig. 9A-a) and sham group (Fig. 9A-b) which revealed non-significantly different results when compared with the control group. In contrast, caspase 3 immunopositive neurons in the CCI group (Fig. 9A-c) were apparently detected, showing a significant up-regulation in caspase 3 expression compared to the sham group. However, treatment with either pregabalin (Fig. 9A-d) or low dose of TF (Fig. 9A-e) tends to decrease the number of immunopositive neurons

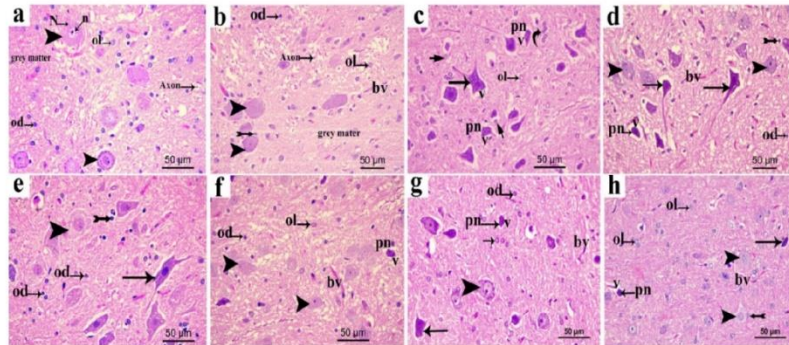


Figure 8. Representative photomicrographs in sections of brain stem from various groups (a) control group; (b) sham group; (c) CCI group; (d) pregabalin group; (e) TF (p.o., 200 mg/kg); (f) TF (p.o., 400 mg/kg); (g) TA (p.o., 200 mg/kg); (h) TA (p.o., 400 mg/kg). Arrowhead, arrow, short arrow bifid arrow illustrate normal neurons, affected neurons with dark stained cytoplasm and nuclei, perineural glial cell nuclei rarified lightly stained cytoplasm and nuclei, respectively; pn; pyknotic nuclei; N; Nissl granule; n; nuclei; bv, normal blood vessel; v; vacuolated cytoplasm, Ol; lightly stained glial cell, Od; deeply stained glial cell. Scale bar, 50 μm × 400.

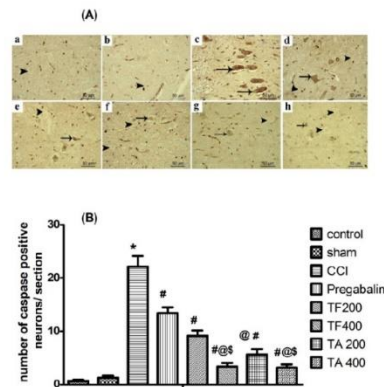


Figure 9. (A) Representative images showing the expression of the apoptotic neurons in different experimental groups through caspase-3 immunostaining of brain stem sections (a) control group; (b) sham group; (c) CCI group; (d) pregabalin group; (e) TF (p.o., 200 mg/kg); (f) TF (p.o., 400 mg/kg); (g) TA (p.o., 200 mg/kg); (h) TA (p.o., 400 mg/kg). Arrow indicating dark brown staining of the cytoplasm of immunopositive neurons and arrowhead indicating the negative immunostaining neurons. Scale bar, 50 μm. (B) Bar graph showing differences in the number of caspase positive neurons in all study groups in the brainstem areas. The immunopositive neurons were counted over the entire 6 animals/group in 3 non-overlapping fields from × 200 magnification. Statistical analysis was carried out using one-way ANOVA, followed by a post-hoc test by Tukey test. Values are shown as mean ± SEM (n = 6). *Significant difference from the sham group, $p < 0.05$; #Significant difference in comparison to the CCI group, $p < 0.05$; @Significant difference compared to the pregabalin group, $p < 0.05$; \$Significant difference compared to the low dose TF group, $p < 0.05$.

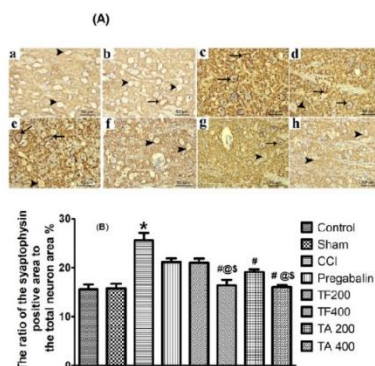


Figure 10. (A) Representative photomicrographs showing the expression of the synaptophysin in the neurons of sections in brain stem in different experimental groups. (a) control group; (b) sham group; (c) CCI group; (d) pregabalin group; (e) TF (p.o., 200 mg/kg); (f) TF (p.o., 400 mg/kg); (g) TA (p.o., 200 mg/kg); (h) TA (p.o., 400 mg/kg). Arrowhead indicating coarsely fine beaded reactivity at the neuron surface and arrow indicating dense bands of reactivity at the periphery of the neurons. Scale bar; 50 μ m. (B) Bar chart showing the ratio of the synaptophysin positive reactivity on the surface of the neuron to the total area of the neuron in the brainstem sections of all experimental groups. Statistical analysis using one way ANOVA followed by Tukey post hoc test. Values are set to mean \pm SE (n = 6). *Significant difference in comparison to the control group, $p < 0.05$; #Significant difference from the diseased group, $p < 0.05$; @Significant difference compared to the pregabalin group, $p < 0.05$; \$Significant difference compared to the TF200 group, $p < 0.05$.

but still significant from the sham group. The number of immunopositive neurons revealed down-regulation in low dose of TA (Fig. 9A-g) which revealed significant difference from the sham group. Interestingly, the latter effect was better than the effect observed in the pregabalin group. On the other hand, treatment with high dose of TF (Fig. 9A-f) and TA (Fig. 9A-h) resulted in greater reduction in caspase 3 immunoreactivity and restored its level to the levels of the sham (Fig. 9).

Effect of extracts on synaptophysin (SYN) expression. Synaptophysin reactivity was noticed, at the surface of the neuron in the brain stem of control and sham groups, under coarsely fine beaded reactivity form. As shown in the Fig. 10a,b, the dispersion of the reactive granules was also observed between the neurons. Chronic sciatic ligation resulted in an increase in SYN reactivity which was noticed in a form of dense bands at the periphery of the neurons and within the space between them (Fig. 10c). Treatment with either pregabalin or low dose of TF slightly decreased SYN immunoreactivity. (Fig. 10d,e). However, Treatment with a higher dose of TF or TA (400 mg/kg) revealed a significantly lower SYN reactivity compared to lower doses (200 mg/kg).

The ratios of the synaptophysin positive reactivity on the surface of the neuron to the total area of the neuron were similar in both the control nerve group ($15.60 \pm 0.98\%$) (Fig. 10A-a) and in the sham group ($15.79 \pm 0.95\%$) (Fig. 10A-b). In CCI group (Fig. 10A-c), the ratios of synaptophysin positive reactivity on the surface of the neurons to the total area of the neurons was significantly increased ($25.61 \pm 1.52\%$) compared to the control. However, pregabalin group (Fig. 10A-d) ($21.14 \pm 0.802\%$) and low dose TF group (Fig. 10A-e) ($21.00 \pm 0.89\%$) revealed significant decrease in the ratio compared to CCI group but still significantly different from the sham group. Interestingly, the use of high dose of either TF (Fig. 10A-f), low dose TA (Fig. 10A-g), or high dose TA (Fig. 10A-h) resulted in a greater reduction in the synaptophysin positive reactivity on the surface of the neuron to the total area of the neuron ($16.43 \pm 1.092\%$, $19.12 \pm 0.55\%$ and $16.04 \pm 0.44\%$, respectively). Notably, the later effects were significant compared to CCI, TF and pregabalin groups, however, the differences were not statistically significant in comparison with the sham rats (Fig. 10B).

Effect of extracts on CCI-induced oxidative stress. The present study showed that the oxidative status was higher in the CCI rats' sciatic nerves and the brain stems (Fig. 11A). This increase was revealed by significantly ($p < 0.0001$) high NADPH oxidase (NOX1) contents and lower CAT activity in comparison with the sham group. However, groups with CCI treated with both doses of TA were able to improve their oxidative status through a decrease in the levels of NOX1 accompanied by a dose-dependent augmentation in the CAT activity in comparison with the sham rat values (Fig. 11A). However, TF extract (200 mg/kg) did not attenuate the increase

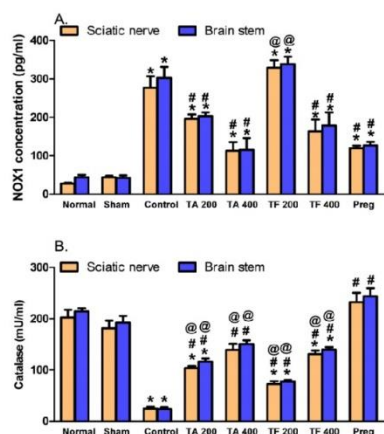


Figure 11. *T. algeriensis* (TA) or *T. fontanesii* (TF) extract (200 and 400 mg/kg, p.o) effects on CCI-induced increase in levels of NOX1 (A) and catalase activity (B) in the sciatic nerves and brain stems of CCI rats. Statistical analysis was performed using one way ANOVA, followed by Tukey post hoc test. Values are presented as mean \pm SE, $n=5$ rats per group. * $p < 0.05$, vs. Sham group; # $p < 0.05$, vs. CCI group; @ $p < 0.05$, vs. pregabalin group (Pre). NOX1, NADPH oxidase.

in NOX1 level and mildly improved catalase activity. Doubling the dose of the extract led to a significant reduction in NOX1 level and elevation in catalase activity compared to CCI rats treated with the vehicle (Fig. 11B).

Effect of extracts on CCI-induced increase in COX2, LOX and PGE2. CCI rats (14 days) showed substantially ($p < 0.05$) increased levels of sciatic nerve and brain stem COX2 (4.1 and 4.6 folds), LOX (4.2 and 3.95 folds) and PGE2 (2.8 and 3.1 folds) relative to sham tests, respectively. On the other hand, both TA and TF (200 and 400 mg/kg) attenuated inflammatory response after 14 days of treatment, rats showed a significant reduction in COX2 (58–65 and 22–62% respectively), LOX (40–52 and 35–59% respectively) and PGE2 (17–53 and 16–59% respectively) compared to CCI control values. Noteworthy, TA reduces PGE2 levels to higher extent compared to TF (Table 1).

Effect of extracts on NF- κ B, TNF- α and iNOS. Sciatic nerve and brain stem of rats subjected to CCI for 14 days revealed significantly high levels of NF- κ B (5 and 4.7 folds, respectively), TNF- α (8.7 and 7.4 folds, respectively) and iNOS (3 and 3.5, respectively) compared to sham rats. While, sciatic nerve and brainstem isolated from rats treated with *T. algeriensis* or *T. fontanesii* extract (200 and 400 mg/kg, p.o, 14 days) showed abrogated CCI-induced increase in NF- κ B and TNF- α and attenuated the increase in iNOS compared to CCI control group. Notably, while the effect of both extracts on NF- κ B and TNF- α was superior to that of pregabalin, all treatments have similar effects on iNOS levels (Table 1).

Discussion

Neuropathic pain, which can affect the peripheral and the central nervous systems, is always referred to a chronic pain condition that follows peripheral or central nerve injury caused either by trauma or systemic diseases such as diabetes, viral infection, multiple sclerosis and cancer. The available treatments for chronic neuropathic pain have limited efficacy in most patients²¹. Therefore, comprehensive studies are required to develop a better treatment for neuropathic pain. Here, we explored the possible protective effects of two species of thymus, *T. algeriensis* (TA) and *T. fontanesii* (TF) in a neuropathic pain rat model, sciatic nerve CCI model, and their mechanism of action. The main findings of our work are: (1) TA and TF administration substantially amended neuropathic pain behavior in the CCI model represented by hyperalgesia and allodynia induced by thermal and mechanical stimuli; (2) the structural derangements of both sciatic nerve and brain stem were improved following TA and TF treatments that was dose dependent and comparable to pregabalin in low doses and better than pregabalin at high doses; (3) both extracts improved synaptophysin expression in brain stem and suppress brain stem apoptotic marker caspase-3; (4) both extracts improved sciatic nerve integrity and maintain myelin sheath in CCI rats; (5) oxidative and nitrosative stress markers, such as iNOS, NOX1 and catalase were improved in both brain stem

Sample	COX2 (ng/mL)	LOX	PGE2 (pg/mL)	NF-κB	TNF-α	iNOS (U/mL)
Normal						
Sciatic	3.84 ± 0.40	0.84 ± 0.09	21.12 ± 1.28	49.04 ± 1.93	34.42 ± 2.99	3.60 ± 0.30
Brain stem	4.56 ± 0.49	0.99 ± 0.09	20.18 ± 1.31	57.48 ± 7.04	43.60 ± 6.11	3.75 ± 0.5
Sham						
Sciatic	6.22 ± 0.76	0.80 ± 0.09	24.68 ± 1.17	50.12 ± 3.54	38.76 ± 4.91	3.78 ± 0.47
Brain stem	6.92 ± 0.51	1.06 ± 0.09	24.54 ± 1.39	63.48 ± 3.35	52.12 ± 6.10	4.10 ± 0.43
CCI						
Sciatic	25.62 ± 1.15*	3.30 ± 0.40*	68.10 ± 6.58*	200.40 ± 13.31*	335.80 ± 26.66*	11.52 ± 0.78*
Brain stem	32.00 ± 1.64*	3.96 ± 0.29*	75.98 ± 7.11*	297.20 ± 22.14*	386.92 ± 27.25*	13.82 ± 0.44*
TA (200 mg/kg)						
Sciatic	10.75 ± 1.96**	1.85 ± 0.19	56.82 ± 5.63*	78.20 ± 6.70*	54.65 ± 6.75**	7.60 ± 1.94
Brain stem	21.00 ± 5.77**	2.36 ± 0.25*	56.51 ± 8.27*	81.46 ± 7.97**	58.43 ± 9.08**	8.08 ± 1.33*
TA (400 mg/kg)						
Sciatic	8.92 ± 1.12†	1.98 ± 0.58	31.42 ± 3.85*	51.51 ± 6.34**	31.80 ± 3.34**	6.88 ± 1.57
Brain stem	13.41 ± 0.64†	2.14 ± 0.17*	31.18 ± 3.88*	55.38 ± 13.16**	33.36 ± 4.25**	6.60 ± 1.55*
TF (200 mg/kg)						
Sciatic	9.57 ± 0.64**	1.83 ± 0.40	51.73 ± 6.73*	66.1 ± 3.37**	60.20 ± 6.21**	7.50 ± 2.27
Brain stem	24.84 ± 3.26**	2.11 ± 0.65*	64.22 ± 17.43*	69.92 ± 2.62**	65.55 ± 5.53**	8.10 ± 2.36*
TF (400 mg/kg)						
Sciatic	10.68 ± 2.01**	1.60 ± 0.38*	40.64 ± 11.28	41.12 ± 4.82**	35.34 ± 3.27**	9.68 ± 1.69
Brain stem	12.41 ± 0.62†	1.62 ± 0.49*	48.93 ± 4.58	44.60 ± 4.34**	37.42 ± 4.66**	10.33 ± 1.81*
Pregabalin						
Sciatic	10.64 ± 0.76**	2.20 ± 0.27	32.30 ± 6.38*	114.08 ± 9.17**	124.6 ± 4.27**	7.28 ± 0.65**
Brain stem	10.11 ± 0.86*	2.58 ± 0.17**	47.00 ± 1.83**	128.18 ± 10.19**	139.38 ± 3.28**	8.44 ± 0.63**

Table 1. Effect of *T. algerensis* (TA) and *T. fontanesii* (TF) extracts (200 and 400 mg/kg) on different inflammatory markers. Statistical analysis was performed using one way ANOVA, followed by post hoc testing by Tukey test. Values are presented as mean ± SE, n = 5 rats/group. *p < 0.05, vs. Sham group; †p < 0.05, vs. CCI group; ‡p < 0.05, vs. pregabalin group. COX2, cyclooxygenase 2; LOX, lipoxigenase; PGE2, prostaglandin E2; NF-κB, nuclear factor kappa B; TNF-α, tumor necrosis factor alpha; iNOS, inducible nitric oxide synthase.

and sciatic nerve; (6) TA and TF extracts treatment protect HaCaT cell lines from UVA induced oxidative stress; (7) proinflammatory enzymes (COX 2 and LOX) and proinflammatory mediators (TNF-α, NF-κB and PGE 2) were reduced after administration of both extracts in the brain stem and the sciatic nerve of CCI model rats.

The CCI model is a widely used neuropathic pain models. The peripheral nerve injury as a result of the sciatic nerve ligation leads to both structural and functional alteration in the injured nerve that can ultimately lead to both local inflammation and pain sensitization which peak two weeks following the nerve injury²². The ongoing peripheral damage is usually associated with central inflammation and sensitization; hence an effective therapeutic approach to treat neuropathic pain should target both the peripheral and central components of the disease.

Here, we demonstrated that rats developed both mechanical and thermal hyperalgesia in addition to the cold and dynamic allodynia especially when tested after days 7- and 14- post-surgery. In contrast to the study conducted by Chen et al. 2018²³, the authors observed that hyperalgesia condition was obvious from day 3 to day 14 post CCI surgery of sciatic nerve with the peak on day 7. Our study showed that hyperalgesia condition appeared at day 7 and was more prominent at day 14 post-surgery. The obtained results showed an attenuation of the CCI-induced neuropathic pain after the once-daily administration of both extracts. Their effects were dose dependent and superior to pregabalin, the reference standard used in the present study.

Intact peripheral nerves consist of resident macrophages, neurolemmocytes (or Schwann cells), fibroblasts, and the peripheral nervous system wrapping glia. Because, either central or peripheral components can orchestrate the neuropathic pain, we examined in our model, the effect of different treatments on the structural alterations induced by CCI in both the brain stem and the sciatic nerve. We were interested in studying brain stem area because several previous studies showed that chronic neuropathic pain is associated with ongoing functional alterations in the brain stem endogenous pain-modulation system^{24,25}. Intact sciatic nerves consist of closely packed nerve fibers of the nerve fascicle that are surrounded by a perineurium. The myelinated nerve fibers are formed from axoplasm bounded by white of myelin and the nuclei of neurolemmocytes that appear between the nerve fibers. In the CCI model, the sciatic nerve is loosely ligated and chronically constricted. In the present study, H & E staining of the constricted sciatic nerves showed disorganization of nerve fascicles and wide separation of nerve fibers from each other and from overlying perineurium. Moreover, Osmic acid staining showed distortion of the myelin sheath in the CCI group. In previous studies, the afferent sensory neurons were reported to be first excited and the axons were then degenerated, resulting in a demyelination of these neurons¹⁶. This process causes the occurrence and establishment of peripheral neuropathy²⁷. The present study showed that pregabalin

and the low doses of TA and TF extracts established most of the normal situation of nerve fascicles, however, the nerve fibers remain separated in some areas and they did not reverse distortion of myelin sheath. On the other hand, high doses of TA and TF groups showed apparently normal myelin sheath and normal fascicles with slightly separated nerve fibers in few areas.

Both satellite glial cells and microglia, which represent the tissue-resident macrophages in the CNS, play an important role in restoring the physiological pain in sensory ganglia, particularly in dorsal spinal ganglia²⁷. In the present study, we looked at brain stem that is responsible for a key role in the pain pathway. Our results showed degeneration and pyknosis of most neurons and the presence of perineural glial cells closely linked to other degenerated CCI neurons. Different previous papers indicated that glial cells are involved in neuron inflammation within the CNS²⁸. Pregabalin and low doses of TA and TF extracts produce partial improvement, while high doses of extracts produce greater improvement.

Synaptophysin (SYN), the presynaptic protein marker, is localized in small synaptic vesicles and elevated in various neuropsychiatry disorders^{29,30}. Our results indicated dendritic spine deterioration in brain stem following CCI due to alteration of expression levels of synaptic proteins, SYN. The expression levels of SYN in spinal cord were consistent with the duration of heat hyperalgesia caused by sciatic nerve CCI in rats revealing that CCI modulated SYN heat hyperalgesia³⁰. Also, nerve transection significantly elevated the expression levels of SYN in the spinal cord horn³¹. The elevated SYN may be attributed to increased LOX and TNF- α observed in the present study. This note is supported by the finding that, 12/15-lipoxygenase overexpression elevates central SYN levels and triggers anxiety-related behavior and that TNF- α stimulates SYN expression in cultured endometrial stromal cells in a dose-dependent manner^{29,31}. Both thymus extracts decreased synaptophysin expression in dose dependent manner with high doses exert more potent effect than pregabalin or low doses likely via attenuation of both LOX and TNF- α expression in brain stem.

Oxidative stress has been recognized as the contributor to chronic neuropathic pain. We showed previously that TA and TF have powerful antioxidant effects more than ascorbic acid *in vitro*³². In this work, we examined the TA and TF antioxidant effects, using the HaCaT cells exposed to UVA light. UVA light induced oxidative stress was abolished by both extracts. This protective effect was due to Nrf-2 pathway in the case of TF extract. Nrf2 and its downstream pathway play an important role in maintaining the cellular redox status upregulated by means of different antioxidant enzymes, such as the NQO1 and IJO-1. Further, we investigated the antioxidant potential of both extracts in CCI model. Our previous studies showed that catalase is decreased while, NADPH oxidase-1 (NOX-1) is increased in sciatic nerve and brain stem of CCI rats^{6,10,31}. Catalase enzyme is one of the endogenous antioxidant enzymes present in peroxisomes and catalyzes the breakdown of H₂O₂ to H₂O and O₂. Excessive ROS formation in sciatic nerve and brain stem observed in our study may be responsible for the consumption of catalase activity 14 days post-surgery. Because of their antioxidant potential, both TA and TF extracts increased catalase activities in a dose dependent manner and give better effects than pregabalin. NOX-1 activation is the principal source of superoxide anion. Microglia, neurons, astrocytes, and macrophages in the dorsal root ganglion (DRG) and CNS expressed NOX1 during nerve injury³². ROS produced by NOX1 induction, in dorsal root ganglionic neurons, is responsible for pain amplification. Thermal and mechanical hyperalgesia was significantly attenuated in mice lacking Nox1^{32,33}. The reduction of NOX-1 by both extracts may contribute to their protective effects against neuropathic pain. Our findings are consistent with those of a study that reported that TA extract has antioxidant potential and neuroprotective effect in a rat model of H₂O₂-induced brain injury³⁴. According to previous studies, the sciatic nerve injury was reported to be responsible for the increase in gene expression of iNOS and NO in spinal cord microglial cells by the 5th day post surgery. We showed previously and in the current study that iNOS expression is also increased in sciatic nerve and brain stem 14 days post-surgery^{6,10}. Activation of iNOS does not only increase the NMDA receptor GluN1 subunit phosphorylation but was reported to be also responsible for developing neuropathic pain following peripheral nerve injury³²⁻³⁴. Inducible NOS produces high concentration of NO which binds with superoxide anion produced by NOX-1 producing powerful peroxynitrite (PN) radical which causes different pain etiologies in the spinal and periphery cord³⁴. The PN inhibits opioid signaling in the rostral ventromedial medulla (RVM) in the brain stem by nitroxidative modifications of endogenous opioid, enkephalin and formation of functionally inert neuropeptides thus causes chronic pain and central sensitization. Inhibition of peroxynitrite formation by inhibiting both NOX-1 and iNOS enzymes may contribute to the neuroprotective effects of TA and TF extracts.

Nitrosative products and ROS cause activation of NF κ B and p38 via degradation/inhibition of I κ B and MAPK phosphatases, that both causes inflammatory and neuropathic pain. Furthermore, NOX activity is essential for downstream NF κ B- and p38 MAPK-dependent cytokine production. It is known that the inflammatory processes are mainly modulated by the NF κ B factor, in glial and neuronal cells³⁵. Our results showed an increase in the TNF- α (proinflammatory cytokine) and the NF- κ B both in brain stem and sciatic nerve at the 14th day post-surgery indicating a neuro-inflammatory response. Both TA and TF abrogated the increased NF- κ B and TNF- α levels at all dose levels tested. Their effects were superior to pregabalin. It was shown that the pain behavior and the inflammation that follow the nerve injury were decreased in rats with transgenic inhibition of glial NF κ B³⁵. This result is in agreement with our finding findings.

High NF κ B and TNF- α gene expression was linked to high LOX, COX-2 and PGE2 levels in sciatic nerve and brain stem 14 days post-surgery. Our findings are in accordance with others who reported that sciatic nerve injury is associated with higher NF- κ B, TNF- α , LOX and PGE2 levels^{36,37}. Notably, the changes in those inflammatory markers were abrogated by both TA and TF at all dose levels, an effect that was comparable to pregabalin. Our findings reveal that both extracts (TA and TF) are able to protect against peripheral nerve injury-induced neurogenic inflammation.

TNF- α binds to TNF- α receptor (TNFR) in Schwann cells causing the induction of apoptosis. The increased level of TNF- α causes intensification of neuronal death in the rat spinal cord. TNF- α was elevated around the injury area after spinal cord injury. We found that caspase-3, an apoptotic marker, was increased in brain

stem of rats 14 days post-surgery. The increase in brain stem apoptosis observed in our rats is supported by others who reported that peripheral neuropathy is associated with neuronal loss and apoptosis in the rostral ventromedial medulla (RVM), a brainstem region involved in nociception³⁸. The administration of TA and TF extracts decreased caspase-3 level in a dose dependent manner. Notably, the effect of high doses was better than pregabalin. Collectively, our findings suggest that TA and TF exert anti-inflammatory and analgesic effects and protects against peripheral neuropathic pain injury. Moreover, both extracts can suppress neuronal cell death following nerve injury.

Conclusions

Thymus algeriensis and *T. fontansii* extracts could effectively protect against painful peripheral neuropathy. Their underlying mechanisms may be through suppression of oxidative stress-induced neuroinflammation and apoptosis. Both extracts may be considered as promising therapeutic options for management of neuropathic pain and associated illnesses.

Received: 19 June 2020; Accepted: 4 November 2020

Published online: 25 November 2020

References

- Cohen, S. P. & Mao, J. Neuropathic pain: mechanisms and their clinical implications. *BMJ* **348**, f7656–f7656 (2014).
- Llana, C. *et al.* Neuropathic pain. *Nat. Rev. Dis. Primers* **3**, 17 (2017).
- van Hecke, O., Anastasi, S. K., Khan, R. A., Smith, B. H. & Torrance, N. Neuropathic pain in the general population: a systematic review of epidemiological studies. *Pain* **155**, 654–662 (2014).
- Woolf, C. J. Evidence for a central component of post-injury pain hypersensitivity. *Nature* **306**, 686–688 (1983).
- Biella, M. L. S. Contribution of central sensitization to the pain related abnormal activity in neuropathic rats. *Somatosens. Mot. Res.* **17**, 32–38 (2000).
- Sobeh, M. *et al.* Salix tetrasperma Roxb. extract alleviates neuropathic pain in rats via modulation of the NF- κ B/TNF- α /iNOS pathway. *Antioxidants* **8**, 482 (2019).
- Duggett, N. A. *et al.* Oxidative stress in the development, maintenance and resolution of paclitaxel-induced painful neuropathy. *Neuroscience* **333**, 13–26 (2016).
- Salvemini, D., Little, J. W., Doyle, T. & Neumann, W. L. Roles of reactive oxygen and nitrogen species in pain. *Free Radical Biol. Med.* **51**, 951–966 (2011).
- Onodera, Y., Teramura, T., Takehara, T., Shigi, K. & Fukuda, K. Reactive oxygen species induce Cox-2 expression via TAK1 activation in synovial fibroblast cells. *FEBS Open Bio.* **5**, 492–501 (2015).
- Sobeh, M. *et al.* Haematoxylin campechianum extract ameliorates neuropathic pain via inhibition of NF- κ B/TNF- α /iNOS signalling pathway in a rat model of chronic constriction injury. *Biomolecules* **10**, 386 (2020).
- Hegazy, N., Rezaei, S. & Fahmy, A. Remin-angiotensin system blockade modulates both the peripheral and central components of neuropathic pain in rats. Role of calcitonin gene-related peptide, substance P and nitric oxide. *Basic & Clinical Pharmacology & Toxicology* (2020).
- Gaskin, D. J. & Richard, P. The economic costs of pain in the United States. *J. Pain* **13**, 715–724 (2012).
- Sobeh, M. *et al.* *Thymus algeriensis* and *Thymus fontansii*: chemical composition, in vivo anti-inflammatory, pain killing and antipyretic activities: a comprehensive comparison. *Biomolecules* **10**, 599 (2020).
- Guesmi, F., Bellamine, H. & Landoulsi, A. Hydrogen peroxide-induced oxidative stress, acetylcholinesterase inhibition, and mediated brain injury attenuated by *Thymus algeriensis*. *Appl. Physiol. Nutr. Metab.* **43**, 1275–1281 (2018).
- Jouadi, R. *et al.* Differentiation of phenolic composition among tunisian thymus algeriensis boiss. Et reut. (Lamiaceae) populations: correlation to bioactive activities. *Antioxidants* **8**, 515 (2019).
- Petruk, G., Donadio, G., Lanzilli, M., Istitico, R. & Monti, D. M. Alternative use of *Bacillus subtilis* spores: protection against environmental oxidative stress in human normal keratinocytes. *Sci. Rep.* **8**, 1745 (2018).
- Petruk, G. *et al.* An ascorbic acid-enriched tomato genotype to fight UVA-induced oxidative stress in normal human keratinocytes. *J. Photochem. Photobiol., B* **163**, 284–289 (2016).
- Jain, V., Jeggi, A. S. & Singh, N. Ameliorative potential of rosiglitazone in tibial and sural nerve transection induced painful neuropathy in rats. *Pharmacol. Res.* **59**, 385–392 (2009).
- Bancroft, J. D. & Gamble, M. *Theory and Practice of Histological Techniques* (Elsevier Health Sciences, Amsterdam, 2008).
- Chaiprasongsuk, A. *et al.* Activation of Nrf2 reduces UVA-mediated MMP-1 upregulation via MAPK/AP-1 signaling cascades: the photoprotective effects of sulfuraphane and hispidulin. *J. Pharmacol. Exp. Ther.* **360**, 388–398 (2017).
- Finnerup, N. B., Sindrup, S. H. & Jensen, T. S. The evidence for pharmacological treatment of neuropathic pain. *Pain* **150**, 573–581 (2010).
- Jaggi, A. S. & Singh, N. Differential effect of spironolactone in chronic constriction injury and vincristine-induced neuropathic pain in rats. *Eur. J. Pharmacol.* **648**, 102–109 (2010).
- Chen, J. Y. *et al.* Valproate reduces neuroinflammation and neuronal death in a rat chronic constriction injury model. *Sci. Rep.* **8**, 1–11 (2018).
- Mills, E. P. *et al.* Brainstem pain-control circuitry connectivity in chronic neuropathic pain. *J. Neurosci.* **38**, 165–173 (2018).
- Brightwell, J. J. & Taylor, B. K. Noradrenergic neurons in the locus coeruleus contribute to neuropathic pain. *Neuroscience* **160**, 174–185 (2009).
- Xia, T. *et al.* Regulation of the NR2B-CREB-CRTC1 signaling pathway contributes to circadian pain in murine model of chronic constriction injury. *Anesth. Analg.* **122**, 542–552 (2016).
- Costa, F. A. L. & Moreira Neto, F. L. Satellite glial cells in sensory ganglia: its role in pain. *Revista brasileira de anestesiologia* **65**, 73–81 (2015).
- Thompson, K. K. & Tsirka, S. E. The diverse roles of microglia in the neurodegenerative aspects of central nervous system (CNS) autoimmunity. *Int. J. Mol. Sci.* **18**, 504 (2017).
- Joshi, Y. B., Di Meco, A. & Praticò, D. Overexpression of 12/15 lipoxygenase increases anxiety behavior in female mice. *Neurobiol. Aging* **35**, 1032–1036 (2014).
- Zhang, H.-H. *et al.* Increased synaptophysin is involved in inflammation-induced heat hyperalgesia mediated by cyclin-dependent kinase 5 in rats. *PLoS ONE* **7**, e46666 (2012).
- Lin, J. Y., Peng, B., Yang, Z. W. & Min, S. Number of synapses increased in the rat spinal dorsal horn after sciatic nerve transection: a stereological study. *Brain Res. Bull.* **84**, 430–433 (2011).
- Grace, P. M. *et al.* Nitrosidative signaling mechanisms in pathological pain. *Trends Neurosci.* **39**, 862–879 (2016).

33. Nayernia, Z., Jaquet, V. & Krause, K.-H. New insights on NOX enzymes in the central nervous system. *Antioxid. Redox Signal.* **20**, 2815–2837 (2014).
34. Starowicz, K. *et al.* Full inhibition of spinal FAAH leads to TRPV1-mediated analgesic effects in neuropathic rats and possible lipoygenase-mediated remodeling of anandamide metabolism. *PLoS ONE* **8**, e60040 (2013).
35. Perrière, A. F. *et al.* Ultramicronized palmitoylethanolamide and paracetamol, a new association to relieve hyperalgesia and pain in a sciatic nerve injury model in rat. *Int. J. Mol. Sci.* **21**, 3509 (2020).
36. Leong, M. L. *et al.* Neuronal loss in the rostral ventromedial medulla in a rat model of neuropathic pain. *J. Neurosci.* **31**, 17028–17039 (2011).
37. Rahbardar, M. G., Amin, B., Mehri, S., Mirnajafi-Zadeh, S. I., & Hosseinzadeh, H. Anti-inflammatory effects of ethanolic extract of *Rosmarinus officinalis* L. and rosmarinic acid in a rat model of neuropathic pain. *Biomed. Pharmacother.* **86**, 441–449 (2017).
38. Jaggi, A. S., & Singh, N. Role of different brain areas in peripheral nerve injury induced neuropathic pain. *Brain Res.* **1381**, 187–201 (2011).

Acknowledgments

The authors would like to thank Dr. Mohammed Cheurfa for providing the plant material and UM6P for APC support.

Author contributions

S.R. performed neuropathic pain experiments and wrote the manuscript. A.E.A. performed the histopathological experiments and drafted the results. L.D. performed the antioxidant activities in cells. A.M.E. commented on the manuscript. D.M.M. wrote the antioxidant activities in cells. M.S. performed the extraction, revised the manuscript, and designed and conceived the study. M.F.M. performed the neuropathic pain experiments, wrote the manuscript, and designed and conceived the study. All authors read the manuscript and validated it.

Competing interests

The authors declare no competing interests.

Additional information

Supplementary information is available for this paper at <https://doi.org/10.1038/s41598-020-77424-0>.

Correspondence and requests for materials should be addressed to M.S. or M.F.M.

Reprints and permissions information is available at www.nature.com/reprints.

Publisher's note Springer Nature remains neutral with regard to jurisdictional claims in published maps and institutional affiliations.

 **Open Access** This article is licensed under a Creative Commons Attribution 4.0 International License, which permits use, sharing, adaptation, distribution and reproduction in any medium or format, as long as you give appropriate credit to the original author(s) and the source, provide a link to the Creative Commons licence, and indicate if changes were made. The images or other third party material in this article are included in the article's Creative Commons licence, unless indicated otherwise in a credit line to the material. If material is not included in the article's Creative Commons licence and your intended use is not permitted by statutory regulation or exceeds the permitted use, you will need to obtain permission directly from the copyright holder. To view a copy of this licence, visit <http://creativecommons.org/licenses/by/4.0/>.

© The Author(s) 2020

***Thymus algeriensis* and *Thymus fontanesii* exert neuroprotective effect against chronic constriction injury-induced neuropathic pain in rats**

Samar Rezq¹, Amira E. Alsemeh², Luigi D'Elia³, Assem M. El-Shazly⁴, Daria Maria Monti³, Mansour Sobeh^{5,*}, Mona F. Mahmoud^{1,*}

¹Department of Pharmacology and Toxicology, Faculty of Pharmacy, Zagazig University, Zagazig 44519, Egypt

²Department of Anatomy and Embryology, Faculty of Medicine, Zagazig University, Zagazig, Egypt

³Department of Chemical Sciences, University of Naples Federico II, Complesso Universitario Monte Sant'Angelo, via Cinthia 4, 80126 Naples, Italy

⁴Department of Pharmacognosy, Faculty of Pharmacy, Zagazig University, Zagazig 44519, Egypt

⁵AgroBioSciences Research Division, Mohammed VI Polytechnic University, Lot 660–Hay MoulayRachid, 43150 Ben-Guerir, Morocco

* Correspondence: mansour.sobeh@um6p.ma, mfabdelaziz@zu.edu.eg

Materials and methods:

Biochemical analysis in sciatic nerve and brainstem tissue

Following the last behavioral assessment, blood samples were collected via cardiac puncture under anesthesia (thiopental, 50 mg/kg, i.p.) followed by heart removal. The progression of NP involves both peripheral and central components, therefore, the anti-inflammatory potential of the extract was investigated in the sciatic nerve as well as in the brainstem, which is known to be greatly involved in maintenance of NP^{1,2}. Ipsilateral sciatic nerves, including the injured site and approximately 5 mm of surrounding tissues on both sides (~10 mm), were excised. Brainstems were then harvested. The collected tissues were either flash frozen in liquid nitrogen and maintained at -80 °C or preserved in formalin for the histochemical analysis. Tissues homogenization was done in PBS followed by centrifugation (14,000 rpm for 20 min, 4 °C). Total protein of the supernatant was estimated using Bradford assay (Bio-Rad, 1000 Alfred Nobel Drive, Hercules, California 94547, USA). NADPH oxidase 1 (NOX1), cyclooxygenase-2 (COX-2), 5-lipoxygenase 1 (5-LOX), catalase, TNF- α , and NF- κ B were detected using rat ELISA kits obtained from Cusabio (TX, USA), while Inducible nitric oxide synthase (iNOS) and Prostaglandin E2 (PGE2) were determined by ELISA kits from MyBiosource (San Diego, CA, USA) and Cayman (Michigan, USA), respectively, according to the manufacturers' instructions^{3,4}.

Immunohistochemical staining of brain stem synaptophysin and caspase-3

Paraffin sections of perfused brain stem from all studied groups were used for detecting, the synaptic protein, synaptophysin (SYN), and the apoptotic marker, caspase -3, immunoreactivity. The sections were de-waxed and incubated for 1hr at room temperature in 0.3% hydrogen peroxide in phosphate-buffered saline, pH 7.6 (PBS). The slides were washed 3 times (10 min. each) in the same buffer to quench endogenous peroxidase activity. They were

incubated for 16 hr at 4 °C in PBS containing 2% normal goat serum (NGS) and 0.5% triton X-100, and then washed again in PBS at room temperature. This was followed by overnight incubation at 4°C with the primary monoclonal antibody of anti-SYN (1:150, CST, MA, USA) or anti-caspase-3 (1:500, CST, MA, USA), then washed 3 time in PBS-2% NGS. The primary antibodies were bounded by a rat adsorbed biotinylated anti-mouse secondary antibody (1:200, Vector Labs, Burlingame, CA, USA), in PBS for 1hr at room temperature. Slides were incubated in avidin-biotin complex linked to peroxidase (ABC Kit, Vector Labs, Burlingame, CA, USA). Peroxidase was seen with 0.03% diaminobenzidine hydrochloride and 0.005% hydrogen peroxide in 0.1 M Tris buffer. All sections were counter stained with hematoxylin dehydrated, cleared, and mounted in Canada balsam. The Image J analysis software (Fiji Image J; 1.51 n, NIH, USA) was used to estimate the ratios of the synaptophysin positive reactivity on the surface of the neuron to the total area of the neuron and to count the immunopositive caspase-3 nuclei^{3,4}.

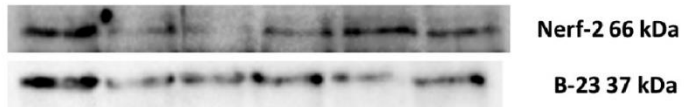
2.5.8. Sciatic nerves staining with osmic acid

For the morphometrical assessment of the sciatic nerve, osmic acid was used to stain the myelin sheath of the nerve, as previously described^{3,4}

. 3- μ m sections were fixed with 4% paraformaldehyde, incubated with 2% osmic acid solution for 3 days, transferred to 75% alcohol (2 h) then embedded in paraffin. Myelin sheaths were stained with a dark brown color upon examination by light microscopy (LEICA ICC50 W, Leica Microsystems (Schweiz) AG, 9435 Heerbrugg, Switzerland). The ratio of the myelinated area to the total nerve fibre area (including the myelin sheath) was detected and represents the integrity of the sciatic nerve. Additionally, the percentage of degenerated nerve fibers (fibers that lack the normal concentric lamellar structure of the myelin sheath or has myelin invagination into the axon and axonal swelling) to the total count of nerves was also estimated by a histologist who did not know the treatments¹.

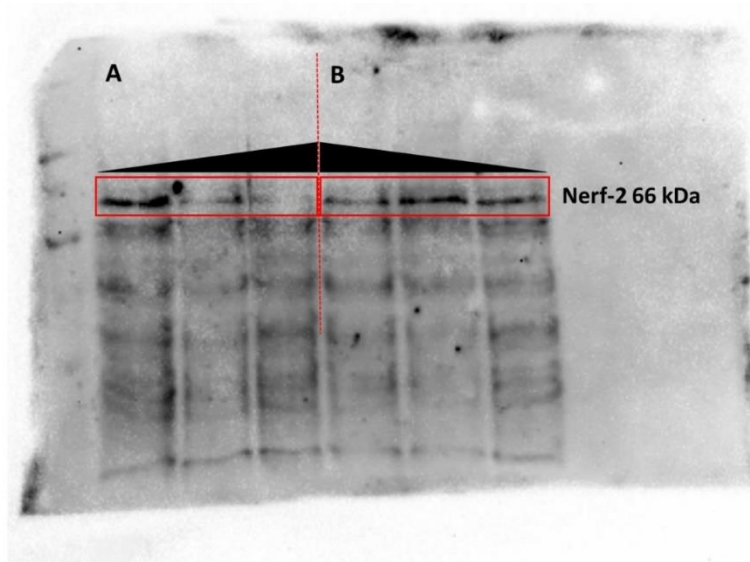
BLOT TA & TF 50 µg/mL 15' and 30' incubation

untreated TA15' TA30' TF30' TF15' untreated



Nerf-2	B-23	Nerf-2/B-23	%
2118	4844	0.43724195	100
1230	1854	0.66343042	152
753	2322	0.32428941	74
1769	3341	0.52948219	100
2246	1840	1.22065217	231
1642	3525	0.4658156	88

BLOT TA & TF 50 $\mu\text{g}/\text{mL}$ 15' and 30' incubation



BLOT TA & TF 50 $\mu\text{g}/\text{mL}$ 15' and 30' incubation

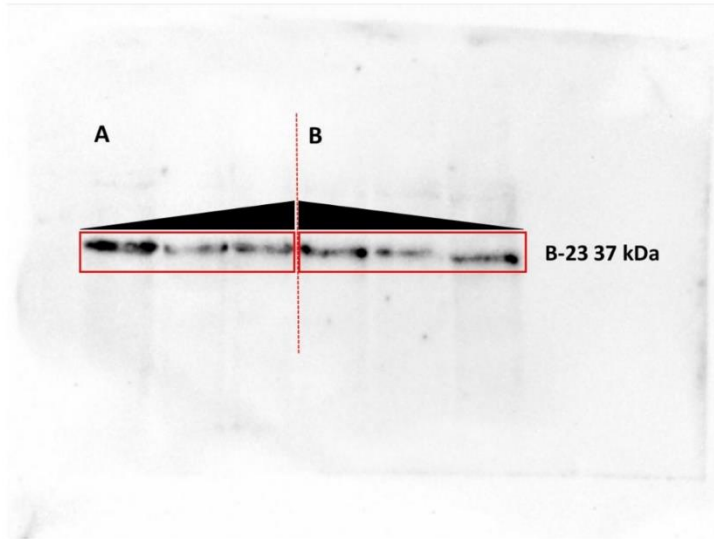
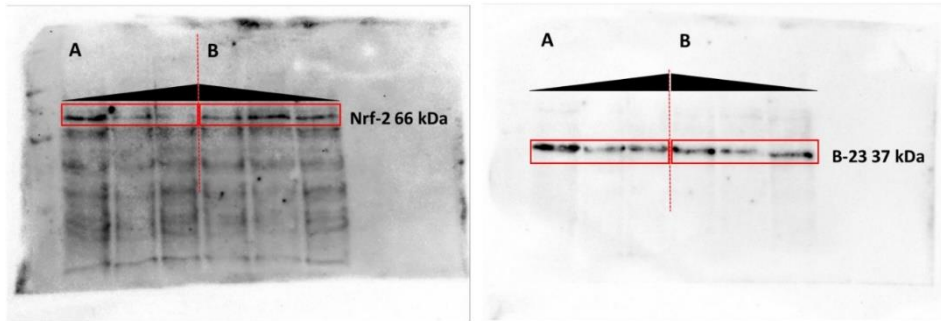


Figure 3



References

1. Colloca, L. *et al.* Neuropathic pain. *Nature reviews Disease primers* **3**, 1–19 (2017).
2. Mills, E. P. *et al.* Brainstem pain-control circuitry connectivity in chronic neuropathic pain. *Journal of Neuroscience* **38**, 465–473 (2018).
3. Sobeh, M. *et al.* Salix tetrasperma Roxb. extract alleviates neuropathic pain in rats via modulation of the NF- κ B/TNF- α /NOX/iNOS pathway. *Antioxidants* **8**, 482 (2019).
4. Sobeh, M. *et al.* Haematoxylon campechianum Extract Ameliorates Neuropathic Pain via Inhibition of NF- κ B/TNF- α /NOX/iNOS Signalling Pathway in a Rat Model of Chronic Constriction Injury. *Biomolecules* **10**, 386 (2020).

La borsa di dottorato è stata cofinanziata con risorse del
Programma Operativo Nazionale Ricerca e Innovazione 2014-2020 (CCI 2014IT16M2OP005),
Fondo Sociale Europeo, Azione I.1 "Dottorati Innovativi con caratterizzazione Industriale"



UNIONE EUROPEA
Fondo Sociale Europeo

